TURBOGENERATOR TRANSIENT BEHAVIOUR UNDER LARGE SYSTEM DISTURBANCES

A STUDY OF PERFORMANCE IMPROVEMENTS BY FAST ACTING CONTROLS

by

K. Jenkins, B.Sc.

This thesis is submitted for the Degree of Doctor of Philosophy to the Faculty of Applied Science, The University of Newcastle upon Tyne

December 1972

TO MY WIFE, SYLVIA

SUMMARY

Mathematical models of varying complexity for representing turbo-generators and associated excitation and prime mover control systems are developed. Special reference is made to the application of these models for digital computer solution to determine turbogenerator transient performance under large system disturbances.

A parametric study of the effect of differing generator designs and control systems configurations, on the transient behaviour is performed, using the digital computer model. In particular, the capabilities of the latest high speed control systems, such as thyristor exciters and electrohydraulic governors, are assessed. Novel methods of stabilisation of these systems and the effects of both single and combined control action are investigated. In choosing the most appropriate computer model, the aim was to achieve the highest possible complexity, taking into account the limitations on available machine data.

A full account of the results of fault tests on a full scale turbo-generating system with thyristor excitation, in which the author participated, is given. These were intented to verify some of the control policies developed, and provide an accuracy check on the computer programme to give confidence in the modelling technique for future simulations. Fast response instrumentation for obtaining specialised feedback signals for the site tests is described, together with a full set of equipment for laboratory investigation on a model power system.

Although a number of difficulties with the instrumentation were encountered in the tests, the results serve to illustrate the capabilities of fast thyristor excitation systems, and the high degree of accuracy obtained by the digital computer simulation techniques.

ACKNOWLEDGEMENTS

The author wishes to thank his project supervisor Mr. J.L. Dineley, and former colleagues of the Power Systems Group in the Department of Electrical and Electronic Engineering, the University of Newcastle upon Tyne, for advice, assistance and ecnouragement throughout the duration of the project. Thanks are also due to Professor R.L. Russell for providing the research facilities in that Department.

The author's sincere gratitude is also expressed to Mr. B. Berger and C.A. Parsons & Co. Ltd., for assistance in completing the work reported in this thesis, and to present colleagues of the Applied Physics Department of that Company for co-operation and helpful technical discussions during the later stages of the project. In addition, the financial backing of A. Reyrolle & Co. Ltd., is also gratefully acknowledged.

Thanks are also given to Mr. W. Fairney and members of the Scientific Services Department, CEGB, Leeds, for allowing the author to participate during the Doncaster system tests and for providing photographs and other material for the thesis.

Finally, thanks should go to those who helped in the production of this thesis, in particular to Mrs. A. Hudson for typing the complete work and to Mrs. E. Tripp and Mr. L. Davidson for reproducing the graphs and diagrams.

CONTENTS

CONTENTS (Cont'd)

CONTENTS (Cont'd)

1 INTRODUCTION

The unprecedented increase in size of individual generating units in post war years has only been achieved by large research investments and intense design activity. However one of the most radical changes in the design of overall turbogenerating systems is taking place in the control field and although this has partly been brought about by the increase unit size, another major influence has been the rapid developments in solid state electronics.

In the excitation system the development of high power silicon diodes facilitated the transition from DC to AC exciters which permitted higher power capabilities,whilst the introduction of thyristor rectifiers removed the control limitations of the rotating machine with its inherent time delays,and thus provided a fast method of direct adjustment of field voltage. The rest of the excitation control loop which normally consists of a voltage regulating feedback system, has also benefited from the use of semiconductors which for example removed the restrictions imposed by the non-linearities of magnetic amplifiers and provided a further improvement in the response of the control system.

In the prime mover control field the centrifugal or Watt governor has had a long history being universally used since the inception of turbo-type generators and even before this on reciprocating machines. These are being superseded, particularly in Europe and the USA by electrohydraulic systems in which the flyball governor is replaced by an electronic speed sensing device and the direct conversion of an electrical signal into hydraulic pressure in the electrohydraulic actuator eliminates most of the mechanical linkages. With these systems, particularly the latest designs, a greater accuracy and faster response is achieved together with a very small dead band giving an extremely flexible control tool.

An influential factor for turbogenerator control systems development has been the increasing concern for the growing problem of power system stability, although this is not the sole reason for the evolution of the new systems, the development of which was dictated by advances in technology. Nevertheless the latest systems exhibit the performance characteristics of accuracy and flexibility which also satisfy the requirements for improving system stability both under small disturbances (steady state stability) and large disturbances or system faults (transient stability).

One reason for the decline in system stability is illustrated by Fig.1.1

GROWTH IN PRODUCTION OF TURBO/GENS
TOTAL MW DESPATCHED

a

b

c

660MW

800MW

GROWTH OF SINGLE LINE
AC GENERATORS

——— ≥3000rpm

- - - BELOW 3000rpm

MW

50,000
10,000
5,000
1000
500
100
50
10
5
1

1880 1890 1900 1910 1920 1930 1940 1950 1960 1970 1980

YEAR

which shows the trends in production of turbogenerators by a British manufacturer. Curve (a) shows the accumulative production of generating plant which reflects the increase in world power demands, since it is an international company. Curves (b) and (c) show the increase in outputs of individual units which, it should be emphasised, are plotted on a logarithmic scale. It is observed that the rate of increase in outputs of both four and two pole sets has escalated in the last twenty years so that curves (b) and (c) are now tending to converge upon curve (a) Hence a single generator now represents a much greater portion of the total system capacity and the whole system is becoming more sensitive to the behaviour of individual units. In addition the new large generator designs are more economical in the use of materials producing reduced inertia constants which make the performance more oscillatory.

A contributing factor to the acceleration of turbogenerator manufacture has been the consuming of world hydro-electric power potentials which has caused hydro utilities such as in Scotland and in Canada to invest in large nuclear powered steam turbine generator installations. Besides the obvious undesirable effects on the system stability produced by size increase of the steam sets over their hydro counterparts, the situation is exacerbated by the bulk transportation of electricity from the large power stations over long transmission lines to the major load centres. This is necessary since the generation zones are usually situated in remote areas near to abundant water supplies such as the North American Great Lakes. This method of transmission involves operation at leading power factors and large load angles which has detrimental effects on the operation by reducing the transient stability margin and the synchronising power.

From the above discussion it is clear that the development of methods of counteracting the decline in the stability picture is of paramount importance. On the system side these methods are well known and include: uprating the working voltage, using parallel transmission lines, using VAR compensation, and judiciously placing transformers, interconnections, etc. However in the design of turbogenerators and control systems the main attention has been given to means of improving steady state stability and although a large amount of computer studies and laboratory and site tests have been performed, there is as yet little evidence of new plant being installed specifically to improve the transient stability. This is due to the lack of precise design philosophy emerging from the previous work as the control systems have generally been too slow and the computer

modelling techniques too simple for the highly complex processes occurring during this mode of operation. The aim of this thesis is to formulate an effective overall control systems policy for excitation and prime mover using the latest developments in these aspects. This is facilitated by the formulation of an accurate turbogenerator digital computer programme for transient stability studies which has been validated by large scale site tests on a 30 MW generator.

2 MODELLING OF TURBOGENERATORS

2.1 Introduction

The power systems engineer can gain very little knowledge of synchronous machine dynamic performance from observations during normal operating conditions. In order to obtain an understanding of the transient behaviour, a disturbance has to be applied to the system and resulting oscillations of the various machine and system quantities recorded and analysed. This is by nature an expensive and occasional process only performed a limited number of times under a carefully planned and strictly controlled programme. Such tests have been performed on the British power system at a rate of about one every two years and these have provided power systems analysts with some valuable material.

The best solution at this stage of development is to use some form of modelling technique. This incurs minimum cost and the great advantage is that tests can be repeated many times until satisfactory results are obtained. However the use of modelling techniques entails the introduction of constraints and assumptions which detract from their accuracy according to which type of technique is chosen for a particular study. Thus an engineer must select carefully the type of technique which is best suited in each individual case and if it is an analytical method, a further selection of the most suitable mathematical representation and accuracy of solution is also necessary.

2.2 Modelling techniques

2.2.1 AC network analysers

The original method of modelling power systems was by network analysers[1]. These employed scaled physical representations of inductors, resistors and capacitors to represent the inductance, resistance and capacitance of equivalent transformers, transmission lines and other system components. Generators were represented by an AC voltage which was usually variable in magnitude and phase, in series with an inductance and a resistance. This is often referred to as the voltage behind reactance representation. The frequency of this voltage was usually very much higher than the actual power system frequency in order to reduce the values and hence the physical size of the analyser components.

The basic AC network analyser has the disadvantage that the simplicity of the generator representation renders it unsuitable for transient stability studies, although the method was extended by using transient reactances and

representing transient saliency[2]. This was remedied on later machines by using a DC analogue for generators and an AC analogue for the transmission system[3], but practical difficulties arise in interfacing the two systems. The standard AC analyser still finds some application in load flow and steady state stability studies by power system authorities and manufacturers as the presentation of information is more readily comprehensible than a digital computer print out.

2.2.2 DC analogue computers

Due to size and capital cost restrictions, DC analogue computer studies are usually limited to those involving a small number of generators[4,5]. In these studies the mathematical representation of generators is usually of only moderate complexity but programming the full two axis representation is possible. As this required approximately 30-40 amplifiers however, only single machine studies can be attempted on most computers with models of this complexity. On occasion, the CEGB have assembled large analogue systems for special studies[6]. The great advantage of using analogue computers is the speed at which desired results can be obtained by repeating tests at various parameter settings. Often the machine can be programmed to work faster than the real time enabling the transient decay of generator oscillations (which may last for several seconds) to be displayed as a stationary trace on an oscilloscope screen. The effect of any parameter on the transient performance can then be assessed by simply adjusting the appropriate potentiometer, voltage or feedback impedance.

The biggest problem with early machines was that of drift in the DC amplifiers but present day computers usually employ silicon transistor amplifiers with field effect transistor chopper stabilisers to overcome this. The extensive incorporation of semiconductors has reduced the overall physical size of computers but the cost per amplifier is still prohibitive for most analytical studies.

Because the analogue computer can operate in real time however, it is the ideal alternative for use in on-line control systems which require a mathematical model of the system to be referred to. Two of these are the high speed predictive and model reference adaptive system[7] but due to high development costs, little practical work has been performed on these systems so far.

2.2.3 Digital computers

Due to the rapid increase in speed and core size, the digital computer has become the most popular tool for power system studies in recent years.

Another reason for their popularity is that the computer is shared by many users, each one paying for only the time that his particular programme is being processed. However the computation time is still very slow for reasonable accuracy of modelling, being of the order of one minute for calculating one second of real-time machine response. Thus, optimisation of machine and control system variables using the digital computer is inherently a lengthy process. This has been improved upon with the latest generation of fast computers using time-shared terminal systems. For investigations using highly complicated representations and large scale multimachine studies, the large modern digital computer system is ideally suited as it provides almost unlimited capability. As an example, a recent paper[8] describes a multimachine stability programme with a capability of 2000 buses, 3000 lines and 600 generators using a 128 K-byte computer. This is by no means a very large machine by present day standards.

Nevertheless, digital computers are still too slow for on-line control of fast transients in large systems. The main reason for the slow speed of digital computation is that the mathematical process of integration has to be performed by an iterative method which involves many cycles of the differential equations for each calculation step. Thus it follows that the computation time will depend upon the choice of the method of integration, but this choice should not be made on speed requirements alone as some of the more basic methods such as Simpson's Rule tend to be too inaccurate for calculation of results during the subtransient period. The more complicated methods such as Runge-Kutta are satisfactory if a short step length is used, but this wastes computer time for the calculations subsequent to the subtransient period where a longer step length would suffice. An obvious answer is to change the step length artificially at some predetermined point in the programme but this requires prior knowledge of the length of the subtransient period. A more satisfactory approach is to use a Kutta-Merson type of integration which automatically reduces the step length until some required accuracy parameter is satisfied. However a disadvantage is that the subdivision of the step length is carried out from the same starting point each time. This has been improved upon by predictor-corrector methods which predict a value of step length from information 'remembered' from the previous step. The most suitable form for power system transient stability studies appears to be that developed by Hammings[9] and the author has experienced an economy of up to 30% on computer time using this method as compared to Kutta-Merson integration.

Due to the increase of computing speed as new processors are developed it may now be feasible to use digital computer models of turbogenerators for on-line control. At the present time computers find wide application in large power stations for data logging, boiler control and programmed run-up and synchronisation, and direct digital control of turbogenerator dynamical behaviour would seem an obvious progression in the near future.

2.2.4 Laboratory alternator systems

Small industrial alternators and laboratory teaching machines are not generally suited for modelling large turbogenerators as their parameters are not equivalent on a per unit basis (i.e. referred to machine rating). The major discrepancies occur in the values of winding resistances which are too high and inertia constant which is too small. These cause substantial differences in important aspects of the dynamic behaviour, notably angular backswing and oscillation frequency. Some improvement can be gained by derating the machine but this reduces iron saturation effects which should be included for correct simulation. The introduction of the microalternator[10,11] which was specially designed for power system transient stability studies offset some of these difficulties. The most common set in the United Kingdom is manufactured by Mawdsleys of Dursley, Gloucestershire. This machine utilises a large frame so that large cross-section windings can be incorporated to reduce resistances, also a flywheel is mounted on the shaft with detachable annular weights for adjustment of the inertia constant. Good approximation is obtained to most turbogenerator parameters except that the rotor time constants are too small. These depend to a certain extent upon the volume of iron in the machine and an attempt to achieve a correct value would lead to a design with impractical dimensions. Since time constant is an L/R ratio, it can be increased by reducing resistance, or conversely by inserting 'negative resistance'. This is performed electronically as shown in Fig.2.1.

The winding F is the field winding which has an auxiliary winding S wound alongside it that experiences the same flux changes. Amplifier A is a combined error and power amplifier whose output voltage is given by the expression

$$e = k \times \left[V_f - \left(rI + n \frac{d\phi}{dt} \right) \right] \qquad \ldots(2.1)$$

where k is the overall gain of the amplifier system and r is the resistance

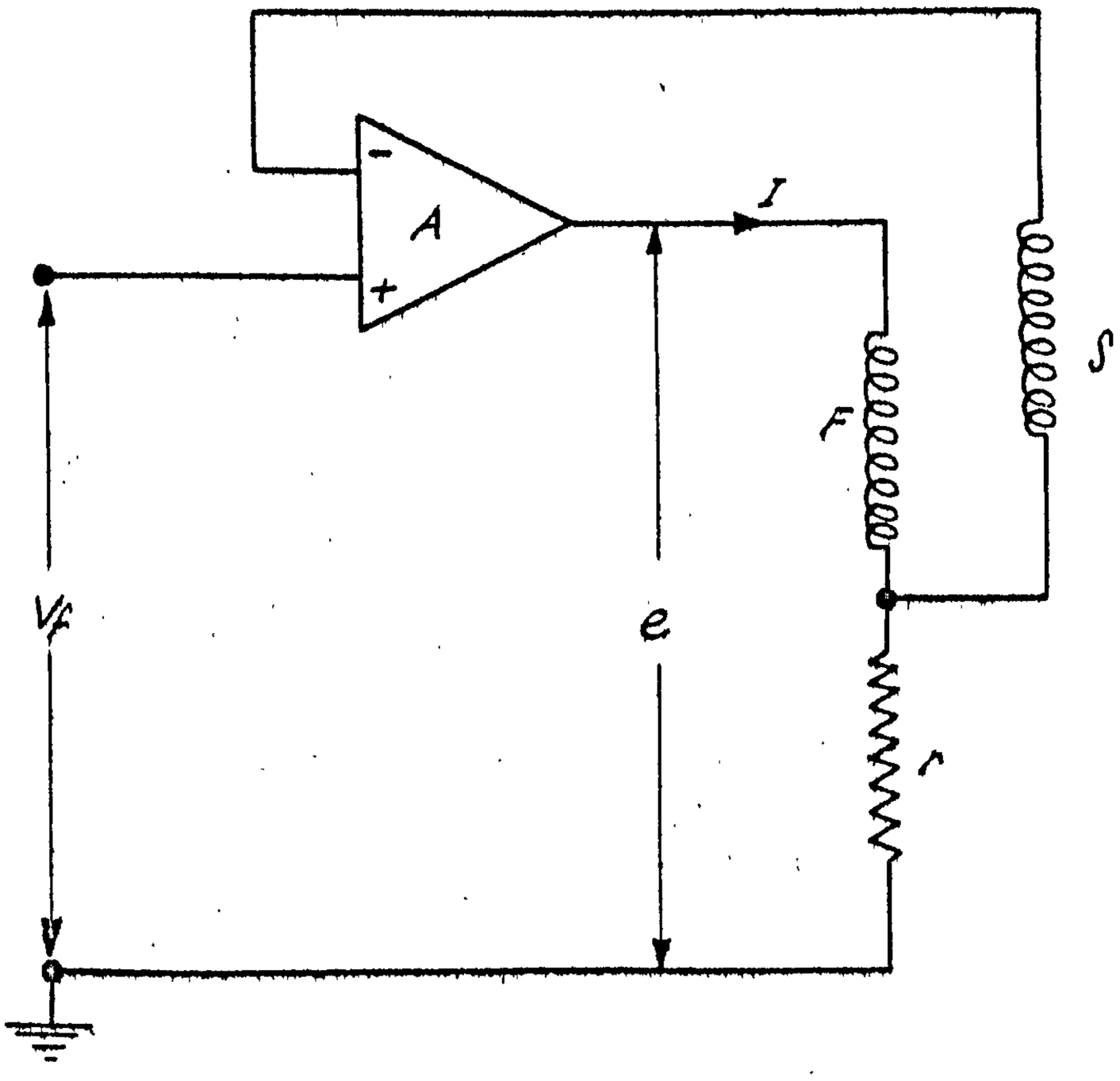

BASIC CIRCUIT OF TIME CONSTANT REGULATOR

FIG 2.1

of a shunt which is inserted in the field circuit.

If the gain k is made very high, then from equation (2.1) the effective input voltage to the field supply system is given by

$$V_f = rI + \frac{nd\phi}{dt}$$

Comparing this with the equation for the voltage across the field,

$$V_F = RI + \frac{nd\phi}{dt}$$

it is seen that so far as the new input voltage to the field system is concerned, the effective resistance is equal to the artificially inserted value r, which can be varied at will in order to achieve any desired field time constant.

In practice the power amplifier is often a thyristor controlled bridge system, but limitations on speed of operation when used at mains frequency make this unsuitable for use on the rotor damper circuits. Using a higher supply frequency of say 1000 Hz is a possible solution but with the additional requirement of voltage reversal the system is very costly requiring two thyristor bridges and a separate motor-generator set. Transistor amplifiers are now available with high enough power ratings and these may be employed, providing the four fields are paralleled to give a sufficiently low voltage requirement.

The area where the most differences occur between the laboratory and large scale machines is that of damping representation. On a present day turbogenerator the damping circuits are very complex and may include the effect of the solid iron of the rotor, any damper bars, the slot wedges and the end caps. The laboratory machine usually has a laminated rotor construction which is sometimes fitted with a fixed damper cage, and the micromachine has a separate damper winding, the two ends of which can be connected to an external circuit by means of slip rings. None of these arrangements can successfully simulate the effect of the solid rotor eddy current path, which changes in geometry with varying frequencies, causing the resistance and reactance to alter. This is due to the frequency dependence of the depth of penetration of flux which is smallest at high frequencies, So that during subtransient conditions a much higher resistance path is presented to the rotor eddy currents than during dynamic conditions when the flux is varying relatively slowly.

2.3 Mathematical modelling

The mathematical model to be described is intended for digital computer solution using iterative methods of integration as described earlier. Although most of the equations could be adapted for an analogue computer this method of solution is out of the scope of the present work and is not specifically referred to further.

The acknowledged method of analysis is by the 'two axis' theory which was developed for the synchronous machine by Park[12,13], and as the derivation of basic synchronous machine equations using this theory is covered by many textbooks (e.g. Adkins[14] and Jones[15]), it is not treated here. The equations are developed using the per-unit system[16,17] whereby all the parameters are referred to appropriate base values which are usually derived from the rating of the machine. This system simplifies the equations and makes it possible to compare the parameters and performance of machines of widely differing ratings. The derivation of the base values and the transfer of rotor to stator quantities (see Ref, 18) is treated later.

The elemental mutual and leakage reactances as in Park's original analysis are used throughout because in the author's view, the commonly used 'transient' and 'sub-transient' reactances are obsolete and too limiting in scope for complex machine studies.

2.3.1 Equations for the standard model

The standard 'benchmark' model to be described is a compromise between the limitations of presently available generator data and a high enough complexity for the required studies (see Table 1). Much work is currently proceeding to improve upon the acknowledged deficiency in generator data[19].

Fig.2.2 shows in diagrammatic form the equivalent arrangement of the coils of the synchronous machine under the two axis theory for the standard model. These consist of direct and quadrature axis coils for armature and damper windings and a single field coil which is assumed to be situated on the direct axis. A further field coil is added on the quadrature axis if it is desired for study of doubly-excited machines. The two-phase representation is of course entirely fictitious, being a mathematical device to overcome the difficulties of analysis. The conversion of the actual three-phase machine into this form is covered by the two axis theory.

The expressions for the flux linkages in each coil are written in terms of self and mutual components:

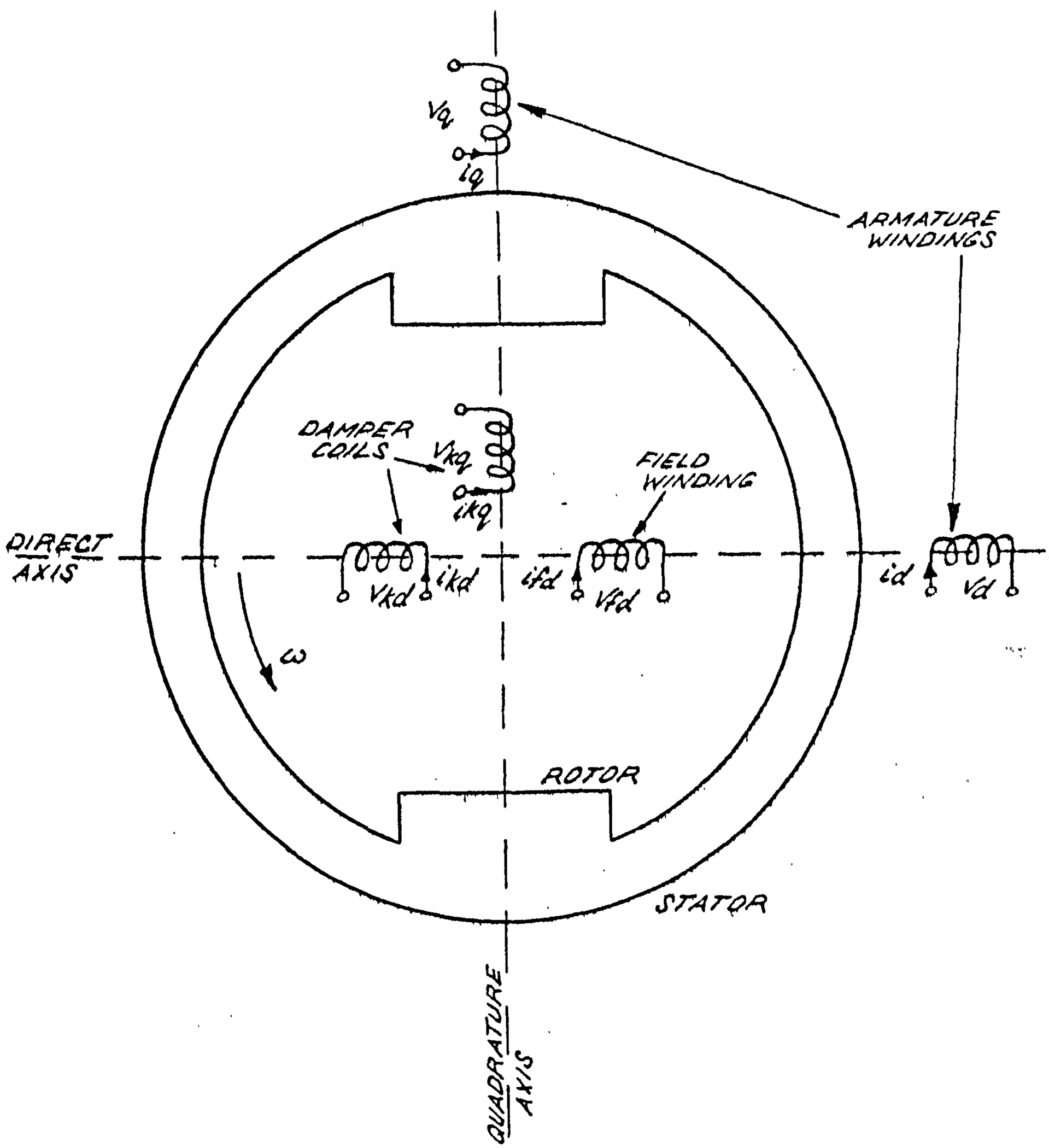

DIAGRAM OF SYNCHRONOUS MACHINE IN TWO AXIS FORM

FIG 2.2

$$\psi_{fd} = \frac{1}{\omega_o}\left[\chi_{fd}\, i_{fd} + \chi_{md}\, i_{kd} - \chi_{md}\, i_d\right] \qquad \ldots(2.2)$$

$$\psi_d = \frac{1}{\omega_o}\left[\chi_{md}\, i_{fd} + \chi_{md}\, i_{kd} - \chi_d\, i_d\right] \qquad \ldots(2.3)$$

$$\psi_q = \frac{1}{\omega_o}\left[\chi_{mq}\, i_{kq} - \chi_q\, i_q\right] \qquad \ldots(2.4)$$

$$\psi_{kd} = \frac{1}{\omega_o}\left[\chi_{md}\, i_{fd} + \chi_{kd}\, i_{kd} - \chi_{md}\, i_d\right] \qquad \ldots(2.5)$$

$$\psi_{kq} = \frac{1}{\omega_o}\left[\chi_{kq}\, i_{kq} - \chi_{mq}\, i_q\right] \qquad \ldots(2.6)$$

In these equations it is assumed that all the mutual reactances are equal and reciprocal and the ratio of per unit$_{\lambda}^{base}$ reactance to per unit$_{\lambda}^{base}$ inductances is the base frequency ω_o which is chosen to be synchronous speed. Hence the need for including the $1/\omega_o$ terms.

The expressions for the voltage across each stator coil will contain resistive and rotational terms and in addition the often neglected stator transients or '$p\psi$' terms. The rotor coils are not cutting flux and therefore no rotational voltages are present.

$$V_d = p\psi_d - R_a\, i_d - \omega\psi_q \qquad \ldots(2.7)$$

$$V_q = p\psi_q - R_a\, i_q + \omega\psi_d \qquad \ldots(2.8)$$

$$V_{fd} = p\psi_{fd} + R_{fd}\, i_{fd} \qquad \ldots(2.9)$$

$$V_{kd} = 0 = p\psi_{kd} + R_{kd}\, i_{kd} \qquad \ldots(2.10)$$

$$V_{kq} = 0 = p\psi_{kq} + R_{kq}\, i_{kq} \qquad \ldots(2.11)$$

Electrical torque is considered to be developed by the interaction of flux in one axis with the current in the other, i.e.

$$T_e = \omega_o\,(\psi_d\, i_q - \psi_q\, i_d) \qquad \ldots(2.12)$$

And finally, to complete the electrical equations for the generator the active

and reactive power are derived from summation of the quadrative components.

$$P = V_d i_d + V_q i_q \qquad ...(2.13)$$

$$Q = V_q i_d - V_d i_q \qquad ...(2.14)$$

Considering the dynamic performance of the generator, the system is in equilibrium if the input torque from the turbine equals the total electrical torque and if the latter is altered suddenly by some electrical disturbance the rotor will be subjected to an angular acceleration. Losses due to friction and windage may also need to be taken in account by the inclusion of constant and speed dependent terms respectively. The mechanical equation of motion is then:

$$\frac{2H}{\omega_o} \ddot{\delta} = (T_L - T_i - k_d\omega) - T_e \qquad ...(2.15)$$

The inertia constant H is used in preference to the moment of inertia J as it is more compatible with the per unit system. It is the specific inertia and may be regarded as moment of inertia 'referred' to rated KVA and speed so having a similar magnitude for machines of different ratings.

For the single machine studies contemplated, the generator is assumed to be connected to an infinite capacity busbar through a single transmission line. This represents all transformer, compensator and transmission line reactance and resistance between the busbar and generator terminals. The transmission line equations contain busbar voltage, resistive, reactive and transient components as follows:

$$V_d = V_b \sin\delta + R_t i_d - \chi_t \frac{\omega}{\omega_o} i_q + \frac{\chi_t}{\omega_o} p i_d \qquad ...(2.16)$$

$$V_q = V_b \cos\delta + R_t i_q + \chi_t \frac{\omega}{\omega_o} i_d + \frac{\chi_t}{\omega_o} p i_q \qquad ...(2.17)$$

Transformer magnetising currents and line charging currents have been neglected in the above as they are usually small, but if long transmission lines are studied then the capacitive charging currents must be taken into account.

2.3.2 Re-arranging the standard equations for solution

For accurate solution by computer, a set of simultaneous first order differential equations have to be extracted from the basic equations. As

there are five coils in this particular representation then it should be possible to extract a minimum of five differential equations. The five integratable variables as chosen to be ψ_{fd}, ψ_{kd}, ψ_{kq}, i_d, i_q and all other variables are eliminated. Early digital computer models[20] failed to eliminate all the unwanted variables, and to obtain unknown differentials the method of finite differences was used. This assumed a linear relationship of the variable between steps, i.e. if the values of the parameter in the n-1, and n^{th} steps are f(n-1) and f(n), then the differential is given by:

$$f'(n) = \frac{f(n) - f(n-1)}{h}$$

where h is the time between steps.

The present analysis is based upon the work of Harley and Adkins[21] who extracted a complete set of simultaneous equations. Thus the fast varying transients during a large disturbance are able to be simulated to a high degree of accuracy. However the rather limiting 'prime' and 'double prime' parameters were retained but the following synthesis is based upon Park's[12,13] parameters throughout.

The first step is to eliminate i_{fd}, i_{kd} and i_{kq} from the flux equations (2.2) to (2.6), giving expressions for ψ_d and ψ_q as:

$$\psi_d = \frac{X_1}{X_{\ell fd}} \psi_{fd} + \frac{X_1}{X_{\ell kd}} \psi_{kd} - (X_1 + X_{\ell d}) \frac{i_d}{\omega_o} \qquad \ldots(2.18)$$

$$\psi_q = \frac{X_2}{X_{\ell kq}} \psi_{kq} - (X_2 + X_{\ell q}) \frac{i_q}{\omega_o} \qquad \ldots(2.19)$$

where $X_1 = \dfrac{X_{md} \cdot X_{\ell fd} \cdot X_{\ell kd}}{X_{md}X_{\ell fd} + X_{md}X_{\ell kd} + X_{\ell fd}X_{\ell kd}}$, and $X_2 = \dfrac{X_{mq} \cdot X_{\ell kq}}{X_{mq} + X_{\ell kq}}$

As the eliminated variables will be required later they are worked out in terms of the integratable variables:

From equations (2.2) and (2.3)

$$i_{fd} = \frac{\omega_o (\psi_{fd} - \psi_d) - X_{\ell d} i_d}{X_{\ell fd}}$$

then substituting for ψ_d from (2.18)

$$\hat{i}_{fd} = \frac{\omega_o}{X_{\ell fd}} \left[\left(1 - \frac{X_1}{X_{\ell fd}}\right)\psi_{fd} - \frac{X_1}{X_{\ell kd}}\psi_{kd} + \frac{X_1}{\omega_o} i_d \right] \quad \ldots(2.20)$$

Similarly

$$i_{kd} = \frac{\omega_o}{X_{\ell kd}} \left[\left(1 - \frac{X_1}{X_{\ell kd}}\right)\psi_{kd} - \frac{X_1}{X_{\ell fd}}\psi_{fd} + \frac{X_1}{\omega_o} i_d \right] \quad \ldots(2.21)$$

$$\hat{i}_{kq} = \frac{\omega_o}{X_{\ell kq}} \left[\frac{X_2}{X_{mq}}\psi_{kq} + \frac{X_2}{\omega_o} i_q \right] \quad \ldots(2.22)$$

Substituting equations (2.20)-(2.22) in the voltage equations (2.9)-(2.11) gives the first three differential equations_

$$P\psi_{fd} = V_{fd} - \omega_o \cdot \frac{R_{fd}}{X_{\ell fd}} \left[\left(1 - \frac{X_1}{X_{\ell fd}}\right)\psi_{fd} - \frac{X_1}{X_{\ell kd}}\psi_{kd} + \frac{X_1}{\omega_o} i_d \right] \quad \ldots(2.23)$$

$$P\psi_{kd} = \omega_o \cdot \frac{R_{kd}}{X_{kd}} \left[\frac{X_1}{X_{\ell fd}}\psi_{fd} - \left(1 - \frac{X_1}{X_{\ell kd}}\right)\psi_{kd} - \frac{X_1}{\omega_o} i_d \right] \quad \ldots(2.24)$$

$$P\psi_{kq} = -\omega_o \cdot \frac{R_{kq}}{X_{\ell kq}} \left[\frac{X_2}{X_{mq}}\psi_{kq} + \frac{X_2}{\omega_o} i_q \right] \quad \ldots(2.25)$$

To obtain expressions for pi_d and pi_q, equations (2.7) and (2.16), and (2.8) and (2.17) are equated to eliminate V_d and V_q respectively giving:

$$\frac{X_t}{\omega_o} \cdot pi_d = p\psi_d - (R_a + R_t)\, i_d - \omega\psi_q - V_b \sin\delta + X_t \frac{\omega}{\omega_o} i_q \quad \ldots(2.26)$$

$$\frac{X_t}{\omega_o} \cdot pi_q = p\psi_q - (R_a + R_t)\, i_q + \omega\psi_d - V_b \cos\delta - X_t \frac{\omega}{\omega_o} i_d \quad \ldots(2.27)$$

However the unwanted terms of $p\psi_d$ and $p\psi_q$ still remain and expressions for these are obtained by differentiating equations (2.18) and (2.19) to give

$$p\psi_d = \frac{X_1}{X_{\ell fd}} \cdot p\psi_{fd} + \frac{X_1}{X_{\ell kd}} \cdot p\psi_{kd} - \frac{(X_1 + X_{\ell d})}{\omega_o} pi_d \quad \ldots(2.28)$$

$$p\psi_q = \frac{X_2}{X_{\ell kq}} p\psi_{kq} - \frac{(X_2 + X_{\ell q})}{\omega_o} pi_q \quad \ldots(2.29)$$

equations for $p\psi_{fd}$, $p\psi_{kd}$, $p\psi_{kq}$ are substituted into (2.28) and (2.29) from (2.23)-(2.25) giving expressions for $p\psi_d$ and $p\psi_q$ containing only the desired integratable variables. These can then be substituted in (2.26) and (2.27) to give the final form

$$pi_d = A\,V_b \sin\delta - B\,V_{fd} + Ci_d - D\,\omega i_q - E\,\psi_{fd} - F\,\psi_{kd} + G\,\omega\psi_{kq} \quad \ldots(2.30)$$

$$pi_q = -I\,V_b \cos\delta - J\,i_q - K\omega i_d - L\,\psi_{kq} + M\,\omega\psi_{fd} + N\,\omega\psi_{kd} \quad \ldots(2.31)$$

The constants A-G and I-N are given in the Appendix 11.1. This completes the differential equations for the electrical quantities of the generator and finally the mechanical equations of motionhave to be written in a similar form to make the equations truly simultaneous (a procedure that was not performed by Harley and Adkins[21]). The electrical torque is first obtained in terms of the integratable variables by substituting equations (2.18) and (2.19) in the torque equation (2.12). This is then substituted in the mechanical equation which is written as two differential equations:

$$p\omega = \frac{\omega_o}{2H}\left[T_L - T_i - \omega_o\left(\frac{X_1}{X_{\ell fd}}\psi_{fd} + \frac{X_1}{X_{\ell kd}}\psi_{kd} - (X_1+X_{\ell d})\frac{i_d}{\omega_o}\right) i_q - \omega_o\left(\frac{X_2}{X_{\ell kq}}\psi_{kq} - (X_2+X_{\ell q})\frac{i_q}{\omega_o}\right) i_d - k_d\omega\right] \quad \ldots(2.32)$$

$$p\delta = \omega \quad \ldots(2.33)$$

A complete set of seven simultaneous differential equations for the generator have now been formed, i.e. (2.23)-(2.25) and (2.30)-(2.33). These are integrated over the step length period to determine updated values of ψ_{fd}, ψ_{kd}, ψ_{kq}, i_d, i_q, ω and δ. From these parameters all the other generator quantities can be calculated, excepting the field voltage V_{fd} and mechanical torque T_L, which are calculated separately from the AVR and governor equations respectively as these are regarded as the controllable quantities.

The remaining fluxes ψ_d and ψ_q are calculated first from equations (2.18) and (2.19) and the stator transients $p\psi_d$ and $p\psi_q$ from equations (2.28) and (2.29). This enables the direct and quadrature axis armature voltages V_d and V_q to be obtained using equations (2.7) and (2.8). From these the generator terminal voltage is calculated as:

$$E_{tm} = \sqrt{V_d^2 + V_q^2} \quad \ldots(2.34)$$

This is required as an input for the AVR, and the speed ω, which is calculated directly from the differential equations, is required for the governor.

2.3.3 Setting up of initial conditions

The initial conditions are calculated directly from the vector diagram of Fig.2.3 in which the resistances have been omitted for clarity. They are, however, included in the computer programme calculations otherwise a transient is produced when the differential equations are processed.

The equations are stated directly, all the parameters being covered in the Nomenclature section.

$$E_f' = \sqrt{\left[I_a\chi_q \sin (90^o-\phi)\right]^2 + \left[V_T + I_a\chi_q \cos (90^o-\phi)\right]^2} ,$$

$$\delta' = \arctan \left[\frac{I_a\chi_q \sin (90^o-\phi)}{V_T+I_a\chi_q \cos (90^o-\phi)}\right] ,$$

$$E_f = E_f' + I_a (\chi_d-\chi_q) \cos (90^o-\phi-\delta') ,$$

$$V_b = \sqrt{\left[I_a\chi_t \sin (90^o-\phi)\right]^2 + \left[V_T- I_a\chi_t \cos (90^o-\phi)\right]^2} ,$$

$$\sigma = \arctan \left[\frac{I_a\chi_t \sin (90^o-\phi)}{V_T-I_a\chi_t \cos (90^o-\phi)}\right]$$

$$\delta = \delta' + \sigma$$

Also,

$$I_d = I_a \sin (\delta' +\phi) ,$$

$$I_q = I_a \cos (\delta' +\phi) ,$$

$$I_{fd} = \frac{E_f}{\chi_{md}} ,$$

$$V_{fd} = I_{fd} R_{fd}$$

and $$E_{fd} = V_{fd} E_{fdo} \text{ volts.}$$

If saturation is included (see Section 2.5) then the calculated values of

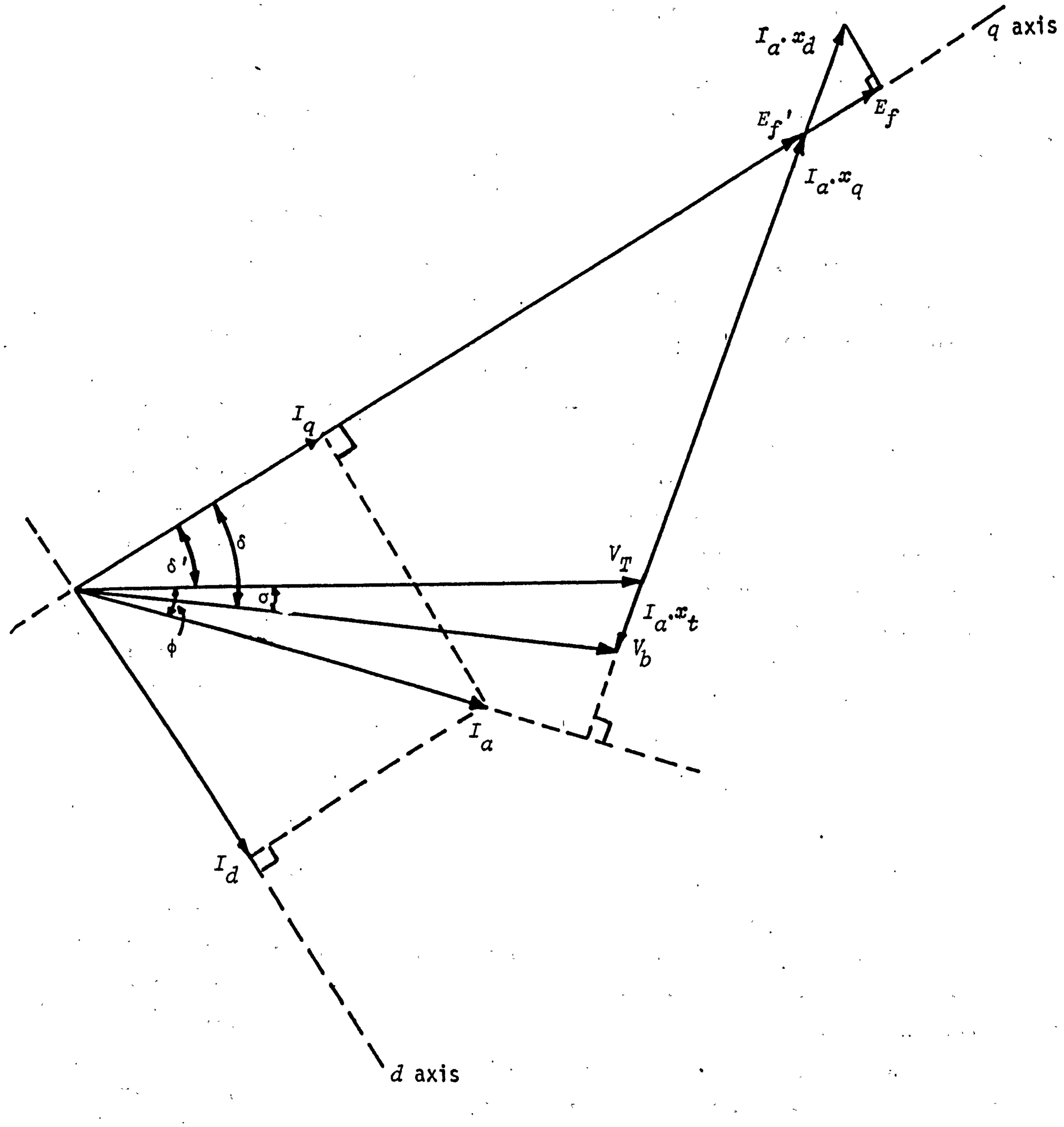

STEADY STATE VECTOR DIAGRAM WITH RESISTANCES NEGLECTED

FIG. 2·3

field and armature currents (initial damper currents = 0) are used to obtain temporary saturated values of χ_{md} and χ_{mq}. These are substituted in place of the unsaturated reactances in the above equations and new values of the 'saturated' currents are calculated. The process is repeated continuously in an iterative cycle until successive calculations yield answers which differ by less than a predetermined margin giving the true saturated conditions.

Data input required forthe initial conditions is basically line voltage, V_T, armature current I_a, and phase angle ϕ in addition to the machine and system reactances and resistances. Of these only the terminal voltage is usually specified directly, the other two quantities being obtained from the electrical load P_e and power factor cos ϕ. In simulating site test conditions it is often desired to set the machine at some desired rotor angle but this is not a normal data input parameter for the equations. To overcome this ,trial values of the normal input quantities are inserted and the calculated rotor angle compared with the desired value. If there is an error then one of the input parameters (usually power factor) is altered slightly and the process repeated until the error is minimised to within acceptable limits. If both saturation and accurate rotor angle setting are required then two nested iteration loops are performed with the saturation loop innermost.

Finally, the initial values of flux are calculated from equation (2.2)-(2.6) and all the integrator inputs set accordingly.

2.3.4 Simple synchronous machine models

Depending upon the requirements of a particular application, machine models of widely differing complexities may be chosen. Economy in computing time can be obtained by selecting the simplest practicable model of the generator. For multi machine studies such economy becomes essential and great engineering skill is needed to choose the minimum complexity. However, as the standard model previously described was selected for all the computations for this thesis, other models are only described briefly.

Table 1 shows the range of the most important models available and they will be described in turn.

The simplest of all models is known as the 'constant voltage behind transient reactance' or 'classical' representation. As it requires the solution of only two differential equations the calculation time is very rapid and for this reason the model is often used for multimachine studies

involving a very large number of generators. Prediction of the first swing of rotor angle is fairly accurate but as no damping is taken into account, it is unsuitable for multi-swing stability studies where dynamic interaction between generators may not be neglected[22].

The mathematical principle relies upon the fact that the flux linking an inductive circuit cannot change rapidly even if transient changes occur in mutually coupled circuits, i.e. it is a 'constant flux linkage' method. Hence a constant voltage E' developed by the armature flux under transient conditions can be defined as in the vector diagram of Fig.2.4 If subtransient parameters are known then the voltage behind the subtransient reactance E'' could be used.

To simplify the method as much as possible, the following assumptions are usually made:

(a) No saliency, i.e. $\chi_d = \chi_q$.

(b) No transient saliency, i.e. $\chi'_q = \chi'_d$.

(c) Speed effects can be neglected.

(d) Stator and field transients can be neglected.

(e) Armature resistance is negligible.

(f) No electrical damping is included.

With these assumptions the vector E' lies on the quadrature axis and can be calculated initially from:

$$|E'| = |E_{tm} + jX'_d I| \qquad \ldots(2.35)$$

The simple system diagram of Fig.2.5 is used for single machine studies where it is assumed that the fault is applied to the busbar. The fault current is then calculated simply as

$$I_L = \frac{E'}{R_t + j(X'_d + X_t)} \qquad \ldots(2.36)$$

With assumptions (c),(d) and (e) above,the Park's voltage equations become:

$$V'_d = -\psi_q = 0 \qquad \ldots(2.37)$$

$$V'_q = \psi_d = E' \qquad \ldots(2.38)$$

The torque equation is therefore

$$T_e = \omega_o (\psi_d i_q - \psi_q i_d) = \omega_o E' i_q \qquad \ldots(2.39)$$

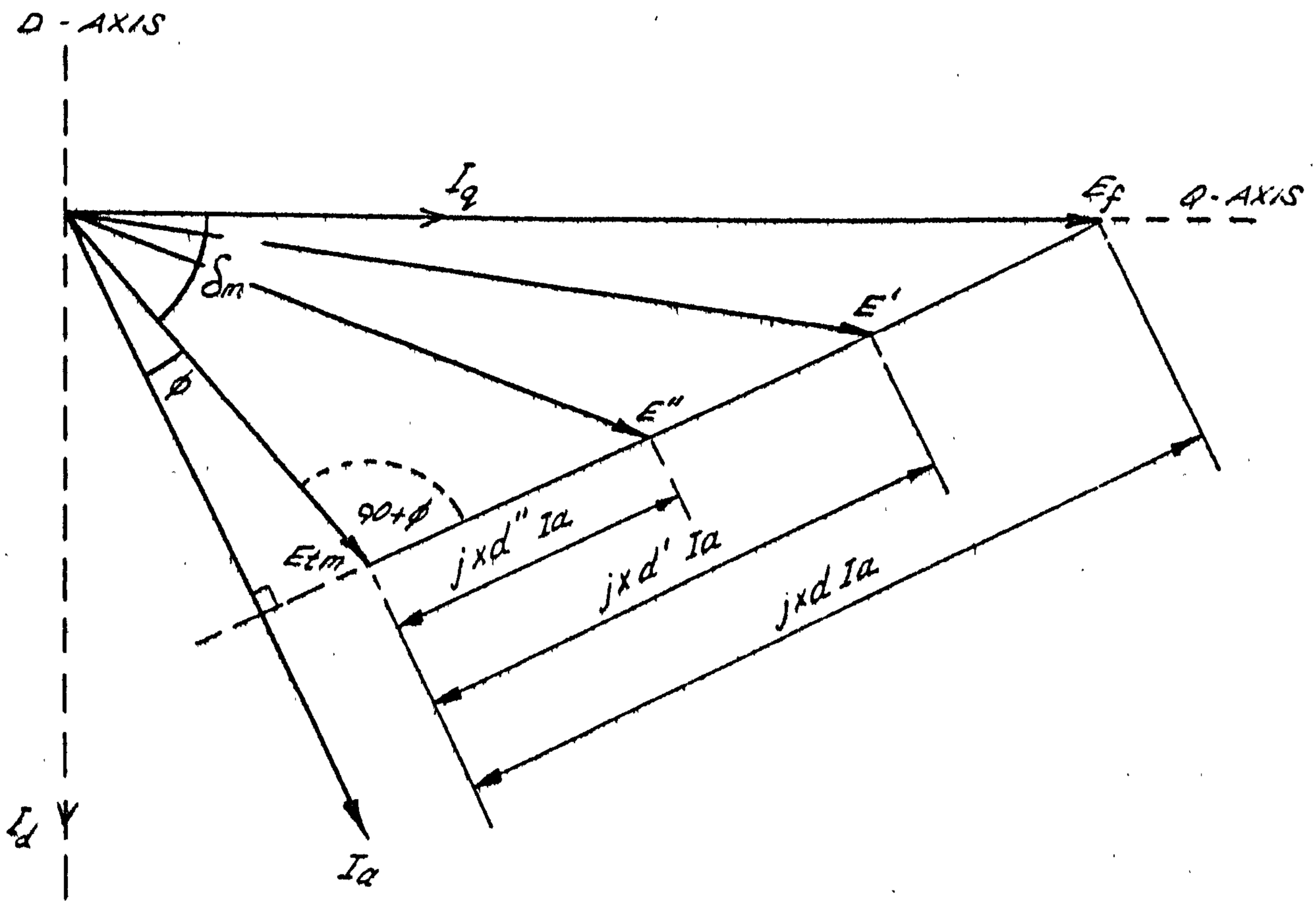

VECTOR DIAGRAM FOR SIMPLE MODEL

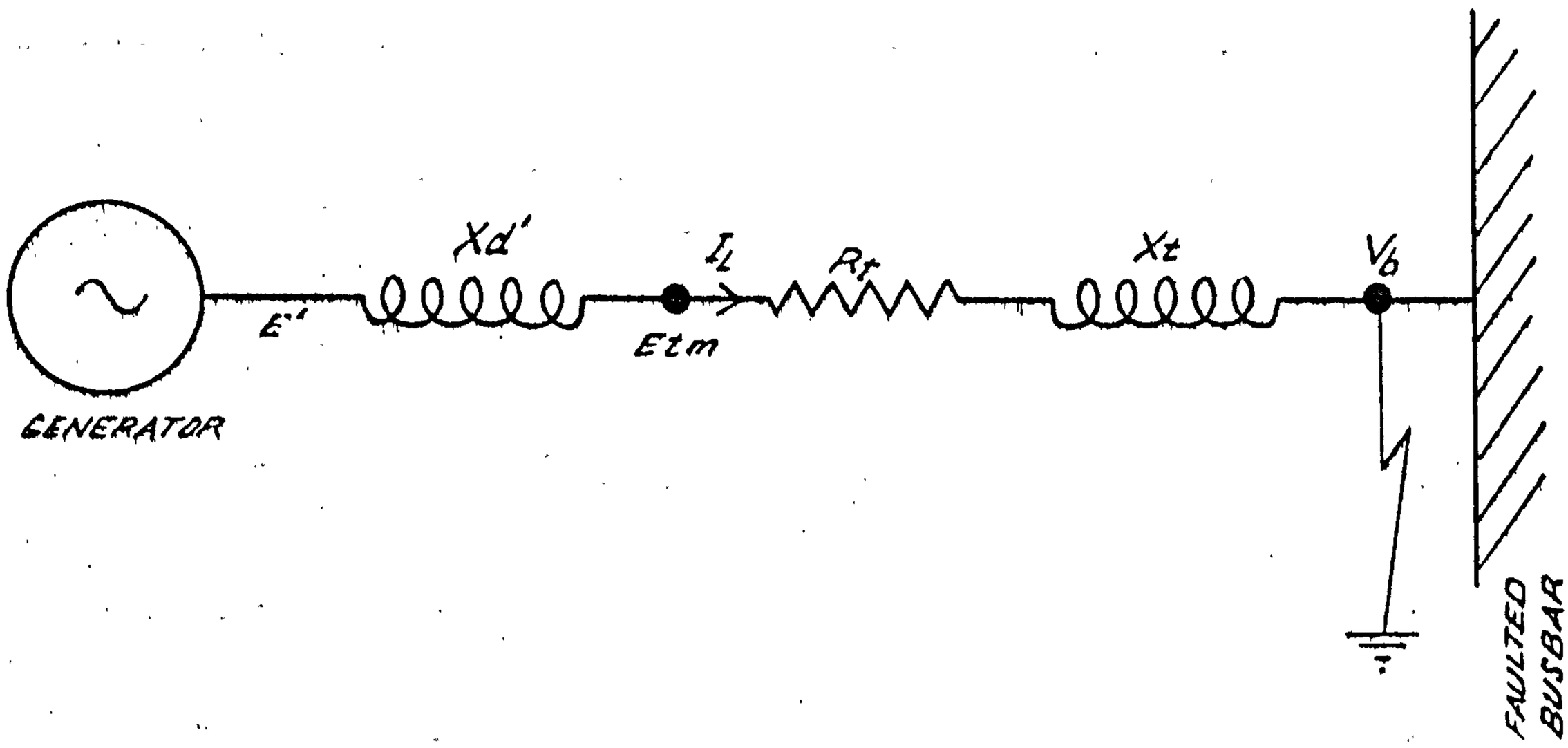

SYSTEM CONFIGURATION FOR SIMPLE MODEL

FIG. 25

This can then be substituted in the same mechanical equation of motion as used for the standard model (2.15) to obtain the rotor angle swing curve.

Model 2 in Table 1 includes the effects of field transients and is the simplest model based on Park's analysis. The following simplifying assumptions apply:

(a) Speed effects can be neglected.

(b) Stator transients can be neglected.

(c) Damping is represented by an extra speed dependent term in the dynamic equation.

(d) Armature resistance is negligible.

The full Park's equations (2.2)-(2.11) now reduce to the following:

$$\psi_{fd} = \frac{1}{\omega_o}\left[\chi_{fd}\, i_{fd} - \chi_{md}\, i_d\right] \qquad \ldots(2.40)$$

$$\psi_d = \frac{1}{\omega_o}\left[\chi_{md}\, i_{fd} - \chi_d\, i_d\right] \qquad \ldots(2.41)$$

$$\psi_q = \frac{1}{\omega_o}\left[\quad - \chi_q\, i_q\right] \qquad \ldots(2.42)$$

$$V_{fd} = p\,\psi_{fd} + R_{fd}\, i_{fd} \qquad \ldots(2.43)$$

$$V_d = -R_a\, i_d - \psi_q \qquad \ldots(2.44)$$

$$V_q = -R_a\, i_q + \psi_d \qquad \ldots(2.45)$$

Due to assumptions (a) and (b) the instantaneous currents can be calculated from the vector diagram (Fig.2.6) as:

$$i_d = \frac{\chi_{md}\, i_{fd} - V_b \cos\delta}{(\chi_d + \chi_t)} \qquad \ldots(2.46)$$

$$i_q = \frac{V_b \sin\delta}{(\chi_q + \chi_t)} \qquad \ldots(2.47)$$

Substituting (2.46) in (2.40) an expression for field current in terms of field flux is arrived at:

$$i_{fd} = \frac{(\chi_d + \chi_t)\,\omega_o\,\psi_{fd} - \chi_{md}.V_b.\cos\delta}{(\chi_d + \chi_t)\,\chi_{fd} - \chi_{md}^2} \qquad \ldots(2.48)$$

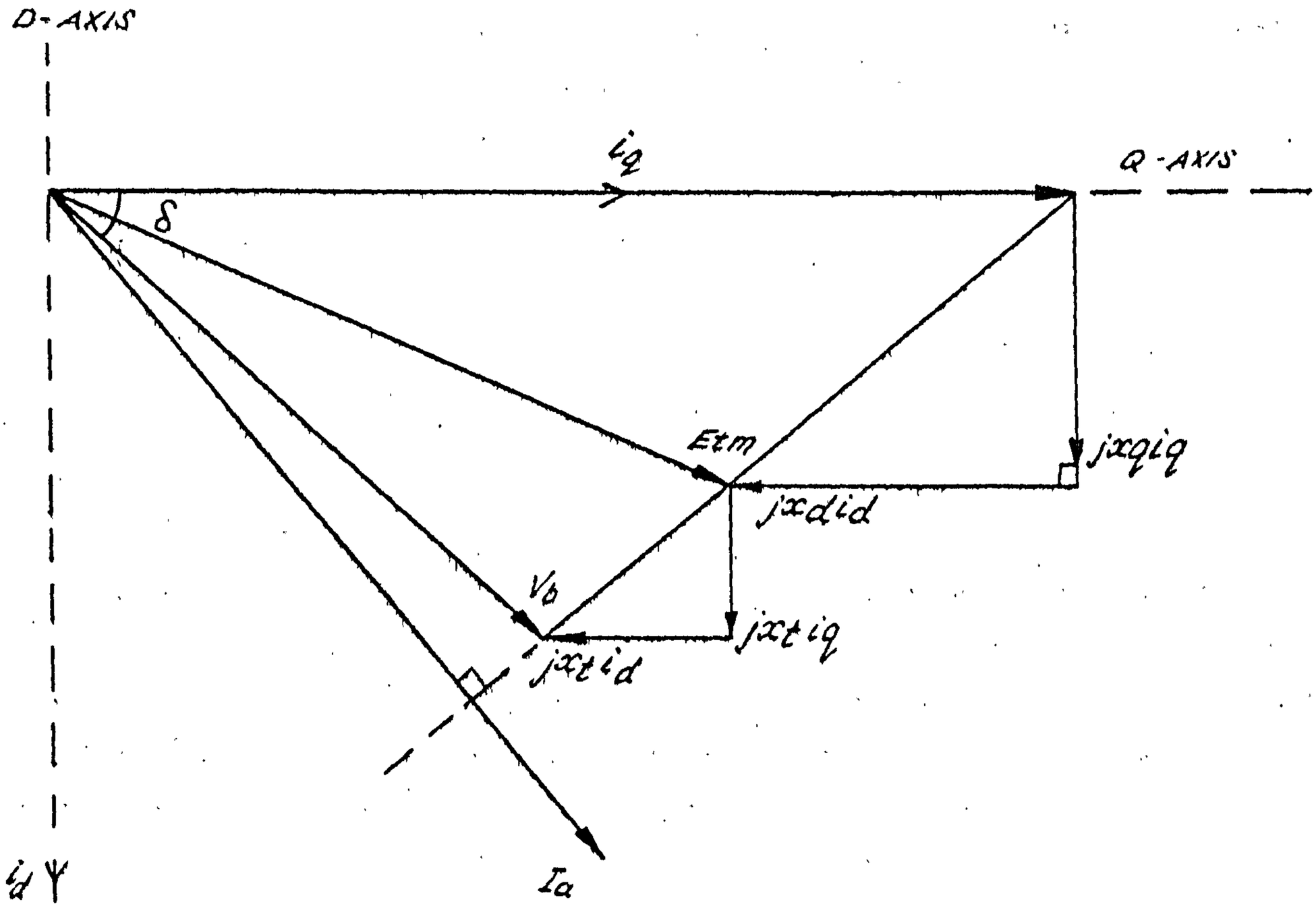

VECTOR DIAGRAM FOR 3rd ORDER MODEL

FIG 2.6

This is then substituted in equation (2.43) to give a homogenous differential equation suitable for solution by integration as explained earlier.

$$p\psi_{fd} = v_{fd} - R_{fd}\left[\frac{(X_d + X_t)\,\omega_o\,\psi_{fd} - X_{md}\,V_b\cos\delta}{(X_d + X_t)\,X_{fd} - X_{md}^2}\right] \qquad \ldots(2.49)$$

The new values of ψ_{fd} obtained every step, are used to calculate i_{fd} from equation (2.48). The sequence of calculations is then: i_d and i_q from equations (2.46) and (2.47), ψ_d and ψ_q from equations (2.41) and (2.42), and finally, torque T_e from the standard torque equation (2.12). The mechanical equation of motion contains an electrical damping term which is proportional to speed as well as the mechanical damping term,

$$\frac{2H}{\omega_o}\ddot{\delta} - K_{dm}\,\omega = (T_L - T_i - k_d\,\omega) - T_e\ ,$$

and the two mechanical differential equations are obtained as before:

$$p\omega = T_L - T_i - T_e + (K_{dm} - k_d)\,\omega \qquad \ldots(2.50)$$

$$p\delta = \omega\ . \qquad \ldots(2.51)$$

This method of damping representation is questionable as it is extremely difficult to obtain a value for the damping constant K_{dm} from design or test information, and also the full Park's equations invalidate the assumption that damping is proportional to speed. The usual procedure for obtaining K_{dm} is by performing optimisation runs simulating known site results, but it has been found that the value obtained does not hold for other tests performed under different conditions.

Model 3 contains all the assumptions of Model 2 except that damping is represented by a single coil on the quadrature axis. This is feasible since it is known that quadrature axis damping parameters have the most effect under transient conditions and this is especially true for turbogenerators with damper bars in the top of the field winding slots.

The quadrature axis equations of Model 2 are developed to include the damping terms while the direct axis equations (2.40), (2.41) and (2.43) remains unchanged. The new equations are:

$$\psi_q = \frac{1}{\omega_o}\left[X_{mq}\,i_{kq} - X_q\,i_q\right] \qquad \ldots(2.52)$$

$$\psi_{kq} = \frac{1}{\omega_o}\left[X_{\ell kq}\,i_{kq} - X_{mq}\,i_q\right] \qquad \ldots(2.53)$$

$$V_{kq} = 0 = p\,\psi_{kq} + R_{kq}\,i_{kq} \qquad \ldots(2.54)$$

Substituting (2.47) in (2.53) gives the damper current:

$$i_{kq} = \frac{\omega_o\,\psi_{kq} + \dfrac{X_{mq}}{(X_q+X_t)}\,V_b \sin\delta}{X_{\ell kq}} \qquad \ldots(2.55)$$

This is then substituted in the voltage equation (2.54) to give the new differential equation:

$$p\psi_{kq} = -\frac{R_{kq}}{X_{\ell kq}}\left[\omega_o\,\psi_{kq} + \frac{X_{mq}}{(X_q+X_t)} \cdot V_b \sin\delta\right] \qquad \ldots(2.56)$$

2.3.5 Complex synchronous machine models

The rotor of a turbogenerator is usually machined out of a solid steel forging which then provides an infinite number of damping current paths according to the depth of flux penetration and changing flux distribution under transient conditions Hence the correct two-axis representation of the damping circuits would be an infinite number of damper coils on the d and q axes, for which it is impossible to give parameter values.

An attempt at solving this dilemma was proposed by Jackson and Winchester[23] who developed an equivalent circuit which simulated each separate physical flux path in the machine by an individual coil. However very little information was provided for calculating or measuring the parameters of the coils, so that their contribution remains an academic reference.

To reduce this approach to more practical proportions, a useful model is produced by assuming one damper coil on the direct axis and two on the quadrature axis. The parameters of the first quadrature axis coil are calculated to represent damping during the high frequency conditions during a fault (usually rated frequency) and the second represents damping when the machine is swinging against the busbar after the fault has been removed. During the latter condition the rotor experiences a slowly oscillating flux wave of frequency usually around 1 Hz which penetrates past the rotor teeth deep into the main body of the rotor. Hence there is an abrupt change in reluctance and it follows that the use of two quadrature axis damper coils is feasible.

The equations for the direct axis are identical to those of the standard model but one more differential equation is required to take into account the extra q-axis damper coil. As there are now two rotor coils on each axis the d and q-axis equations are of a similar form, the new quadrature axis equations are given overleaf.

$$\psi_q = \frac{1}{\omega_o}\left[\chi_{mq}\ i_{kq1} + \chi_{mq}\ i_{kq2} - \chi_q\ i_q\right] \qquad \ldots(2.57)$$

$$\psi_{kq1} = \frac{1}{\omega_o}\left[\chi_{kq1}\ i_{kq1} + \chi_{mq}\ i_{kq2} - \chi_q\ i_q\right] \qquad \ldots(2.58)$$

$$\psi_{kq2} = \frac{1}{\omega_o}\left[\chi_{mq}\ i_{kq1} + \chi_{kq2}\ i_{kq2} - \chi_q\ i_q\right] \qquad \ldots(2.59)$$

$$V_{kq1} = 0 = P\ \psi_{kq1} + R_{kq1}\ i_{kq1} \qquad \ldots(2.60)$$

$$V_{kq2} = 0 = P\ \psi_{kq2} + R_{kq2}\ i_{kq2} \qquad \ldots(2.61)$$

These are rearranged as before to give the new differential equations:

$$p\psi_{kq1} = \omega_o \frac{R_{kq1}}{\chi_{\ell kq1}}\left[\frac{X_3}{\chi_{\ell kq2}}\psi_{kq2} - \left(1 - \frac{X_3}{\chi_{\ell kq1}}\right)\psi_{kq1} - \frac{X_3}{\omega_o} i_q\right] \qquad \ldots(2.62)$$

$$p\psi_{kq2} = \omega_o \frac{R_{kq2}}{\chi_{\ell kq2}}\left[\frac{X_3}{\chi_{\ell kq1}}\ \psi_{kq1} - \left(1 - \frac{X_3}{\chi_{\ell kq2}}\right)\psi_{kq2} - \frac{X_3}{\omega_o} i_q\right] \qquad \ldots(2.63)$$

The above representation is equivalent to Model 6 in Table 1.

The ultimate representation (Model 7 in Table 1) is an attempt to produce a practical model which allows for a more accurate simulation of solid rotor damping effects. Instead of having an infinite number of damper coils each with fixed resistance and reactance, only a single coil is assumed on each axis with an infinite number of parameters depending upon the frequency of the alternating incident flux waves ψ_{kd} and ψ_{kq}. It is feasible that the relationships between the damping parameters χ_{kd}, χ_{kq}, R_{kd}, R_{kq} and frequency $(\omega - \omega_o)$ can be obtained by special test procedures[19], these could be stored on the computer as polynomials enabling the exact reactances and resistances to be read for any value of instantaneous slip frequency.

2.4 Calculation of base values

The parameters used in the preceding equations are expressed in the widely used 'per unit'[16,17] form. For the calculation of these parameters from absolute quantities certain base values have to be defined. These are usually taken

as the rated quantities of the machine but certain ambiguity can arise over the rotor base values. One definition of the base field voltage is "that which is required to produce one per unit armature voltage on open circuit at rated speed". This is anomalous as the value will vary depending upon the rotor temperature and it is more correct in the first instance to define a base field current as this quantity induces the armature voltage. In order to do this the following definitions are made:

(a) The base armature current and voltage used in determining the base field values are taken as the maximum instantaneous values of rated phase current and phase voltage respectively, i.e.

I_{ao} is the peak rated phase current,

E_{ao} is the peak rated phase voltage

and VA_o is $\frac{3}{2}.I_{ao}.E_{ao}$

(b) The volt-ampere base of the field and all other rotor circuits must be equal to the generator stator volt-ampere base. This condition is essential to give reciprocal per unit mutual inductances between rotor and stator, i.e.

$$M_{fd} = M_{df} = M_{kd} = M_{dk} = L_{md}$$

(c) The base field current is that which will induce in each stator phase, a voltage equal to $\omega_o L_{md} I_{ao}$ with the generator on open circuit.

Using the above definition the field base quantities are calculated by the following procedure

$$L_{ao} = \frac{E_{ao}}{I_{ao}} \div \frac{1}{\omega_o} \text{ Henrys} \qquad \ldots(2.64)$$

From the open circuit curve the field current I_{fa} amps, required to give the rated terminal voltage on the air gap line is determined. Then, since $E_{ao} = \omega_o L_{afd}.I_{fa}$ volts,

$$L_{afd} = \frac{E_{ao}}{\omega_o I_{fa}} \text{ Henrys} \qquad \ldots(2.65)$$

Now, $\chi_{md} = L_{md}$, per unit, therefore

$$L_{md} = \chi_{md} L_{ao} \text{ Henrys} \qquad \ldots(2.66)$$

From definition (c)

$$\omega_o L_{afd} I_{fdo} = \omega_o L_{md} I_{ao}$$

therefore,

$$I_{fdo} = \frac{L_{md} I_{ao}}{L_{afd}} \text{ amps} \qquad \ldots(2.67)$$

Also from definition (b)

$$E_{fdo} I_{fdo} = VA_o$$

therefore

$$E_{fdo} = \frac{VA_o}{I_{fdo}} \text{ volts} \qquad \ldots(2.68)$$

Using this method for calculating the field base values gives a full load field current in per unit of around unity. However due to the condition that the volt ampere bases of field and stator are the same, the base field voltage is extremely high, rendering a very small value of field voltage E_{fd} in per unit. This conflicts with the basic purpose of the per unit system and it is often most convenient to use another per unit field voltage V_{fd} for comparison purposes which has been referred through the mutual reactance to the stator. It is defined from:

$$i_{fd_{pu}} = \frac{E_{fd}}{R_{fd}}\bigg|_{rotor} = \frac{V_{fd}}{\chi_{md}}\bigg|_{stator}$$

i.e. $$V_{fd} = E_{fd} * \frac{\chi_{md}}{R_{fd}} \qquad \ldots(2.69)$$

2.5 Representation of magnetic saturation

All the machine inductances are interlinked by ferromagnetic circuits but as the leakage flux paths are predominately in air it is assumed, for the mathematical representation, that only mutual inductances are affected by saturation. However recent evidence suggests that certain anomolies in representing system faults may be attributed to neglecting the saturation of leakage inductances and this is an important area for further investigation.

Saturation depends upon the resultant air gap flux and in order to calculate this under all conditions it is assumed that the load saturation curve is of the same shape as the open circuit curve as used in the case of zero power factor by Potier.

The direct and quadrature axis components of the resultant unsaturated air gap flux are given by:

$$\psi_{d\ unsat.} = \chi_{md\ unsat.}\ (i_{fd} + ik_{d} - i_{d})$$

and $$\psi_{q\ unsat.} = \chi_{md\ unsat.}\ (i_{kq} - i_{q})$$

The total unsaturated flux is

$$\psi_{T\ unsat.} = (\psi_{d}^{2}\ _{unsat.} + \psi_{q}^{2}\ _{unsat.})^{\frac{1}{2}}$$

$$\therefore \quad \psi_{T\ unsat.} = \left[\chi_{md}^{2}\ _{unsat.}\ (i_{fd}+i_{kd}-i_{d})^{2} + \chi_{mq}^{2}\ _{unsat.}\ (i_{kq}-i_{q})^{2}\right]^{\frac{1}{2}}$$

If the ratio $\frac{\chi_{mq\ unsat.}}{\chi_{md\ unsat.}} = A$, then an equivalent magnetising current, i_{eq}, acting through $\chi_{md\ unsat}$, necessary to produce $\psi_{T\ unsat}$, can be defined as

$$i_{eq} = \left[(i_{fd} + i_{kd} - i_{d})^{2} + A^{2}\ (i_{kq} - i_{q})^{2}\right]^{\frac{1}{2}} \qquad ...(2.70)$$

Saturation is represented by a factor, K, where

$$\frac{\psi_{T\ sat}}{\psi_{T\ unsat}} = \frac{\chi_{md\ sat}}{\chi_{md\ unsat}} = \frac{\chi_{mq\ sat}}{\chi_{mq\ unsat}} = K\ .$$

The open circuit curve is used to determine this factor for any i_{eq} giving

$$K = \frac{f(i_{eq})}{m i_{eq}} \qquad ...(2.71)$$

where $f(i_{eq})$ is a polynomial expression representing the saturation curve, in which the abscissa is the unit field current and the ordinate is in arbitrary units,

and m is the slopeof the air gap line drawn to the saturation curve with the same units as $f(i_{eq})$.

The slope m is easily calculated from the open circuit characteristic and fed directly as data into the digital computer programme. The function $f(i_{eq})$ can be obtained using a curve fitting programme or subroutine but as this can unnecessarily waste computer time, the following simpler approach is recommended. The open circuit curve is supplied as data input in the form of a series of x and y coordinates. A straight line

approximation is assumed between adjacent points which gives a reasonable enough accuracy when weighed against the initial assumptions with minimum computer time wastage.

Saturation can now be represented by modifying the mutual inductances χ_{md} and χ_{mq} after each integration step, by calculating i_{eq} from equation (2.70) and K from equation (2.71).

In the above calculations it has been assumed that the quadrature axis saturates by the same amount as the direct axis. This may appear to be questionable but the assumption seems reasonable as very accurate simulation of steady state test conditions which depend mainly upon χ_q have been obtained. However, the errors caused by the assumptions in simulating saturation under transient conditions are difficult to assess and further work in improving saturation representation when more accurate tested information is available is clearly needed.

2.6 Performance of digital computer programme for solution of standard mathematical model

2.6.1 Accuracy and efficiency of integration technique

The digital computer programme (see Appendix 11.2) was originally developed using a Kutta-Merson variable step length integration routine. When development was completed a study was performed using two alternative integration methods namely Runge-Kutta and Hammings fourth order predictor-corrector method. A standard initial step length of 1 millisecond was used but the Hammings and Kutta-Merson methods automatically reduced this to a much lower value during conditions of fast transients to achieve the desired accuracy, whereas the Runge-Kutta used a fixed value throughout. The results using this fixed step length method were considerably devious from those obtained using the variable step length methods but good agreement was obtained if the step length was reduced to .0001 seconds. However the Runge-Kutta method was very inefficient in computation time at this fixed value of step length when compared with the other two methods which adjusted to 0.001 seconds to achieve the same accuracy. In addition the Hammings predictor corrector method was approximately 30% faster than the Kutta-Merson.

Increasing the step length induced mathematical instability using all three methods giving unintelligible results. This occurred after a step length of around 12 milliseconds with the Runge-Kutta and Kutta-Merson methods and 25 milliseconds with the Hammings predictor-corrector method.

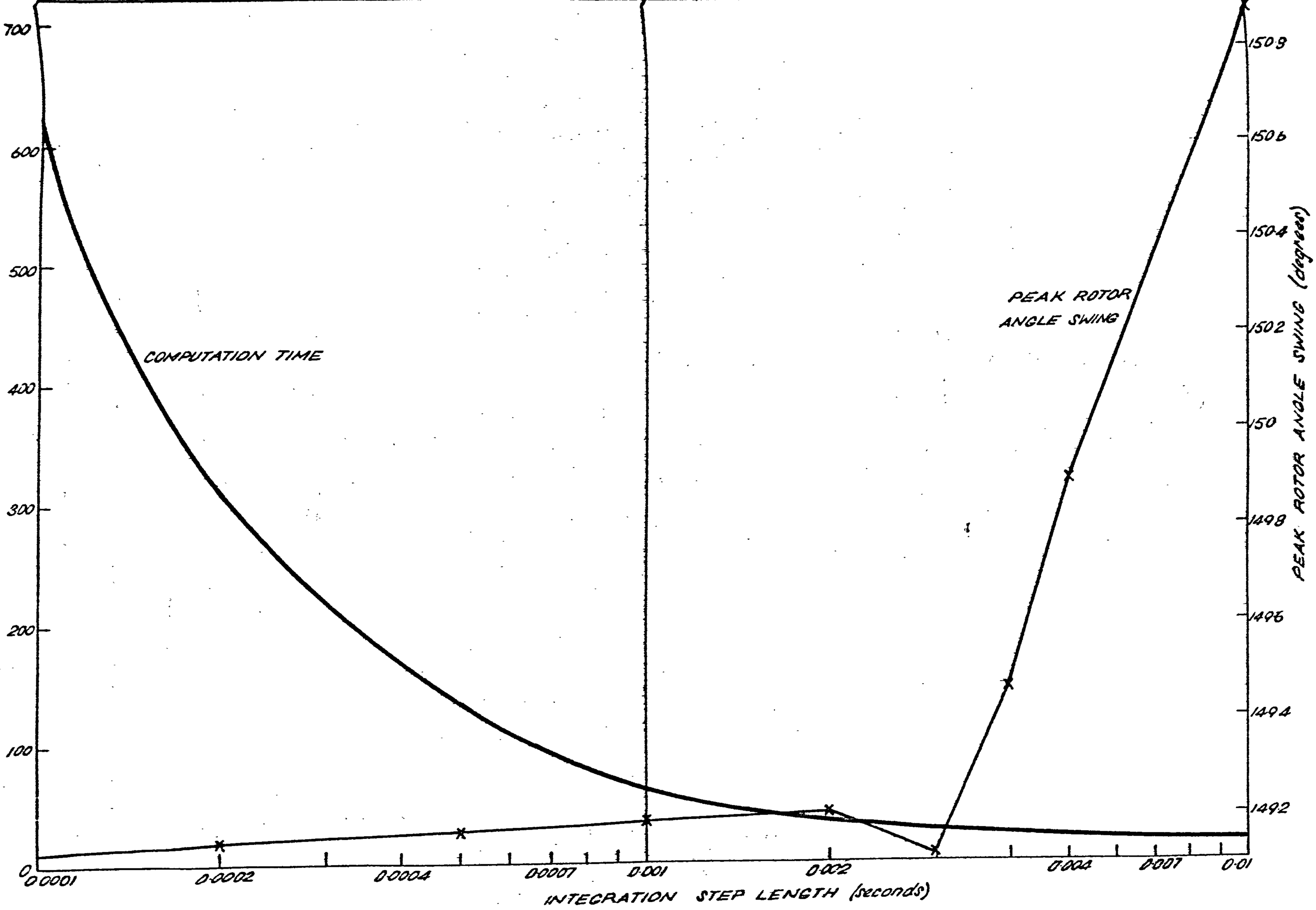

COMPUTER PROGRAMME PERFORMANCE WITH DIFFERENT STEP LENGTHS

FIG 2.7

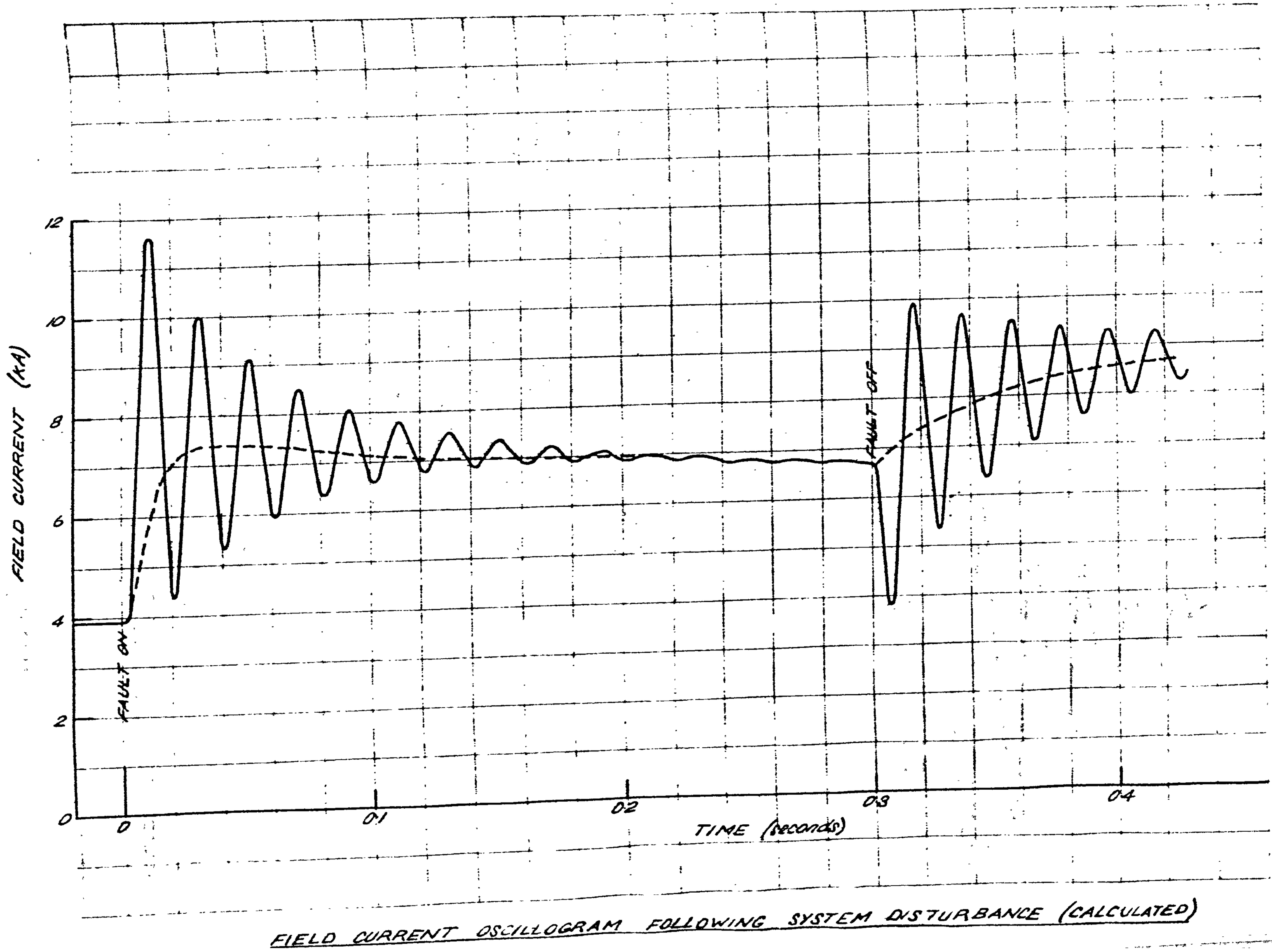

FIELD CURRENT OSCILLOGRAM FOLLOWING SYSTEM DISTURBANCE (CALCULATED)

FIG 2.8

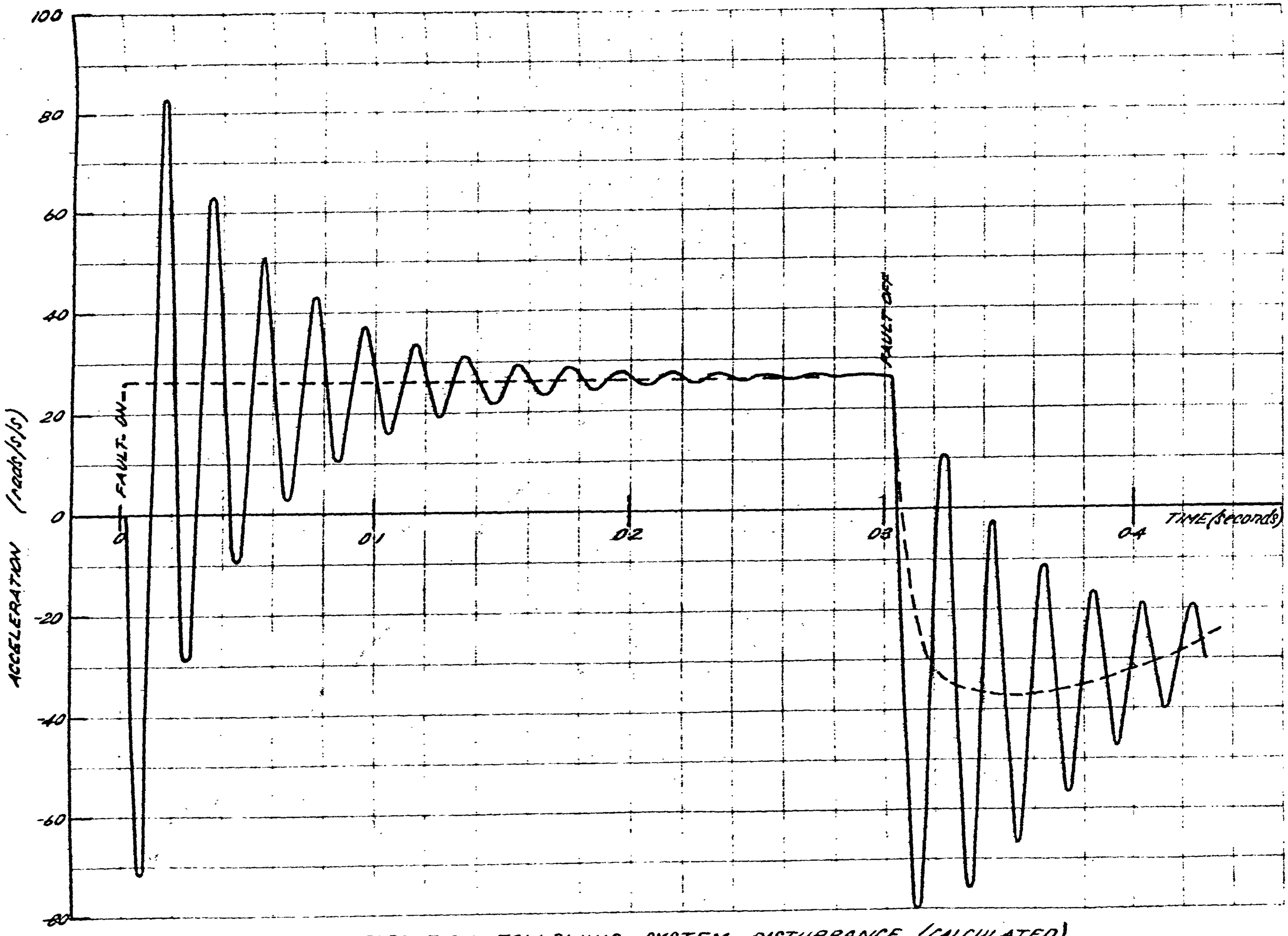

SHAFT ACCELERATION FOLLOWING SYSTEM DISTURBANCE (CALCULATED)

FIG 27

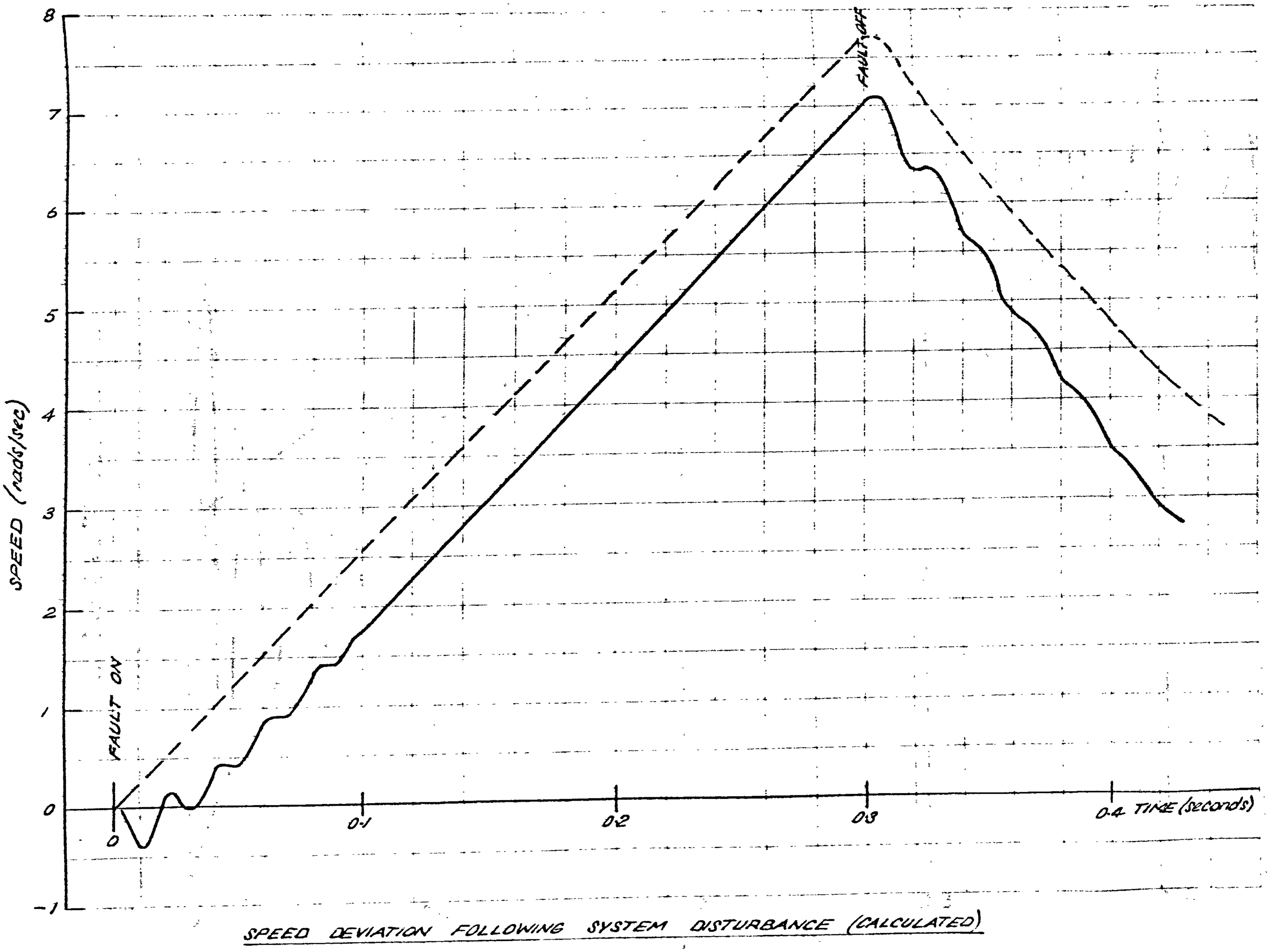

SPEED DEVIATION FOLLOWING SYSTEM DISTURBANCE (CALCULATED)

FIG 2.16

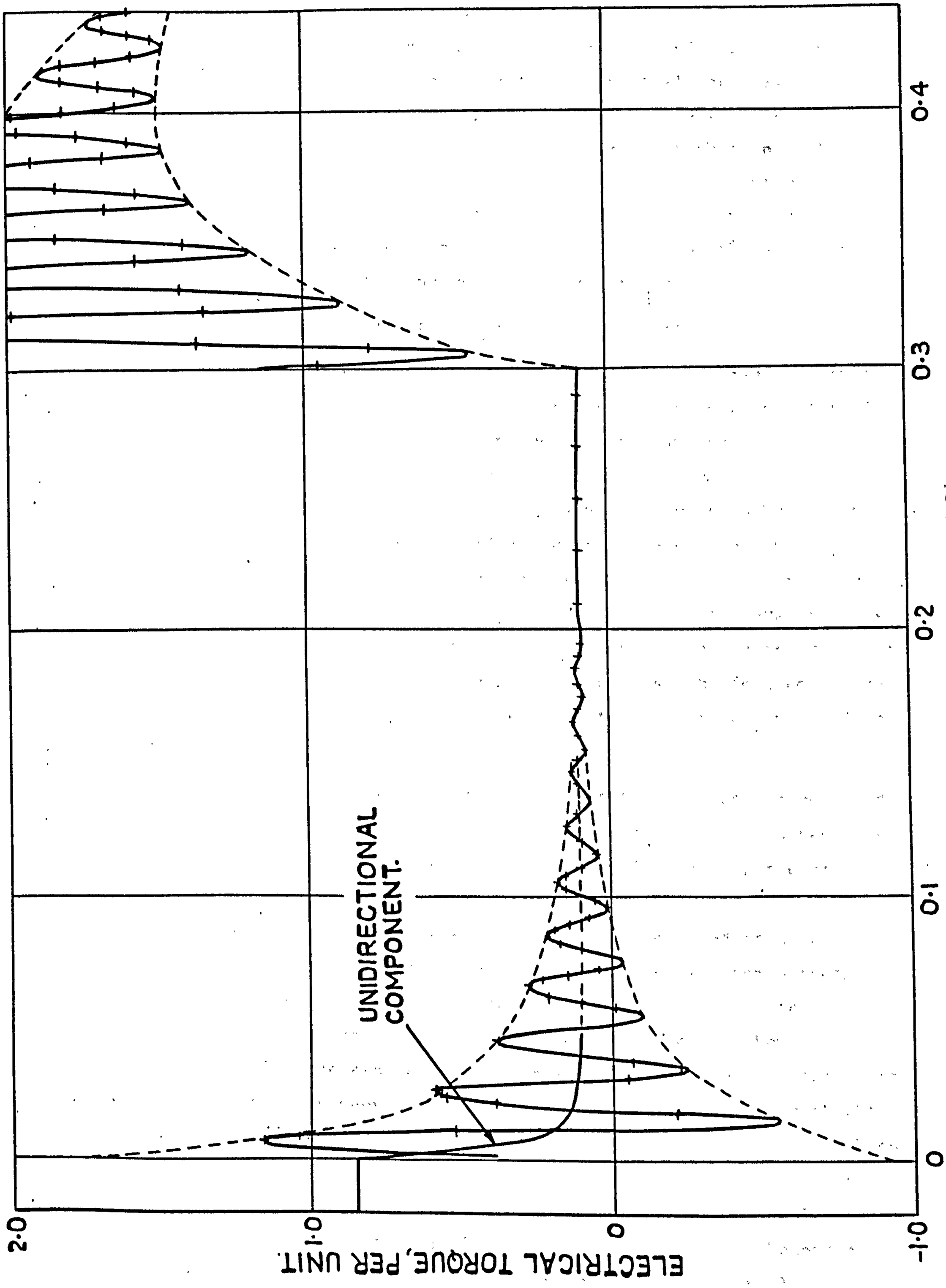

TORQUE OSCILLATIONS FOLLOWING SYSTEM DISTURBANCE. (CALCULATED)

FIG. 2.11.

On the basis of the above investigation the predictor corrector method was preferred for permanent inclusion in the programme and the performance capability chart of Fig.2.7 obtained. With the original step length of 1 millisecond the computer required approximately 1 minute to calculate results for a solution time of 1 second. From the chart this could be increased to 2 milliseconds with little sacrifice of accuracy but with a saving of nearly 50% in computation time. Little economy would be gained in a further increase in step length and in addition the accuracy in simulating the rotor angle swing would fall off rapidly.

2.6.2 Simulation of fundamental frequency components

Figs.2.8-2.11 are sample results obtained from a three phase symmetrical fault study at full load on a large 500 MW turbogenerator (see Appendix 11.3). These illustrate the effects of including the stator transient terms $p\psi_d$ and $p\psi_q$ in equations (2.7) and (2.8) and the transmission system transients pi_d and pi_q in equations (2.16) and (2.17). In many programmes these are omitted. as in addition to reducing the number of differential equations by two, it saves the complex procedure of re-arranging the basic equations for solution. However once the re-organisation of the equations has been achieved and a set of simultaneous differential equations extracted, as in the present work, it is little extra task for the digital computer to process the full equations and obtain results which are not only more accurate but noticeably different from those obtained by the simpler model.

In these figures, the dotted portions represent typical results obtained from the simpler model (transients neglected) and the full line curves were obtained from the complete equations. The major difference is the presence of oscillations at power system frequency excited by the application and removal of the faults which are present in all the calculated machine quantities. The field current oscillations are well known from both site recordings of fault tests and manufacturers sudden short circuit tests (from open circuit conditions) for obtaining generator parameters. However the oscillations on shaft acceleration and the smaller oscillations on speed are rarely recorded due to inadequate instrumentation, and in fact very slight fundamental frequency components are present in the rotor angle result which has been hitherto an unknown phenomenon. Oscillations in the direct and quadrature armature voltages and currents can be interpreted as amplitude modulations when converted into the absolute AC values. This phenomena was noticed on the Doncaster fault test recordings (see Chapter 9). Fundamental fluctuations in power and torque are important for studies of

the mechanical behaviour of the rotor shaft and couplings for which the programme could be adapted.

2.6.3 Rotor angle backswing

It is observed from Figs.2.9 and 2.10 that immediately after fault application the rotor is decelerated producing a slight negative speed deviation. These results were calculated for full load and the effect on the rotor angle is to produce a slight dwell period before it starts increasing. However at low loadings there is a much greater negative speed deviation producing an appreciable initial downward swing of the rotor angle sometimes referred to as the backswing. Fig.2.12 is the result for a 500 MW machine operating at a quarter of rated full load where a backswing of 3^{o} was produced. Although this is fairly small compared to the forward swing of the machine, the important factor is the period of delay before the rotor accelerates, which has effectively increased the critical clearing time by nearly 200 milliseconds in this case. In addition, any error in computing the duration of the backswing would cause a phase discrepancy in the rotor angle time - dependent oscillation which would be significant in multimachine studies.

Early explanations[21,24] of the backswing attributed to the unidirectional component of torque (see Fig.2.11) which takes a finite time to decay and dissipates energy in the form of electrical power in the field and damper resistances. Because this is damping power it would tend to oppose the torque unbalance during a disturbance and act against the prime mover, thus reducing the initial rate of angle change. However this torque never exceeds the prime mover torque and so could not cause a backswing alone. A later theory due to Shackshaft[25] attributes the cause to the fundamental frequency oscillations which also dissipate power (in this case AC power) in the field and damper circuits. This is a feasible explanation since the oscillatory component of torque is many times the steady state prime mover torque before the disturbance. This explanation is strenghthened by the fact that backswing is only predicted by models that include the stator transient effects which greatly emphasises the superiority of this type of model.

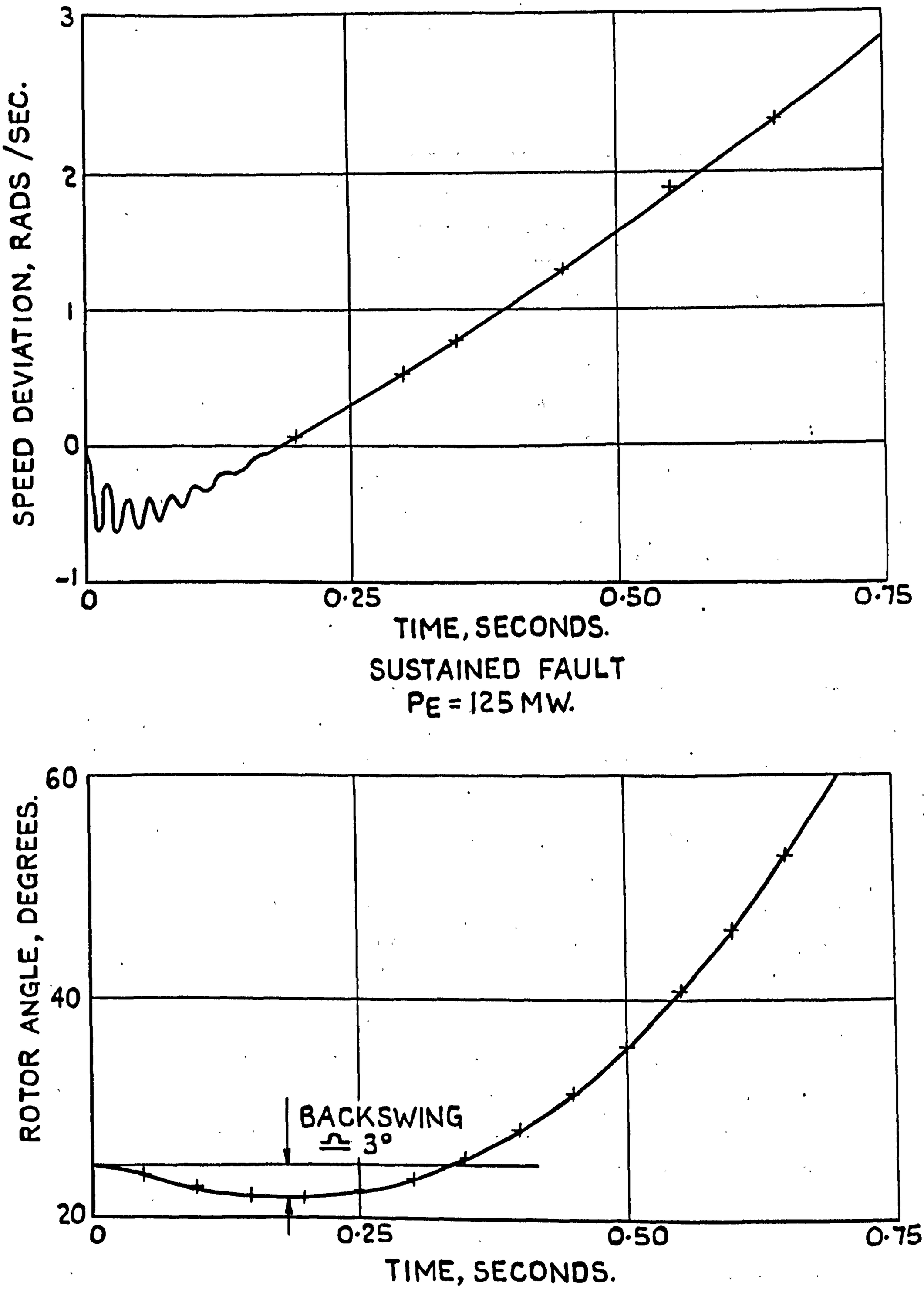

ROTOR ANGLE BACKSWING EFFECT AT LOW LOADING.

FIG. 2.12.

3 MODELLING OF EXCITATION AND TURBINE CONTROL SYSTEMS

3.1 Control systems developments

3.1.1 Control techniques

Control technology applied to turbogenerating systems has so far been confined to electrical and mechanical analogue methods. Very little evidence of the practical application of digital computers for direct digital control (DDC) of turbogenerators is to be found, but due to rapid expansion of technology in this field it may become a viable proposition in the near future, and some initial work has already been published[26-29]. The main objections to digital computer control at the moment are on the grounds of poor reliability and this may preclude their use in this application for some time to come. However an appreciation of this technique would form a logical extension to the present project.

Fluidic control in the governing system is another possibility, but although this technique has gained wide acclaim in certain industrial processes, it has remained undeveloped in the turbogenerator control field.

3.1.2 Developments in excitation systems

The main aim of excitation control is to provide stabilisation of generator terminal voltage to within prescribed limits at various operating conditions, which is usually achieved by feedback. A secondary aspect is the control of reactive power flow and an under-excitation limit is necessary for limiting the VAR's in the leading power factor region. A new requirement in recent years has been a faster speed of response for controlling the dynamic performance of the generator, and the major developments in excitation systems have been allied to this requirement in addition to the need to provide larger power gains as the size of units increased.

When the design and size limitations of DC exciters were reached they were replaced by AC exciter/rectifier combinations, the latest designs having rotating rectifiers which eliminate brushes and the associated current collection problems at high powers. The amplification system in the automatic voltage regulator (AVR) has progressed from static (mag.-amp.) and rotating (amplidyne) magnetic amplifiers to fast thyristor systems. This reduced the AVR time constant to a very small value but the overall excitation system response is still not instantaneous due to the rotating exciter, which has a typical lag of 0,5 seconds. A subsequent development was thyristor excitation systems which placed fast high power control devices immediately

in front of the generator field, giving a typical response of less than 10 milliseconds. The ultimate development in excitation systems is the rotating thyristor system[30] which not only provides a fast response but also overcomes current collection problems.

The elimination of brushes and sliprings in rotating diode/thyristor systems does not in itself affect the excitation system representation but due to the rotor circuits being inaccessible, no exciter feedback stabilising signal can be obtained. This is overcome by using equivalent forward loop stabilisation as in Fig.3.1b. For the original feedback stabilisation of Fig.3.1a, the transfer function is:

$$V_f = \frac{K_e}{(1+pT_e)}\left[V_i - \frac{K_s.p}{1+pT_s} . V_f\right] \qquad \ldots(3.1)$$

equation (3.1) can be re-arranged to obtain an equivalent forward loop as follows:

$$V_f\left[1 + \frac{K_e.K_s.p}{(1+pT_e)(1+pT_s)}\right] = \frac{K_e}{1+pT_e} V_i$$

$$\therefore \quad V_f = \left[\frac{(1+pT_e)(1+pT_s)}{(1+pT_e)(1+pT_s)+K_e.K_s.p}\right] \frac{K_e}{1+pT_e} . V_i$$

$$= \left[\frac{1+p(T_e+T_s)+p^2T_eT_s}{1+p(T_e+T_s+K_e.K_s)+p^2T_eT_2}\right] \frac{K_e}{1+pT_e} . V_i \qquad \ldots(3.2)$$

A first order filter, usually suffices for achieving stabilisation and neglecting p^2 terms, equation (3.2) reduces to:

$$V_f = \left[\frac{1+p(T_e+T_s)}{1+p(T_e+T_s+K_eK_s)}\right] . \frac{K_e}{1+pT_e} V_i \qquad \ldots(3.3)$$

equation (3.3) is the transfer function of Fig.3.1b where

$K_i = T_e+T_s$, and $T_i = T_e+T_s+K_eK_s$

Equation (3.3) can be used to give a guide to parameters of the forward stabiliser for the brushless exciter if the equivalent feedback stabiliser has already been established on a previous design. The final transfer function is usually arrived at by manual adjustment of the parameters to obtain optimum performance during commissioning tests.

(a) FEEDBACK LOOP STABILISATION

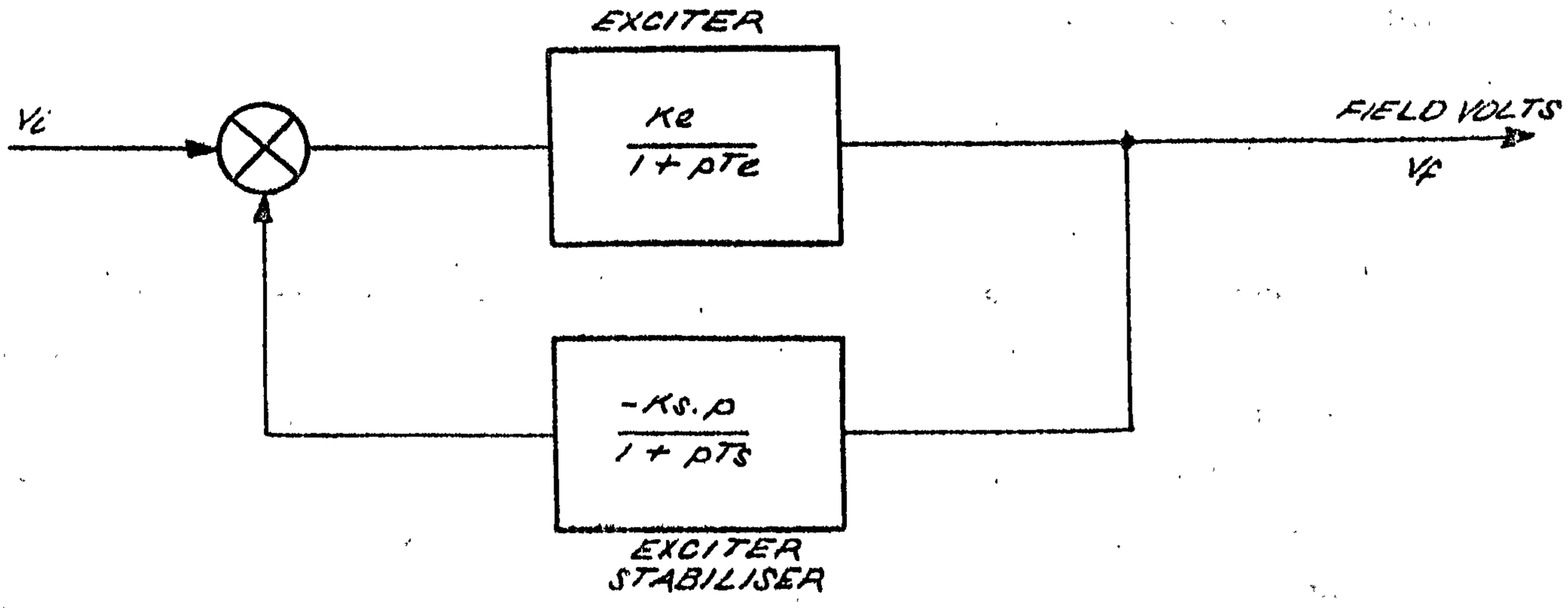

(b) FORWARD STABILISATION

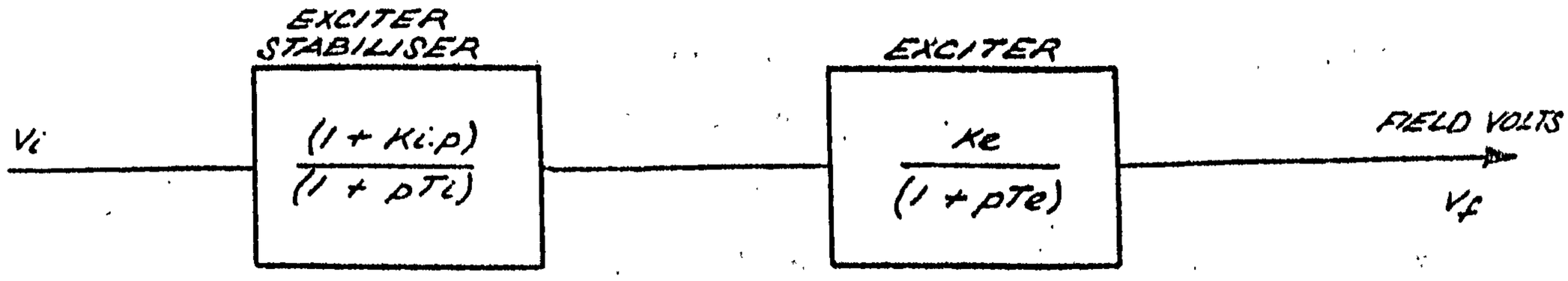

METHODS OF EXCITER STABILISATION

FIG 3.1

3.1.3 Developments in prime mover control

The primary function of controlling the turbine is speed governing and load control but once more developments have been dictated by a requirement for a faster speed of response. To meet the needs for increased power gains the majority of the mechanical linkages in earlier systems were replaced by hydraulic amplifiers which also reduced some of the friction and deadbands within the system.

To reduce the response time, electrohydraulically actuated valves were developed and the flyball or Watt governor which has remained basically unchanged in principal since the development of the steam engine, has been replaced by an electronic speed measuring device. However, due to uncertainty about the long term reliability of electronic equipment, a complex arrangement of system duplication with majority voting has to be used but operational experience may show that this is not essential.

Turbine response time has also been reduced by the use of interceptor valves. These control the steam outlet to the intermediate and low pressure stages thus by-passing the reheater with its associated large time lag.

3.2 Digital computer representation of transfer function building blocks

Most of the control system transfer functions can be decomposed into a combination of three elements namely lag, lead and lead-lag. It is a very simple matter to represent these on an analogue computer by using the operational amplifier circuits shown in Fig.3.2.

If the inverting amplifier A is assumed to have an infinite gain, then by standard theory the input terminal or 'summing junction' of the amplifier is always restored to zero voltage by the negative feedback, i.e. a 'virtual earth' is established. Thus the input current equals the current in the feedback loop and the following may be written:

$$\frac{V_i}{Z_i} = \frac{V_o}{Z_f}, \quad \therefore \quad \frac{V_o}{V_i} = \frac{Z_f}{Z_i} \qquad \ldots(3.4)$$

Applying equation (3.4) to Figs.3.2a,b and c respectively gives the following expressions for the analogue representation of the transfer function blocks:

(a) lag $\quad \frac{V_o}{V_i} = \frac{R_f/R_i}{1+j\omega C_f R_f}$ i.e. $K \equiv \frac{R_f}{R_i}$, $T \equiv C_f R_f$, etc.

(b) lead $\quad \frac{V_o}{V_i} = \frac{j\omega C_i R_f}{1+j\omega C_f R_f}$

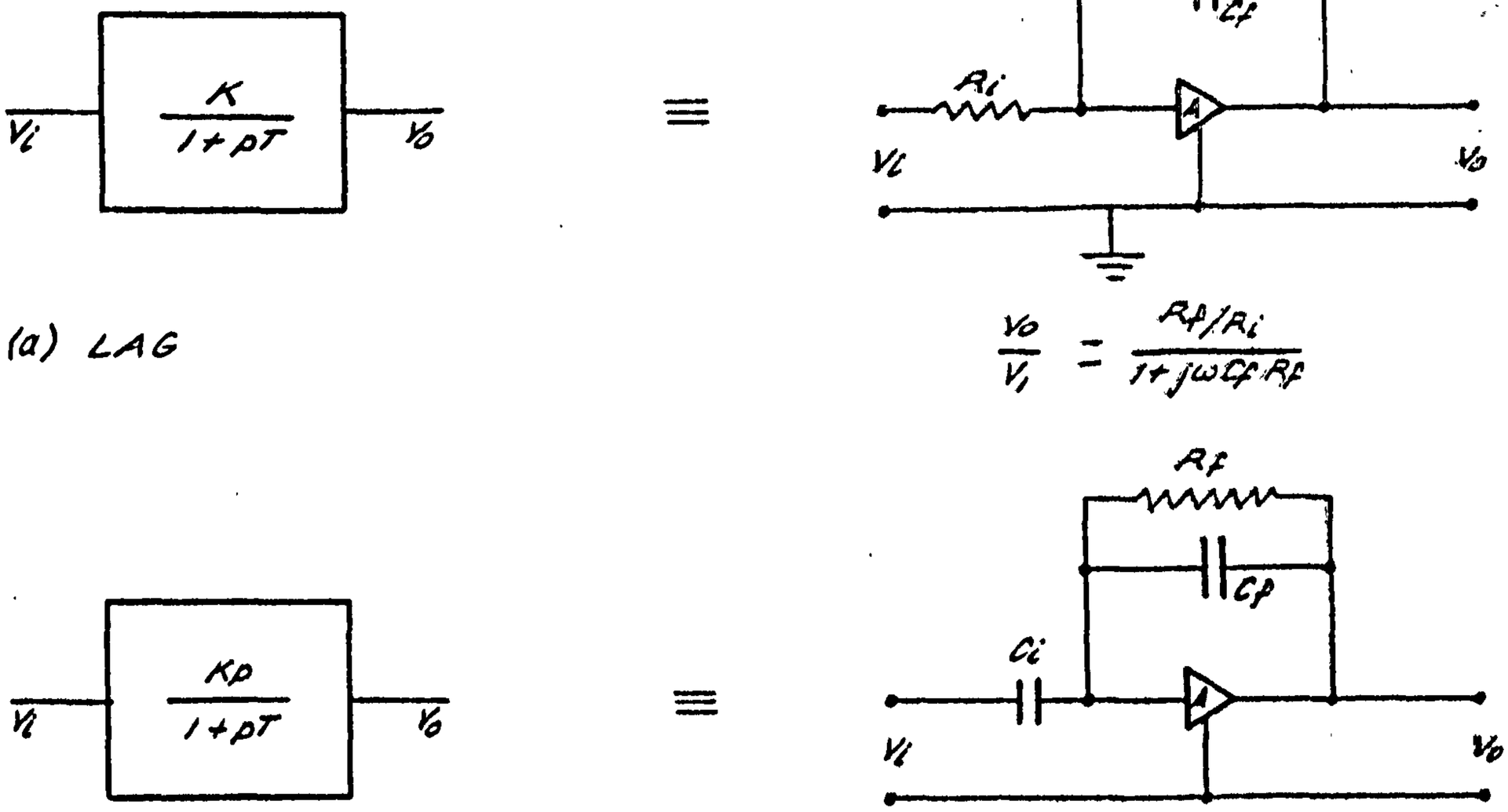

(a) LAG

$$\frac{V_o}{V_i} = \frac{R_f/R_i}{1+j\omega C_f R_f}$$

(b) LEAD

$$\frac{V_o}{V_i} = \frac{j\omega C_i R_f}{1+j\omega C_f R_f}$$

(c) LEAD - LAG

$$\frac{V_o}{V_i} = \frac{R_f/R_i\,(1+j\omega C_i R_i)}{1+j\omega C_f R_f}$$

ANALOGUE COMPUTER PRESENTATION FOR BASIC TRANSFER FUNCTIONS

FIG 3.2

(c) lead-lag $\frac{V_o}{V_i} = R_f/R_1 \frac{(1+j\omega C_i R_i)}{1+j\omega C_f R_f}$

Representation of these function blocks on a digital computer is more difficult due to the impossibility of applying the differential operator 'p' as discussed in the last chapter. Again the functions have to be rearranged in the form of first order differential equations and integrated by an iterative method. However this is a much simpler task than the rearrangement of the generator equations and the procedure for each block is given below.

(a) lag $\frac{V_o}{V_i} = \frac{K}{1+pT}$

$$\therefore \quad V_o (1+pT) = KV_i$$

$$pV_o = \frac{KV_i - V_o}{T}$$

One integrator is required and the output of this gives the output of the function block V_o directly.

(b) lead $\frac{V_o}{V_i} = \frac{Kp}{1+pT}$

$$\therefore \quad V_o (1+pT) = Kp\, V_i$$

$$p(KV_i - TV_o) = V_o$$

One integrator again is required but the output in this case is $(KV_i - TV_o)$ from which a new value of V_o is calculated after every step (assuming V_i is known). This is then used as the input to the integrator for the next calculation and so on

(c) lead-lag $\frac{V_o}{V_i} = \frac{K(1+pT_1)}{1+pT_2}$

$$\therefore \quad V_o (1+pT_2) = KV_i (1+pT_1)$$

$$p(T_2V_o - KT_1V_i) = KV_i - V_o$$

Again only one integrator is required and the auxiliary equation to be processed at the end of each step is:

$$\text{integrator output} = T_2V_o - KT_1V_i$$

from which V_o is calculated and together with a new value of V_i is fed back

into the integrator for the next calculation.

Other functions likely to require modelling are multiplication or division of two quantities and non-linear functions such as limits, logarithms, and trigonometrical functions. Here the digital computer is well suited as all these operations can be programmed directly. For analogue simulation, ready made blocks are available for these functions but these are usually very expensive if any degree of accuracy is required.

3.3 Exciter saturation

Both saturation and regulation effects can be represented as a non-linear feedback term Se^{31} in the input to the exciter as shown in Fig.3.3a.

The open circuit and normal load saturation curves for a typical exciter are plotted in Fig.3.3b and the air gap line has a slope of K_e representing the linear gains in the transfer function block. Thus if no saturation function were applied, an input voltage to the exciter field of V_e would produce an exciter armature voltage output of E_{fd}' as determined by the air gap line. However, the true output voltage E_{fd} is determined by the load curve, and this would also be produced by a voltage v_i behind the linear gain K_e as dictated by the air gap line. Thus, in order to obtain the correct result, a saturation function equivalent to the length χ on the diagram must be subtracted from the input voltage V_e. The value of the saturation function varies with the output voltage and its expression is derived as follows:

from Fig.3.3a, $v_i = V_e - S_e \times E_{fd}$

$$\text{and, } E_{fd} = K_e \times v_i \quad \text{(steady state conditions)}$$

$$\therefore E_{fd} = K_e (V_e - S_e \times E_{fd})$$

$$Se = \frac{V_e}{E_{fd}} - \frac{1}{K_e} = \frac{V_e - v_i}{E_{fd}}$$

$$\text{i.e. } Se = \frac{\chi}{E_{fd}}$$

In order to represent exciter saturation therefore, first of all a load curve must be available, and various measurements of χ taken to obtain values of Se throughout the whole range. These values are then stored on the digital computer either as a polynomial expression or as an incremental straight line approximation to the curve of Se versus E_{fd}.

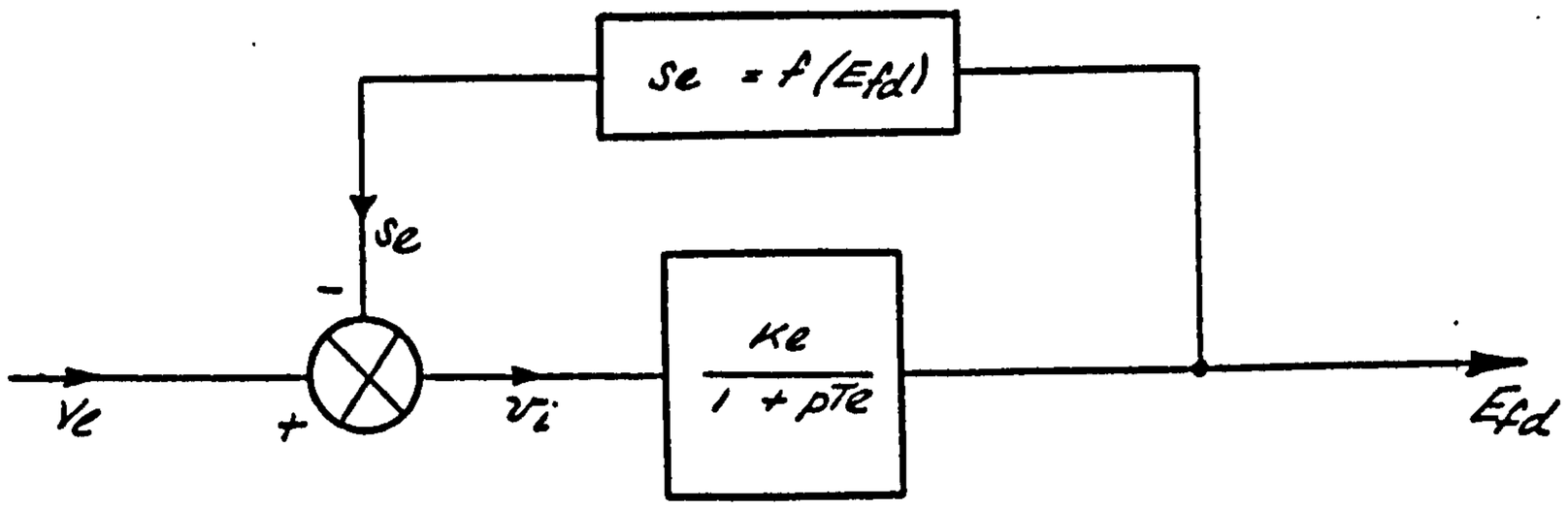

(a) TRANSFER FUNCTION BLOCK

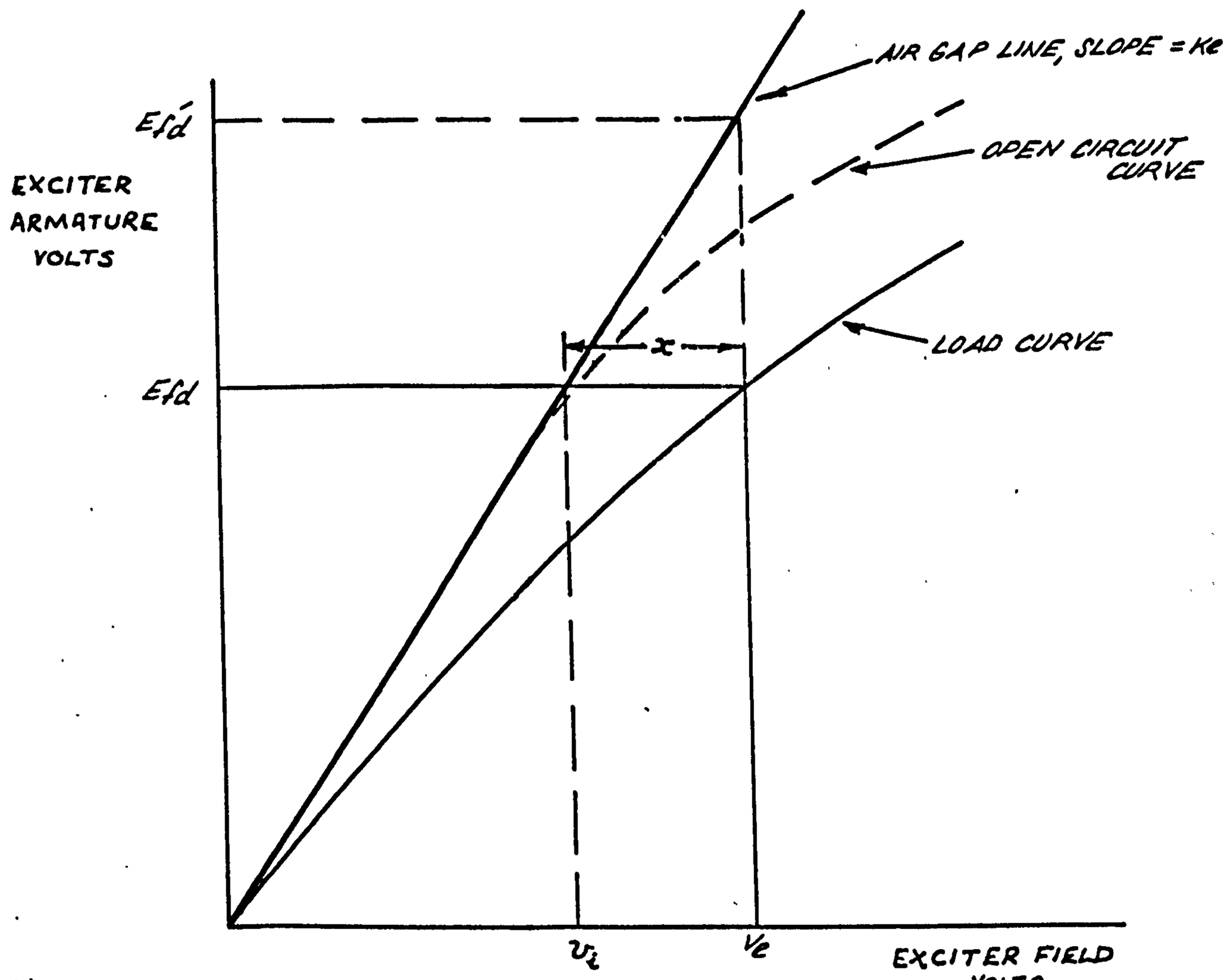

(b) LOAD SATURATION CURVE

REPRESENTATION OF EXCITER REGULATION AND SATURATION

FIG 3.3

The appropriate value of Se is selected from the stored curve after each integration step and the expression Se × E_{fd} subtracted from the exciter field voltage to allow for the prevailing regulation and saturation effects.

3.4 Excitation system models

In the following, all the major developments of excitation systems as in Section 3.1 are discussed together with their transfer functions in the form of the basic blocks as listed in Section 3.2.

3.4.1 Non continuously acting systems

A typical non-continuously acting regulator is shown in Fig.3.4a in which the exciter field current is supplied by a pilot exciter and is varied by a series rheostat. This is adjusted incrementally by a special electromechanical contactor arrangement to restore the voltage error to zero and a facility for switching the whole resistance in or out in one operation on the receipt of a large voltage error is usually incorporated.

The terminal voltage signal is obtained via a step down transformer and three phase rectifier after which it is passed into a voltage sensitive bridge of the metrosil type. These are semiconductor components which act as non-linear resistors and satisfy the equation

$$V = RI^{\beta}$$

It is arranged that the components in adjacent arms of the bridge have different β values, typically 0.2 and 0.6, and this enables the incoming voltage to be backed off at a certain current setting which is adjusted by the bridge rheostat.

Thus the output of the bridge will be zero when

$$R_1 I^{0.2} = R_2 I^{0.6} \text{ (assuming zero loading on bridge output)},$$

i.e. when

$$I = \left(\frac{R_1}{R_2}\right)^{2.5}$$

If the input voltage changes then the voltages dropped across the metrosils will differ producing an output signal from the bridge. Thus the bridge system acts as a reference, and an output is only produced when the input voltage diverges from this reference which is set by the bridge rheostat.

The transfer function of Fig.3.4b contains an integral term to represent the automatic adjustment of the field rheostat. In actual fact the

(a)

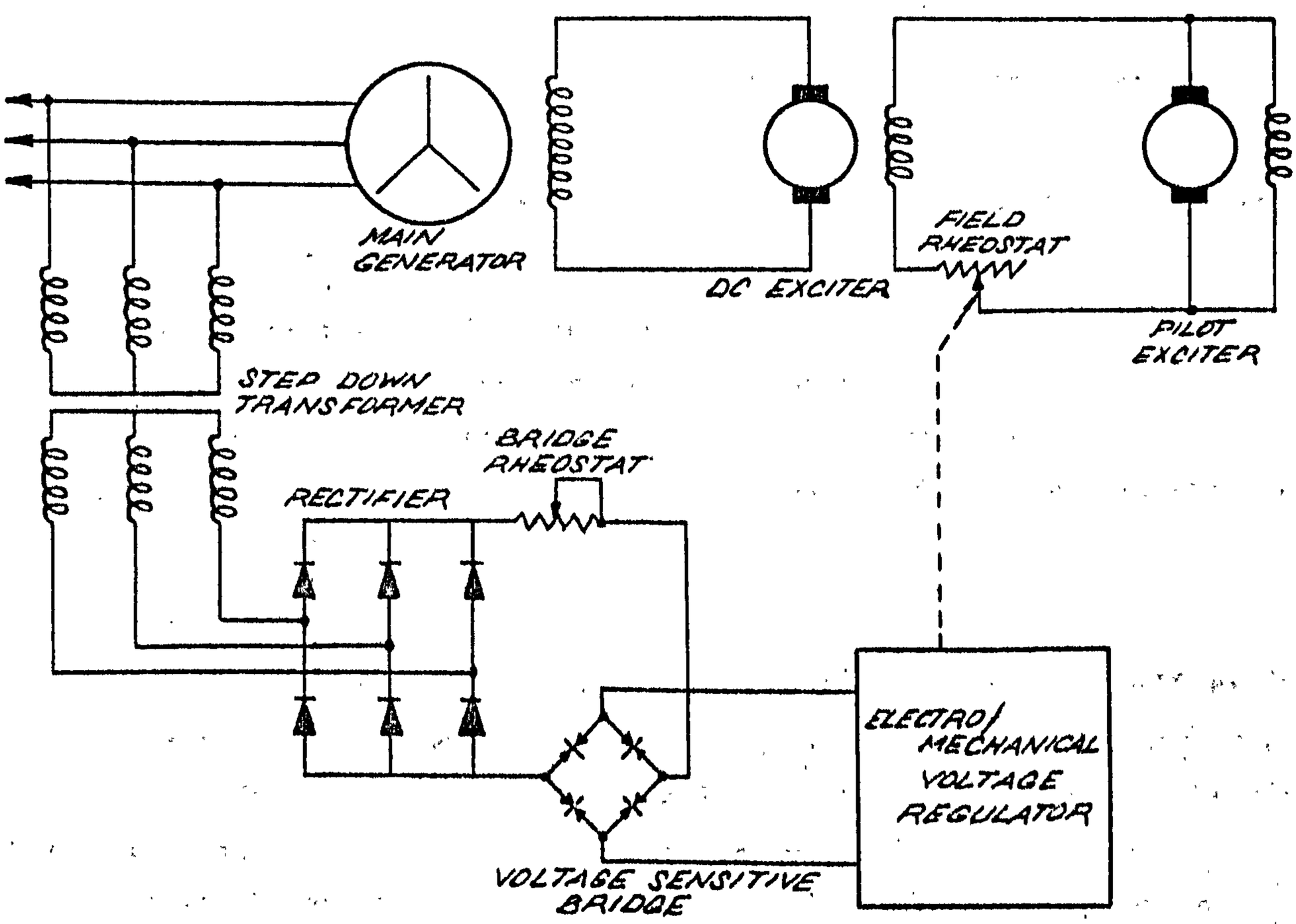

(b)

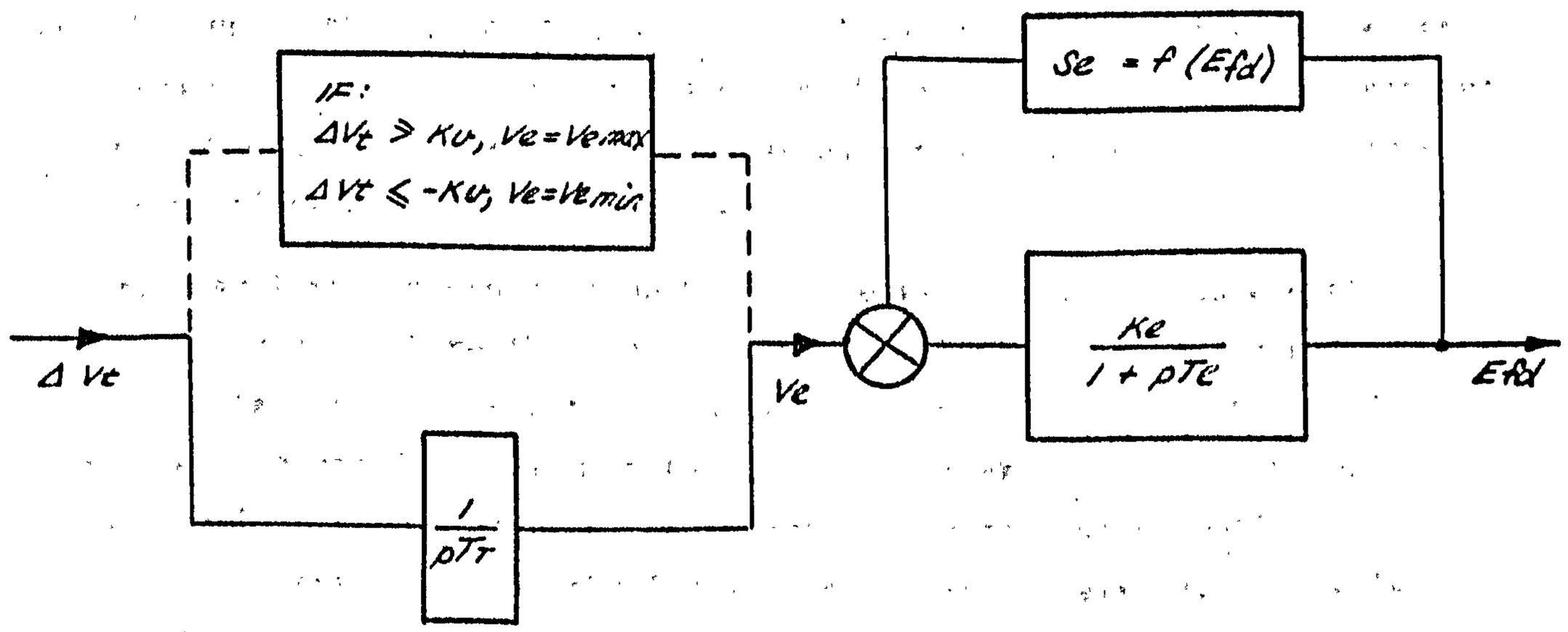

NON-CONTINUOUSLY ACTING VOLTAGE REGULATOR

FIG 3.4

adjustment is made in discrete steps but as the operation time is very slow it is feasible to represent it as a continuous function. An overide is provided for when the whole of the rheostat is switched in or out on receiving a large error signal.

The DC exciter is represented by a single lag and a saturation function can be added if necessary.

The above representation is intentionally not a very accurate one as this type of AVR only remains on old and small machines of which the transient stability aspects are rarely studied. In addition, parameters are usually extremely difficult to obtain for obsolete equipment and thus a more exacting simulation would be pointless.

3.4.2 Early continuously acting systems

Fig.3.5a shows a typical continuously acting AVR for use with a DC exciter[32]. The transformer, rectifier and metrosil bridge are similar to the previous system but some form of smoothing is usually necessary to filter out the ripple as the overall gain is high. Next follows a two stage magnetic amplifier which can drive the exciter field directly on smaller generators but on medium and large size machines, one or more amplidynes or even additional exciters may be used to obtain the necessary power amplification. A passive feedback network is connected from the exciter output terminals as shown for stabilisation and the magnetic amplifiers have their own internal stabilisers. It is only necessary to represent the forward loops of all the amplifiers by a single lag as their time constants are small compared to the exciter and can be represented collectively by one time constant. However care must be taken not to overlook any limit conditions which may be pertinent.

The transfer function can also be used to represent earlier AC exciter/ static diode systems. Here the exciter field is on the rotor and supplied by slip rings. The three phase output from the stator is rectified by static diode banks and returned to the main generator field again via slip rings. The latest versions of this type of equipment employ thyristor amplifiers in the AVR which are stabilised in the forward loop where necessary. This is covered by the next type.

3.4.3 AC exciter-brushless diode systems

The brushless system (Fig.3.6) is fast gaining popularity due to an extremely high reliability record. The continuous on load maintenance required with brushes has been eliminated, and the doubts about the ability of power diodes and fuses to withstand high 'g' forces have been dispelled

(a)

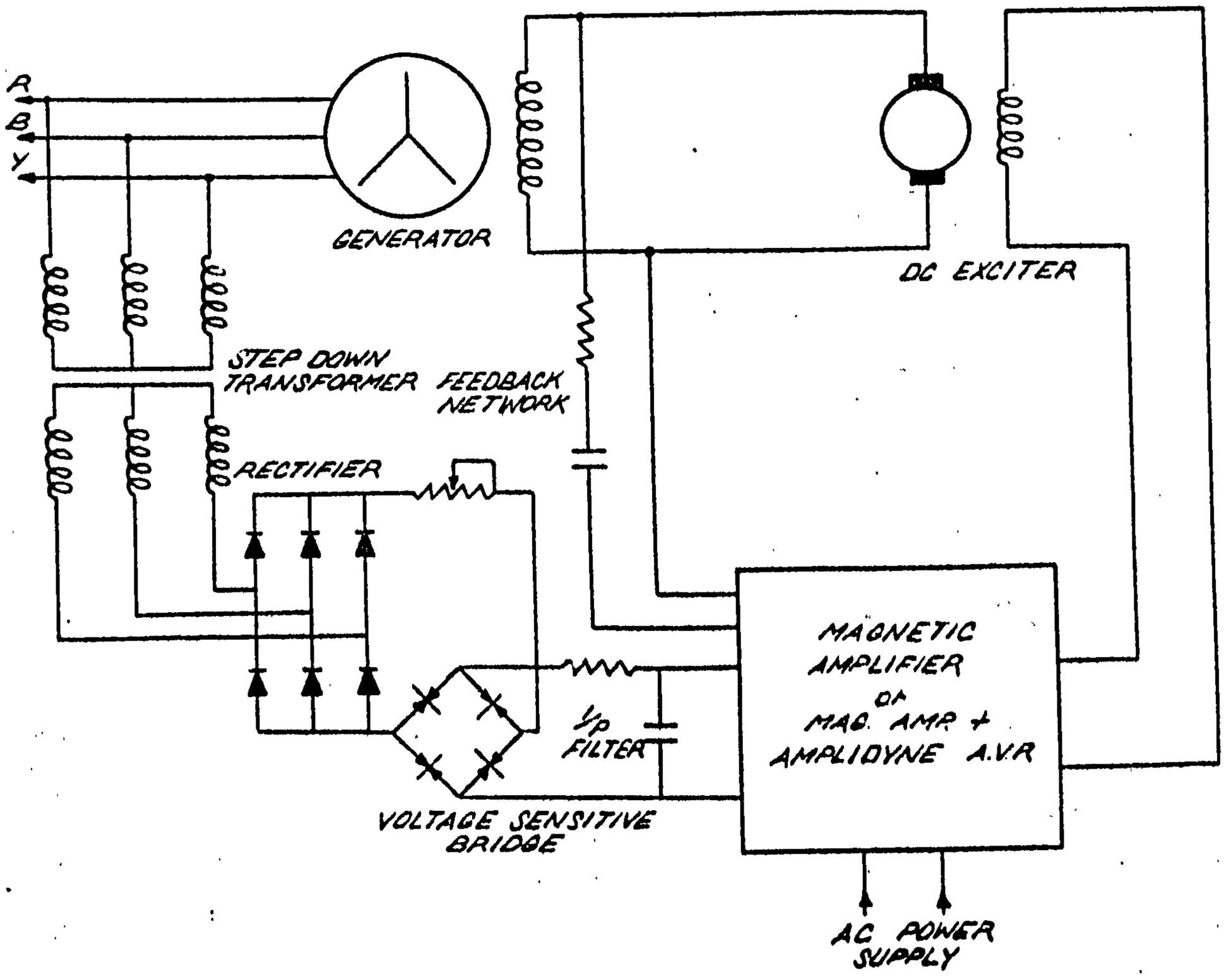

(b)

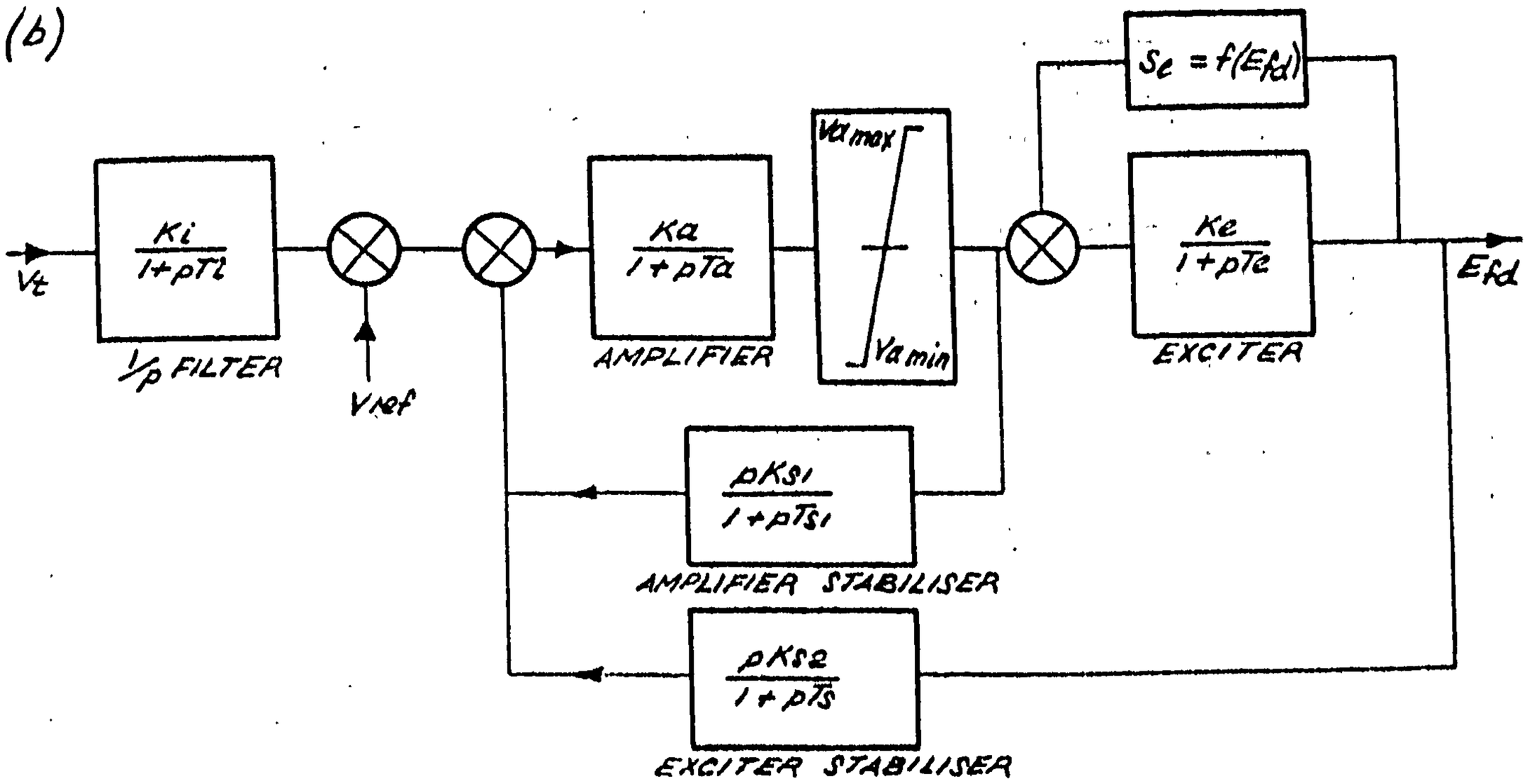

CONTINUOUSLY ACTING REGULATOR

FIG 3.5

(a)

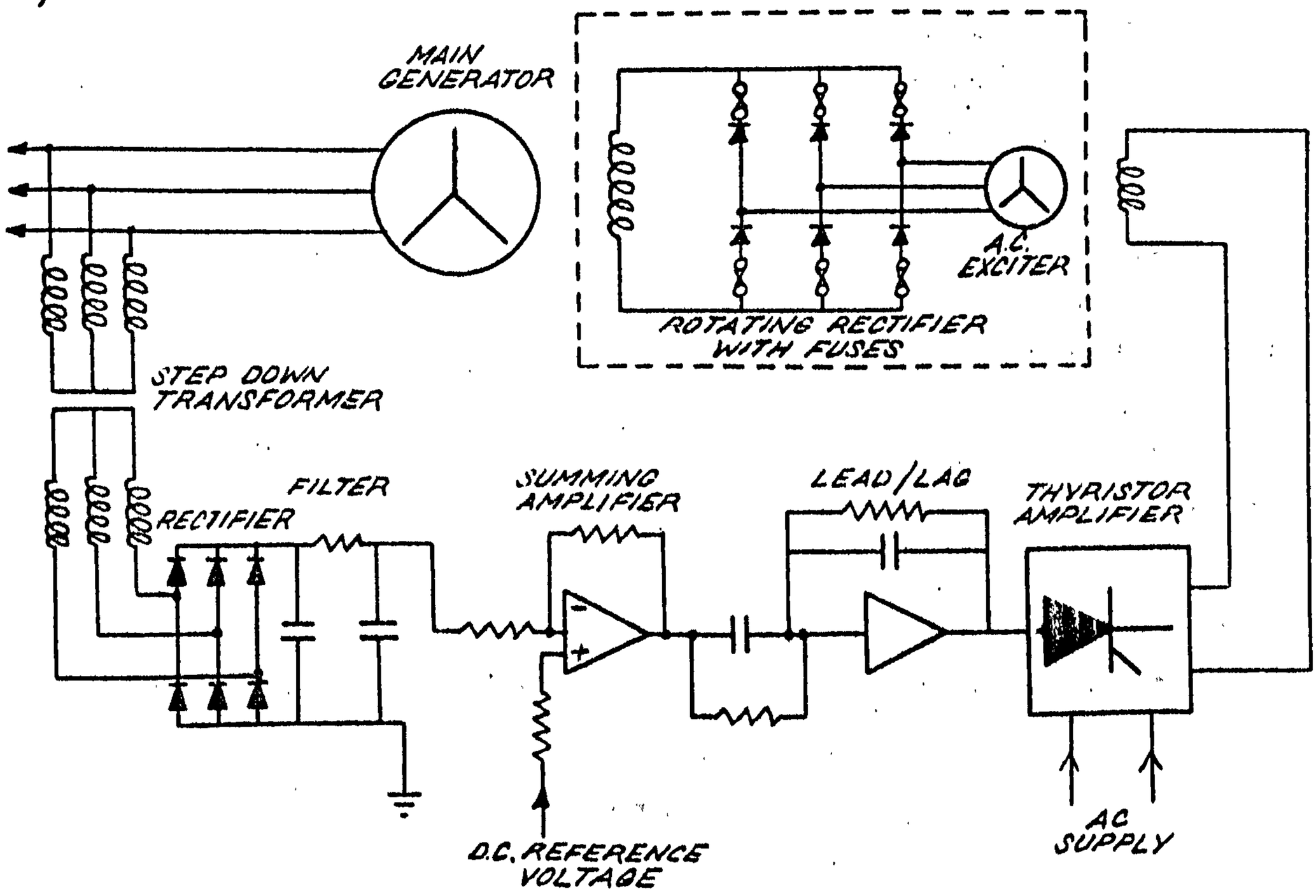

(b)

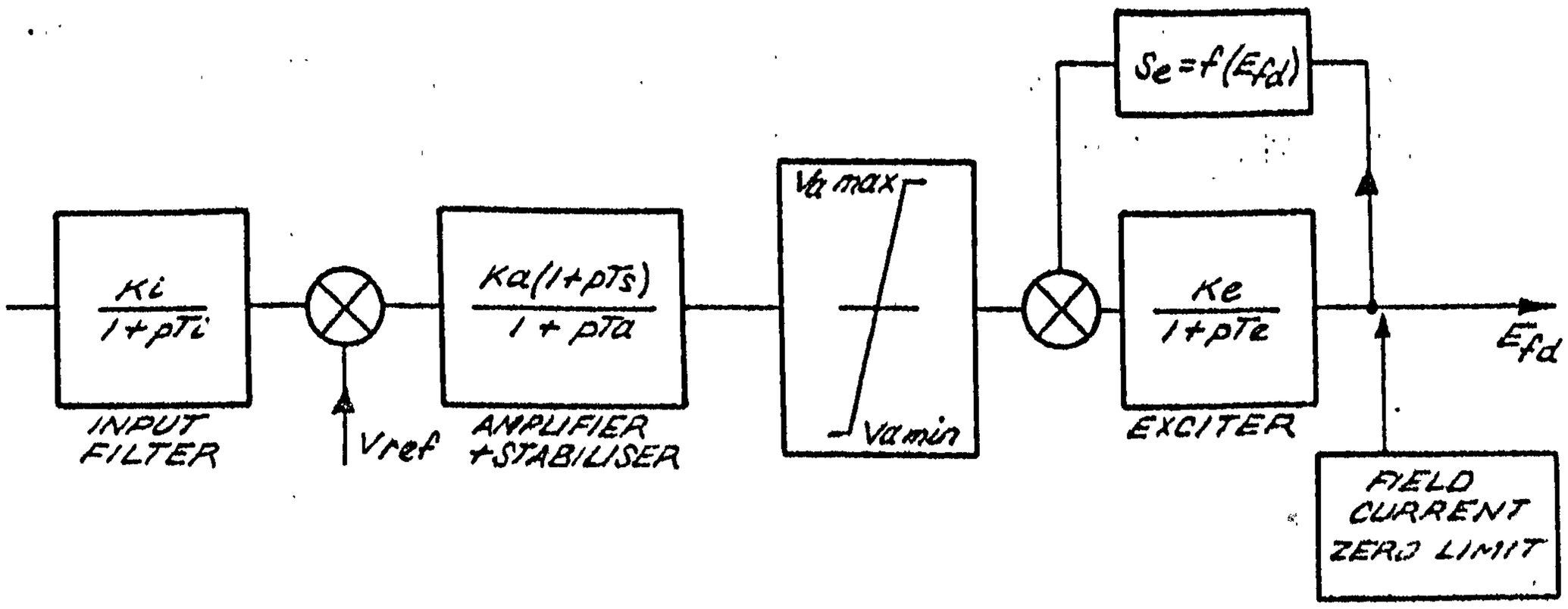

REGULATOR FOR BRUSHLESS DIODE - AC EXCITER SYSTEM

FIG 3.6

by the trouble-free service records of the units installed in the last decade. The increase in voltage ratings of diodes has enabled the brushless system to be used on the largest units to date without the need for series devices, but it is necessary to have two or more devices in parallel per arm to achieve the high excitation currents and allow for redundancy in case of diodes failing.

Fig.3.6a shows a typical brushless excitation system with active elements for subtracting the reference and providing forward loop stabilisation. A thyristor amplifier supplies the field of the AC exciter and the armature voltage is rectified by diodes, mounted on a special flywheel, before feeding the generator field winding. Two AVR channels are usually provided for extra reliability, one channel being kept on standby.

The transfer function is straight forward but an extra point to be taken into account when studying AC exciters is the zero voltage and current limits of the rectifiers.

3.4.4 Thyristor excitation systems

These systems are of the most importance to the present investigation as they are the only ones with a fast enough response to enable the effective use of additional stabilising signals. This is due to the elimination of the exciter time lag by using high power thyristors to control the field voltage directly.

Three different system configurations have been developed:

(a) Static thyristor equipment supplying the generator field via slip rings and deriving AC power from the generator terminals (Ref.33).

(b) As above but deriving power from an AC exciter mounted on the generator shaft (Ref.34).

(c) Rotating thyristor equipment (Ref.30).

The first has the disadvantage that during a fault condition on the system the excitation power supply is depleted by voltage drop, so that field forcing is not possible during the disturbance. Configuration (b) overcomes this disadvantage as there is a constant power supply available from the rotating exciter but the problems of brushes and sliprings still remains. The last system mentioned would seem to be the ultimate in excitation systems as all the previously mentioned problems are eliminated. However this system has not yet been proved in service and certain phenomena perculiar to the system may cause difficulties. To expand on this, there has to be some

method of supplying the rotating thyristor with firing information without using brushes, and so some sort of telemetry system has to be used. A method which is being employed on a British prototype unit[35] is to use a small three-phase control alternator with fields on the direct and quadrature axes which enables the phase of the output voltage to be varied over a full 360° with respect to the shaft. This output voltage is then converted into pulses for driving the gates of the thyristors by shaft mounted firing circuits. It is apparent that the reliability of the system may be impaired by the significant amount of electronic hardware which is mounted on the rotating part and subject to high 'g' forces. However by the careful selection of suitable encapsulated components and the 'potting' of the complete firing circuits in epoxy resins it is hoped that good 'M.T.B.F.' figures will be achieved.

Fig.3.7 shows typical thyristor exciters of the types discussed but due to the novel nature of these systems, practical designs may differ quite widely in detail until proven systems have been established.

Fig.3.7a represents the least expensive system due to the relatively high cost of rotating plant compared to transformers. The rotating thyristor system of 3.7c is the most costly due to the need for special technology for the design of the rotating systems and also the static control circuits are more complex. This is because specialised non-linear function circuits have to be employed to obtain the correct control of firing angle using the split field exciter, and also accuracy demands harmonic-free waveforms on the two fields requiring the use of high power transistorised servo amplifiers.

The exciters have a facility for including extra feedback signals in the input to the thyristor convertor which can be used for increasing the performance of the turbogenerator in both the transient and dynamic zones[36,37]. Depending upon control requirements and the actual signal used, some sort of analogue processing is usually necessary. This is represented as a simple lead/lag in the transfer function of Fig.3.8 but in practice it may be a complex high order function (for example Ref.37). A field current limit is also shown on the diagram which is an additional feature on some systems to prevent the field current building up to damaging proportions should the field voltage remain at ceiling for too long. If the current exceeds a predetermined level then an extra signal is subtracted from the voltage at the input to the thyristor convertor thus reducing the field voltage

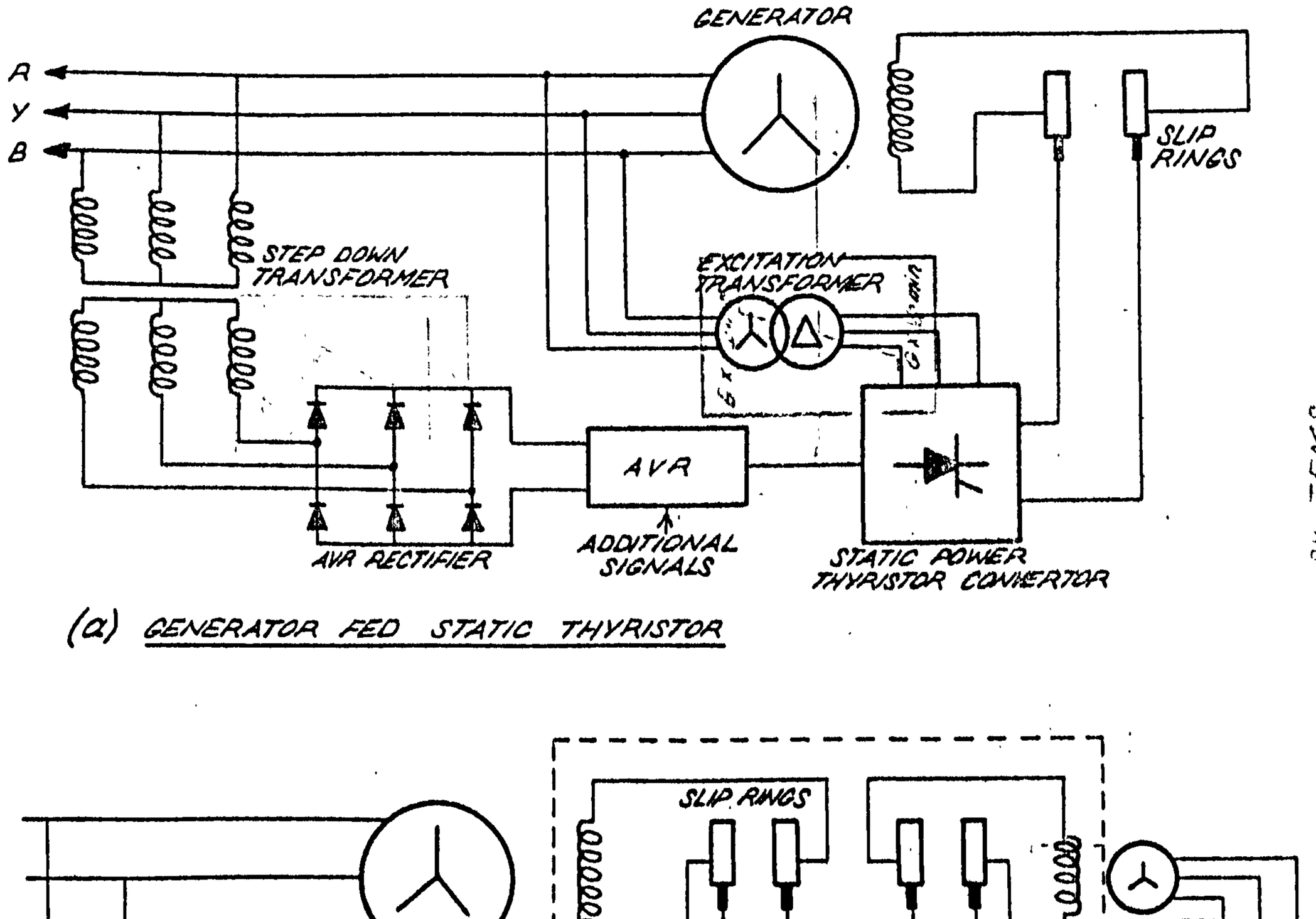

(a) GENERATOR FED STATIC THYRISTOR

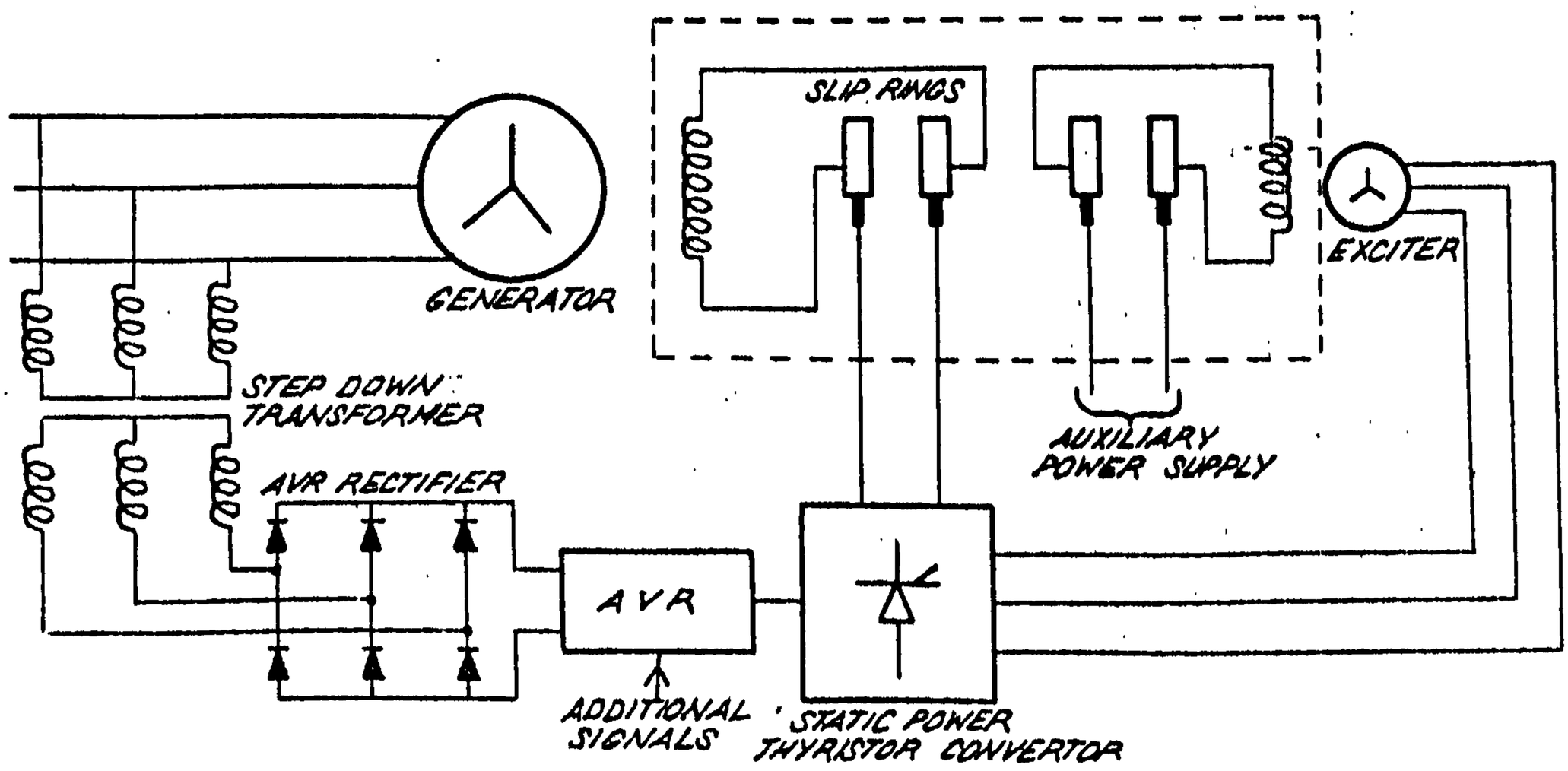

(b) EXCITER FED STATIC THYRISTOR

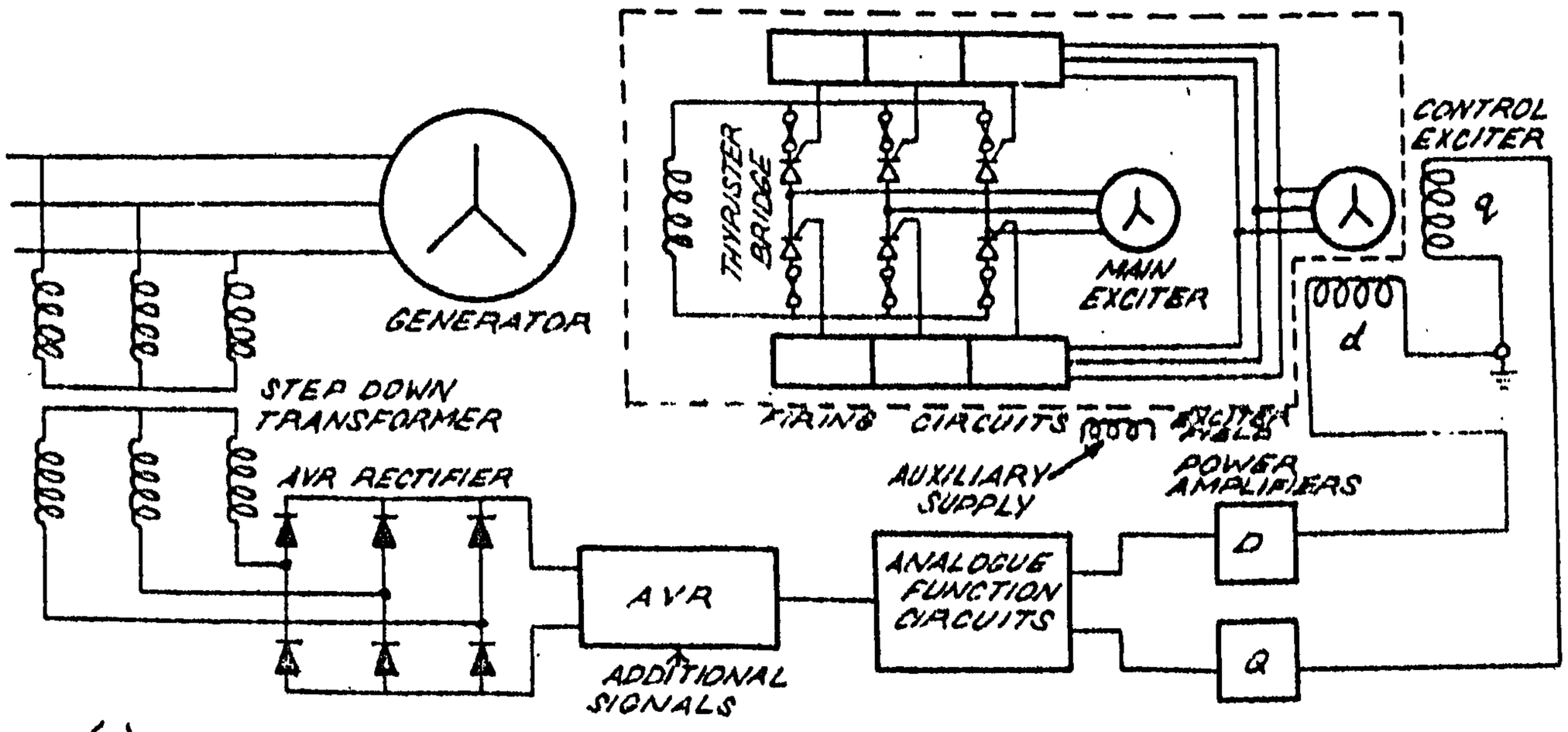

(c) ROTATING THYRISTOR

THYRISTOR EXCITATION SYSTEMS

FIG 3.7

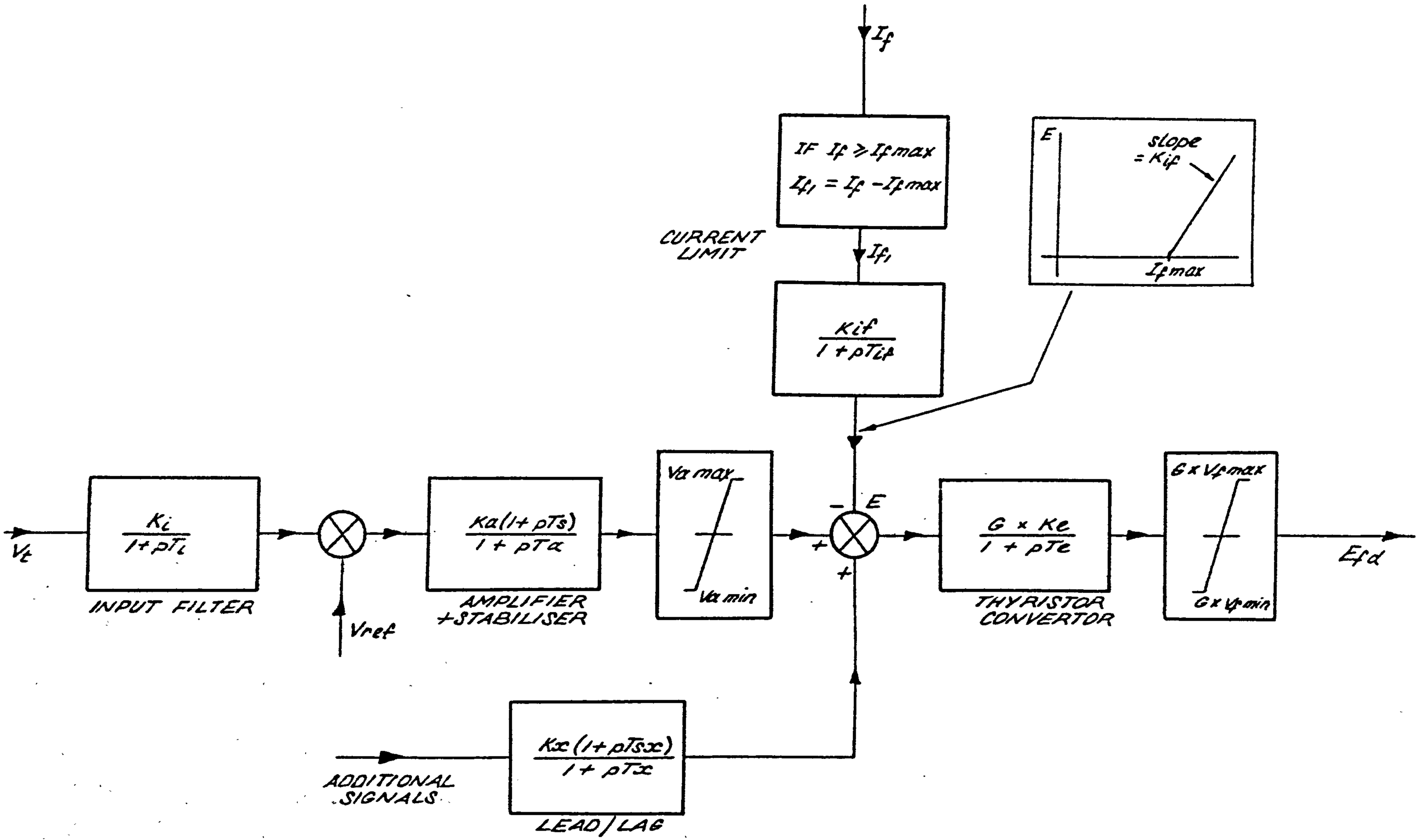

TRANSFER FUNCTION FOR THYRISTOR EXCITATION SYSTEMS

FIG 3.8

To take into account whether the convertor is exciter or generator fed, a factor G is shown on the transfer function which is equal to 1 for the former case and V_t, the terminal voltage in per unit, in the latter. This is used as a multiplier for the gain and limits of the convertor to take into account the reduction of these in the generator fed case during fault conditions.

In some studies it may be necessary to represent the thyristor convertor more accurately. From Ref.38, the output of a mercury arc convertor (which controls the current in the same manner as a thyristor) supplying an inductive load is given by:

$$V_{DC} = \frac{3\sqrt{2}}{\pi} V_{AC} \cos\alpha - X_\ell I \text{ (where } X_\ell I \text{ is the regulation drop)}$$

The firing angle delay α, is varied linearly by the input control voltage V_c, so that when

$$V_c = 0, \qquad V_{DC} = 0, \text{ i.e. } \alpha = \frac{\pi}{2}$$

$$V_c = V_{cmax}, \quad V_{DC} = V_{DCmax}, \quad \alpha = 0$$

Fig.3.9a shows the delay angle characteristic including the regulation effects. In the present application however, the regulation drop at ceiling voltage may not be so high in the transient case due to the time taken for the field current to build up resulting in a higher effective ceiling voltage.

The curve (a) of Fig.3.9b shows the steady state characteristic of the output voltage with respect to the input control voltage V_c. If this voltage is suddenly reversed when the convertor is supplying current into an inductive load, then inversion occurs and the output voltage is reversed according to curve (b) until the output current decays to zero. As the rectifiers cannot pass negative current the output then immediately falls to zero (see Ref.39) until convertor action is demanded again. There is a practical limit on the maximum inversion delay angle of about 150^o as an allowance has to be made for the commutation angle γ', and if α is increased beyond $(180^o - \gamma)$ then inversion failure occurs causing AC to be applied to the generator rotor which could have catastophic affects. Fig.3.10 gives a more explicit operation of the convertor by means of the waveform diagrams.

In some convertors the steady state characteristic is linearised by processing the control voltage according to the characteristic of curve (c) of Fig.3.9b before passing to the firing circuit input. This is done

(a)

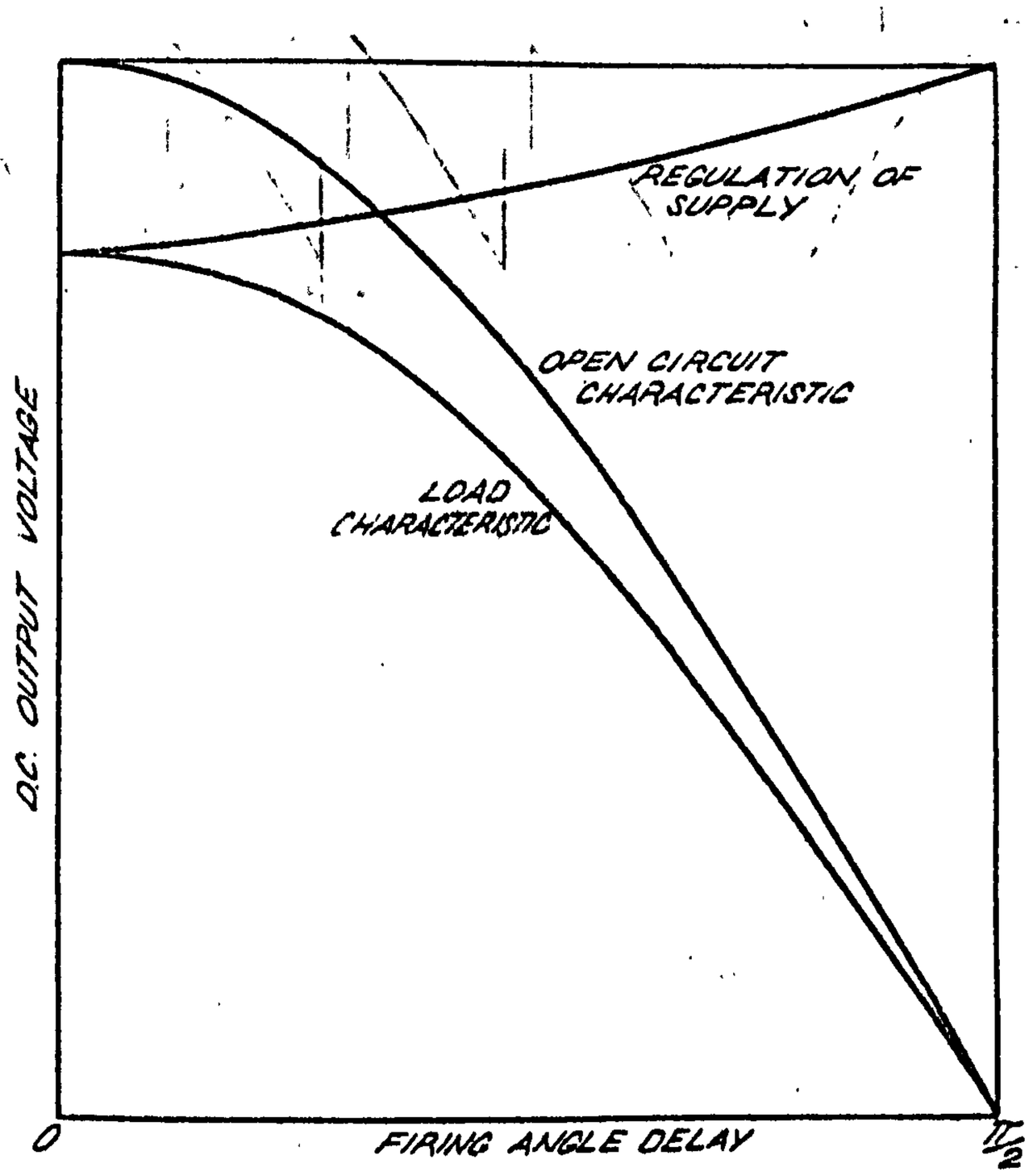

(b)

THYRISTOR CONVERTOR CHARACTERISTICS

FIG 3.9

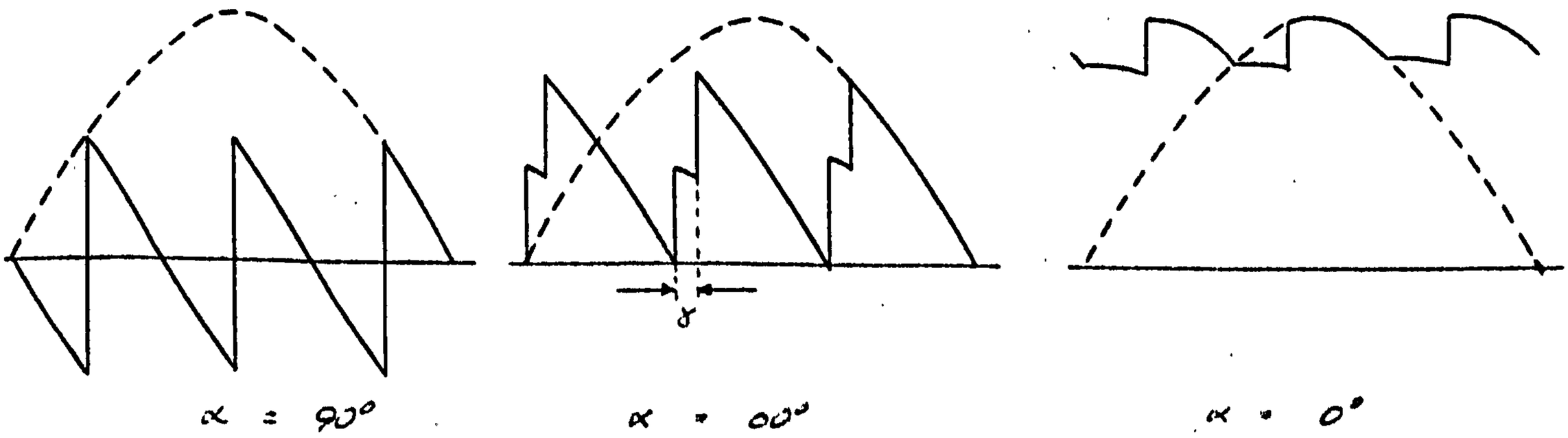

(a) RECTIFICATION MODE

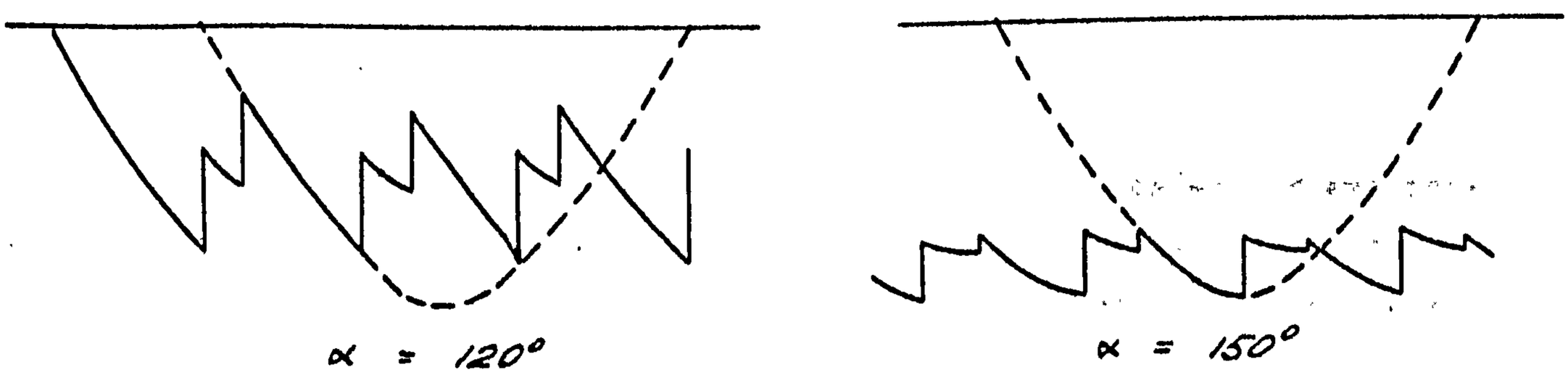

(b) INVERSION MODE

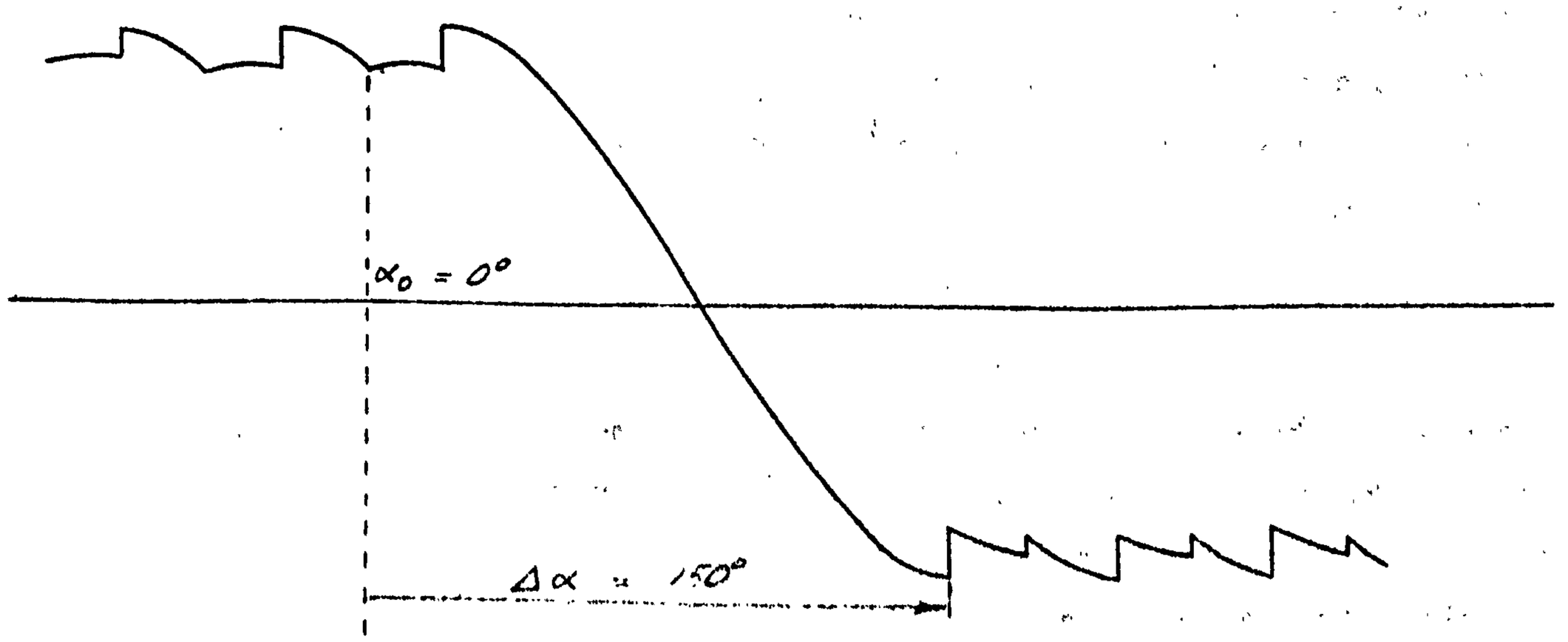

(c) SUDDEN TRANSITION FROM RECTIFICATION TO INVERSION MODE

THYRISTER CONVERTOR OUTPUT WAVEFORMS ON INDUCTIVE LOAD

FIG 3.10

artificially with diode function circuits and is a 'mirror' image of the normal characteristic, curve (a). Thus the output follows the linear characteristic curve (d) which is the median of (a) and (c). If the processed control voltage V_c' then as before,

$$V_{DC} = \hat{V}_{DC} \sin (V_c') \qquad \ldots(3.5)$$

(neglecting regulation)

The equation for curve (d) is

$$V_{DC} = \frac{2}{\pi} \hat{V}_{DC} \cdot V_c \qquad \ldots(3.6)$$

From equations (3.5) and (3.6) therefore, the required characteristic of the non linear function circuit is

$$V_c' = \sin^{-1}\left(\frac{2\ V_c}{\pi}\right)$$

If the convertor is used on a constant load as in turbogenerator exciters, then the regulation can be taken into account in the linearisation. Thus accurate mathematical representation of the thyristor convertor characteristic is possible by a single gain.

The thyristor convertor transient performance does not exhibit an exponential lag but rather a delay depending upon the initial firing angle, and the amount it is varied. However the maximum delay from positive to negative ceiling when operating from a 50 Hz supply will be only 8.33 milliseconds (i.e. $150^{\circ}/180^{\circ} \times 10$ milliseconds) and so for most cases this can be neglected. This is especially feasible for AC exciter fed systems which are normally four or six pole machines generating frequencies of 100 Hz and 150 Hz respectively, resulting in a decrease of the convertor delay time of two or three times.

3.5 Turbine and governor models

Fig.3.11 shows a general schematic of a modern reheat turbine which is used as a basis for the models. Only two basic classifications of prime mover system are considered for simulation purposes; i.e. those with mechanical or those with electronic governors, having in general slow and fast responses respectively. Variations such as the omission of the reheater in single cylinder machines or the use of different droop settings can be catered for by making parameter adjustments without the need for additional models. Boiler dynamics are not considered as the response is slower than 10 secs, and therefore too slow to affect the transient behaviour of the generator, and the operation of the emergency stop valves is not normally studied.

3.5.1 Mechanically governed turbines

Due to the relatively slow operation of mechanical/hydraulic systems and the difficulty of obtaining system parameters only, a greatly simplified representation is used. Fig.3.12 contains only two time constants to represent lags due to governor, steam valves, reheater and steam storage and is economical on computing time as only two integrators are required.

The governor gain Kg is calculated from the turbine setting as

$$Kg = \frac{\text{full load torque (p.u.)} \times 100}{\text{turbine droop (\%)} \times \omega_o \text{ (rads/sec)}}$$

which gives an output torque T_L in per unit that can be fed directly into the mechanical equation of motion for the generator (eqan.2.32).

The parameters K_H and K_L represent the torque complements of the high pressure and intermediate/low pressure cylinders respectively expressed as a per unit (i.e. $K_H + K_L = 1$). This time constant T_1 represents governor, steam value and HP steam storage lags and T_2 represents reheater and IP/LP steam storage. If it is desired to omit the reheater then K_L is simply set to zero and K_H to unity.

Although interceptor valves are present on most modern mechanically governed turbines, they are not used as an operational control device but merely for reheater protection at low loads. As most studies are performed at fairly high loadings, interceptor valve control is not included on the simpler model, but if desired the electronic governor model can be used to represent flyball systems with IV control by adjusting the time constants accordingly.

Another important phenomenon which should be included even on the simpler model is the difference in the valve opening and closing rates. It is essential, in order to preserve an adequate system stability margin, that the valves are closed as soon as possible in the event of a speed rise due to a large system disturbance. However there is not such a demanding requirement on the opening of the valves, and for economic reasons, this can be much slower than the closing rate and so two different time constants are included in the model. This is represented in the computer model by comparing the current speed error with that calculated after the previous integration step to determine whether valve opening or closing is required, and from this the appropriate time constant inserted in the differential equations for the next iteration.

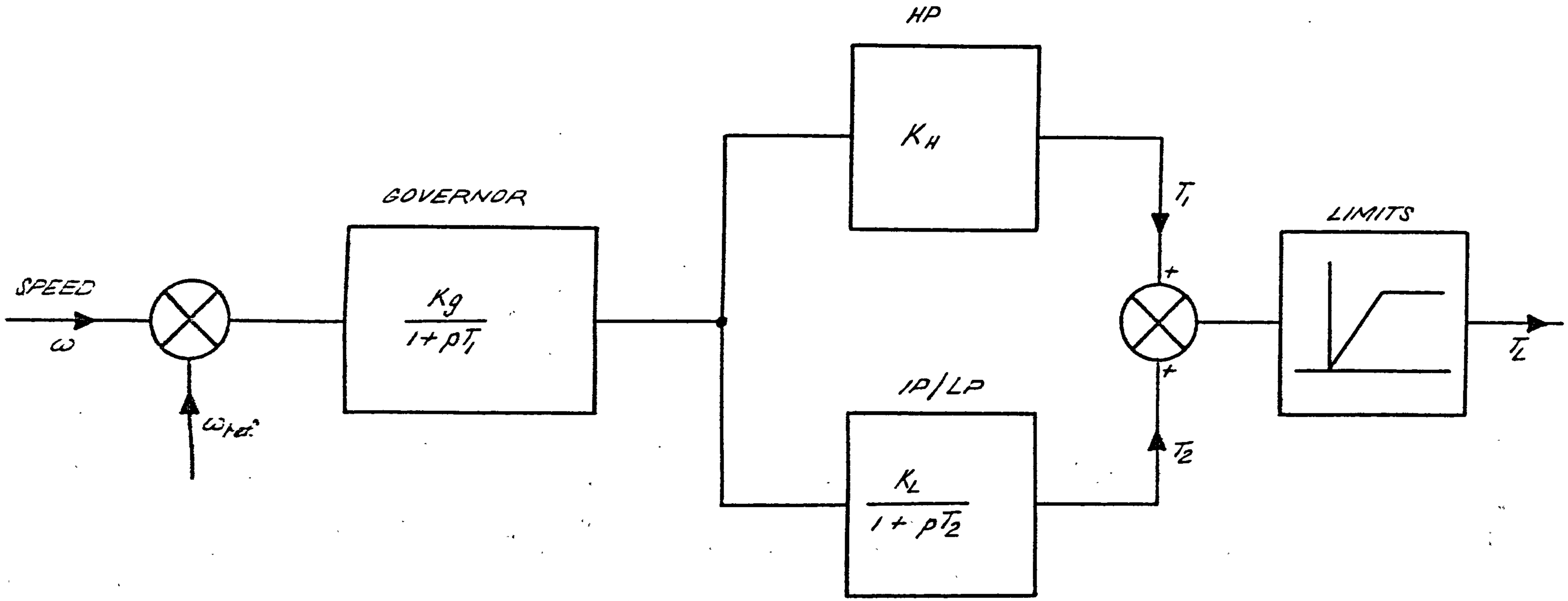

BLOCK DIAGRAM REPRESENTATION OF MECHANICALLY GOVERNED TURBINE

FIG 3.12

To complete the model, limits on the output torque of the turbine which are equivalent to zero and full load torque are included.

Dead band effects due to play and sticktion in the mechanical system are often represented for flyball systems but the present models are only intended for large disturbances where it is considered that these effects can be neglected.

3.5.2 Electrohydraulic systems

In the electrohydraulic or electronic governor systems, the majority of the mechanical delays of earlier systems have been eliminated, thus enhancing the role of the prime mover in controlling the transient behaviour. The system representation of Fig.3.14 is of necessity much more complex as all the transducer, valve and steam lags are included as separate entities. The velocity transducer includes an artificial phase advance term T_s to compensate for delays and provide intrinsic stabilisation, and the output electric analogue signal is divided into two channels for simultaneous control of governor and interceptor valves. The representation of the electrohydraulic valves at the present time is questionable as very few details of their operation are available, these being limited to total valve closure times at the moment. However, small signal perturbation tests have revealed that the valves exhibit a first order lag transfer function with a time constant of approximately the same as the closure time. This leads to the characteristic shown inset in Fig.3.13 which is the valve response to a 'fully open' command from the closed position. The travel is sharply limited when t is equal to the opening rate which corresponds to the control linkage hitting against a stop. The output in the representation is used as a multiplier for steam pressure and varies between zero and unity. In order to cater for a wide range of demands, the input to the lag function must also be limited to give a constant valve closure demand for large step inputs. This is calculated as follows:

The response for a first order lag to a step function is

$$\frac{V_o}{V_i} = 1 - e^{-t/T} \quad \text{where T is the time constant}$$

at $t = T$, $\frac{V_o}{V_i} = 1 - \frac{1}{e} = 0.632$

Substituting $V_o = 1$ gives $V_i = 1.582$ which is the input limit.

Even with throttle valves it is feasible to assume linear valve gains K_1

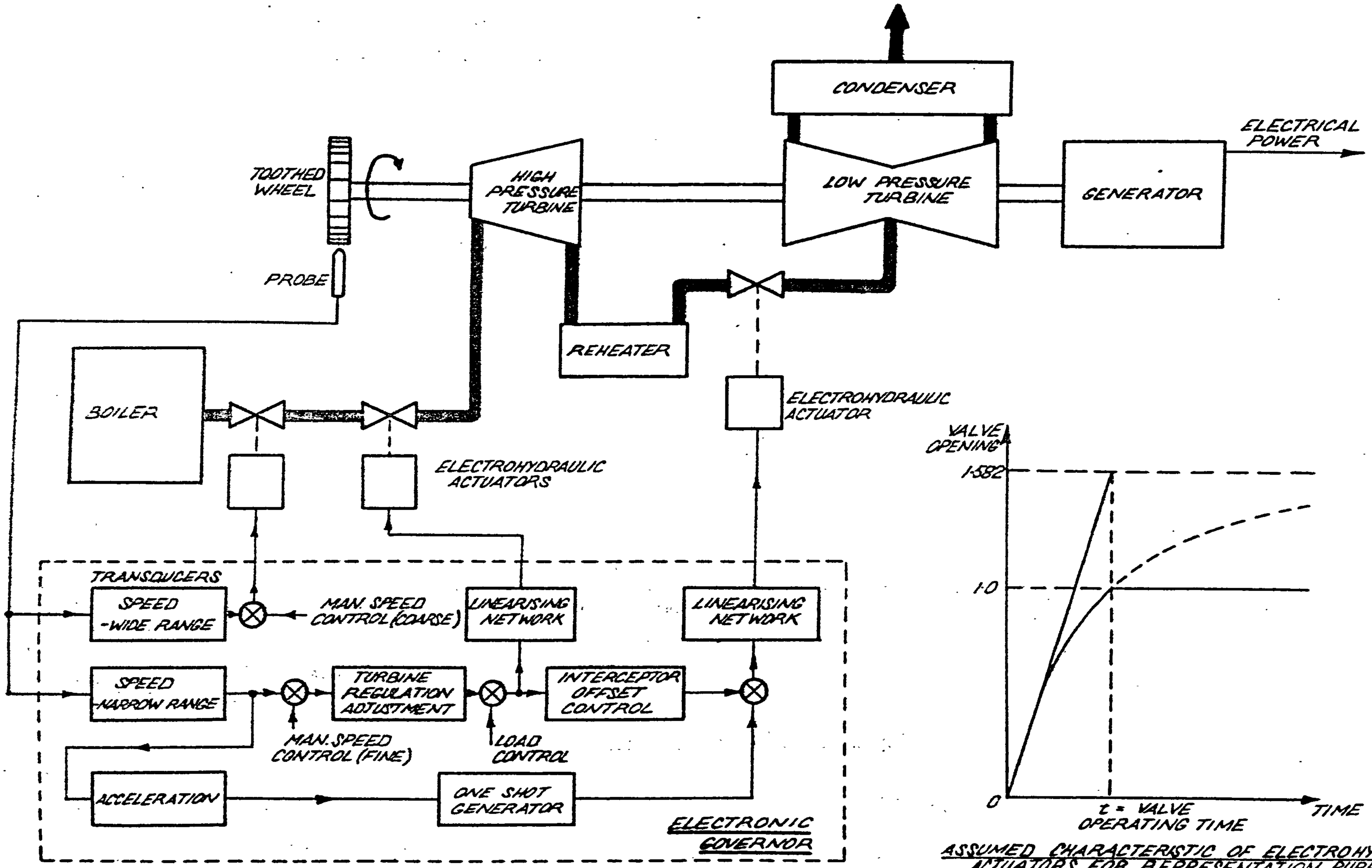

ELECTROHYDRAULICALLY GOVERNED TURBINE SYSTEM

FIG 3.13

and K_2 as artificial linearisation is provided either in the mechanical system by a cam arrangement, or in the electronic drive circuits by diode function generators.

The governor valves act upon the constant boiler pressure P_B in the multiplier M1, and the output feeds the HP turbine which is represented by the steam storage delay T_3. If desired, boiler dynamics could conveniently be added by making P_B the output of a series of boiler differential equations.

From the output of the HP turbine the HP torque complement (K_H) is extracted in a similar manner to the mechanically governed turbine model and the exhaust steam passes into the reheater which has a time constant T_{RH} which is very long. The interceptor valves control the reheated steam which passes into the LP sections and the steam storage delays are represented by T_4, after which the LP torque complement is extracted (K_L). The output mechanical torque is the sum of the HP and LP torque complements TL1 and TL2 as in the previous case.

In setting the initial loading conditions the valve settings are assumed to equal to ratio of initial load TLO to full load TFL (e.g. at half load the valves are set at half travel). The value of the torques before K_L and K_H must equal TLO.

$$\text{Reheater pressure } P_R = \frac{\text{TLO}}{\text{TLO/TFL}} = \text{TFL}$$

which is the correct result, as in practice the reheater pressure is constant down to very low loads. However, the gain of the reheater is now equivalent to TFL/TLO which is inversely proportional to the initial loading.

An added practical feature is the intercept value offset, represented as a constant bias, which can be used to set the LP stages at a proportionally higher loading factor than the HP cylinder.

Acceleration inputs are shown to the governor and interceptor circuits but these are for academic purposes at the moment. However an acceleration sensitive trip is provided on the latest systems which closes the interceptor valves for a certain length of time if the acceleration exceeds a set threshold level as for example under system fault conditions.

It must be noted that in order to simplify gain calculations, the portion of the governor/turbine model after the control valves is represented in per unit form thus giving direct relationships between pressures and torques. This is in contrast to the AVR systems where absolute values are used throughout.

4 GENERATOR DESIGN OPTIMISATION FOR INCREASED TRANSIENT STABILITY LIMITS

4.1 General

The transient stability limit of a power generating system will depend upon the following:

(a) Generator excitation and prime mover control systems,

(b) Turbogenerator design parameters,

(c) Transmission system configuration,

(d) Circuit breaker fault clearing times,

The effects of (c) and (d) above are widely appreciated and item (a) is dealt with in detail in Chapters 5, 6 and 7. Concerning item (b), very few turbogenerator design changes were made in the past, specifically for improving transient performance, but when the rapid increase of individual unit sizes took place in the early sixties it was apparent that the large machines would be more oscillatory due to reducing the inertia constants. In addition to this, various rotor design changes have been made in the last few years which have resulted in substantial variations of damping capabilities, and so it is worthwhile studying initially the effects of design parameter changes on the intrinsic stability of the generator.

The following sections are broadly classified into steady state, transient, and sub-transient parameters but the major emphasis in studying the results is applied to the subtransient effects in each case as these most affect the stability limits. Hence the peak of the first rotor angle swing is regarded as the most important quantity because this ultimately indicates whether the machine is stable or unstable, and the subsequent damping during the transient period, although of great interest, is of secondary importance. Other important quantities to be considered when making comparative assessments of results are the terminal voltage recovery and the induced currents in the rotor circuits.

In order to isolate the effects of the design parameters, the studies were performed on a single generator system without any form of excitation or turbine controls operating. The generator is initially operated at full load (500 MW) and rated power factor (0.85 lagging), and a symmetrical three-phase fault is applied to the high voltage side of the generator transformer for a length of time such that the generator just remains stable with the standard parameter set. With these conditions the model is highly sensitive to parameter variation as a detrimental change immediately causes the generator to become unstable and perform pole slipping excursions.

4.2 Steady state parameters

4.2.1 Short circuit ratio and saliency

The steady state parameters are normally decided by operating requirements such as generator active and reactive power output, system voltage, and winding heating, but according to the choice of these parameters, a substantial change in transient stability margin can result.

Fig.4.1 shows the effects obtained using various values of the mutual reactances χ_{md} and χ_{mq}. (For all the graphs, curve (a) is the result obtained using the standard parameter set see Appendix 11.3.1.)

Curves (b) and (c) were the results for varying both χ_{md} and χ_{mq} simultaneously, keeping the saliency constant at the designed value of 0.974. This is analogous to varying the short circuit ratio ($\simeq \frac{1}{\chi_d}$) which is more common in generator design terminology. From the rotor angle curves it is seen that doubling and halving the reactances increases and decreases respectively the initial steady state operating point. This has the effect of varying the transient stability margin or in other words the amount that the rotor is able to swing without becoming unstable.

From Section 2.3.3 the initial steady state rotor angle is calculated as

$$\delta_o = \arctan\left(\frac{I_a\chi_q\cos\phi}{V_T+I_a\chi_q\sin\phi}\right) + \arctan\left(\frac{I_a\chi_t\cos\phi}{V_T-I_a\chi_t\sin\phi}\right)$$

this may be rewritten as

$$\delta_o = \arctan\left[\frac{P}{\left(\frac{\sqrt{3}V_T^{\,2}}{\chi_q}\right)+Q}\right] + \arctan\left[\frac{P}{\left(\frac{\sqrt{3}V_T^{\,2}}{\chi_t}\right)-Q}\right] \qquad \ldots(4.1)$$

Thus for the constant system and loading conditions considered, the initial rotor angle depends directly upon the quadrature axis synchronous reactance only. This is borne out by the rotor angle curves (d) and (e) in which the saliency was altered to 0.5 and 2.0 respectively, keeping the direct axis reactance χ_{md} the same. It is seen that the earlier effects of varying both reactances together are really caused by χ_{mq} alone as almost identical results were obtained varying only this parameter.

From inspection of equation (4.1) it can be seen that a reduction in the steady state rotor angle can also be achieved by either decreasing the transmission reactance or increasing the generator voltage rating. The latter would appear to be more effective due to the squared term, but in

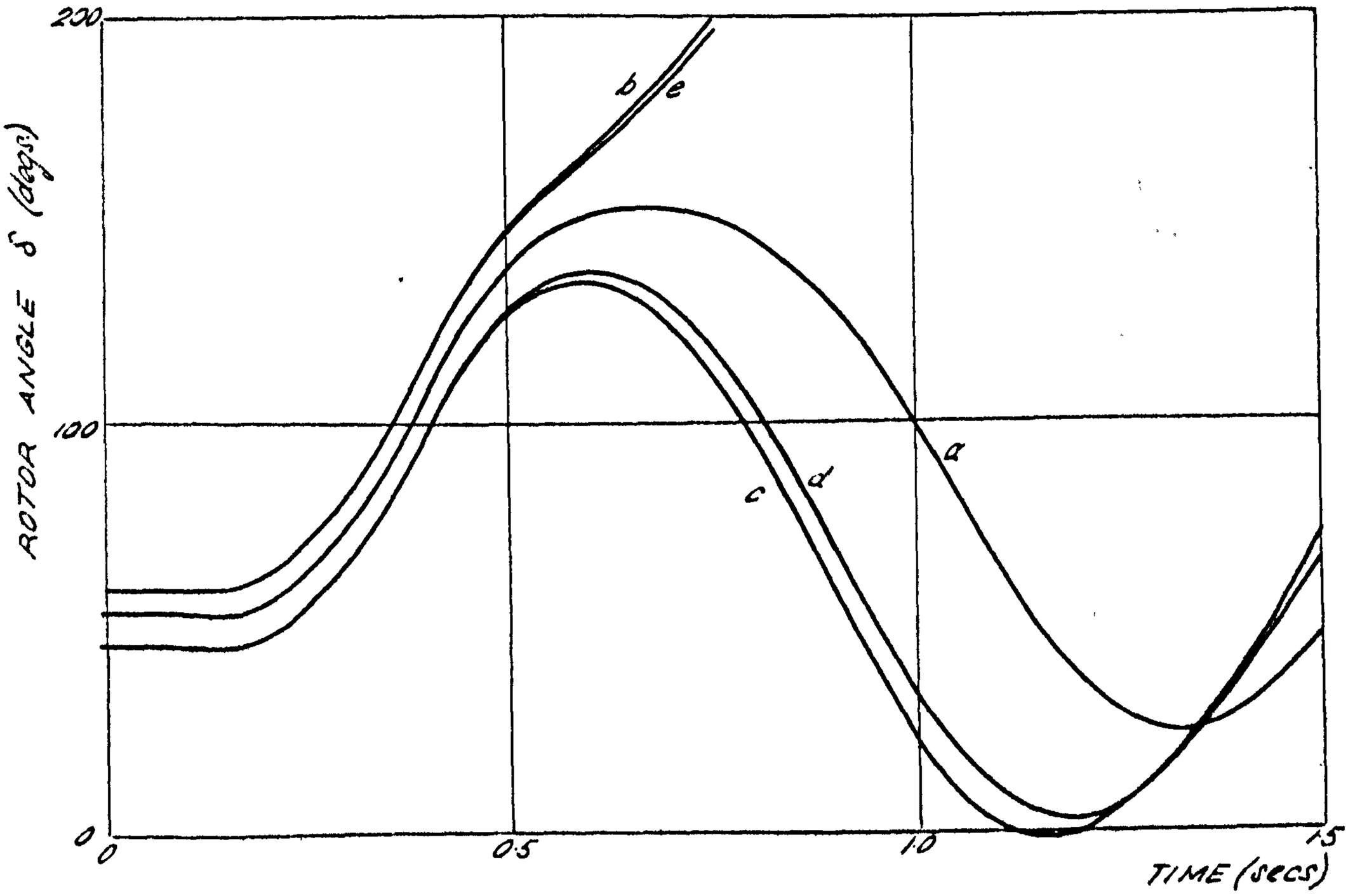

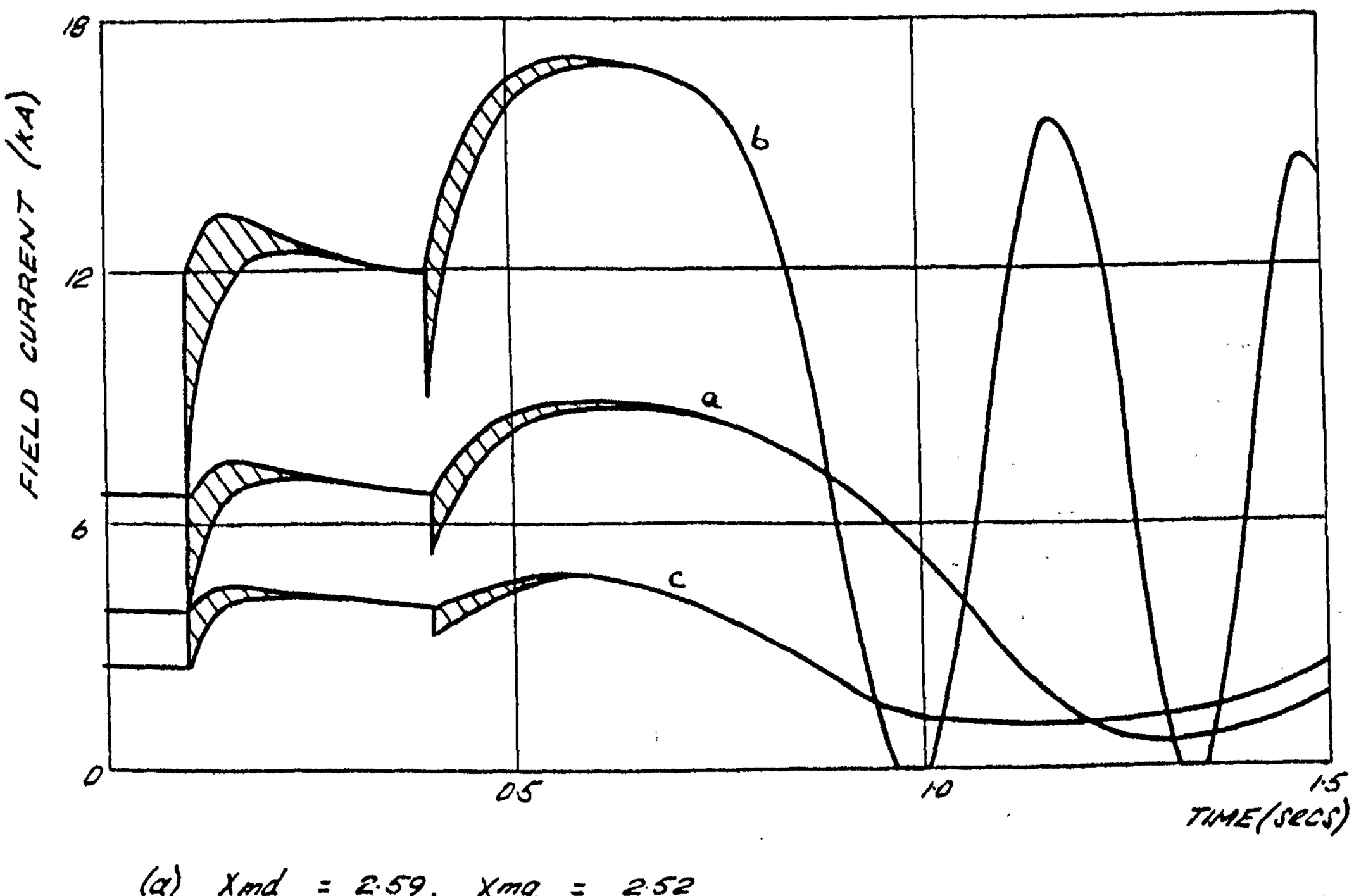

(a) $X_{md} = 2.59$, $X_{mq} = 2.52$
(b) $X_{md} = 5.18$, $X_{mq} = 5.04$
(c) $X_{md} = 1.29$, $X_{mq} = 1.255$
(d) $X_{md} = 2.59$, $X_{mq} = 1.29$
(e) $X_{md} = 2.59$, $X_{mq} = 5.18$

EFFECT OF VARIATION OF SHORT CIRCUIT RATIO AND SALIENCY

FIG 4.1

common with all design changes must be viable on economic grounds.

The plot of an arctangent function is asymptotic to 90^{o}, and therefore any changes in the bracketed quantities of equation (4.1) will have a diminishing return at higher steady state rotor angles. Thus, if the machine is to be operated mainly in the leading power factor region as in the case of a synchronous condenser, little advantage could be gained by consideration of the design changes discussed above.

Changing the synchronous reactances had little or no effect on the oscillatory nature of the generator, the frequency of oscillation and the peak to peak swings of curves (a), (c) and (d) of Fig.4.1 were nearly the same. (Curves (b) and (e) could not be considered due to instability.) The phase change of curve (a) was caused by a prolonged dwell period at the peak of the first swing due to the close proximity to the transient stability limit.

The initial setting of field current was much higher with the increased value of χ_{md}, which is surprising since the reverse would be expected from Section 2.3.3, where field current is calculated initially as

$$I_{fd} = \frac{E_f}{\chi_{md}} .$$

The anomaly was discovered to be due to the value of base field current which had increased by a large proportion, so that although the per-unit field current was smaller when multiplied by the large base value to give the absolute field current, this was abnormally high. The field current base depends upon the field current required to produce one per unit armature voltage on open circuit (I_{fa}). This should be much smaller with a high value of χ_{md} as the slope of the air gap line is increased and so the correct field current base should have been also smaller. As the open circuit curve was only available for the standard parameter set, no values of I_{fa} for the other case considered could be determined. However the results serve to illustrate the pitfalls in studying parameter variations indiscriminately without the consideration of possible secondary effects.

The decay of the field current during the fault and the magnitude of the fundamental oscillations was not noticeably altered. These effects are determined by the direct axis transient reactance and short circuit time constant, which are derived in Ref.14 in terms of Park's parameters as:

$$T_d' = \frac{1}{\omega_o r_{fd}} \left(\chi_{\ell fd} + \frac{\chi_{md} \chi_{\ell d}}{\chi_{md} + \chi_{\ell d}} \right) \qquad \ldots(4.2)$$

$$\text{and } \chi_d' = \chi_{\ell d} + \frac{\chi_{md} \chi_{\ell fd}}{\chi_{md} + \chi_{\ell fd}} \qquad \ldots(4.3)$$

Substituting the standard parameter set for the 500 MW machine in equations (4.2) and (4.3) gives values of T_d' and χ_d' of 0.945 sec. and 0.363 p.u. respectively. If χ_{md} is doubled these values only increase for 0.967 and 0.367, a change of less than 2½% in both cases.

4.2.2 Armature leakage reactance

Referring to Fig.4.2 the value of armature leakage reactance has a marked effect on the rotor angle swing giving a first swing stability improvement of nearly 30^o with the low value of leakage, curve (c). With a high value of leakage reactance, curve (b), the rotor succumbs to instability in a very short time. As the quadrature axis armature leakage was assumed equal to that of the direct axis in all cases, the quadrature axis synchronous reactance would also change by a small amount which gave a slightly increased initial rotor angle as explained in the previous section.

The armature leakage reactance is the major component of both transient and subtransient reactances and reducing this quantity caused an increase in the magnitude of the fundamental frequency components as indicated by the field current oscillogram. However, the decay of these components is reduced and this is borne out by a reduction in the calculated direct axis short circuit time constant from the designed value of 0.945 seconds ($\chi_{\ell d}$=0.21), to 0.61 seconds with a leakage of 0.07 p.u.

Referring to Fig.4.3, 50 Hz components are also predicted on the terminal voltage response which would appear as a pronounced second harmonic on the actual AC voltage waveforms. The recovery of terminal voltage after clearing the fault was also improved with lower values of armature leakage.

4.2.3 Armature resistance

Referring to Fig.4.4, the armature resistance also affected the rotor angle swing considerably and in this case improved stability was obtained with increased values. This is feasible as a larger armature resistance dissipates more power when the fault current is flowing, thus reducing the imbalance of power between generator and prime mover during the fault period. This produces a smaller accelerating torque and hence a lower swing.

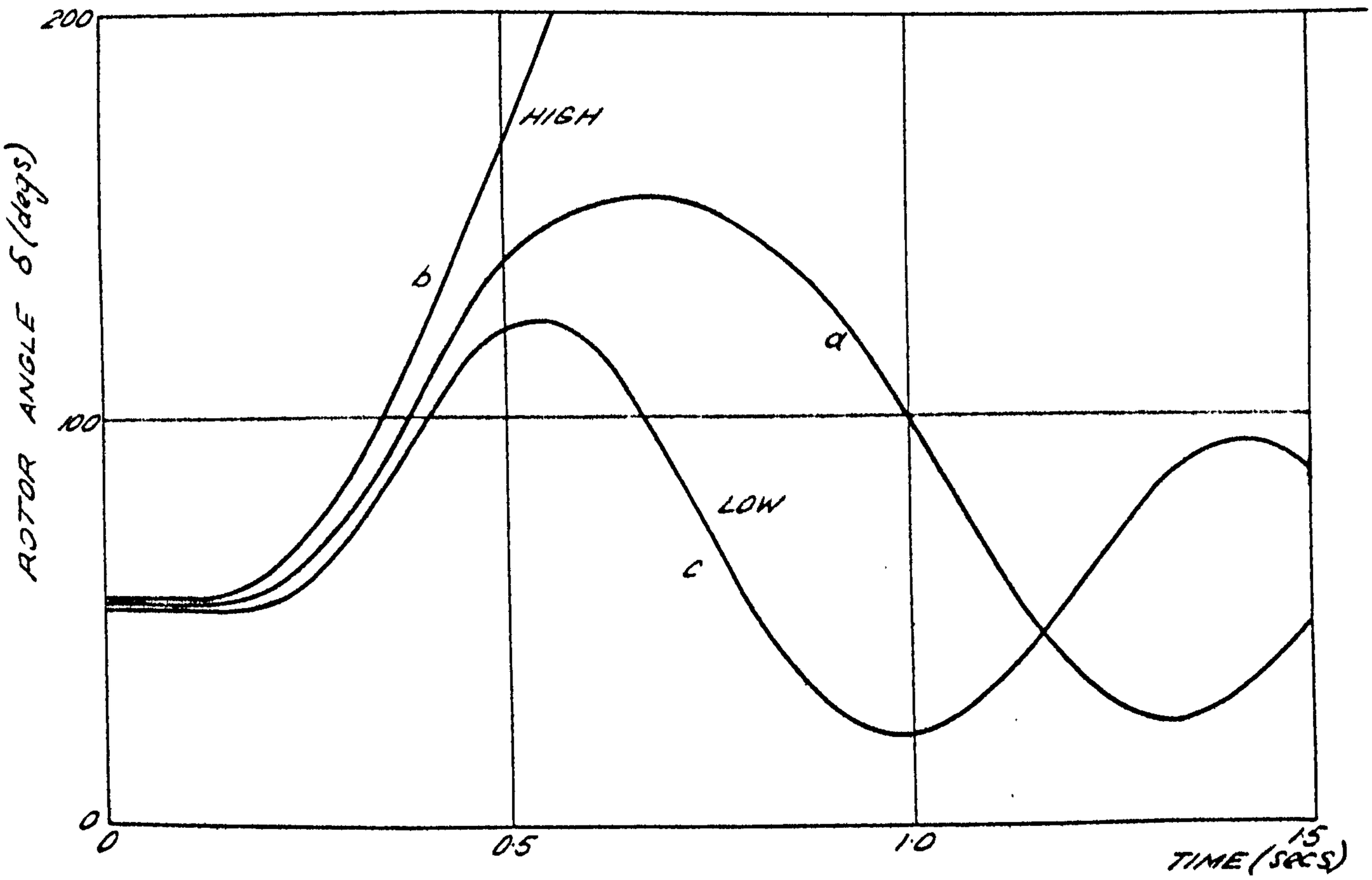

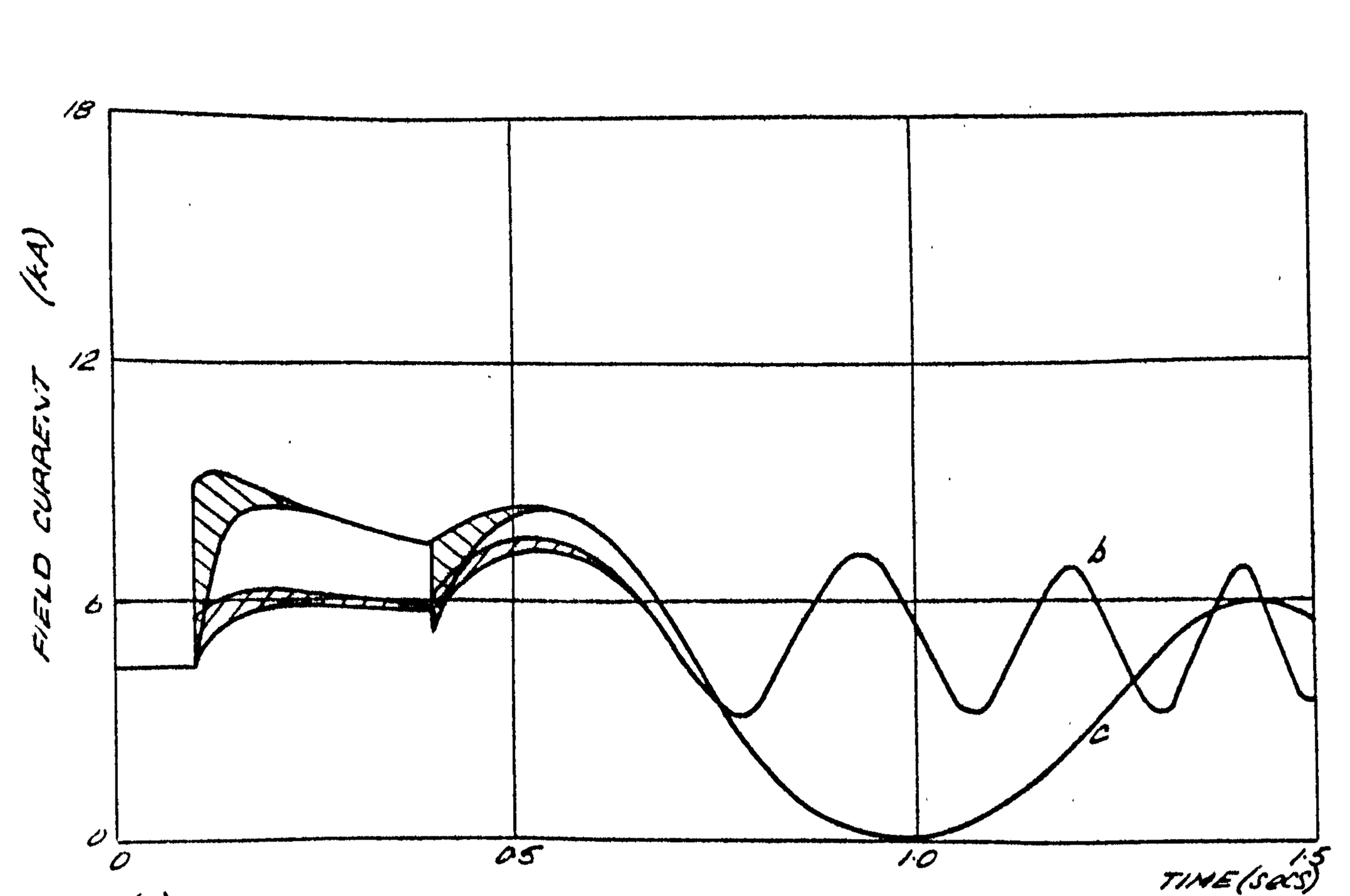

(a) x_{ed}, x_{eq} = 0·21
(b) x_{ed}, x_{eq} = 0·70
(c) x_{ed}, x_{eq} = 0·07

EFFECT OF VARIATION OF ARMATURE LEAKAGE REACTANCE

FIG 4.2

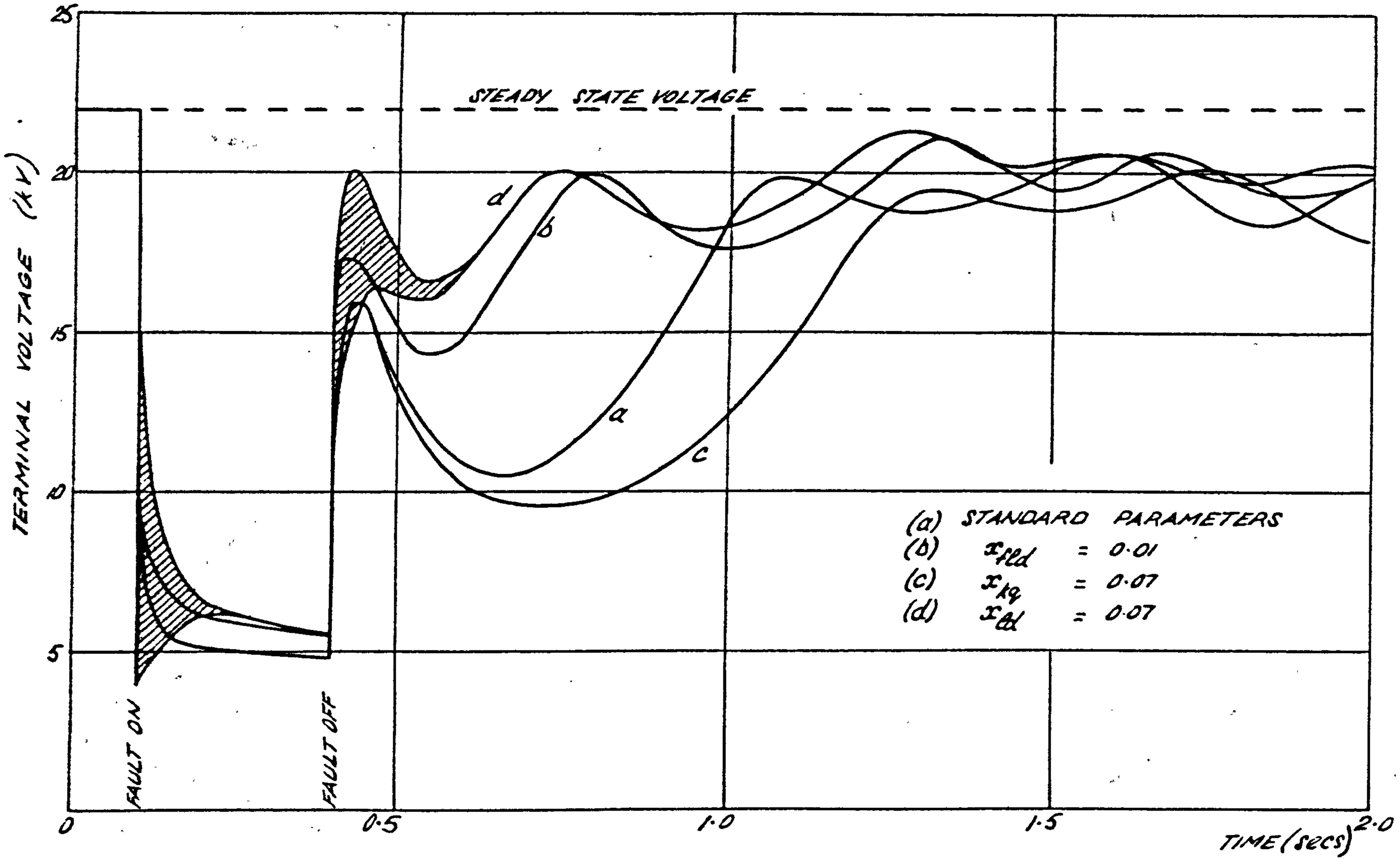

EFFECT OF GENERATOR REACTANCES ON TERMINAL VOLTAGE RECOVERY

FIG 4.3

Very few differences in the field current fundamental frequency quantities were observed but the transient field current swing after clearing the fault was somewhat higher in the unstable case.

A higher armature resistance also improved the terminal voltage recovery (Fig.4.5), but this was accompanied by an increase in the second harmonic component after fault removal.

4.3 Transient parameters

4.3.1 Field leakage reactance

The field leakage reactance represents the so called 'transient', reactance effects of the classical theory but it is seen from Fig.4.6 to affect both transient and subtransient performance. Decreasing the reactance by one order of magnitude gave an improvement of 19^{o} on the first peak rotor angle swing and further, the oscillations were damped out in a shorter period. Increasing the reactance from 0.16 to 0.5 produced instability on the first swing.

A large effect is produced on the field current oscillogram where reducing the field leakage reactance from 0.16 p.u. to 0.01 p.u. increased the fundamental frequency component by approximately five times in addition to increasing the transient effects. From Section 4.2, it is seen that variations in the transient field current swings produced little effect on the rotor angle swing and so in this case the improvement in the swing curves of (b) and (c) may be due to the increase of the fundamental frequency components induced in the field and rotor circuits.

The phenomena of field damping effects is well known and indeed earlier generator models included these effects alone, the electrical damping effects of the damper windings being neglected. This would seem to be anomalous as the damper windings have a large damping contribution, although of shorter duration as they are short circuited. In the case of the field circuit, the current will be affected by the output impedance of the exciter, and when an AC exciter is used the rectifiers prevent the flow of negative field current which effectively open circuits the field winding causing large induced voltages.

Decreasing field leakage reactance also had a beneficial effect on the terminal voltage, curve (b) of Fig.4.3, where the depressed voltage during the fault and the subsequent recovery were both increased. However in all cases without a voltage regulator, the terminal voltage was not restored to the steady state value until the transient had completely subsided, which was of the order of five seconds.

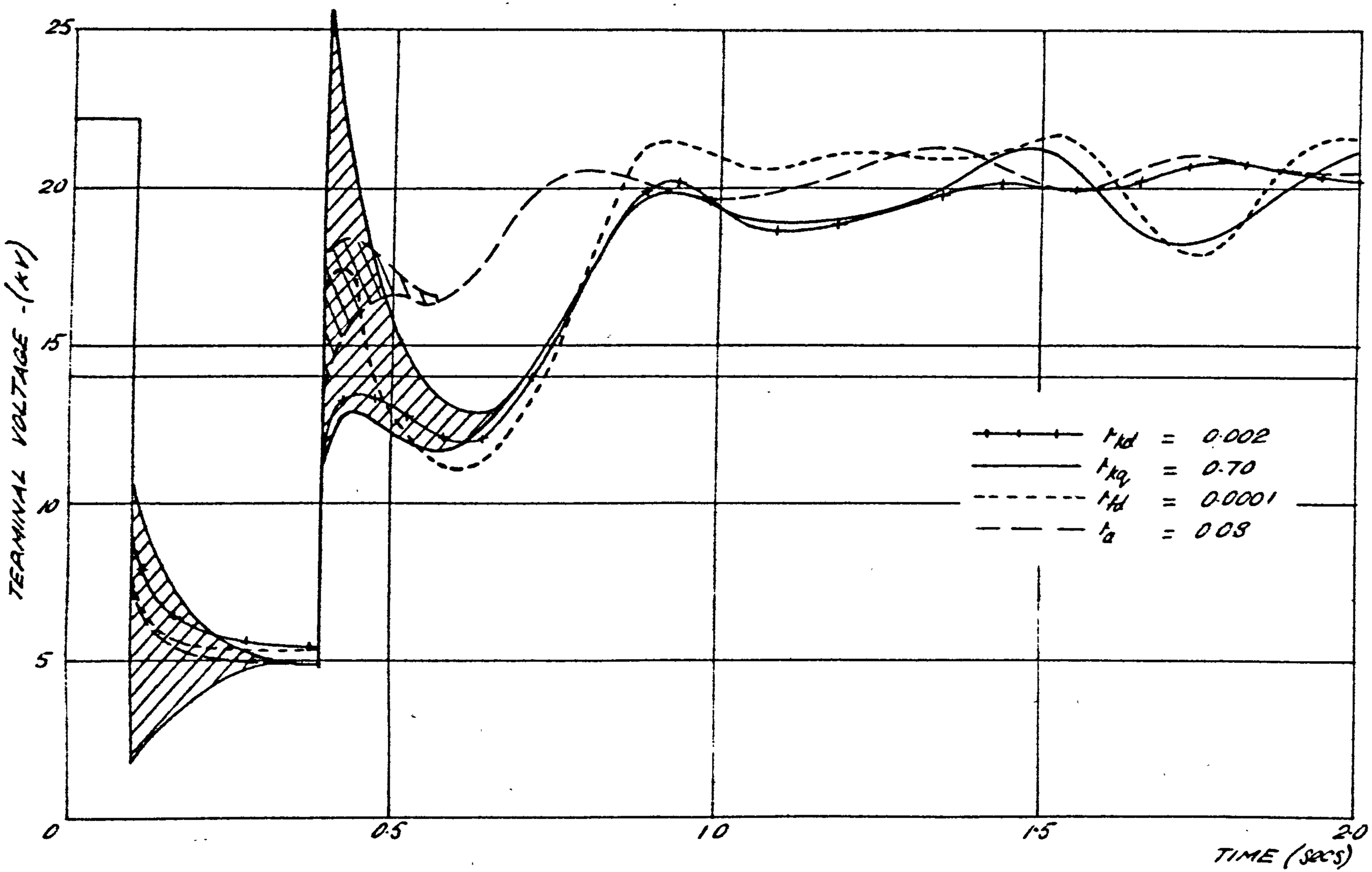

EFFECT OF GENERATOR RESISTIVE PARAMETERS ON TERMINAL VOLTAGE RECOVERY

FIG 4.5

4.3.2 Field resistance

The major effect of this parameter is on the direct axis short circuit time constant of the machine (see equation 4.2). This agrees with the field current oscillograms of Fig.4.7 where using a high value of field resistance produced a fast decay of the mean value of the field current during the fault.

The rotor angle initial swing was improved by decreasing R_{fd} but the benefit was fairly small, being of the order of 4^{o} less on the peak for a change in field resistance of one order. This also produced an undesirable increase in the peak to peak swing so that the first underswing entered the motoring region.

4.3.3 Inertia effects

The inertia is included here under the transient parameters as it affects the frequency of oscillation of the rotor swings. The inertia constant or acceleration time constant H is more commonly used than moment of inertia and Fig.4.8 shows that large values of H cause the rotor to behave in a lethargic manner to a transient disturbance. This is an obvious advantage in withstanding large disturbances as the first peak rotor angle swing is reduced by a large amount and slower exchanges of power with the system are produced. With a low inertia constant the rotor accelerated very quickly during the fault, which is expectable and soon reached instability.

4.4 Subtransient parameters

4.4.1 Damper winding leakage reactances

The direct axis damper leakage reactance had the least effect of all the machine parameters (with the exception of χ_{md}) on the oscillations of rotor angle (Fig.4.9a). Reducing it from the designed value of 0.02 p.u. to 0.007 p.u. produced only a very slight improvement in the peak of the first swing and further reduction to 0.002 p.u. produced virtually no effect whatsoever. Furthermore, a detrimental change caused by increasing χ_{kd} by a factor of ten did not provoke instability as was the case with many of the other parameters.

The main difference in machine performance due to changing χ_{kd} was observed on the fundamental frequency components. These were very much more pronounced with the high value of damper leakage reactance as shown by Fig.4.10. In this and some other respects, the effect is the reverse of that observed by changing field leakage reactance and although the two

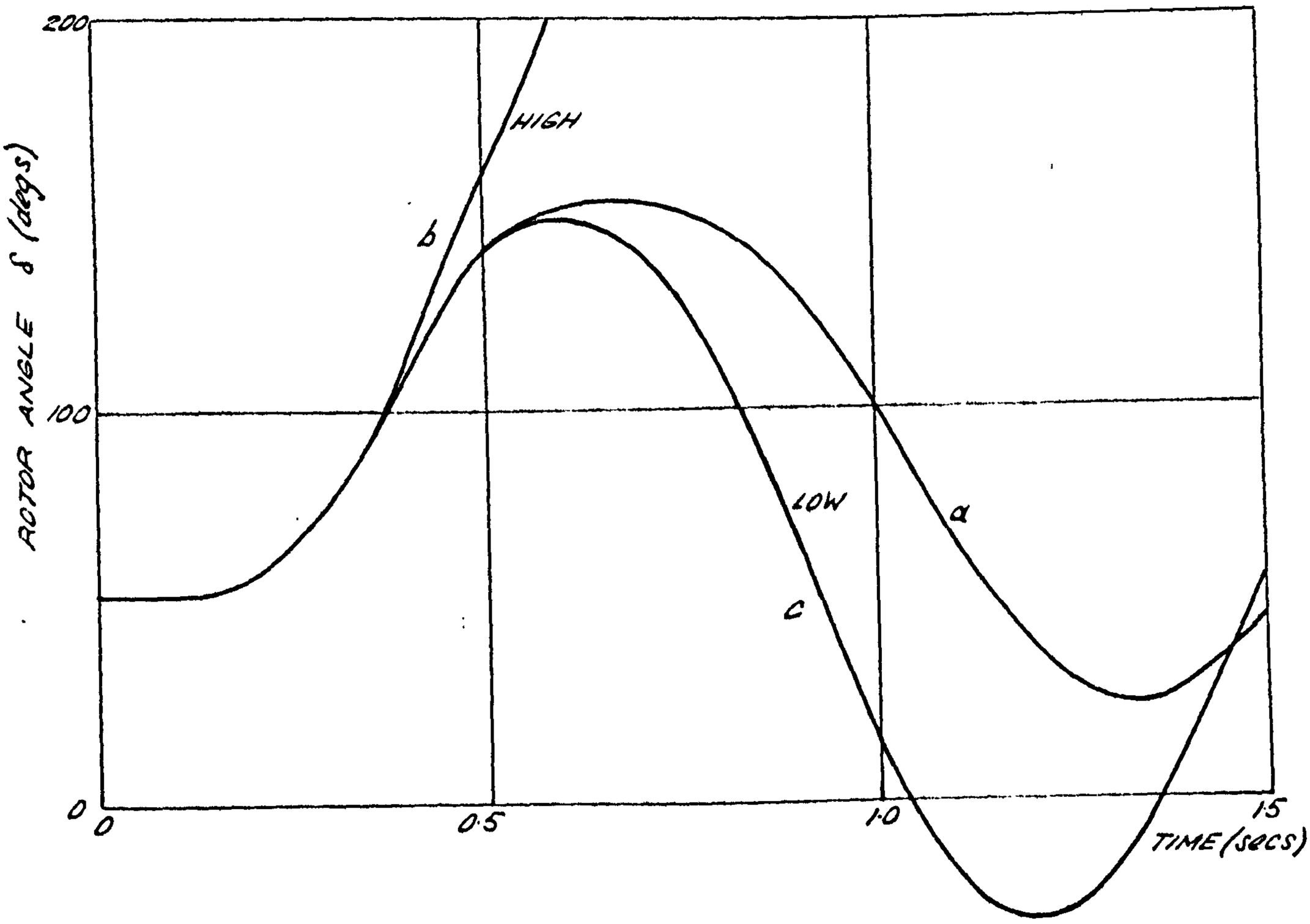

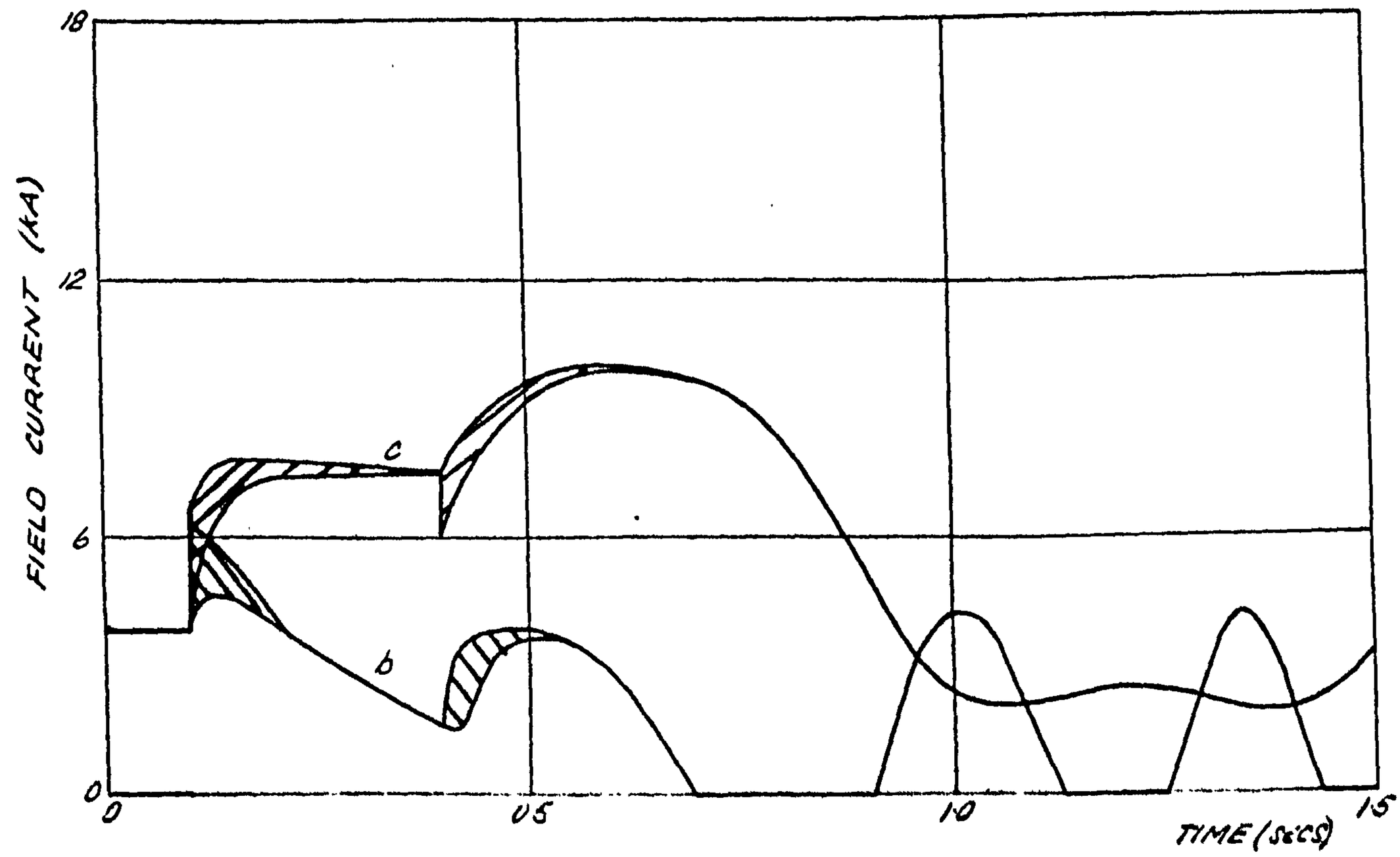

(a) r_{fd} = 0·0012
(b) r_{fd} = 0·01
(c) r_{fd} = 0·0001

EFFECT OF VARIATION OF FIELD RESISTANCE

FIG

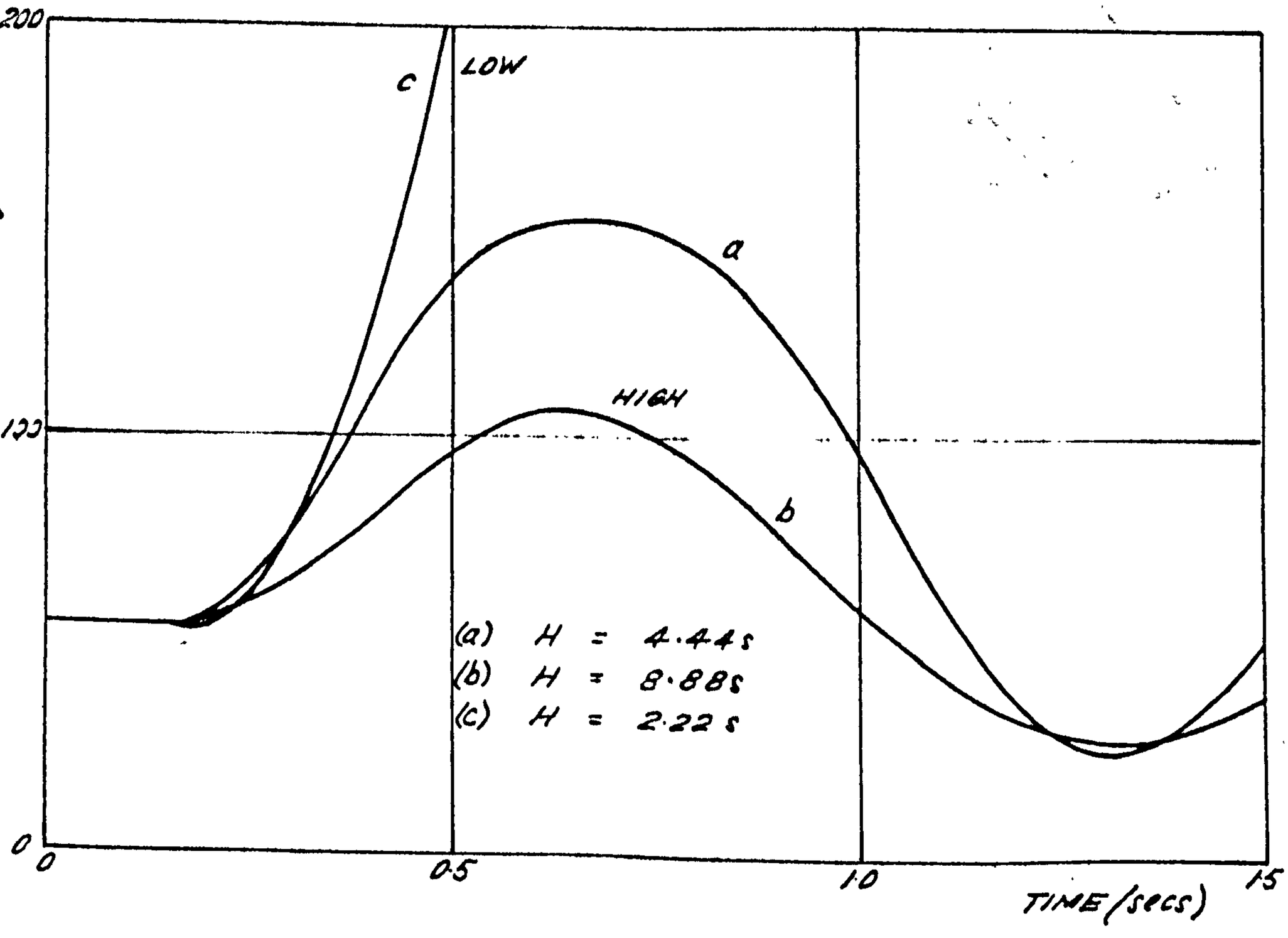

EFFECT OF INERTIA CONSTANT

FIG 4.8

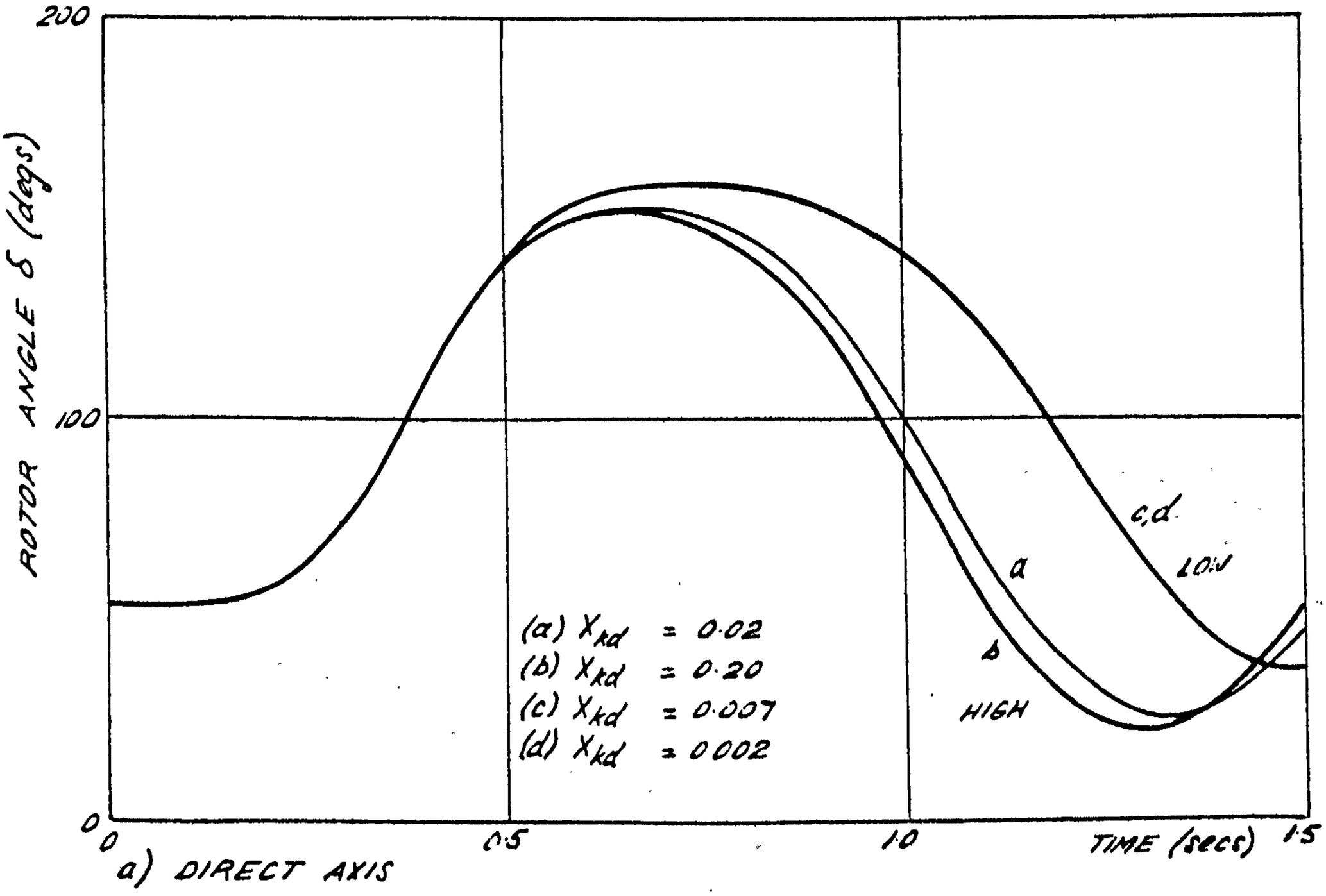

a) DIRECT AXIS

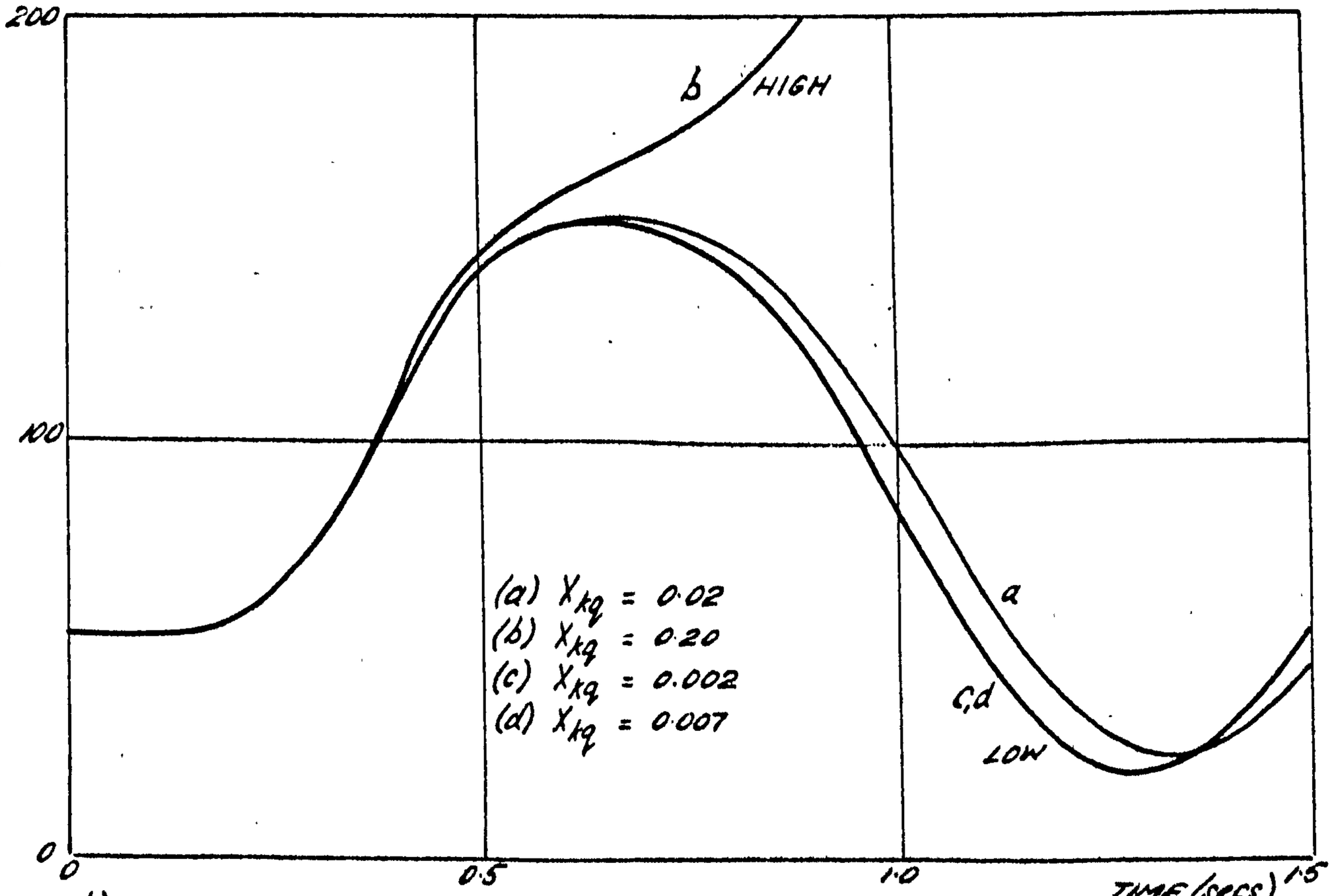

b) QUADRATURE AXIS

EFFECT OF VARIATION OF DAMPER LEAKAGE REACTANCES

FIG 4.9

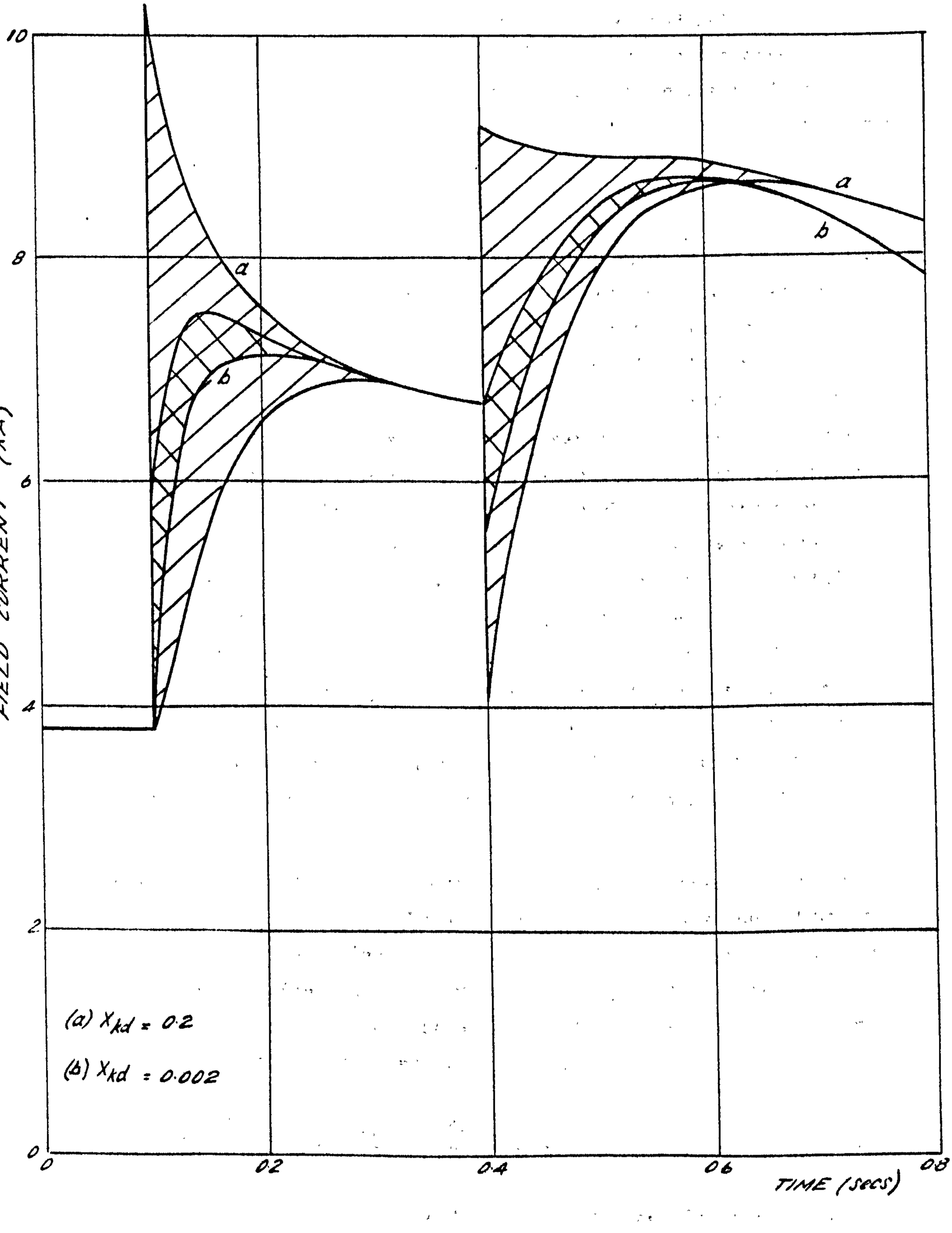

EFFECT OF DIRECT AXIS DAMPER LEAKAGE REACTANCE ON FIELD CURRENT OSCILLATIONS

FIG 4.10

circuits are theoretically in the same positions in the physical fulfilment of the model, they have different electrical characteristics.

Changing the quadrature axis damper leakage reactance had only slightly more effect on the dynamic oscillations to similar changes in the direct axis quantity (Fig.4.9b). In this case no differences were observed on the field current oscillogram but the terminal voltage recovery was deteriorated with increased values of X_{kq}.

4.4.2 Damper winding resistances

Referring to Figs.4.5,4.11 and 4.12, in general, damper resistance changes had a greater effect on the swing curve than equivalent reactance changes. Improved stability was achieved with a lower value of the direct axis resistance, but in the quadrature axis the resistance had to be increased to obtain a performance improvement. It is now not an unusual practice to employ a complete damper winding copper circuit on turbogenerator rotors, but from the above it would appear that the quadrature axis portion is unnecessary and indeed would probably have a detrimental effect on stability if included. However it is not possible to generalise from the relatively few results obtained and this fact can be illustrated by curves (b) and (c) of Fig.4.11b where decreasing R_{kq} to a very small value reversed the trend and caused an improvement in the performance. Hence it appears that there is a worst case setting for the parameter R_{kq} and it is not unlikely that an optimum value also exists as curves (d) and (e) are extremely close. The same may apply for the direct axis damper resistance R_{kd} and the subject would be worthy of a much more exhaustive investigation beyond the scope of the present study.

The magnitude of the field current oscillations was affected by the direct axis damper resistance R_{kd} only. The noticeable features are the extremely large 50 Hz components with a high R_{kd} and a longer build-up time of the mean field current during the fault with a low value of R_{kd}. The latter is explained by the increase of the direct axis subtransient short circuit time constant T_d'' which is inversely proportional to R_{kd}[14]

$$\text{i.e.} \quad T_d'' = \frac{1}{\omega_o R_{kd}} \left(X_{kd} + \frac{X_{md} \cdot X_{\ell d} \cdot X_{\ell fd}}{X_{md}X_{\ell d} + X_{md}X_{\ell fd} + X_{\ell d}X_{\ell fd}} \right) \qquad \ldots(4.4)$$

This time constant is also directly dependent upon the direct axis leakage reactance, the effect of which can just be perceived from Fig.4.10.

Terminal voltage recovery was not affected to any extent by either R_{kd} or

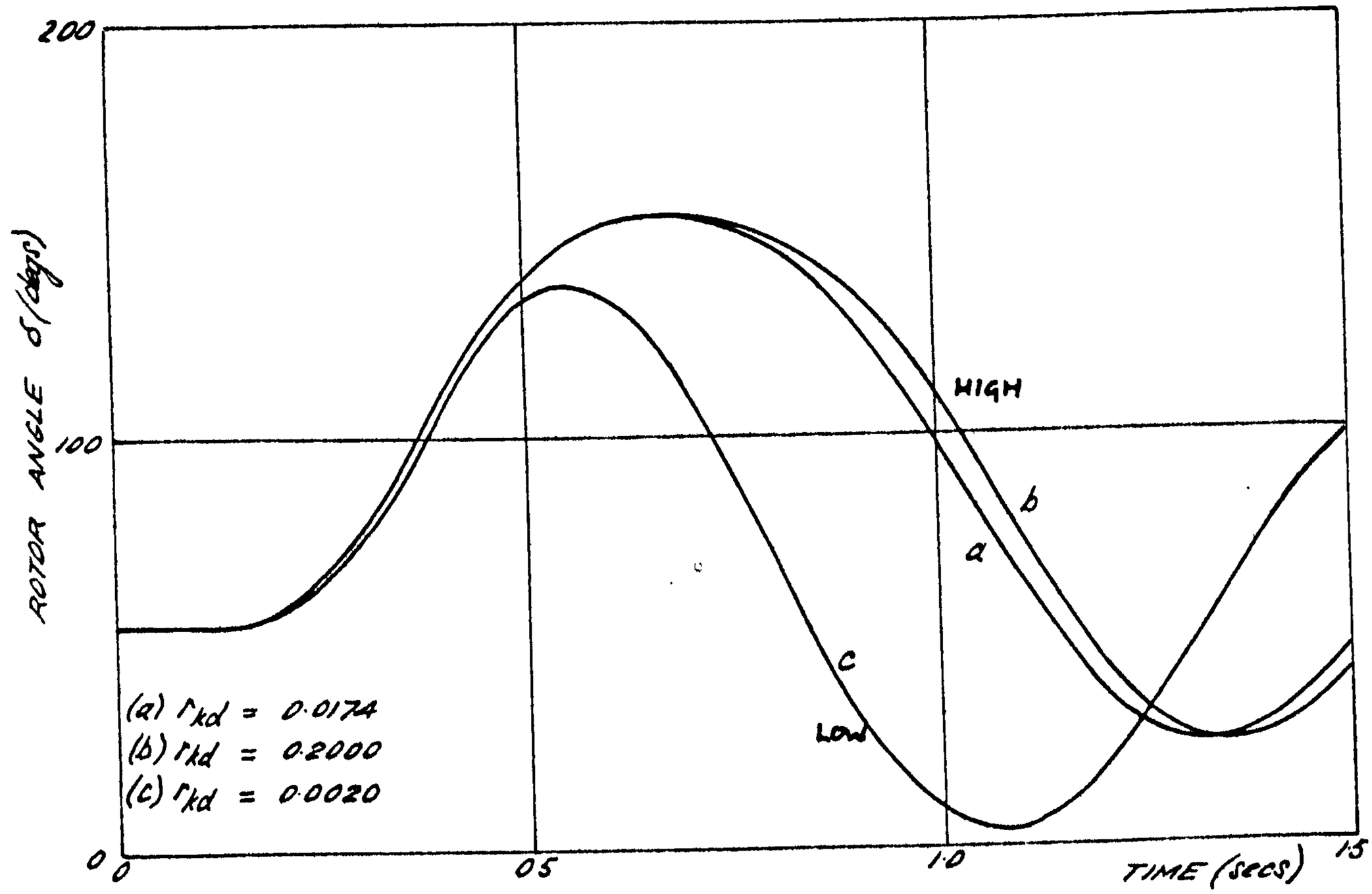

(a) DIRECT AXIS

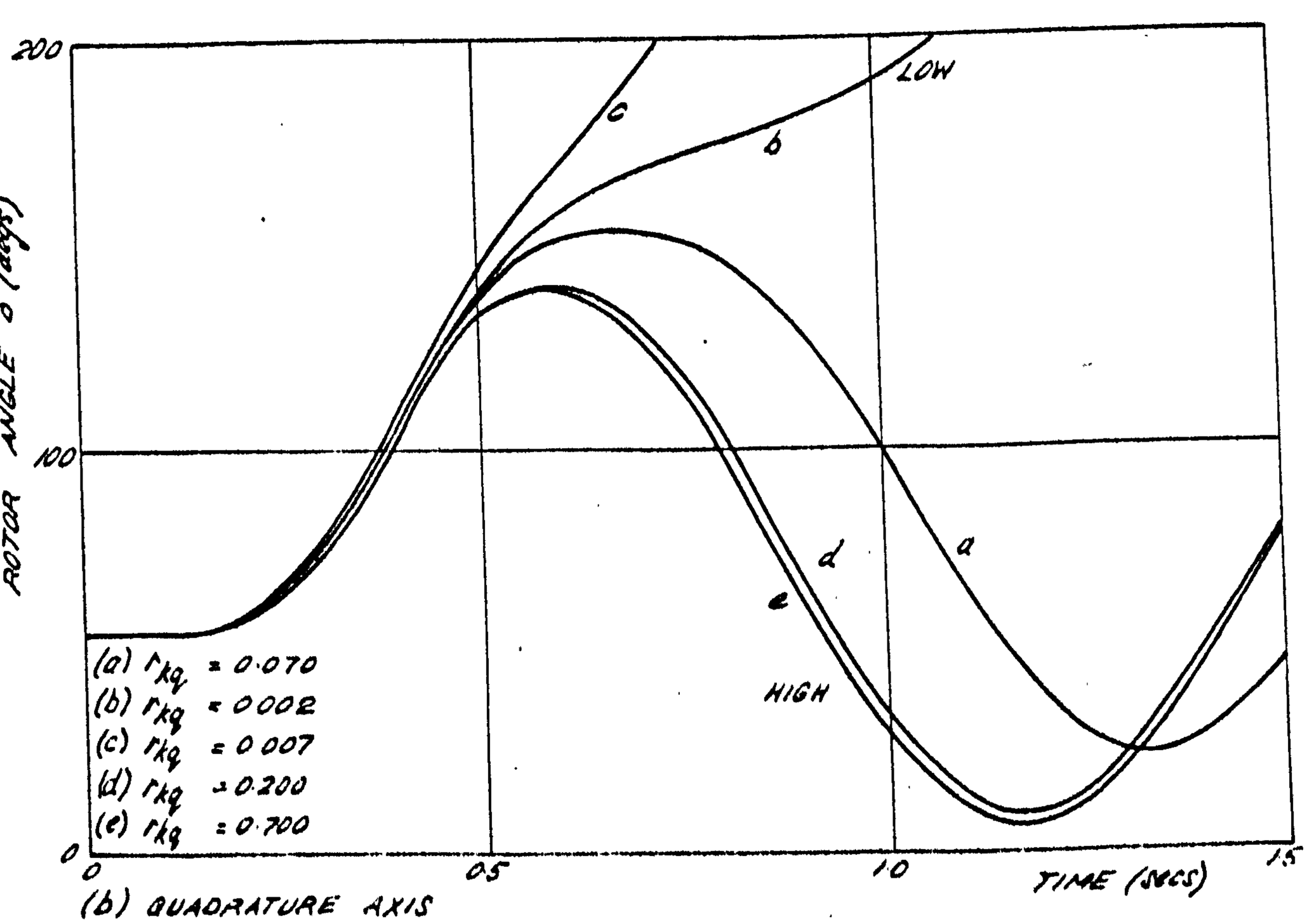

(b) QUADRATURE AXIS

EFFECT OF DAMPER RESISTANCES ON ROTOR ANGLE EXCURSIONS

FIG 4. 11

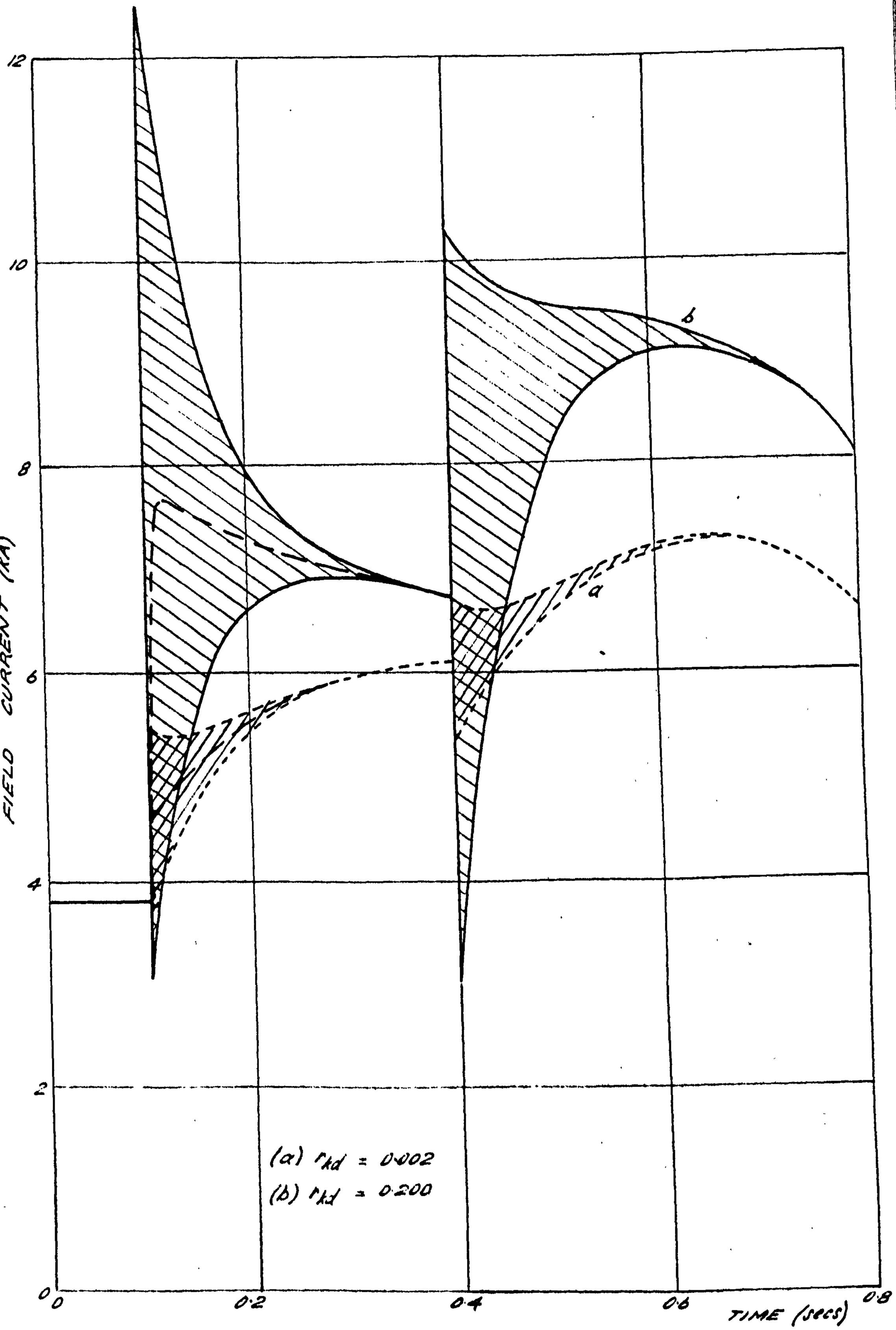

EFFECT OF DAMPER RESISTANCE ON FIELD CURRENT OSCILLATIONS

FIG 4.

R_{kq} but very large second harmonic components were produced both during and after the fault by a high quadrature axis damper resistance.

4.5 Practical scope of generator parameter changes

The design of large generators is usually custom tailored to meet the specified individual power system requirements of each generating station. These are normally steady state load requirements such as voltage and power factor, and the parameters are arrived at after thermal and mechanical limitations have been taken into account. Due to lack of theoretical background on the effect of parameters on the transient behaviour of turbogenerators, little account has been taken in the past of the stability performance of generators at the design stage. As stability problems have become more serious since the early sixties however, the power generating utilities have expressed growing interest in the design of more dynamically stable turbogenerators. The previous sections have given an initial insight into the required alterations in generator parameters for improving the transient performance but this is of little value unless the practical feasibility of implementing these changes is assessed.

From the analysis of the effects of short circuit ratio and saliency it is concluded that the quadrature axis mutual reactance χ_{mq} should be as small as possible to produce the greatest stability margin. This would be achieved if the air gap was increased or the amount of iron in the quadrature axis portion of the rotor reduced. It would seem that these are mutual requirements, because if the air gap is increased, the excitation demands are also increased and a larger field winding is necessary unless more advanced cooling is employed. Thus larger field winding slots are milled out of the quadrature axis portion of the rotor which cause a reduction in χ_{mq}. In order to effect a small increase in the air gap the stator bore would have to be increased in proportion which produces a much larger increase in the weight of the stator causing cost and transport problems.

In the case of all the winding leakage reactances, the best dynamic performance was obtained with the smaller values in every case. To reduce armature and field leakage flux by an appreciable amount is a difficult task, but some improvement can be obtained by alternative slot shapes and dimensions[40,41]. For reducing the leakage of the damper windings, these should be situated as near to the rotor surface as possible. The use of continuous low resistance slot wedges which are shorted at their extremities by the conducting end caps is an arrangement which meets these requirements.

A low field leakage reactance produced large induced currents in the excitation winding and the associated impressed voltages may involve serious insulation problems. With this quantity, and to some extent the armature leakage reactance, any changes must be arrived at after determining whether stability or insulation problems are the most demanding.

For the resistances, no general rule can be formulated to produce a stability improvement. Increasing R_a gave a much reduced peak rotor angle swing, but in practice this would cause additional stator losses and the enormous cost of designing more effective stator cooling, together with the reduced efficiency could not be justified. Only a small improvement was indicated by considering variations of R_{fd} but in this case the desired effect was produced by a reduction in the field resistance. This is viable and as the natural trend is towards increased excitation requirements in any case, the value of R_{fd} will be automatically reduced in future designs.

From the studies of the effects of damper resistances it appears that different requirements occur in the direct and quadrature axes. The best stability improvement was obtained with a high value of R_{kq} and a low value of R_{kd}. The latter also produces more effective field shielding which reduces the induced field components considerably. This indicates that a complete cylindrical damper cage may not be the ideal answer and a better arrangement would be to incorporate some method of impeding the flow of quadrature axis damping currents. For machines without a damper winding which rely on rotor body current damping, this is achieved naturally by the presence of the excitation winding slots. However damper windings are becoming common on the latest fully slotted rotors and one way of obtaining a higher quadrature axis resistance, would be to discontinue the end shorting rings at the inter-polar positions.

Finally, the study of the only mechanical parameter in the generator model, the inertia constant, indicates that this quantity should be large in order to retard the rotor oscillations. Unfortunately the reverse is the general design trend as generator sizes increase due to the increase in length of the machine rather than the diameter which has a lesser effect on the increase of the moment of inertia, i.e. the inertia per MW generated is tending to fall off as specific output increases.

4.6 Summary and conclusions

The studies prove that each electrical parameter of the generator has a realisable contribution to the dynamic behaviour of the rotor under large

disturbance conditions. The one exception is, rather suprisingly, the direct axis mutual reactance. The quadrature axis mutual χ_{mq}, altered the initial rotor angle setting and hence the stability margin of the system. A reduction in any of the leakage reactances produced better performance but the effects due to the resistances did not comply to such a simple formula. The direct axis resistances (i.e. R_{fd} and R_{kd}) needed to be reduced for better stability but the armature and quadrature damper resistances produced the opposite effect. In addition a worst case value for R_{kq} was forecasted.

The induced field current during and immediately after the fault was affected only by the direct axis quantities. The parameters χ_{kd}, R_{fd} and R_{kd} all changed the magnitude of the fundamental frequency components but the only distinct effect on the time constant of decay of these components was caused by the armature leakage reactance. The direct axis damper resistance and to a smaller extent the reactance affected the initial build up of field current while the transient decay depended mainly upon field resistance.

Most of the parameters had some effect on the post fault terminal voltage recovery, in particular field and armature leakage reactances, and armature resistance. However in all cases the voltage did not return to the initial value for at least 5 seconds.

In practice, only the damper parameters can be varied without interfering with the steady state operation of the machine and these should be concentrated upon for future studies. The present analysis has been purposely rather limited in scope in order not to deviate too widely from the main theme of the thesis and there is a great need for further investigations. In particular, a more exacting assessment of the role of the fundamental oscillations in the transient processes would be of great value. This could be facilitated by calculating damper winding currents in both axes which would extend the knowledge already gained from the field oscillations.

5 EFFECTS OF THYRISTOR EXCITATION SYSTEMS ON GENERATOR TRANSIENT PERFORMANCE

5.1 Introduction

The overall and relative merits of the various thyristor excitation systems are numerous (see Chapter 3) and acceptance as the ultimate excitation control tool is becoming realised. The common link of superiority lies in their rapid response characteristic which enables the automatic voltage regulator to act much more effectively. Another important facet is the opportunities for both transient and steady state stability improvements which have been studied by many authors[36,42], mainly in connection with hydro-machine systems. Although the rapid response can produce a decline in stability when using only voltage feedback, more comprehensive control policies can be formulated such as the feedback of external stabilising signals, which make possible substantial increases in system damping due to the reduction of phase lags and non-linearities. A further advantage is gained over diode excitation systems in that the gate control of thyristor convertors can be retarded giving pseudo-inversion whereby the DC output voltage becomes reversed. Thus both buck and boost operation is available provided that the field current never falls to zero. Field current reversal is not likely under synchronous conditions because the decay is determined by the transient short circuit time constant, usually of the order of 1 second. However under pole slipping conditions the field current will attempt to reverse polarity and not only will the output of the thyristor convertor collapse, but also a high induced voltage will be developed across the generator field which may damage the thyristor devices, slip rings, or rotor insulation, unless suitable precautions are taken.

All the following studies were carried out using the full representation of the generator in which damping circuits were simulated by one closed coil on each axis. It has been common practice in the past to neglect amortisseur effects when performing comparative studies of control systems, but from Chapter 4 it is seen that the damper parameters have a large influence on both the power swings and the field system behaviour and in the author's view these effects must be included.

In studying the effects of the various control loops the main area of interest is the rotor angle oscillations resulting from a large system disturbance, but as the primary function of excitation control is the restoration of terminal voltage, this should not be neglected. Small or steady state disturbances are not treated here as the dynamic stability of similar systems has already been established elsewhere[36,43,46].

For purposes of comparison, the same machine constants were used as in the standard parameter set of the previous chapter. In most of the studies the generator was operated at rated conditions and a three-phase fault applied of a duration that was near to critical for the uncontrolled machine case (300 ms). The author feels that these conditions are more exacting for control system assessments than leading power factor conditions as less field forcing capability is available due to the higher initial rotor voltage.

Fig.5.1 shows the excitation system block diagram which is common to all the studies, and it is intended to be perfectly flexible so that most excitation system developments can be investigated. For comparative purposes, only the general trends in performance of the different designs are wanted and so exact representation is unnecessary, but if simulation or prediction of site tests are performed then precise representation of the actual control systems must be attempted. The thyristor convertor is assumed to be linearised and so appears as a fixed gain G_{th} and response time is assumed to be negligbily small when compared to AVR and transducer lags. The representation of the voltage feedback loop is fairly standard being a single lag to represent the combination of step down transformer, rectifier, and filter, and variable lead/lag function to cover the AVR proper. The DC voltage after the filter is compared with a reference voltage V_{ref} and an additional facility is provided for introducing external stabilising signals at the input to the thyristor control circuits. A transducer lag is also incorporated for this channel.

5.2 Voltage feedback capabilities

5.2.1 Consequences of increased regulator response

The common feature in excitation and AVR system development is the successive improvement in the speed of operation with more advanced designs. It is seen from Fig.5.2 that this achieves the desired aim of a better terminal voltage recovery subsequent to fault removal, although little can be done to affect this voltage during the fault period as it depends mainly

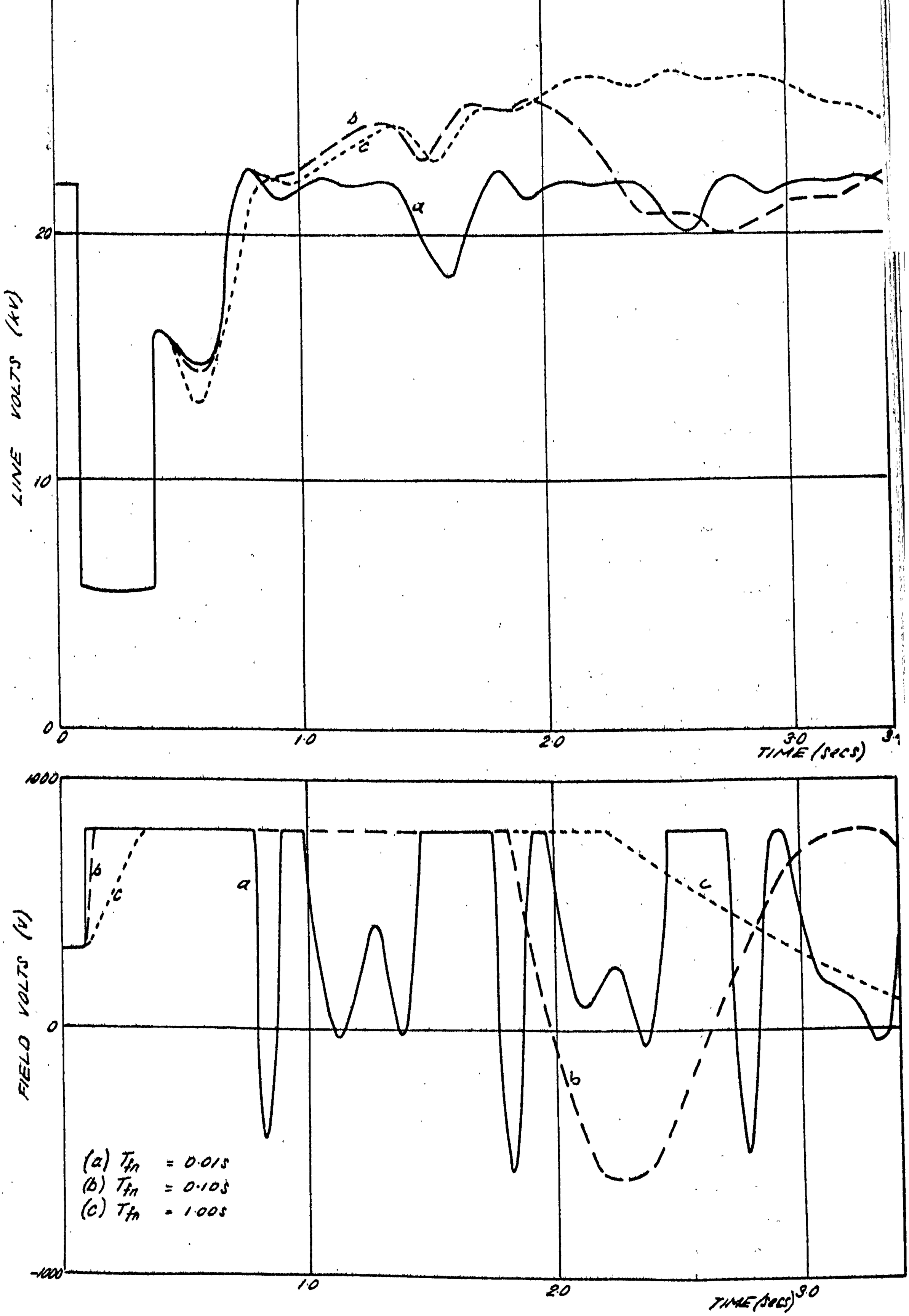

THYRISTOR EXCITATION STUDIES - EFFECTS OF AVR RESPONSE

FIG 5.2

upon the system reactances and proximity of the fault to the generator. With the slower response a substantial overshoot is produced caused by the field voltage lingering at the ceiling value. Even the very slow system reached ceiling during the fault due to the very large terminal voltage error, but after fault removal the error is much smaller and the faster system displays a marked superiority.

Considering the effects on rotor dynamic performance shown in Fig.5.3, this is not as excouraging because although a small reduction in the first peak of rotor angle was predicted, the subsequent oscillations were less damped with a fast response excitation. This is almost certainly not due to a reduction in stability in the regulator itself as very small phase lags are present and the phenomenon has been studied and commented upon previously[43]. The explanation given is that as the terminal voltage is restored quickly after the fault, there is a very small AVR error and hence little flux destroying force available for damping out the power oscillations. With fast excitation more electrical energy is added during the fault by the field voltage rising very quickly to ceiling and this tends to reduce the energy imbalance between generator and prime mover giving a lower initial rotor angle swing. However, when the fault is cleared the field cannot dissipate the energy it supplied during the fault which has to be converted into electro-mechanical energy causing an increase in the rotor oscillations. This explanation may be partly correct but further study reveals that other factors are influencing the operation as discussed in the next sub-section.

5.2.2 Effects of exciter ceiling limits

With a direct current exciter system the output voltage is limited by saturation and mechanical considerations but in an AC exciter/rectifier system the only tangible limitation is the reverse voltage blocking capability of the rectifiers. At the time of writing this limit stands at over 5 kV for high power thyristors giving a maximum safe operating limit of 1.8 kV line (i.e. $\frac{5}{2\sqrt{2}}$) which is equivalent to a DC output voltage of 2.4 kV. In theory this limit could be increased further by using series connected devices, provided some means of voltage sharing is employed. With rectifier excitation systems the ceiling could then be increased to almost any desired value but in practice a constraint has to be applied to protect the generator rotor winding insulation. This is especially true in the case of thyristor rectifiers where the voltage output contains steep wavefronts and spikes which demands a further

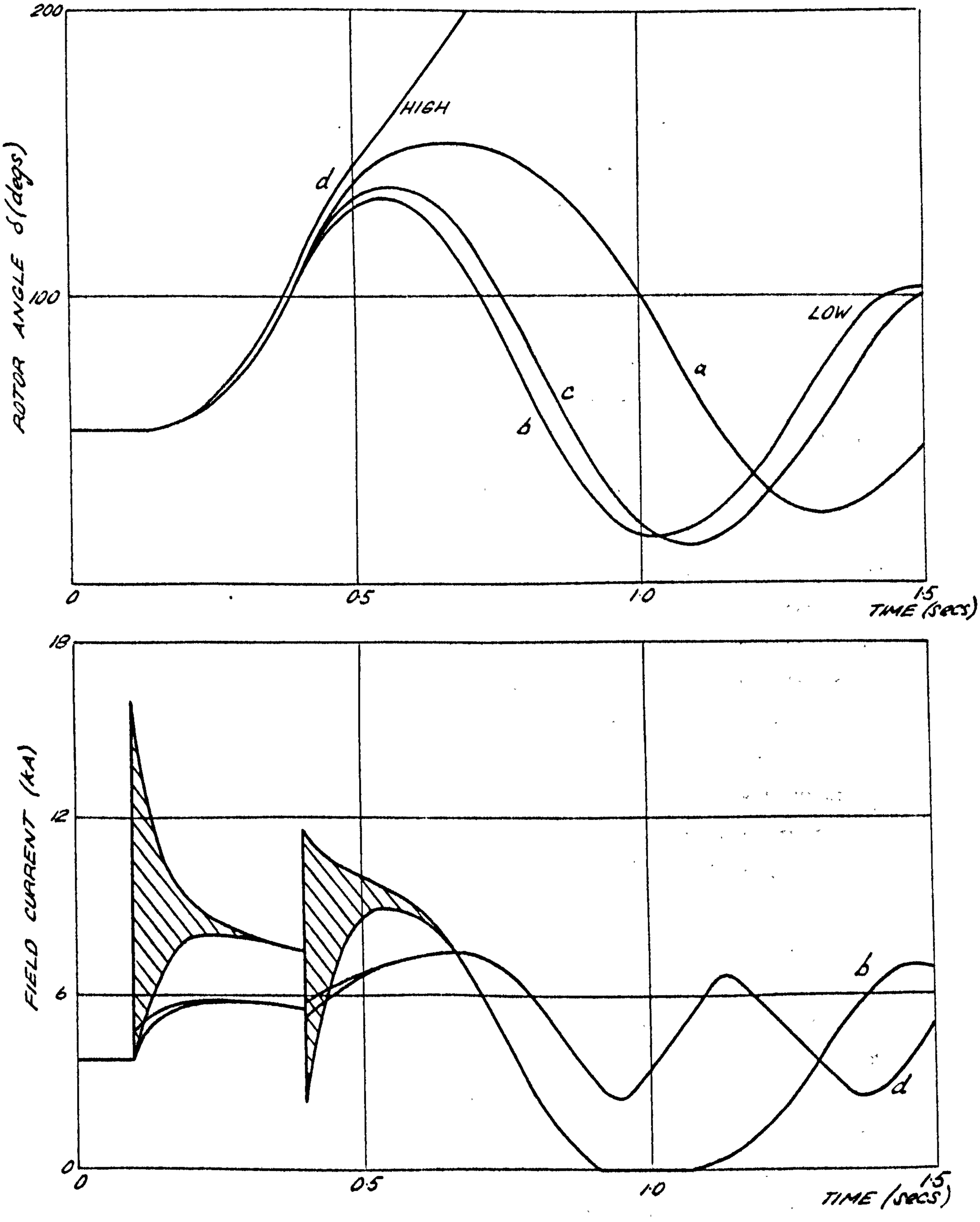

(a) $x_{AFd} = 0.162$
(b) $x_{AFd} = 0.01$
(c) $x_{AFd} = 0.05$
(d) $x_{AFd} = 0.50$

EFFECT OF VARIATION OF FIELD LEAKAGE REACTANCE

FIG 4.6

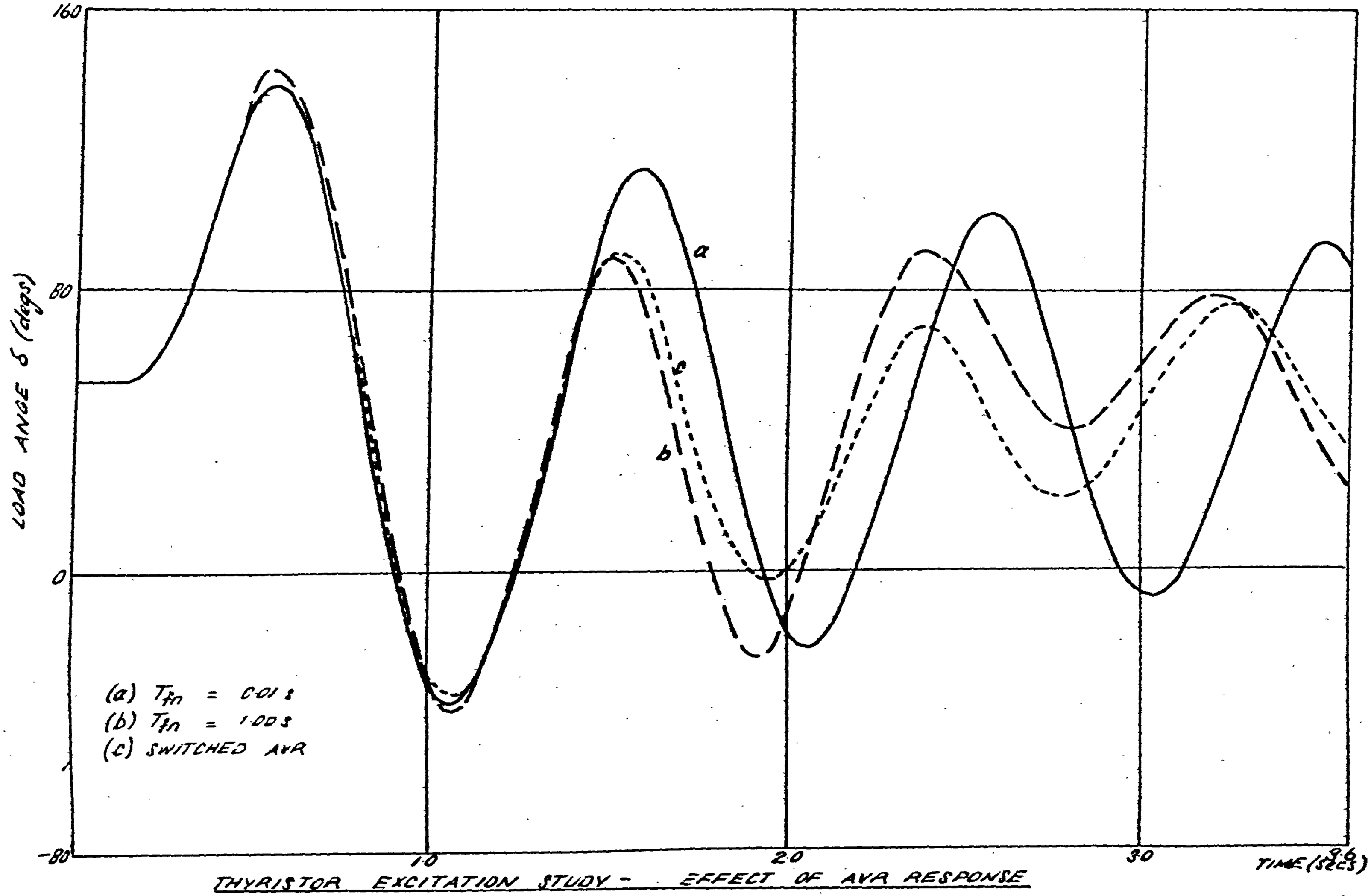

THYRISTOR EXCITATION STUDY - EFFECT OF AVR RESPONSE

FIG 5.3

lowering of the safe operating voltage limit for the insulation, but even so, this is still higher than previous exciter limits. At the present time some of the electric utilities are pressing for fast thyristor excitation schemes with ceiling voltages of unprecedented magnitude. If standard voltage control is employed with these systems then the performance will be totally unsatisfactory as shown by Fig.5.4 where increasing the ceiling from the designed value of 2.5 p.u. (based on 1 p.u. terminal voltage = rated load rated p.f. lag excitation) to 5 p.u. caused a build up of oscillations producing multi-swing instability after 7 seconds. Similar effects were observed by Byerly et al on a water wheel generator[45] and appear to be due to a combination of fast response high ceiling voltage and a large AVR gain, and unless some other means of stabilisation can be applied, one or more of these quantities must be reduced.

If the pole-slipping had been caused simply by conversion of the extra field energy attained during the fault into mechanical energy as discussed in 5.2.1, then instability would have occurred shortly after fault removal. However the gradual build up of oscillations suggests a cyclic injection of kinetic energy which must be produced by the excitation system as transmission system and prime mover quantities were constant after the fault was removed. It is observed from Fig.5.5 that the field is repetitively subjected to full forcing which is caused by a series of corresponding depressions in the terminal voltage. These occur at times corresponding to maximum rotor angle and as the armature current is highest during this period it follows that large voltage drops will appear across the resistance and transient reactance causing the terminal voltage to be depressed. Hence the rotor angle peaks are reflected into the impressed excitation voltage which in effect produces a positive feedback of electrical power.

For economy of calculation time, the saturation facility was excluded from the comparative investigations of control systems, but due to the large excitation voltages present in this particular study, it was felt that saturation effects might play an important role and should be investigated. To substantiate this, the results for the 5 p.u. ceiling voltage case were repeated with saturation included and are presented in curve (d) of Fig.5.4. Although stability was again lost, the inclusion of saturation had a slight stabilising effect which was embodied by a reduction in the rotor angle peak swings. This indicates that the omission of saturation is valid for comparative studies in which the general trends in the effectiveness of different control systems are wanted, and that the results obtained will be on the pessimistic side.

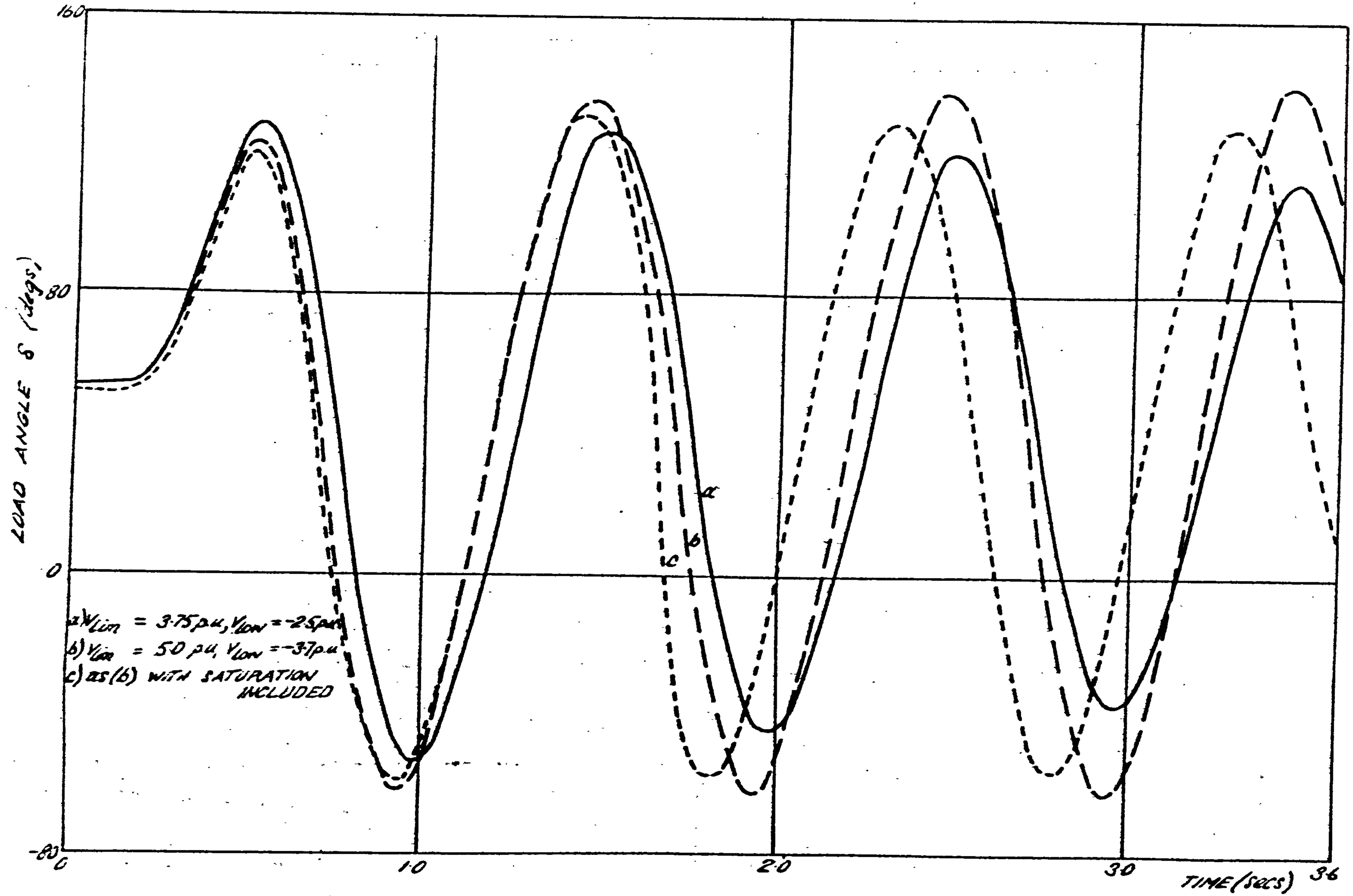

THYRISTOR EXCITATION STUDY - EFFECT OF EXCITER LIMITS ON AVR RESPONSE

FIG 5.4

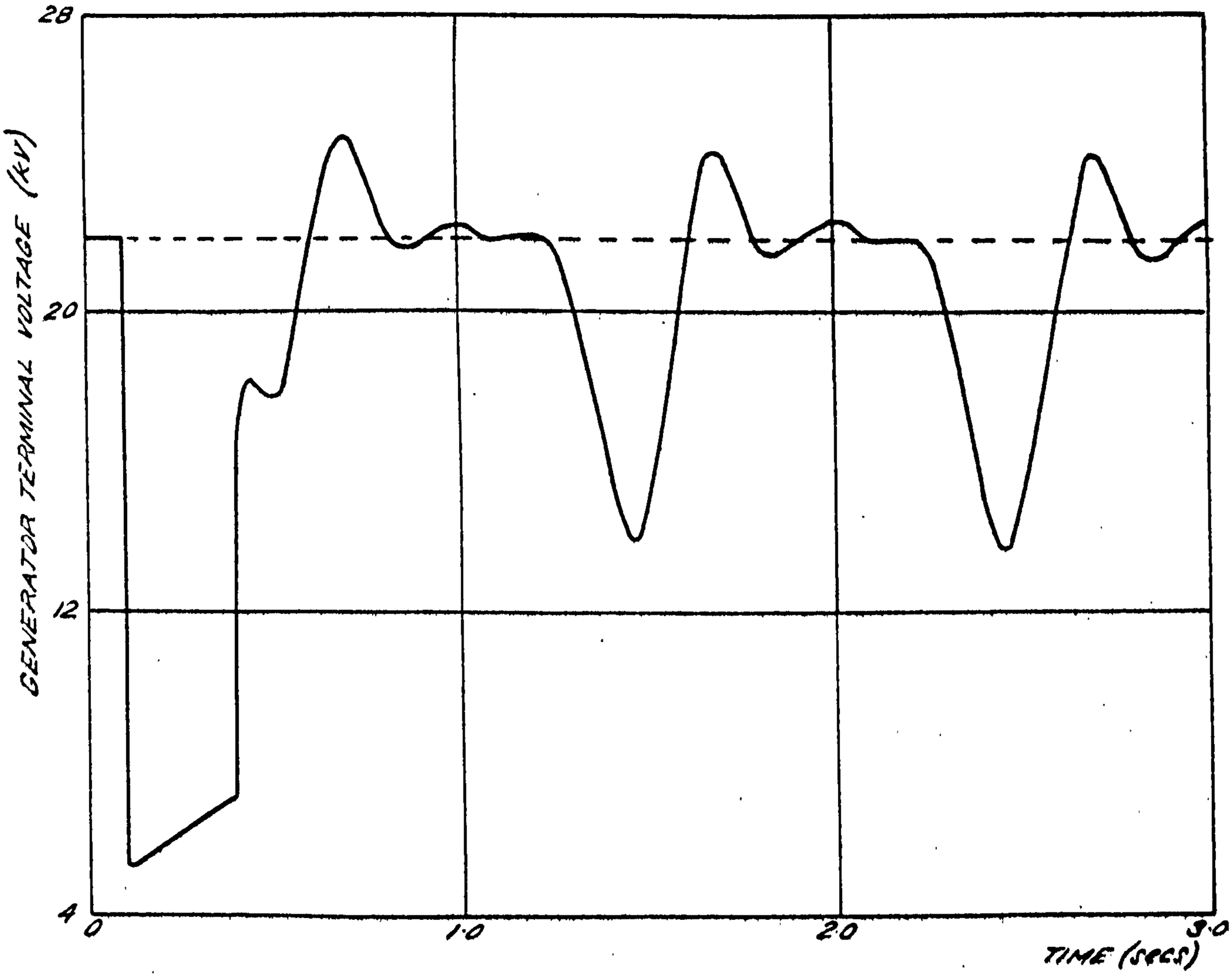

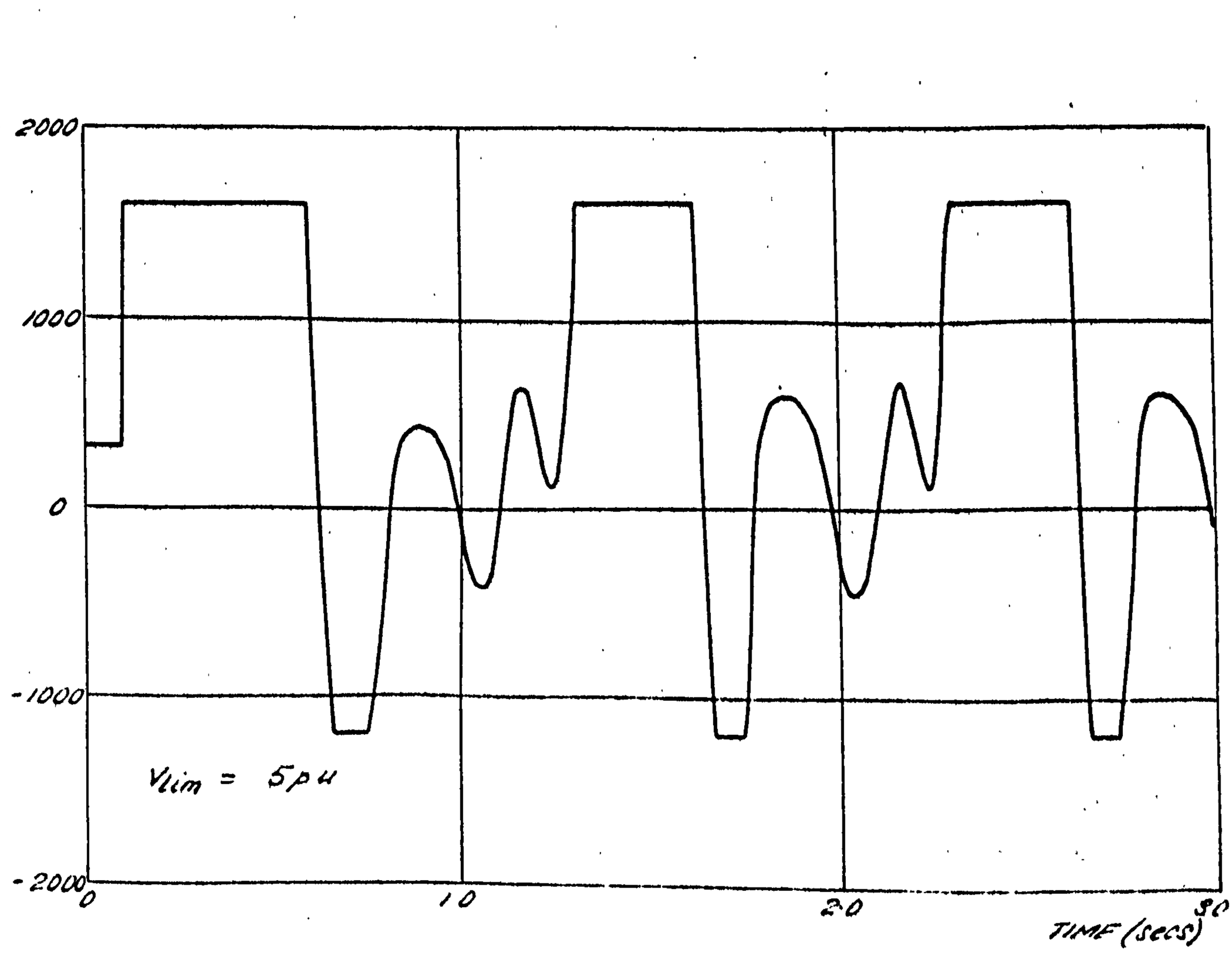

THYRISTOR EXCITATION STUDY - EFFECTS OF EXCITER LIMITS ON AVR OPERATION

FIG 5.5

5.2.3 Stabilisation by rate of change of AVR input voltage

In order to enhance damping of the large oscillations with fast exciters, a rate of change of armature voltage term is often included either as a feedback loop around the AVR (see Ref, 46) or as a phase lead in the forward loop. The latter was simulated in the excitation system model of Fig.5.1 by the constant T_{sv}, and the effect of various values on the damping of oscillations is shown in Fig.5.6. Although a slight increase in the first rotor angle swing results, the underswings are reduced considerably which is brought about by an improvement in the negative forcing of the exciter as in Fig.5.7. This compensates against the effects of the positive field forcing but unfortunately it degrades the terminal voltage recovery. In addition the decay of the oscillations is not affected appreciably by this form of control and other researchers[45] have found that under certain circumstances sustained oscillations with zero damping can be produced.

This control method also stabilised the performance with a high ceiling limit of 5 p.u., a case which was unstable with no phase advance term as discussed previously. Thus with exciters of both fast response and high ceiling the use of a rate of change of voltage term provides an easily implemented and inexpensive method of achieving some degree of stabilisation.

In general, better performance was achieved as the stabilising time constant was increased, thelargest value used in the studies being 1 second. Together with an AVR lag of 0.01 seconds this gives a phase advance of approximately 78°, but to achieve further phase advances approaching or in excess of 90°, a second order transfer function would be necessary of the form:

$$\frac{(1 + P\,T_{sv_1})\,(1 + P\,T_{sv_2})}{(1 + P\,T_{fn})}$$

As the voltage degradation was becoming unacceptable, the effects of further increases of the phase lead were not studied.

5.3 Excitation system external stabilising signals

The same reduction in the first rotor angle swing, as was produced by fast AVR control can be achieved by a switched operation of the excitation voltage which is immediately set to the ceiling value on the detection of a fault by a wired logic circuit or control computer. This has the advantage that an improvement in the first swing stability margin similar to that obtained with a fast thyristor excitation system can be achieved

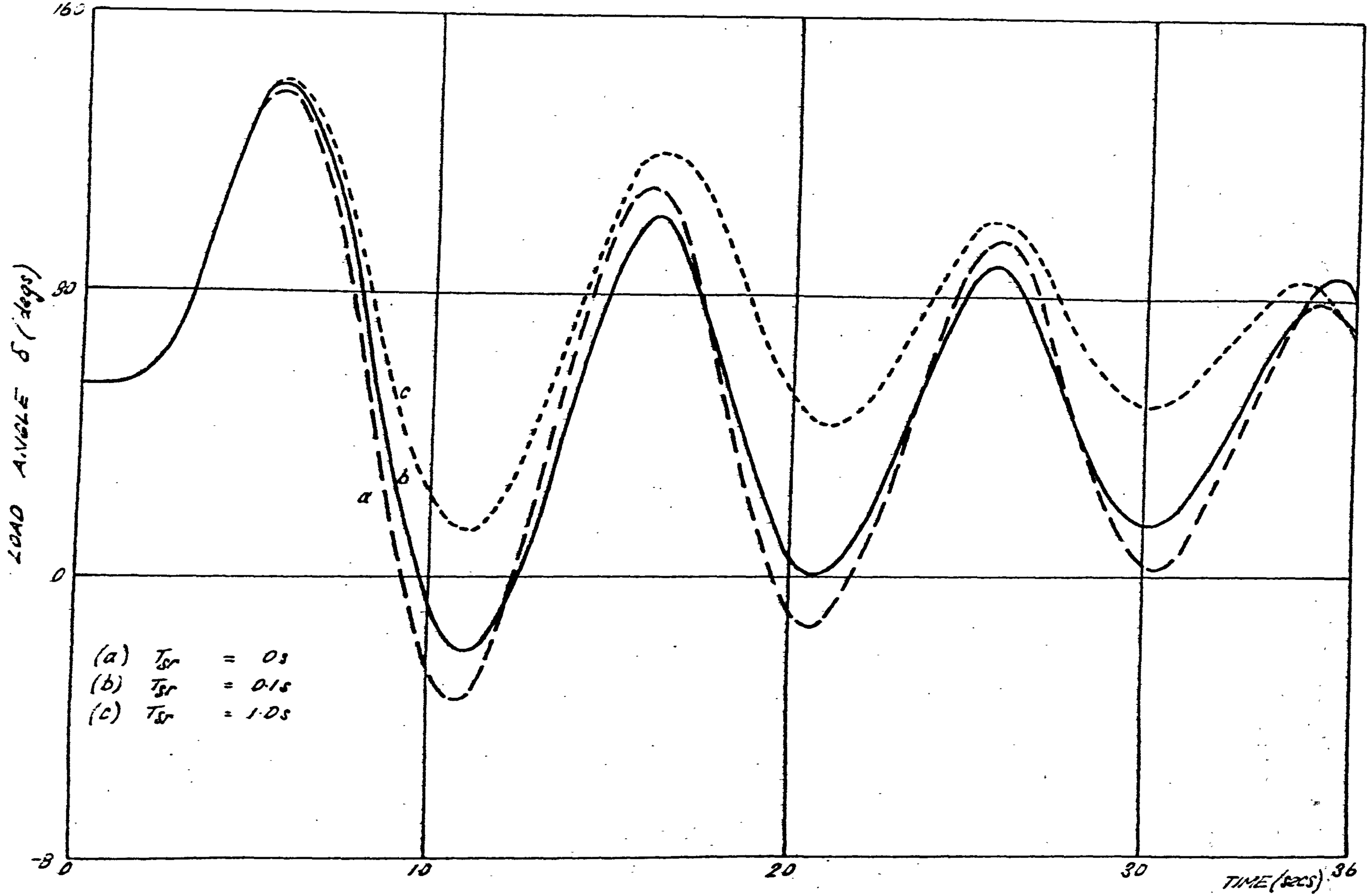

THYRISTOR EXCITATION STUDY - EFFECT OF RATE OF CHANGE OF VOLTAGE STABILISATION

FIG 9.5

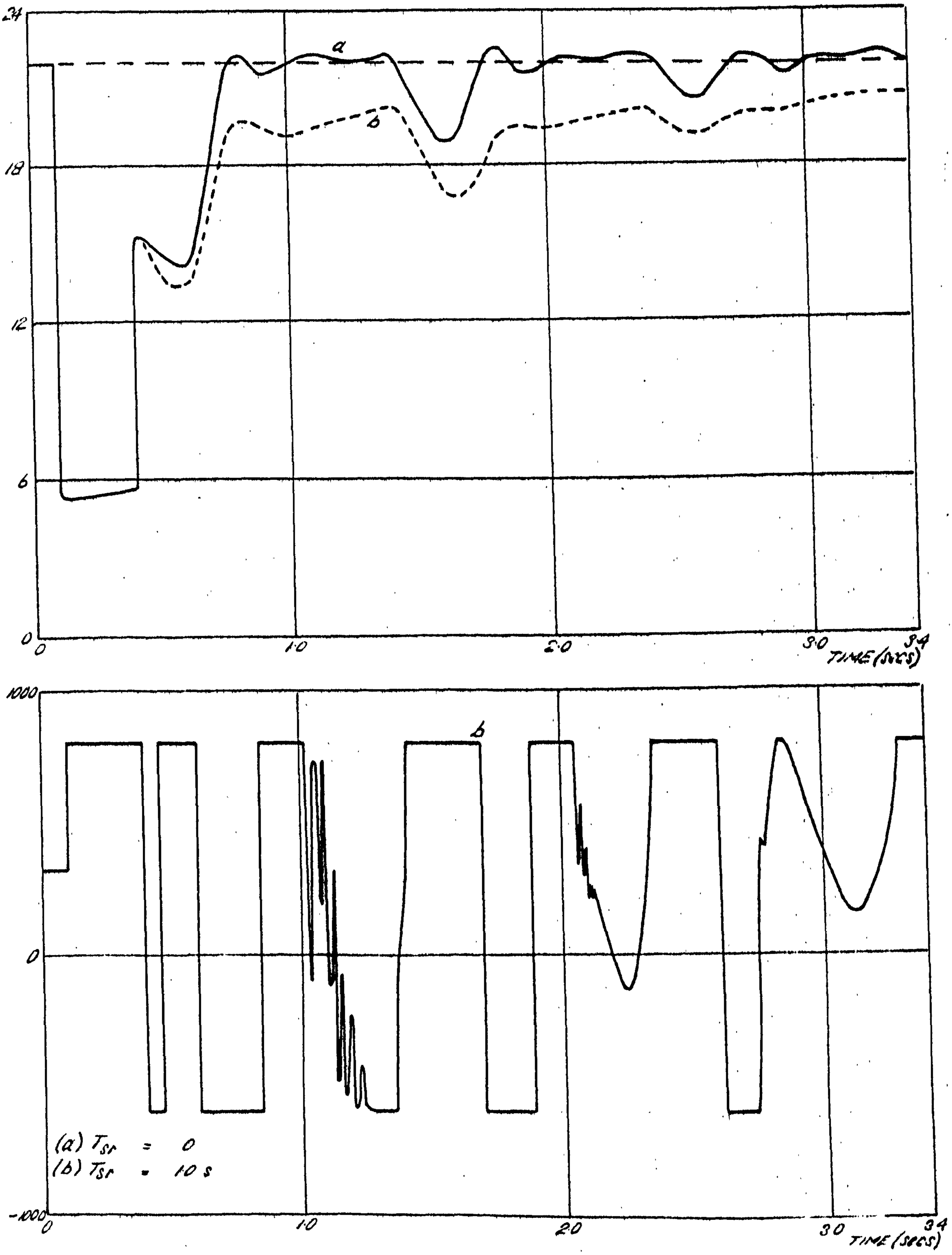

INVRISTOR EXCITATION STUDY - EFFECT OF RATE OF CHANGE OF VOLTAGE STABILISATION

FIG 5.7

with a slow exciter which has the switching facility incorporated. The switching could be performed by a mechanical contactor arrangement, a facility which it was interesting to note, was provided on early non-continuously acting AVR's[53]. Curve (c) of Fig.5.3 shows the swing curve produced by excitation logic that detects a fault by determining whether the acceleration exceeds a threshold value (30 radians/sec^2) and if so, switches the excitation voltage to ceiling until the rotor velocity passes through zero, when normal AVR operation is restored. In this case the controller performed two switching operations and not only is the first peak reduced but also the subsequent swings are more damped. In fact an extremely damped swing can be produced with the switching controller alone, without any form of feedback by manual optimisation of the periods of switching between positive and negative ceiling voltages[43]. Bang-bang control, as this method is termed, is extremely sensitive to loading and other operational conditions and is of no practical use unless some method of on-line optimising of the switching times can be determined, Earlier investigations[47,50] have shown that an approximation to a bang-bang controller could be obtained by feedback of a compound external stabilising signal into the AVR containing velocity and acceleration channels with appropriate gains. An extra AVR input proportional to velocity deviation has been previously investigated for stabilising dynamic oscillations and the signals used by the various authors were derived by three different methods namely from the frequency difference[48], from integral of power error[49], and from direct measurement of shaft velocity[36]. The last mentioned method is presently being explored further to give a noise free signal with a fast response (see Chapter 8) and is the most likely method for future adoption as the first two methods introduce inherent lags into the control loop.

Although a velocity deviation signal seems to be extremely useful for stabilising dynamic oscillations, the advantages to be gained when considering transient response are not as encouraging. This is because the speed only builds up gradually during the fault (c.f. Fig.2.10) and to produce the required bang-bang effect for transient stability improvement, a very high gain has to be used. The effect of this is to increase the offset of the mean of the rotor angle oscillations as shown by Fig.5.8 until stability is lost. With lower gains a fair amount of damping is produced but the ability to reduce the first forward swing is lessened and additionally, in all cases a very poor terminal voltage response was produced as in Fig.5.9a.

By feedback of a signal proportional to shaft acceleration an almost

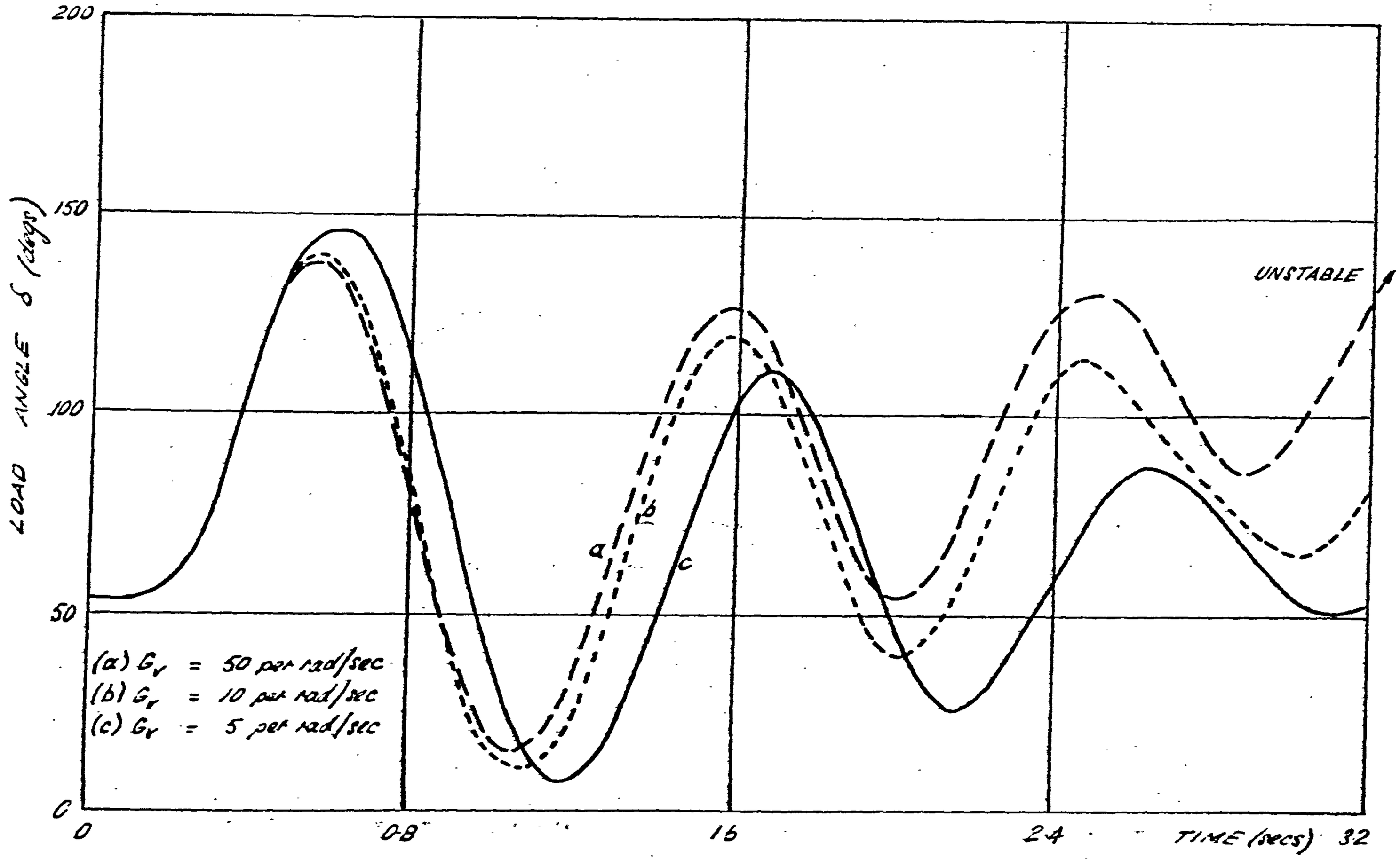

THYRISTOR EXCITATION STUDY - EFFECT OF SHAFT VELOCITY STABILISING FEEDBACK

FIG 5.9

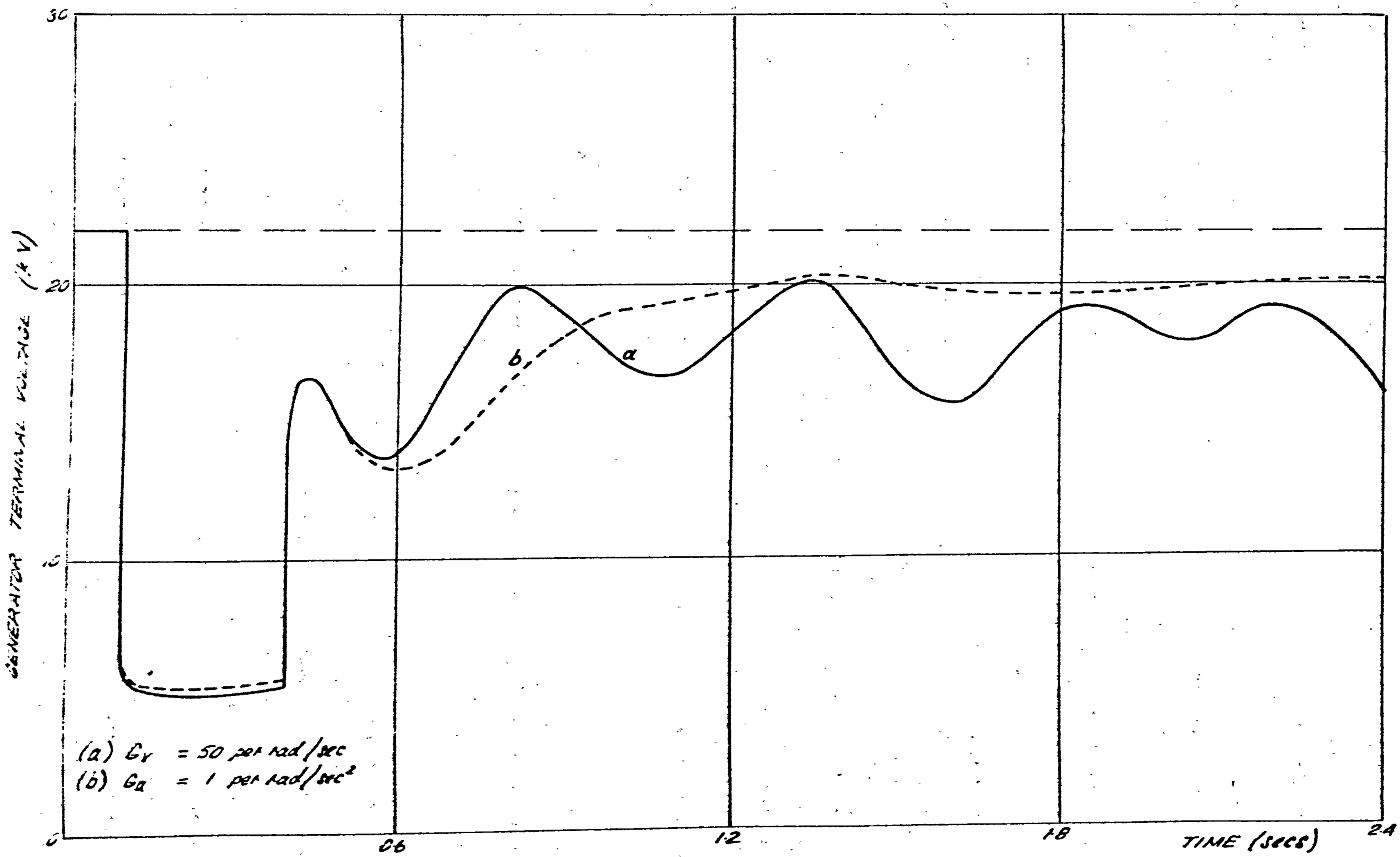

THYRISTOR EXCITATION STUDY - EFFECT OF ACCELERATION AND VELOCITY STABILISING FEEDBACK SIGNAL ON TERMINAL VOLTAGE RECOVERY

Fig 5.9

critically damped response can be obtained, together with a substantial reduction of the first swing as illustrated by Fig.5.10. This means that the power variations injected by the excitation control are in antiphase with the electrical power oscillations caused by the fault which gives the rapid damping effect. In this respect the transient control requirements are contrary to those of the dynamic state where due to the integrating effect caused by the field time constant an acceleration term has very little advantage and the best signal is acceleration phase shifted by 90^{o}, i.e, velocity. However, in the transient state the performance depends upon the ability of the excitation system to maintain the power balance which is dependent directly upon the applied excitation voltage.

After the initial transient the rotor is left at a higher angle than the prefault value and a very slow secondary transient takes place until the original conditions are restored. This is because the excitation system now has linear control over the machine as it is operating well within its ceiling limits and the result is to increase the effective moment of inertia by many times. The terminal voltage is depressed after the initial transient and this also takes many seconds to return to the initial value due to the same effect (Fig.5.9b).

From the equation of motion, neglecting losses torque and assuming constant prime mover torque, we may write

$$2 H_m P^2\delta = T_i - T_e = - \Delta T_e \qquad \ldots(5.1)$$

as the changes in speed, even during a severe disturbance, only amount to a few per cent, then 5.1 approximates to

$$2 H_m P^2\delta = - \Delta P_e \qquad \ldots(5.2)$$

It follows from 5.2 then that if a power error stabilising signal were used[45] it should give similar effects to the acceleration signal previously described. This is substantiated by Fig.5.11 where again a large amount of damping is achieved but this time using a power error signal. With the large value of gain, however, instability was induced and this may be due to the power signal containing both acceleration and velocity components as instability was also produced by a large velocity feedback gain.

The reason for the effectiveness of the dynamic external stabilising signals can be best illustrated by further inspection of the equation of motion. The change in electrical power during a disturbance is composed of damping

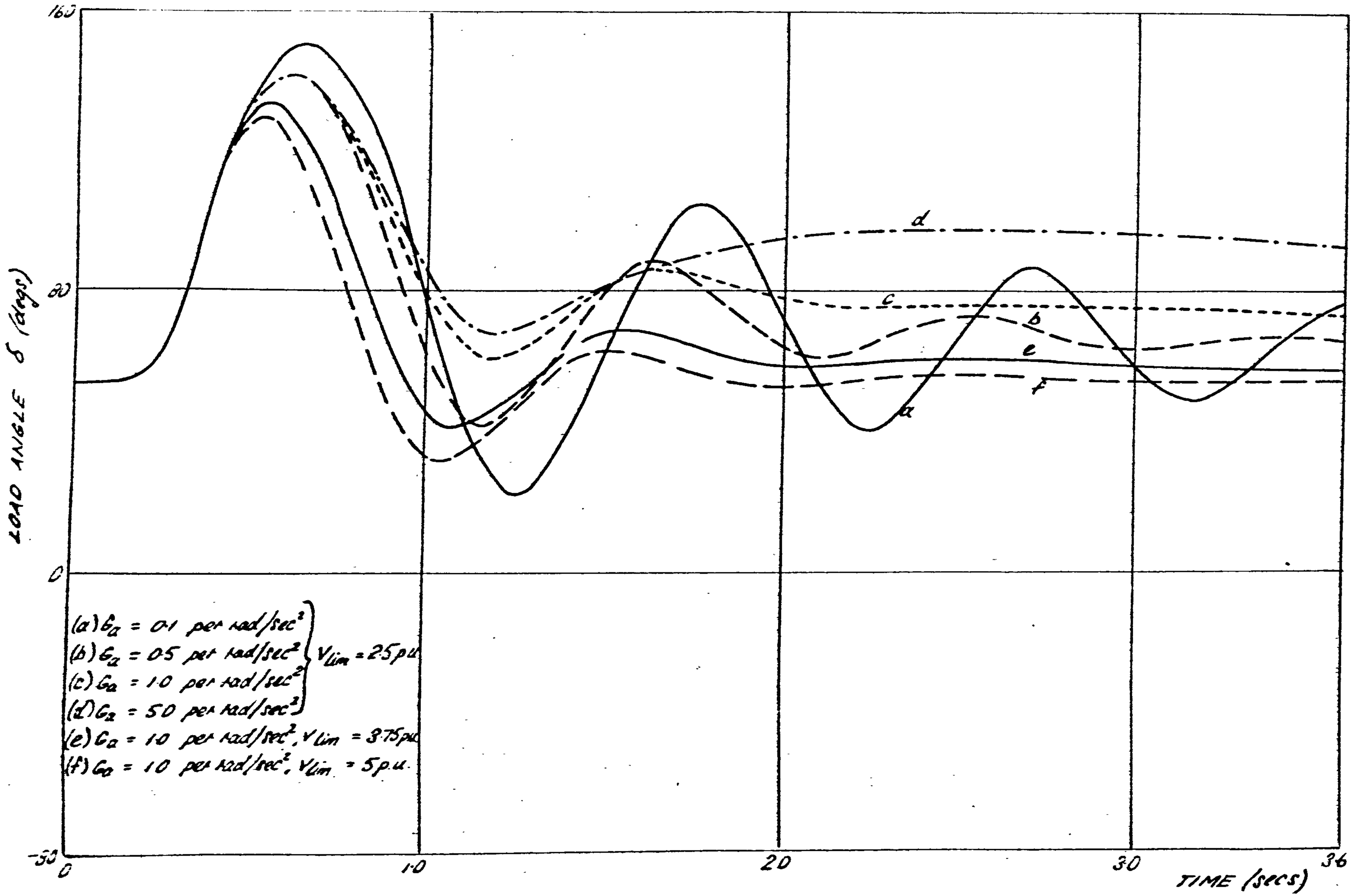

THYRISTOR EXCITATION STUDY - EFFECT OF ACCELERATION FEEDBACK

FIG. 5.10

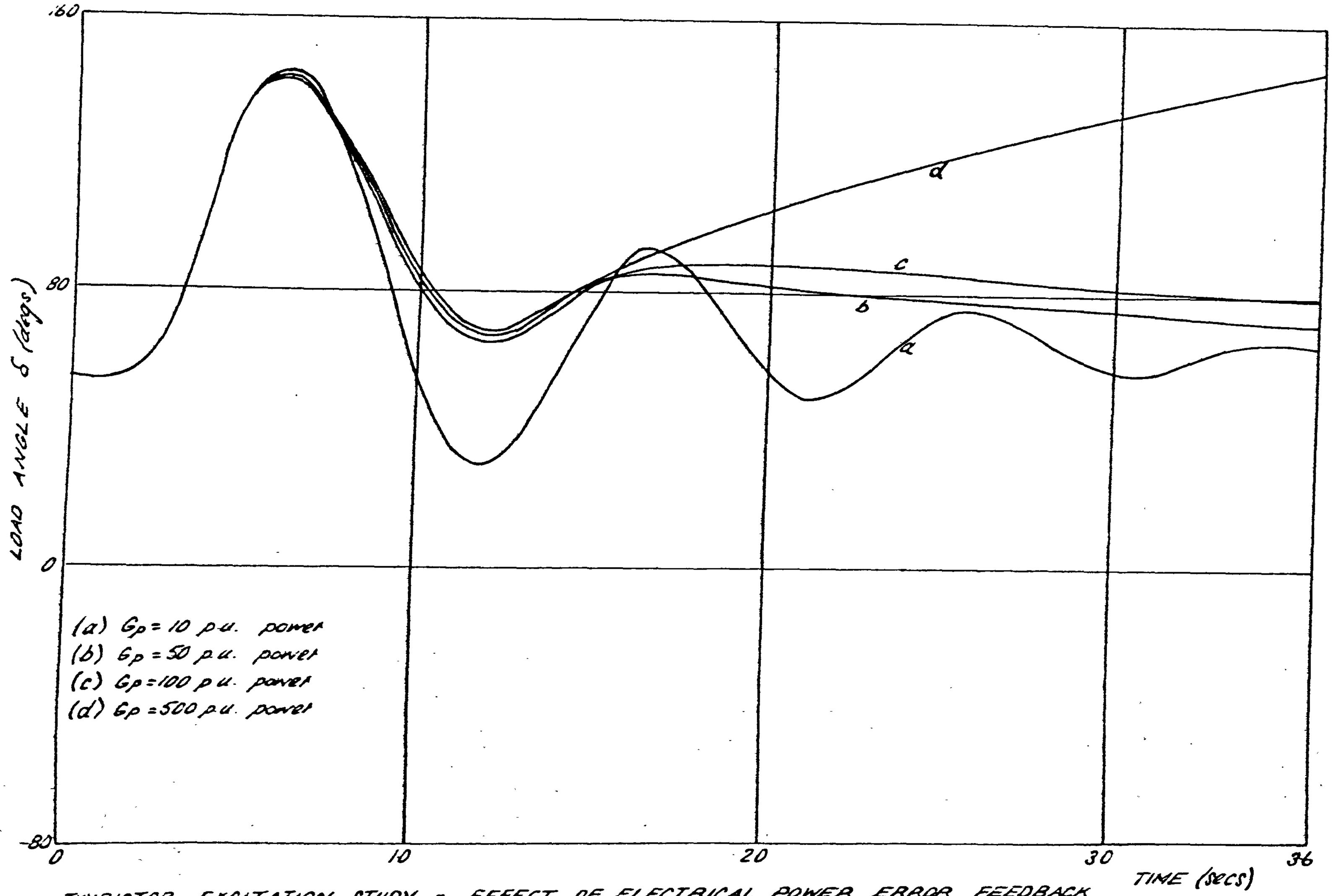

THYRISTOR EXCITATION STUDY - EFFECT OF ELECTRICAL POWER ERROR FEEDBACK

FIG 5.11

components, depending upon the change of speed and the damper winding parameters, and 'synchronising' components which depend upon the generator internal voltage during the transient E'_q, the busbar voltage V_b and load angle δ[43], therefore

$$2 H_m p^2\delta + f_d(p\delta) + f_s (E'_q, V_b, \sin\delta, \sin 2\delta) = 0$$

where f_d and f_s are complex functions of the bracketed terms and the machine reactances.

If for simplicity the simple generator representation is considered where

$$E'_q = \frac{K_{ef}}{1+pT'_d} \cdot \Delta V_f$$ (where K_{ef} is a constant and T'_d the direct axis transient short current time constant)

then we may write,

$$2 H_m p^2\delta + f_{s1}\left(\frac{\Delta V_f}{1+pT'_d}\right) + f_d(p\delta) + f_{s2} (V_b, \sin\delta, \sin 2\delta) = 0$$

Hence if ΔV_f is proportional to acceleration $p^2\delta$, then under fast transient conditions the $\frac{1}{1+pT'_d}$ term will integrate this to give a velocity or in other words a damping effect, but under steady state or conditions ofvery slow changes, the power contribution from the excitation will be directly proportional to acceleration as the $\frac{1}{1+pT'_d}$ term will have little effect at very low frequencies. Thus the acceleration term, i.e. the effective inertia constant is increased. This analysis also explains the effectiveness of a velocity signal in the dynamic state where again the integral term has negligible effect and a direct velocity damping contribution is achieved.

Curves (d) and (e) of Fig.5.10 show the effects of increasing the excitation system ceiling limits with acceleration feedback control. Here there is no deterioration in the damping effect as in the case of voltage feedback and a substantial improvement in the dynamic performance and terminal voltage recovery results.

The reduction of the first peak of the rotor angle swing was not quite as effective with the power and acceleration stabilising feedback as with the fast voltage regulator. It was noted that the field voltage immediately reversed under the stabilising controller when the fault was removed,but the excitation stayed at the positive ceiling for a longer period with voltage control. This was obviously the cause of the difference in the results and is explained by again considering the energy balance. Hence immediately after the fault the generated portion of the electrical power is very high due

to the increased rotor angle, and combined with the large damper power in this period forms the major part of the total electrical power which is greater than the prime mover power causing a deceleration of the rotor. As the electrical power can be controlled by the excitation, if this is kept high after the fault then a larger deceleration will ensue, causing a smaller rotor angle excursion. If the field is boosted for too long however, this produces a larger underswing and unfortunately the optimum time for field reversal is difficult to determine due to the contributions of the damper windings to the energy balance considerations.

5.4 Effects of high speed excitation at leading power factor

In some power system networks, especially those of overseas countries, power has to be transported from the remote generating stations over very long transmission lines to the load centres. Thus a large amount of reactive power is demanded and if separate compensation is not provided this has to be achieved by operating the generators at reduced excitation in the leading power factor region. This lowers the transient stability margin due to the increased steady state operating load angle and in addition, the synchronising power which is proportional to (cosδ), is diminished. Hence operations engineers are very concerned about the performance at leading power factor and much testing and analysis has been performed with a view to obtaining knowledge of the behaviour under these conditions (e.g. References[51] and [52]). In this thesis however an extensive study has not been performed as the author believes that rated conditions are best for assessing relative control system capabilities as discussed earlier. The curves of Fig.5.12 were intended to check the effects of the previously investigated controls in the leading power factor region. A lower fault period of 200 ms had to be used as the value of 300 ms used in the studies at lagging power factor was near critical and obviously caused instability at leading power factor.

The same general effects were observed with voltage and acceleration feedback as previously, i.e. a marked decrease and increase in the damping behaviour respectively, but it was found that after the initial transient with the acceleration feedback case, the rotor angle did not return to normal and a condition of dynamic equilibrium was established. No explanation is tendered for this phenomenon but it may have been that a decay was present but was so slow that it could not be detected on the limited computed results.

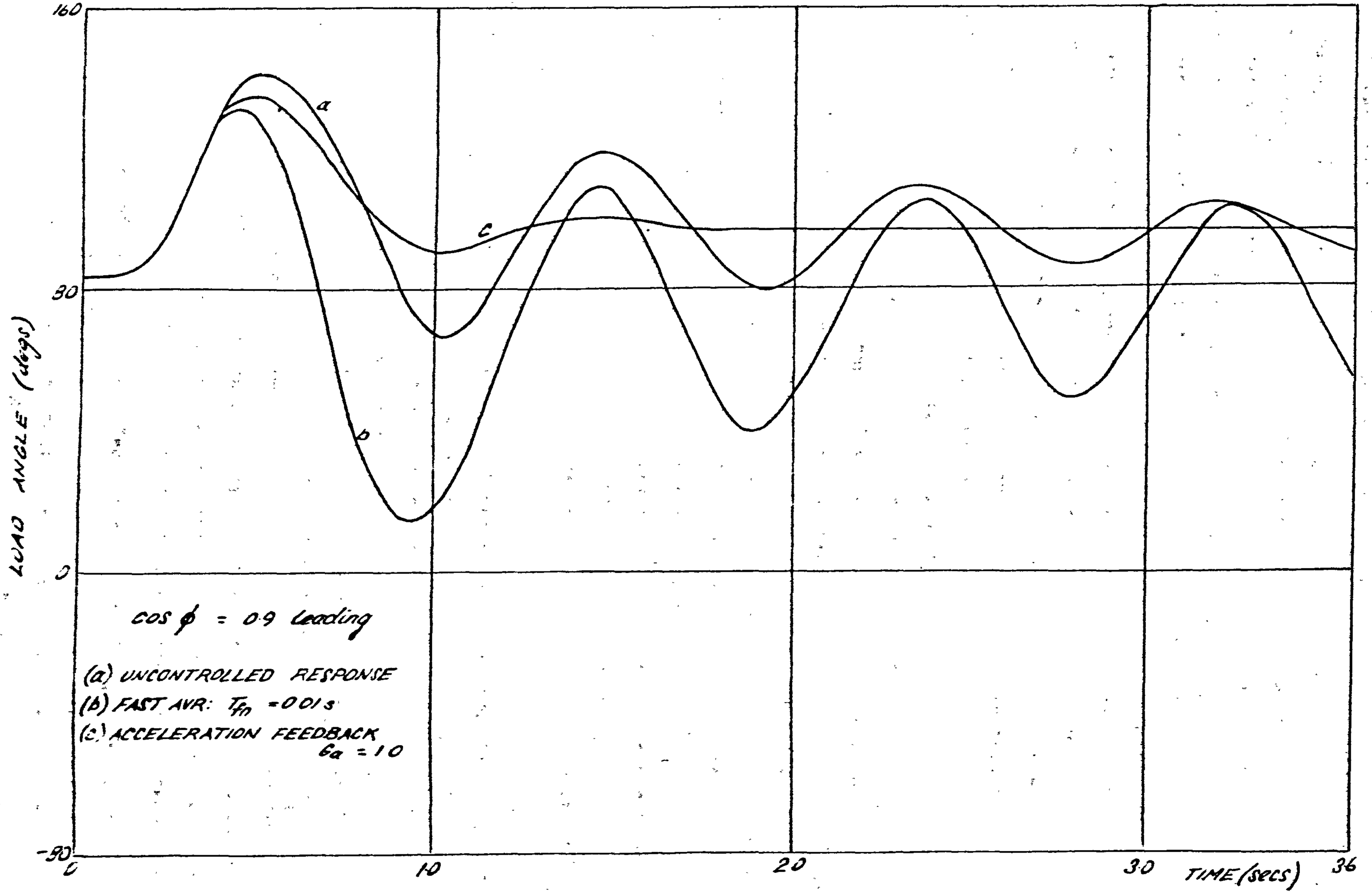

THYRISTOR EXCITATION STUDY - EFFECTS OF FAST EXCITATION AT LEADING POWER FACTOR

21.5 FIG

5.5 Performance of combined voltage regulator and stabilising signal

The stabilising signals have so far been analysed acting independently of a voltage regulating channel. It has been found that with a thyristor exciter acceleration feedback control gives a very high degree of damping of the rotor angle oscillations but the voltage regulation is seriously impaired. On the other hand the use of fundamental voltage control in a fast excitation system tends to make the overall performance more oscillatory. By combining the two different types of feedback one might expect to achieve a compromise between the performances but in practice this is not so, as shown by curve (a) of Fig.5.13 where it is observed that little improvement on the response is obtained by introducing an acceleration signal into the voltage regulator. In fact the voltage regulation effect seems to be entirely dominant as indicated by the fast terminal voltage recovery (Fig.5.14). Curves (b) and (c) of Fig.5.13 show an attempt at separating the actions of the two channels by increasing the AVR time constant whilst keeping a fast acceleration channel. In this manner a better damping is obtained but there is an obvious decline in terminal voltage response and the first rotor angle swing is increased. Fig.5.15 shows the effect of higher ceiling limits with a voltage time constant of three seconds and negligible acceleration lag. After the first transient has diminished, linear control is established but due to terminal voltage error the excitation increases in an attempt to correct for this. However the effective moment of inertia has been increased by the acceleration feedback and a very slow transient ensues which approaches the steady state stability limit.

With an exciter containing a rate of change of voltage term there was also little advantage gained by including an additional acceleration stabilising signal. The gain of the acceleration channel used for the combined control studies was the optimum value for the case of the acceleration feedback acting alone. It is noteworthy that this is no longer optimal when the voltage regulator is added and it is likely that a large increase in G_a would be necessary in order to swamp the AVR effects and achieve good damping. However as the present acceleration gain was very high, further increases were not attempted as it would be impossible to eliminate noise from the signal and still retain fast response, even with the most advanced measurement techniques.

Another method of enhancing the effect of the stabilising term would be to reduce the gain of the AVR channel. This gain is fixed by steady state regulation requirements and was not changed in all the previous studies. The overall gain is calculated as that which will produce full exciter forcing

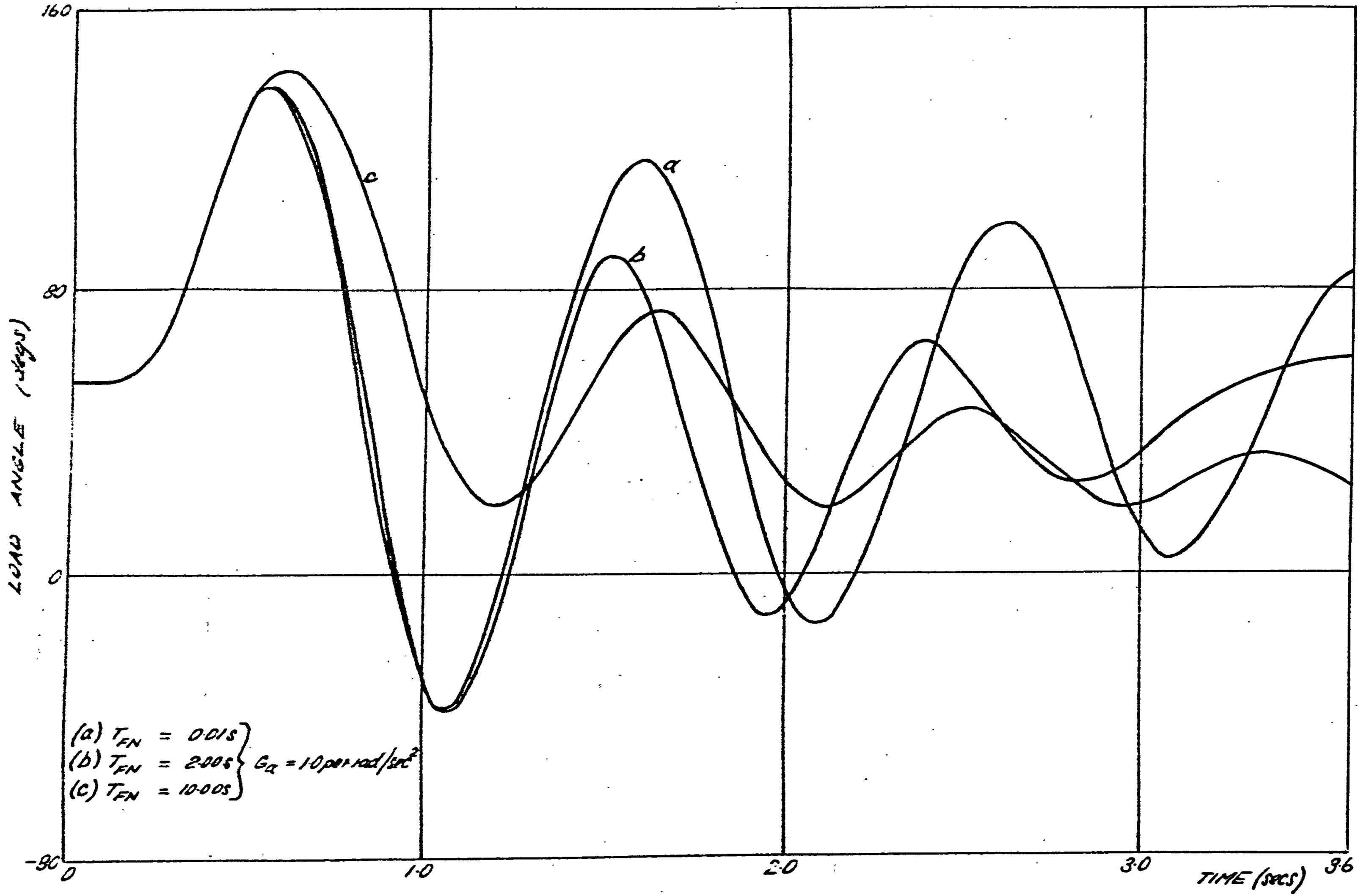

THYRISTOR EXCITATION STUDY - EFFECT OF ACCELERATION AND VOLTAGE FEEDBACK ACTING SIMULTANEOUSLY

SY.5.13 Fig. 9/1

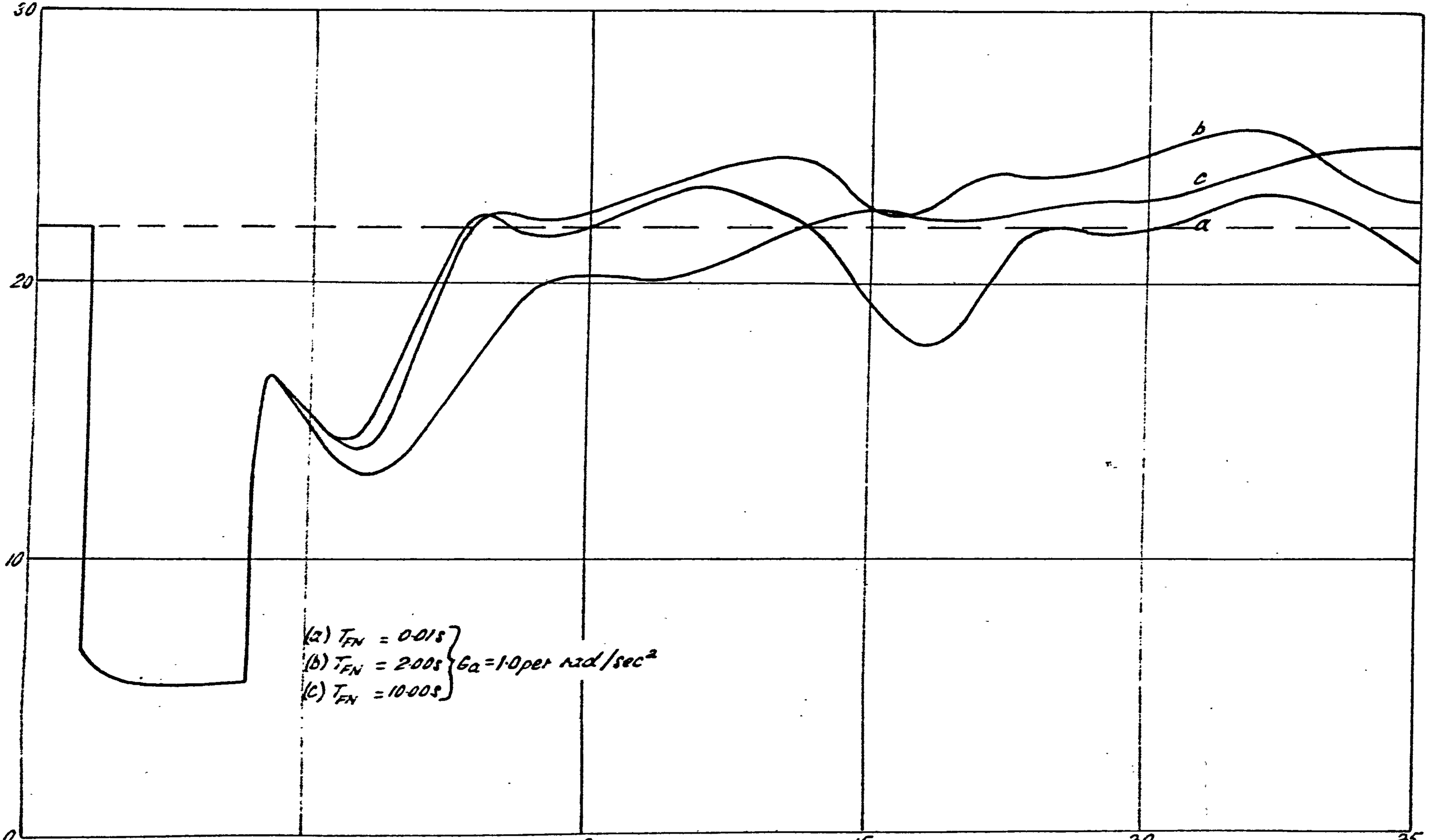

THYRISTOR EXCITATION STUDY - TERMINAL VOLTAGE RECOVERY WITH ACCELERATION AND VOLTAGE FEEDBACK ACTING SIMULTANEOUSLY

W.S. 5.4 F/G

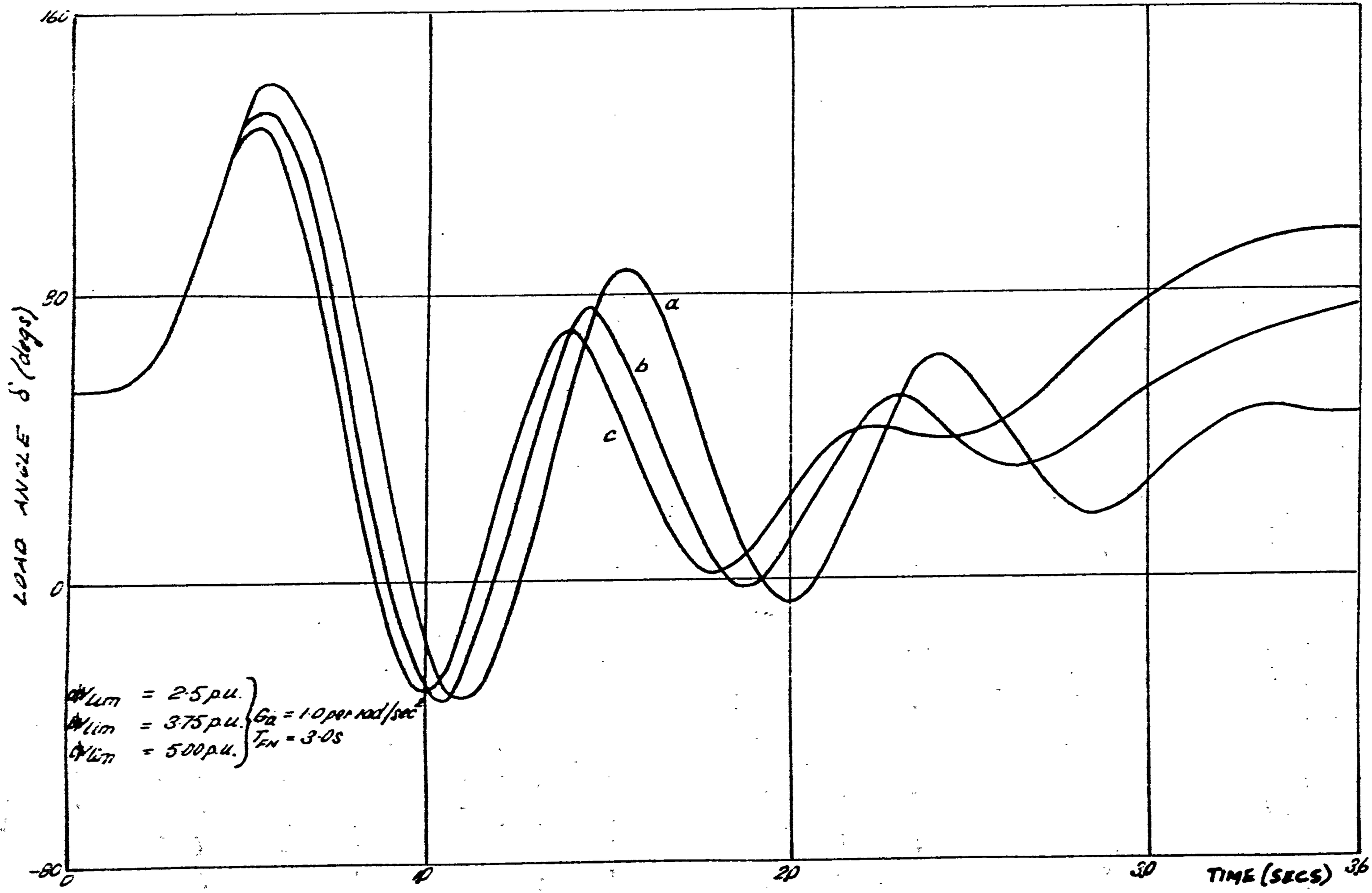

FIG 5.15

THYRISTOR EXCITATION STUDY - EFFECT OF EXCITER CEILING LIMITS WITH COMBINED ACCELERATION AND VELOCITY FEEDBACK

voltage for a terminal voltage depression of 1%. However it is only during transient oscillations that a reduction in gain is necessary and this could be achieved by AC feedback across the AVR calculated to give the correct gain reduction at the frequency of the transient oscillations which is usually around 1 Hz.

5.6 Summary and conclusions

It has been seen from the preceding section that although the thyristor convertor provides a fast flexible high power amplification system, its use as an exciter for a turbogenerator is by no means straight forward. A simple analogue controller to cover all aspects of operation was not forthcoming but the findings of the various systems are summarised in the following.

Fast voltage control gave a very good recovery of terminal voltage after a system fault and the best first swing transient stability margins. However the subsequent oscillations were more severe and with higher ceiling limits this was exacerbated causing multi-swing instability in some cases. The situation was improved a small amount by the introduction of a phase advance or 'rate of change of voltage' term, but only with a corresponding degradation of the voltage recovery.

The incorporation of a velocity stabilising feedback is now a common requirement for thyristor excitation schemes, especially in overseas systems, and has been found by other workers to render a marked improvement in the dynamic stability[36]. Under large disturbance conditions however, a velocity signal had little beneficial effect on the transient performance of the machine and if the gain was too high then instability could be produced. The best signals for the large disturbance case were acceleration and power which had similar effects giving a near critically damped or 'optimal' performance. This was obtained at the expense of voltage control and when an AVR channel was combined with the optimum stabilising feedback the effects of the latter were masked out giving a return of the underdamped oscillations.

It is clear that the creation of an overall control policy for the excitation system acting alone using pure analogue techniques is problematic due to the many functions that we are attempting to fulfil. These are summarised as:

(i) Voltage control, both during steady state to satisfy customer requirements and during transients to prevent stalling of auxiliaries and minimise interaction effects with other machines.

(ii) Field forcing during and immediately after a system fault to produce the maximum transient stability margin.

(iii) Damping of the rotor angle oscillations subsequent to a system fault to reduce system power fluctuations.

(iv) Stabilisation of dynamic performance to minimise 'hunting' effects and provide steady state stability.

It was found that fast voltage feedback covered the functions of (i) and (ii) only and had a negative effect on (iii). The requirements of (iii) and (iv) can be satisfied by acceleration and velocity feedback respectively but generally have an adverse effect on (i) and (ii).

The above observations suggest that a discontinuous control policy is the only true answer as follows:

(a) Steady state - voltage and velocity signals.

(b) During and immediately after a severe disturbance (subtransient period) - voltage only.

(c) Post fault (transient) period - acceleration feedback.

(d) Quasi-stable period (oscillations damped out but terminal voltage in error) - voltage and velocity signals.

6 CONTROLLING CAPABILITIES OF ELECTRO-HYDRAULIC GOVERNORS

6.1 Introduction

The primary function of turbine governor control systems is the regulation of shaft speed, and as this quantity is directly related to the rotor dynamics. the governor representation can be very significant in power system stability studies[65]. Due to the slow response of mechanical governors however, it has been common practice in the past to neglect prime mover effects for transient stability studies by assuming constant mechanical input power. Although this may be valid in the initial subtransient period there is evidence to suggest that the method of governing can affect the oscillations subsequent to the fault and for accurate results, it should not be neglected[54-58].

With the new electrohydraulic governor systems[59-61] (hereafter referred to as EH governors) the time constant and dead band of both governor and valve mechanisms are minimal enabling faster and more accurate control over the full turbine output power. Thus it is possible to restore the power balance more quickly under large disturbance conditions and effect a major contribution to the damping of transient oscillations.

An important feature of EH governing systems is a facility for the control of interceptor valves which give a faster response due to the elimination of the reheater lag. A means for high speed closure of the steam valves on detecting a fault is also incorporated, which can be triggered by an acceleration sensitive device and is commonly referred to as 'fast valving'. With straight through or 'flash' type boilers, fast valving is only performed on the interceptor valves so that the boiler is protected by the reheater buffering effect. Fast valve closure is also available on some of the later mechanically governed turbines, but in this case the tripping device is a mechanical accelerometer which has an appreciable time delay compared to the latest electronic transducers employed in EH systems which are actuated from a toothed wheel and magnetic probe speed detector arrangement.

The new governors also offer greater flexibility of operation. For example, the droop characteristic can be varied with the system on load, and more advanced control configurations such as the feedback of generator load or other similar analogue quantity, and provision for digital or analogue computer control can be incorporated. These are very important aspects of the EH system and in the following chapter the analogue control capabilities will be investigated. Once more the effects of a three-phase fault on a 500 MW generator are studied and in order to isolate the governor action,

constant excitation voltage is assumed. The electrohydraulic governor model described in Chapter 3 (Fig.3.14) is employed as it is simplified enough for representative data to be obtained, and includes most of the system components[62] individually so that comparative studies can be performed to investigate their effects.

6.2 Contribution of speed governor loop to the transient effects

6.2.1 Dynamic response advantages of the electrohydraulic system

The lack of attention to the representation of governors in previous transient stability studies has been due to the slow dynamical response of the mechanical/hydraulic systems caused by governor, reheater and steam valve lags. Thus the governor had negligible effect in controlling fast transients which is illustrated by curves (b) and (c) of Fig.6.1a, where an overall time constant of greater than 0.5 second effected little improvement on the uncontrolled generator transient response. In practice these effects would be even smaller, as the curves were obtained assuming both main and interceptor valve control which is not featured on older systems.

With the EH governor, the response is only effectively limited by the valve operation times as the speed transducer delay is negligible and the effect of the reheater is superseded by control of the interceptor valves. Intensive development of electrohydraulic actuator systems has produced substantial performance improvements since the inception of EH governors, and valve operation times (closing) have been reduced to less than 150 ms on the most modern designs.

Curve (α) indicates that the fast EH governor now makes a substantial contribution to the shorter term rotor dynamic oscillations by a marked reduction in the first and subsequent forward swings. It is interesting to note that little improvement in damping out the oscillations is achieved, and the overall effect is to shift the curve downwards away from the area of instability.

6.2.2 Consequences of slow valve opening rates

In both the electrohydraulic and mechanical/hydraulic systems rapid valve closure is accomplished by exhausting the hydraulic fluid into a reservoir, thus allowing the valve to be closed by the pressure of a heavy spring. This provides fail-safe operation should loss of hydraulic pressure occur. Opening of the valves necessitates forcing the hydraulic fluid from the

accummulators into the valve actuating cylinders by a pumping action against the pressure of the strong return springs. This is by nature a slower process and it is common for valve opening rates to be many times that of the closing value.

The effect on the transient performance is shown by Fig.6.2 where it is seen that although the underswings are increased by slower valve opening rates, there are no detrimental effects on the forward rotor angle swings. To speed up the valve opening rate would require more powerful pump motors and larger accummulators in addition to more advanced valve designs, all of which require higher capital outlay. It would seem that even if system damping is a problem there is little cost justification for fast opening of steam valves as it is questionable whether an effective improvement in performance would be produced.

6.2.3 Variations in the turbine droop setting

On most existing CEGB units there is a standard linearised turbine droop setting of 4%, which means that all machines respond equally to load changes and the valves will eventually fully close, should a speed rise of 4% or more be sustained. However it is seen from Fig.6.1b that even with a fast EH governor system, under a transient disturbance the valves attain less than half closure, and it is clear that for fault conditions a higher overall forward gain is required. This can be achieved by reducing the droop setting, which is the reciprocal of the overall gain of the governor system, and on the EH governor can be carried out on-line either manually or by a control system directive.

Fig.6.3 shows the effect of reducing the droop setting of the EH governor down to 1%, in which case the valves attain full closure in the duration of the fault period. This produces a large improvement in the transient stability margin due to the reduction of the power imbalance between generator and prime mover during the fault. Additionally a small increase in damping is produced but again the whole curve is shifted downwards causing larger underswings.

The operation of small numbers of generators, such as those fitted with EH turbine control at constant low droop settings of say 1% is inadvisable because these machines would attempt to take up the major proportion of the load fluctuations, in preference to generators operating at the 4% setting. A solution to the problem would be to keep the steady state droop setting at 4% and switch to lower values during a disturbance but if reduction of

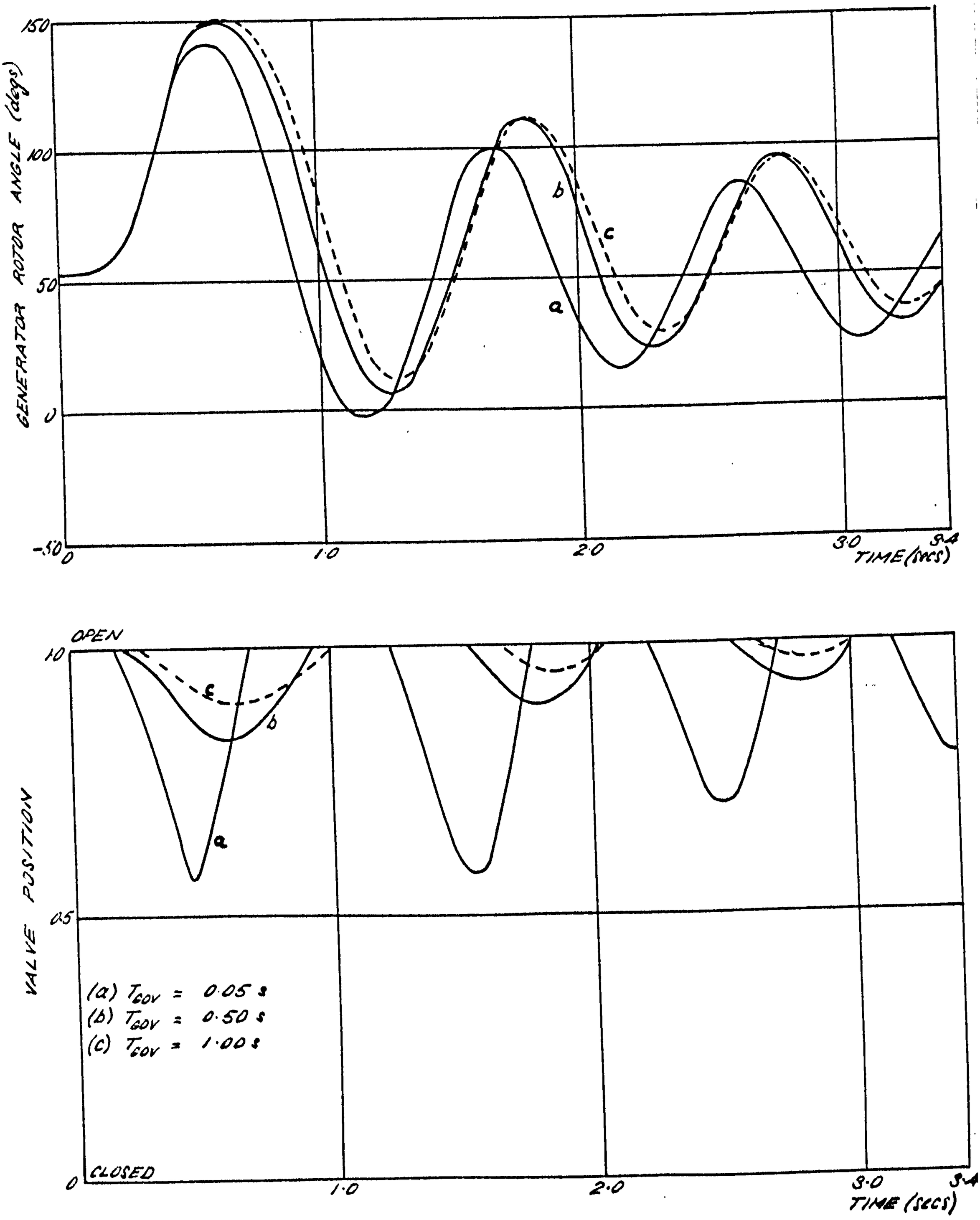

ELECTRO-HYDRAULIC GOVERNOR STUDY-
EFFECT OF INCREASED DYNAMICAL RESPONSE

FIG 6.1

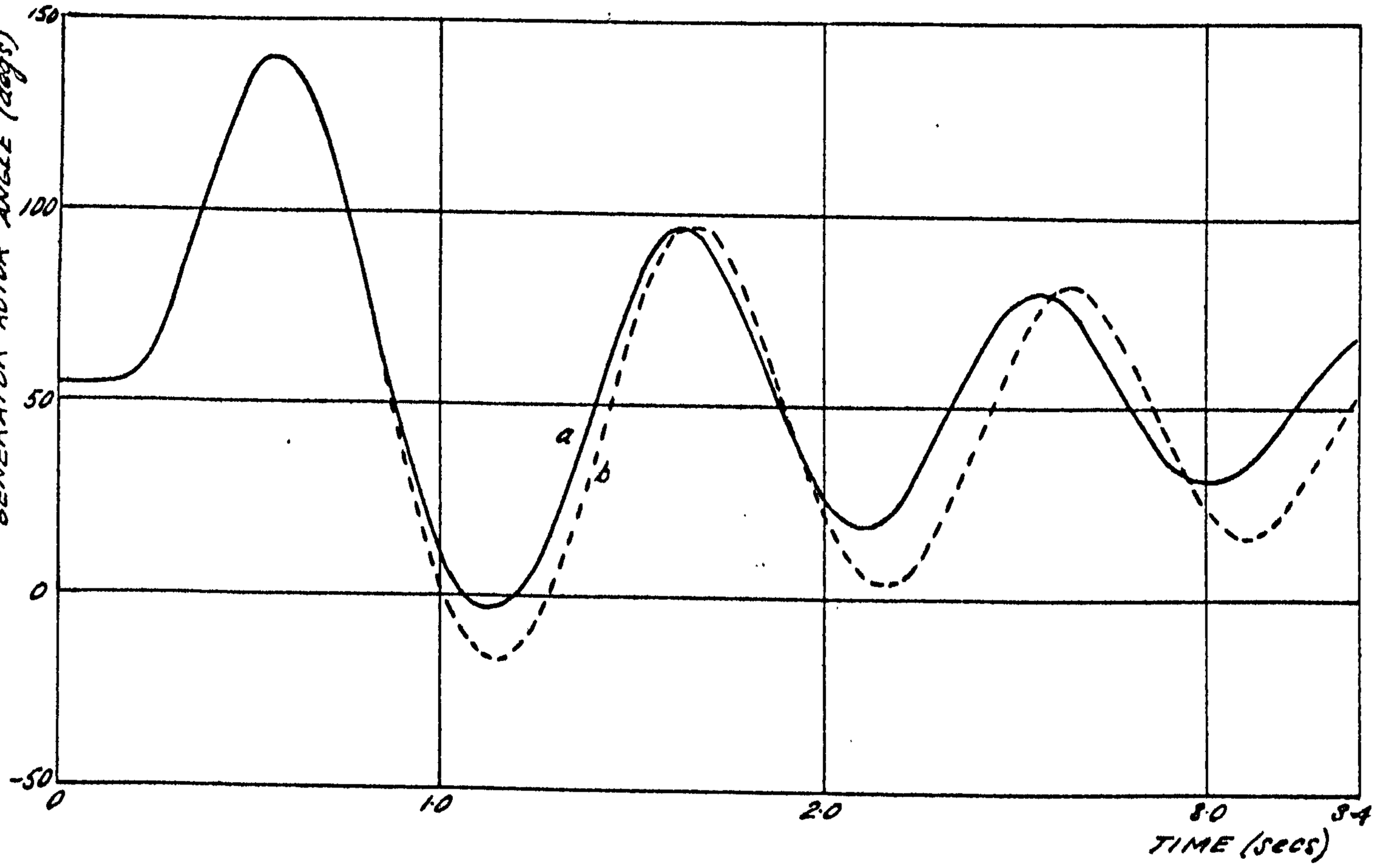

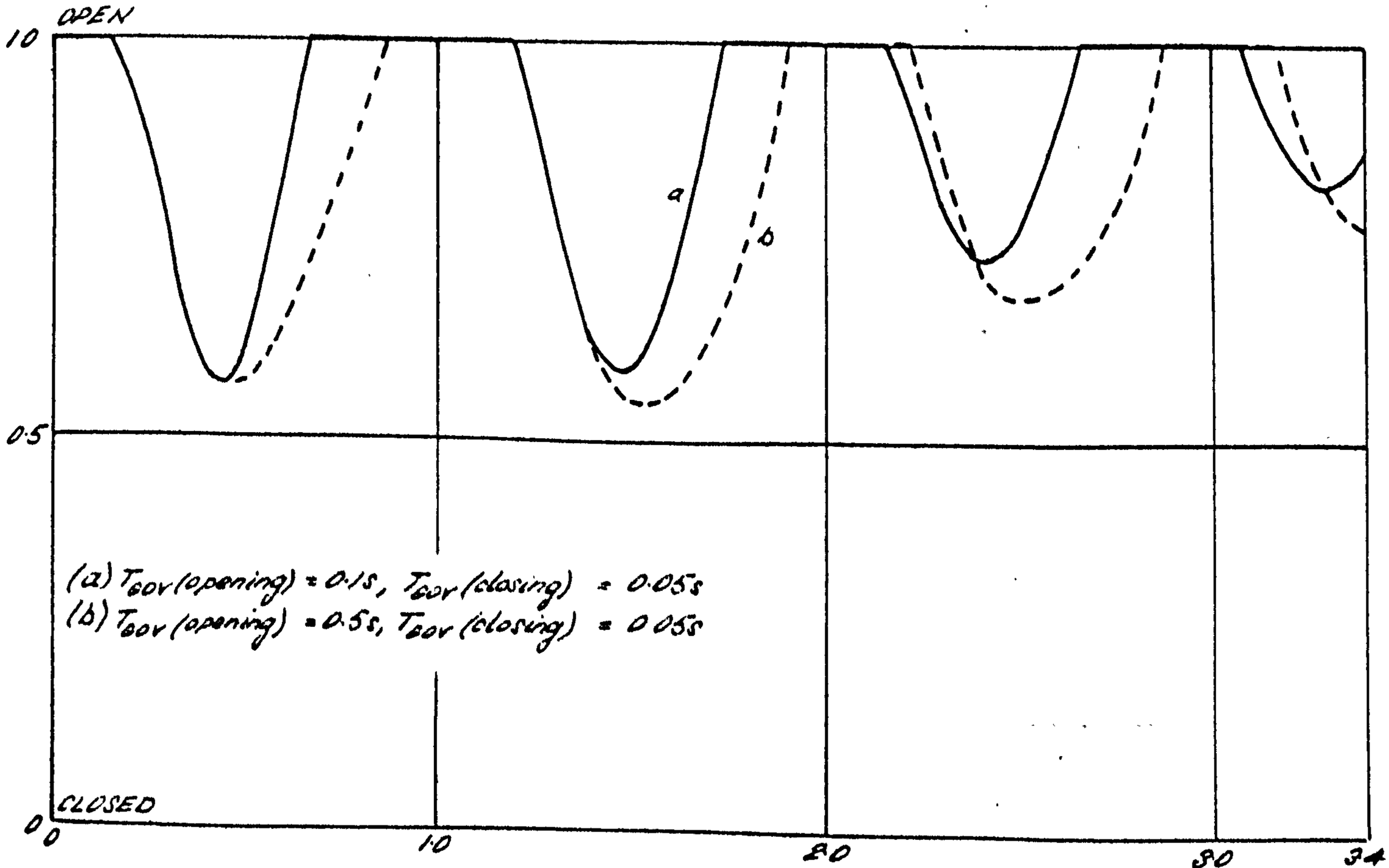

ELECTRO-HYDRAULIC GOVERNOR STUDY-
EFFECT OF SLOWER VALVE OPENING RATE

FIG 6.2

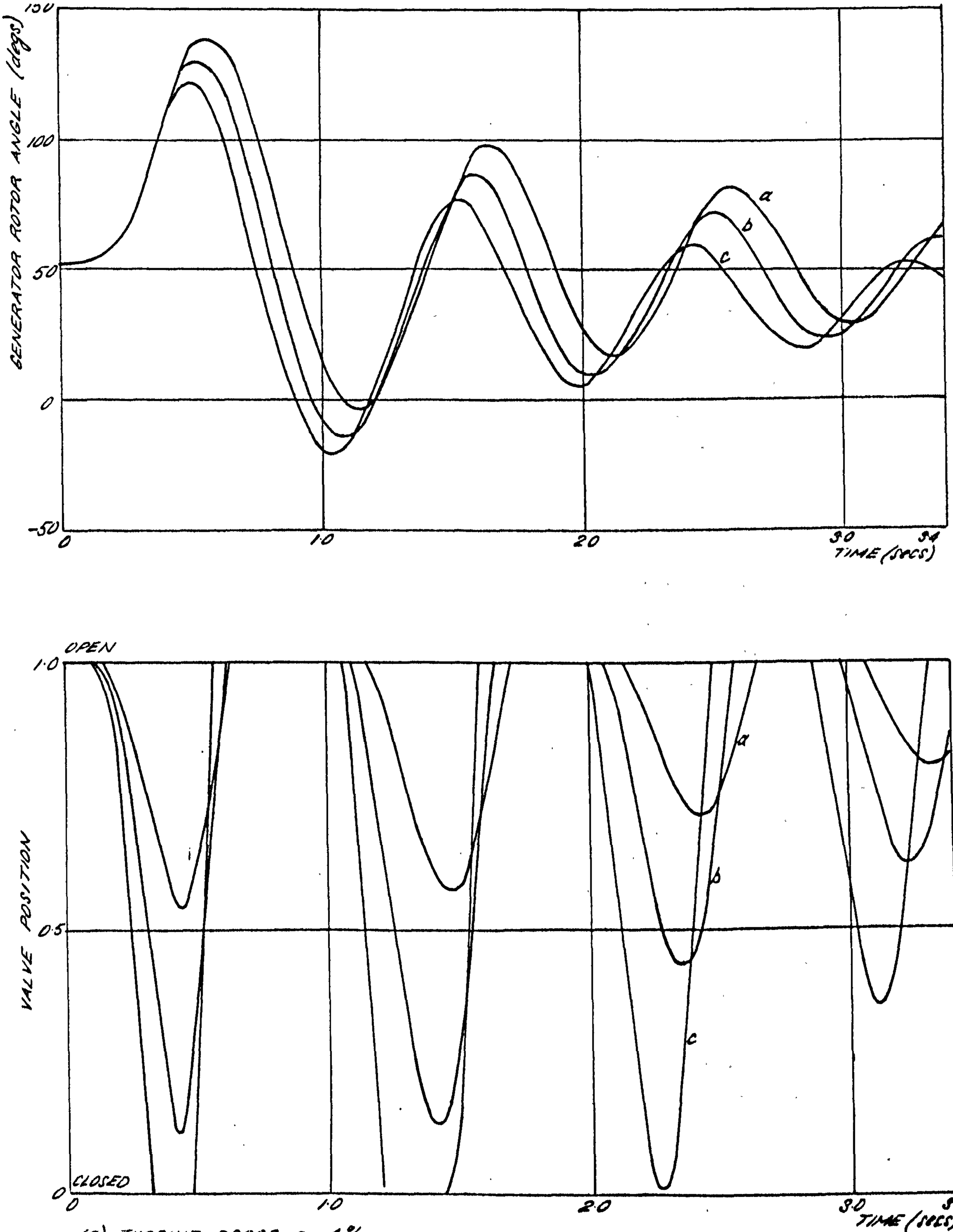

(a) TURBINE DROOP = 4%
(b) TURBINE DROOP = 2%
(c) TURBINE DROOP = 1%

ELECTRO-HYDRAULIC GOVERNOR STUDY -
EFFECT OF TURBINE DROOP SETTING

FIG 6.3

the first swing is only required then logical control or 'fast valving' as covered in the next section, is more effective. This is because the speed cannot rise instantaneously due to the effect of inertia, and therefore it is not the best control signal for during the fault period whatever the value of gain.

6.3 Fast valving

Turbine protection is normally afforded by the emergency stop valves which on an electrically governed turbine can be protectively operated by various quantities indicative of failures such as limiting values of condenser vacuum and temperature in addition to the standard overspeed trip function. However for transient faults it is not necessary to shut down the turbine entirely, and on many of the new systems 'fast valving' is featured whereby the interceptor valves (or both main and interceptor valves) are closed rapidly by a fault sending device. This slows down the acceleration of the machine due to the reduction of the power imbalance during the fault and reduces the first forward swing of the rotor as shown by Fig.6.4. Here the valves were closed for 0.5 second by an acceleration sensing device, after which the system was returned to normal speed governing with a droop setting of 4%. Both main and interceptor valves were closed simultaneously and Fig.6.5 shows the resulting decay in turbine output torque. This only falls off relatively slowly compared to the speed of operation of the valves at a rate of about 50% in 0.5 second, which is caused by steam transport delays in the pipework downstream of the valves and in the turbine cylinders. Due to the fairly low level of acceleration threshold chosen for the study, a further fast valving operation took place at the first rotor underswing after which normal governing was resumed. The actual reduction in the rotor angle peaks will depend upon the reaction time of the fault sensing device (in this case 20 ms) and the valve closure time. Fig.6.4 also shows the effects of slower valve opening rates on the performance with fast valving where again an increase in the underswings was produced as in the case of normal speed governing.

As with the thyristor excitation system, the fast governor could be operated in a bang-bang fashion to obtain large improvements in system damping by optimising the timing and duration of a series of fast valving operations. The ultimate system would be the logical control of both excitation and governor which would require a fast multiple access digital computer operating on-line[63].

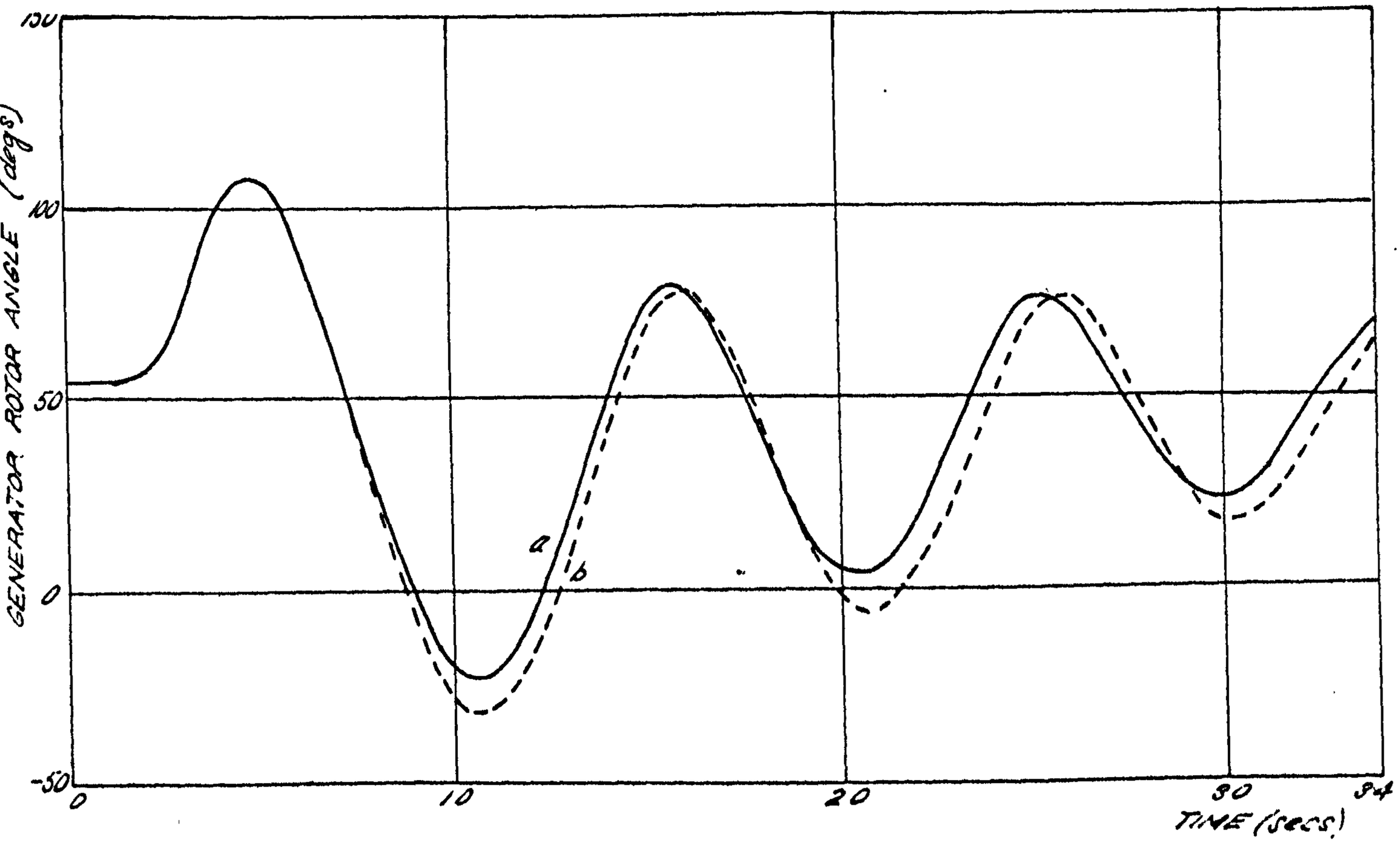

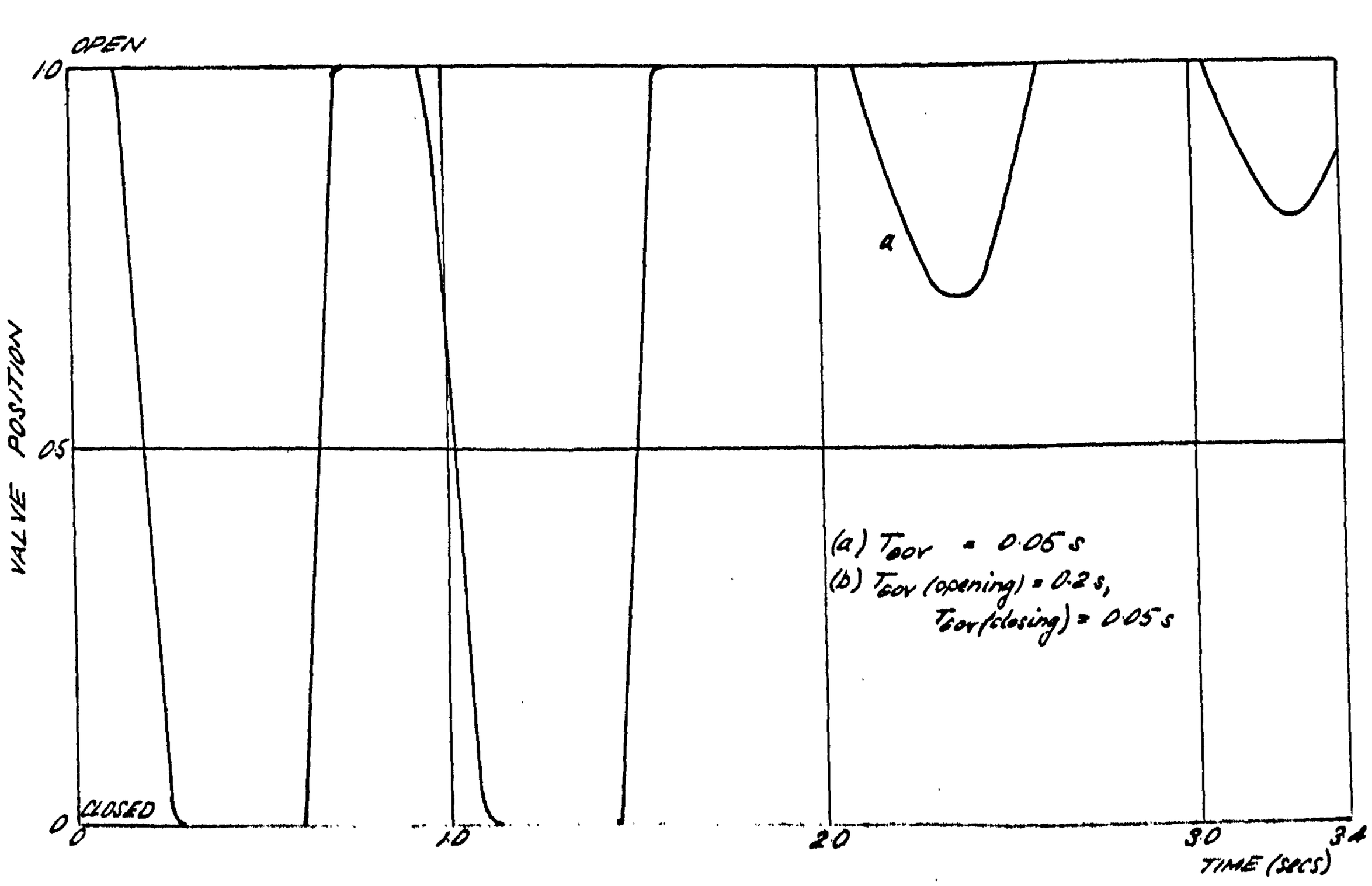

ELECTRO - HYDRAULIC GOVERNOR STUDY - "FAST VALVING"

FIG 6.4

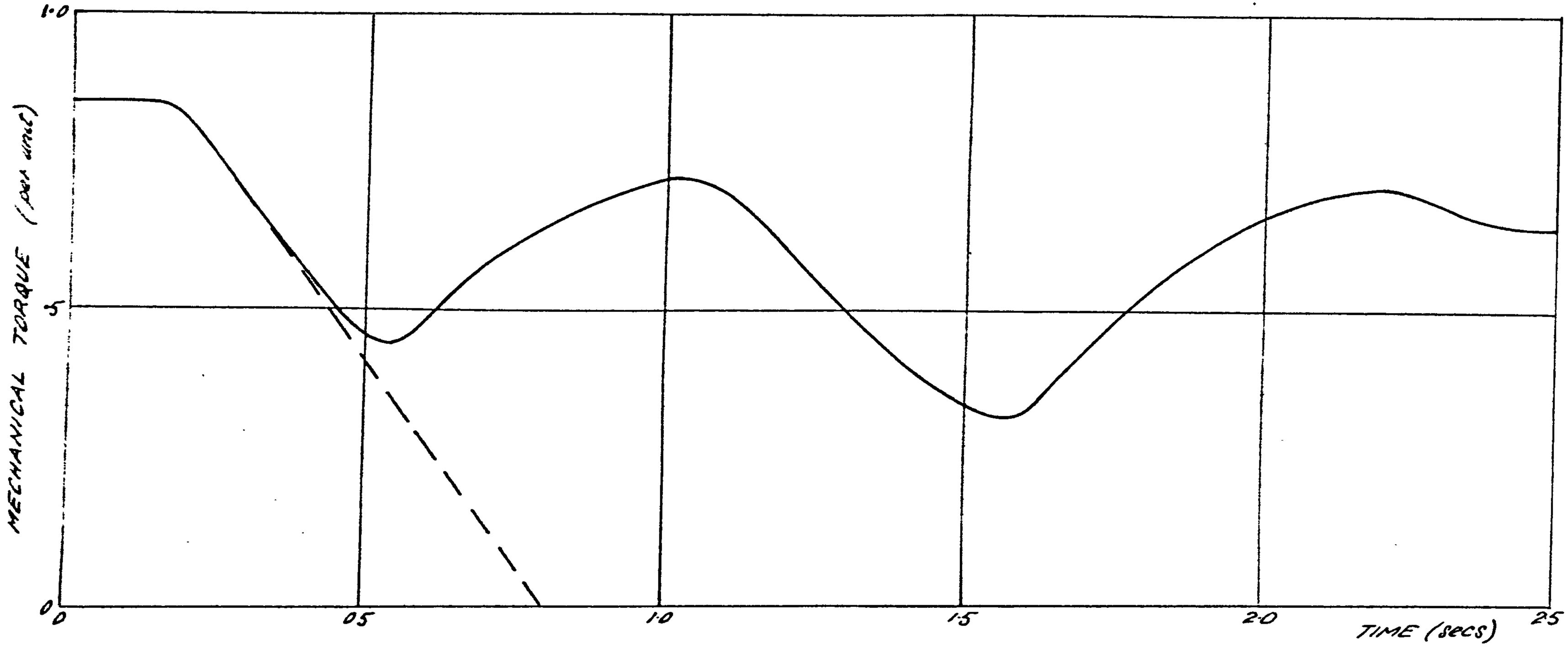

ELECTRO-HYDRAULIC GOVERNOR STUDY- MECHANICAL TORQUE VARIATION DUE TO FAST VALVING

FIG 6.5

6.4 - Advanced governor stabilising techniques

Rate of change of input stabilisation as was investigated in the AVR system, can also be applied to the governor, but only as a forward element in this case as it would be extremely difficult to obtain an output feedback signal (i.e. mechanical torque). Fig.6.6 shows the result of using various values of phase advance on the speed input by varying the time constant T_s of Fig.3.14. Using this type of stabilisation in the governor produces a far greater improvement than in the excitation system, as it compensates for the valve and turbine phase lags to produce effective velocity damping. Also, complete closure of the valves is accomplished directly after fault application, giving rise to large reductions in the first forward swing. Unfortunately, during swings in the negative direction, the valves are also closed causing a very large first underswing as there is not enough mechanical torque to balance the electrical torque that was restored after the fault. Further, if the phase was advanced too far then a long slow second underswing ensued and it appeared there was an optimum value of T_s between 1 and 5 seconds (T_v = 0.01 secs).

Another effect of advancing the phase too far was to induce valve oscillations as shown by Fig.6.6b. The frequency of oscillation was about 5 Hz and is a case for further study using dynamic stability analysis techniques. This phenomenon could be disastrous if the oscillations were large, or if the frequency coincided with one of the natural torsional frequencies of the shaft, in which event the build up of oscillations may take place causing serious damage unless suitable protection is contrived. This problem has been encountered using a speed stabilising signal into a static excitation system[37] and as the dynamic response is increased it is likely that the same effects could be induced by EH governor systems.

The effects of feeding back an acceleration term were identical in the governor case to the effects of the rate of change of velocity stabilisation (Fig.6.7) as they are the same quantity. This is also true for power error feedback (graphs not plotted as they were similar to Fig.6.7) which is present on most electric governors in the form of a load control loop. However, the contribution to system damping will be small as there is usually a large time constant associated with this channel.

The use of a combined acceleration and velocity governor feedback is portrayed by Fig.6.8, where no deterioration of the performance was found. Thus the normal and stabilising signals appear to be compatible and no interaction effects were observed.

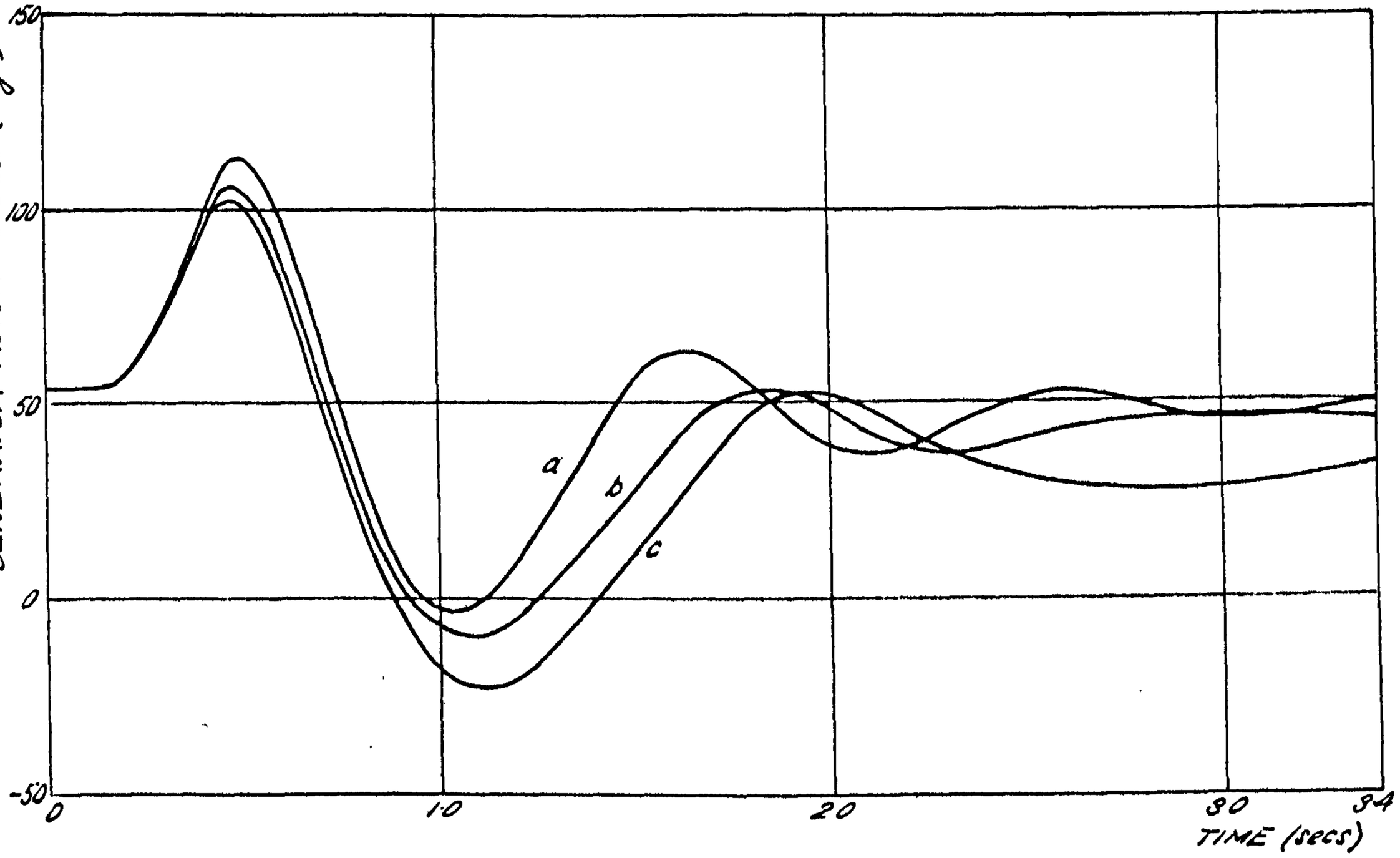

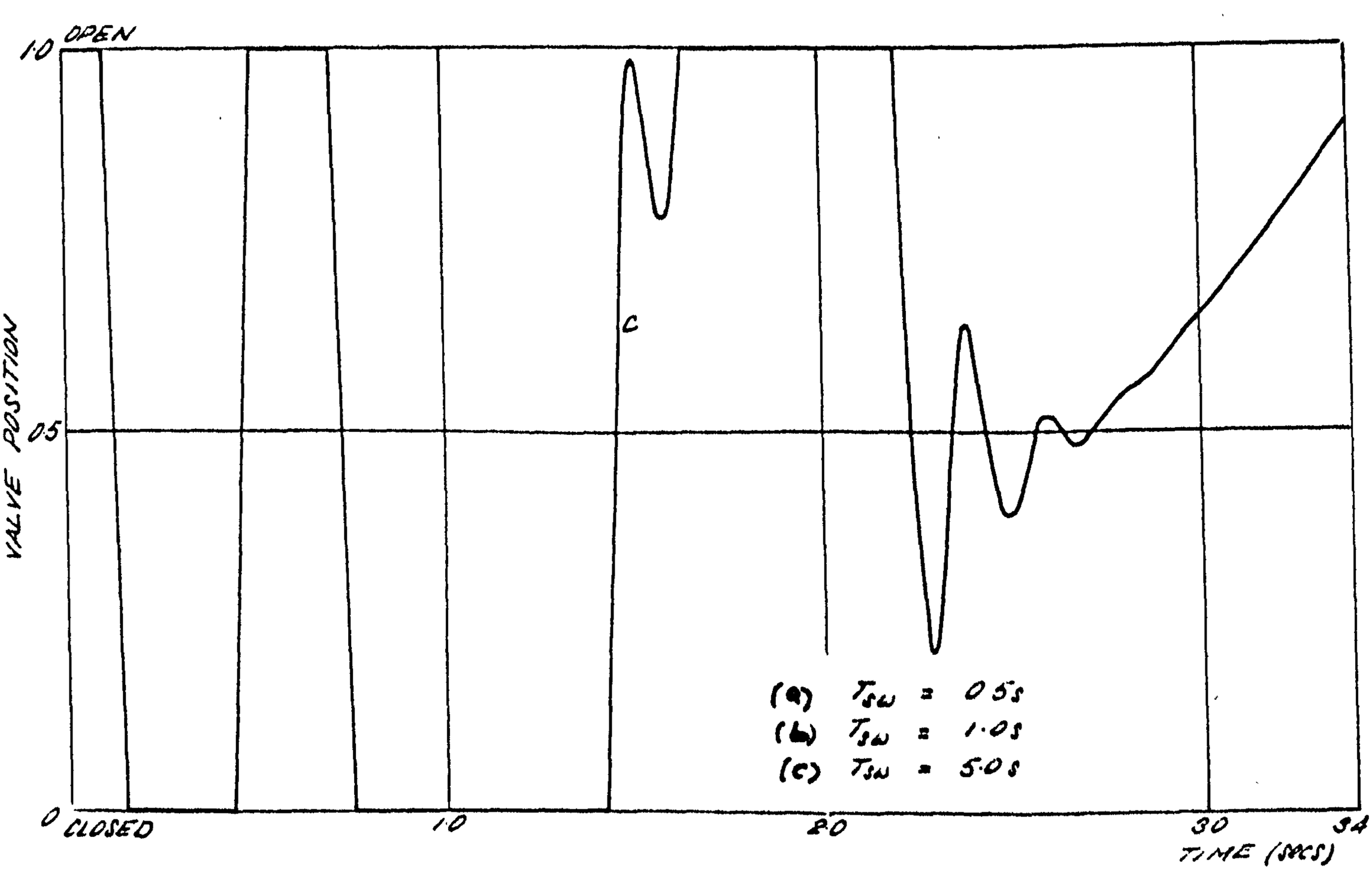

ELECTRO-HYDRAULIC GOVERNOR STUDY-

EFFECT OF RATE OF CHANGE OF VELOCITY STABILIZATION

FIG 6.6

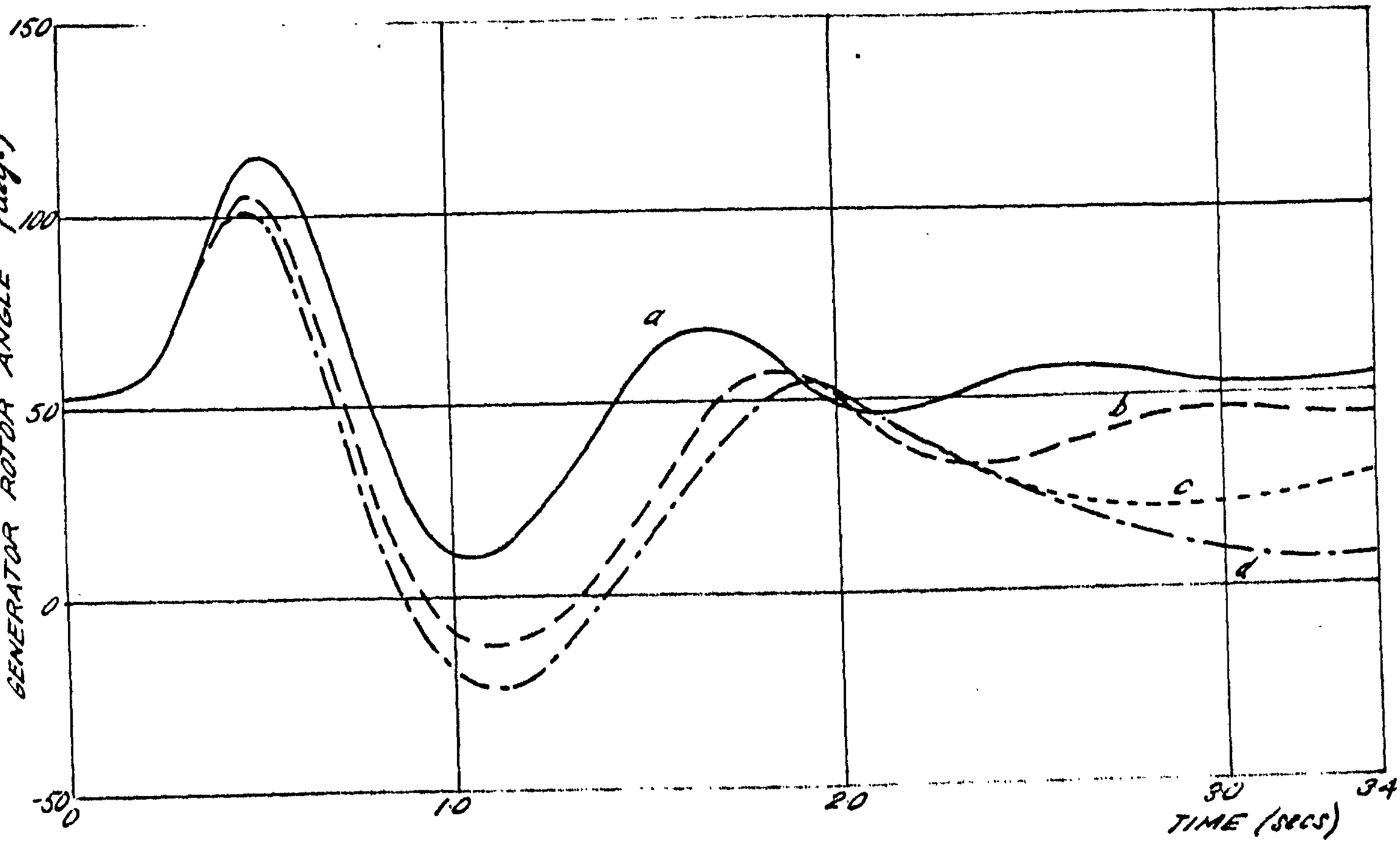

(a) G_a = 0·5 per rad/sec²
(b) G_a = 1·0 per rad/sec²
(c) G_a = 5·0 per rad/sec²
(d) G_a = 10.0 per rad/sec²

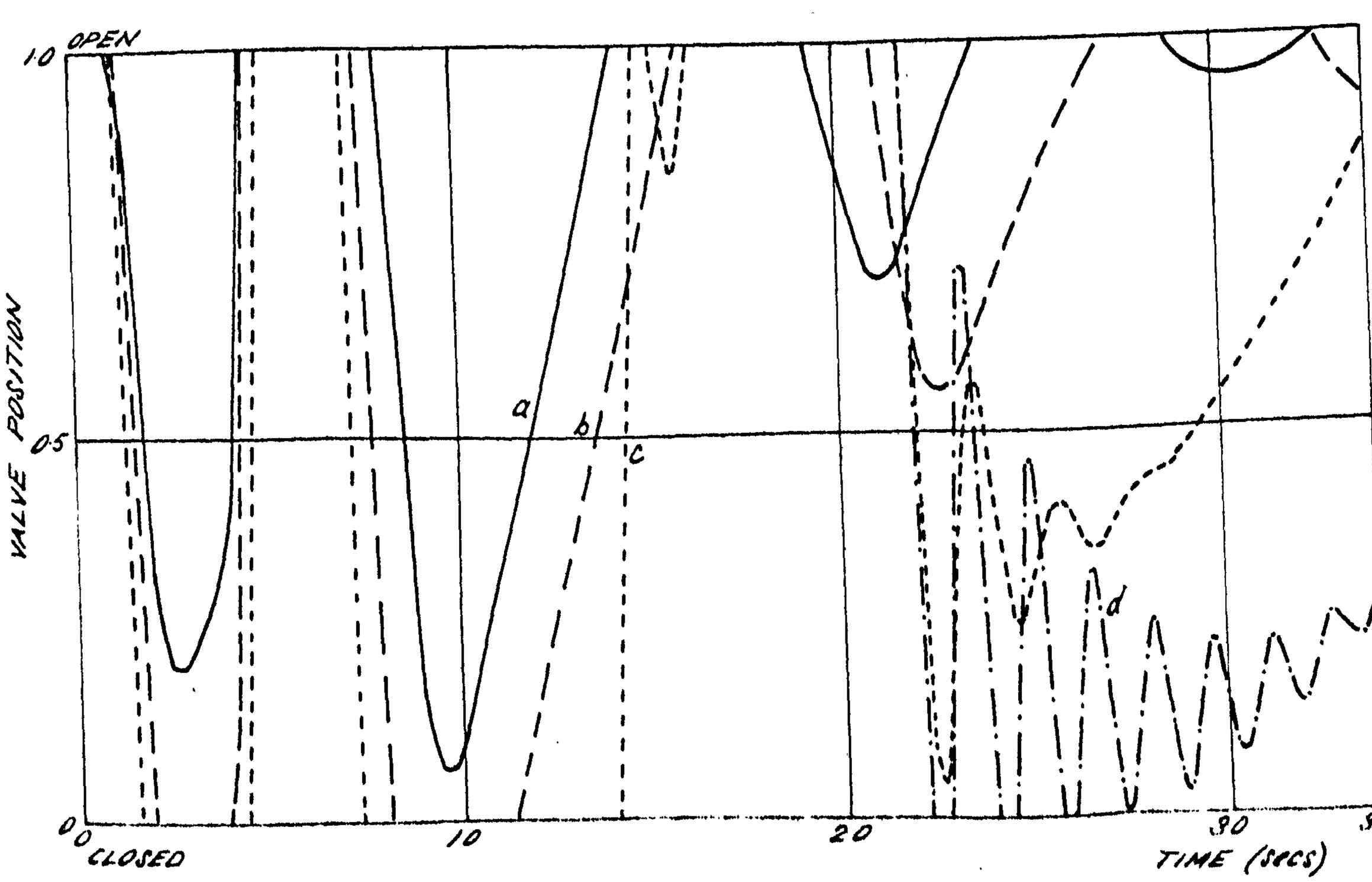

ELECTRO-HYDRAULIC GOVERNOR STUDY-
EFFECT OF ACCELERATION FEEDBACK

FIG 6.7

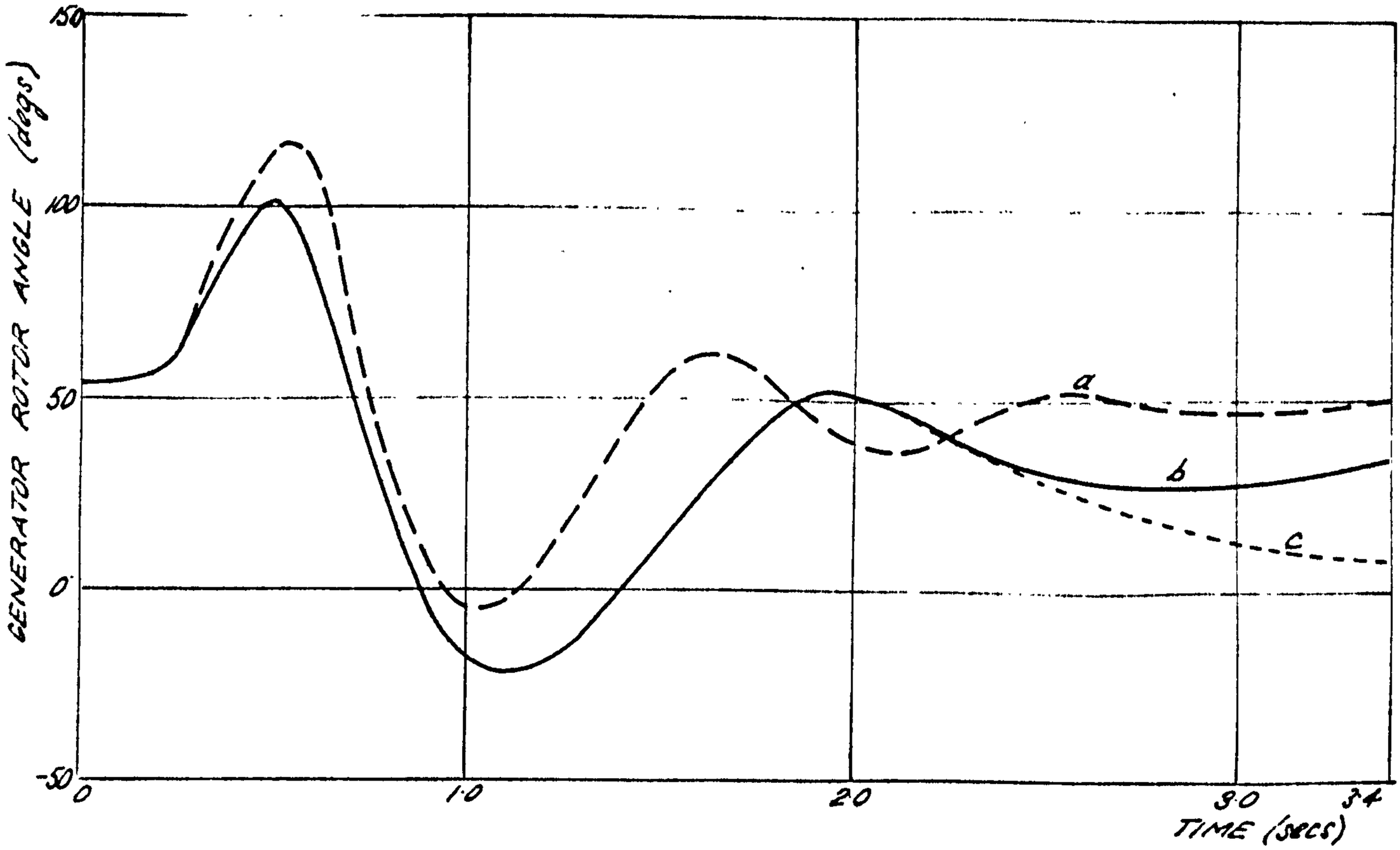

(a) G_a = 0·5 per rad/sec², TURBINE DROOP = 4%
(b) G_a = 5·0 per rad/sec², TURBINE DROOP = 4%
(c) G_a = 5·0 per rad/sec², TURBINE DROOP = 1%

ELECTRO-HYDRAULIC GOVERNOR STUDY-

EFFECT OF COMBINED VELOCITY AND ACCELERATION CONTROL

FIG 6.8

The effectiveness of the governor stabilisation can again be explained by inspecting the mechanical equation of motion as in the case of the AVR studies, i.e.

$$\frac{2H}{\omega_o}\ddot{\delta} = T_L - T_e \quad \text{(neglecting losses)}$$

The mechanical torque during a disturbance will contain a transient variation T_L in addition to the steady state component T_{Lo} which will depend upon the applied control, i.e.

$$\frac{2H}{\omega_o}\ddot{\delta} - \Delta T_L = T_{Lo} - T_e$$

If the governor system had an instantaneous response then ΔT_L would be directly proportional to speed giving a large degree of damping. However a phase lag is introduced by the steam storage delays as deduced from Fig.6.5 reducing the effectiveness ofthe governor damping. This explains the improvement in performance obtained by the rate of change of velocity term which advances the phase to compensate for the steam lags. From Fig.6.5 the approximate time constant of decay of turbine output torque upon sudden valve closure is 0,7 seconds. If the turbine system is represented by a single first order lag, then the phase retardation at the approximate frequency of oscillation of the rotor of 1 Hz is calculated by:

$$f(\Delta T_L)_{j\omega} = \frac{1}{1+j(0.7\times 2\pi\times 1)} \equiv 0.0492 - j(.216)$$

From which the phase lag is

$$\phi_T = \arctan\left(\frac{0,216}{0,0492}\right) = \arctan\ (4.4) = 77.4^{\circ}$$

This is compensated for by the phase advance network

$$f(\dot{\delta})_p = \frac{1+pT_s}{1+pT_v}$$ where T_v is the speed transducer lag which was ,01 secs in the study

and

$$f(\dot{\delta})_{j\omega} = \frac{1+j(2\pi\times T_s)}{1+j(.02\pi)} = \frac{[1+j(2\pi\times T_s)][1-j(.02\pi)]}{1+4\pi^2\times 10^{-4}}$$

$$= \frac{(1+.04\pi^2\times T_s) + j(2\pi\times T_s - .02\pi)}{1+4\pi^2\ 10^{-4}}$$

The phase advance is then

$$\phi_s = \arctan\left(\frac{2\pi \times T_s - .02\pi}{1 + .04\pi^2 \times T_s}\right)$$

If this exactly compensates for the steam system lag then $\phi_s = \phi_T$, i.e.

$$\frac{2\pi T_s - .02\pi}{1 + .04\pi^2 \times T_s} = 4.4$$

From which T_s is calculated as 2.64 secs.

This agrees with the results shown in Fig.6.6 where the best performance was obtained with a stabiliser time constant of between 1 and 5 seconds.

If the governor is over compensated by too much rate of change of velocity then ΔT_L will be mainly acceleration dependent, which increases the effective inertia. This produced a very long slow underswing when linear control was established which commenced at about 2.2 seconds (Figs.6.6 and 6.7).

6.5 Practical considerations

Although the governor model used for these studies is much more involved than the equivalent excitation system model used in Chapter 5, there are a far greater number of simplifying assumptions. There is a pressing need for extensive testing of electrohydraulic governing systems for determining all the characteristics and non-linearities of the system components so that the formulation of more accurate models can be achieved.

In the steam valves there is usually some form of linearisation either by electrical or mechanical means. This only covers the steady state characteristic but under transient conditions it is likely that the assumption of linear variation of steam pressure with valve travel no longer holds. The valve dynamics were represented by a simple gain and time constant lag function which means that they can be made to operate at any speed depending upon the input levels. In practice there will be a limit to the valve travel velocity which is difficult to simulate, and as a temporary measure the input level limits shown on Fig.3.14 were introduced.

Assuming constant boiler pressure may also lead to performance errors, in particular the response after a few seconds or so where the boiler system dynamics will come into effect. This is especially true of flash boilers which contain only a small volume of entrained steam. The reheater pressure was controlled by a single lag with a time constant of 7 seconds, which

again is an over simplification as the reheater response is to some extent pressure dependent.

Finally, the turbine responses were once again simulated by simple first order lag functions but the actual response is determined by the very complex thermodynamical processes taking place inside the turbine. However, contrary to what might be expected, it has been found elsewhere[64] by comparing computed results with site tests that the simplified representation gives a good approximation to the actual response.

Due to lack of operational experience there is at present no universally accepted control mode of EH governors in the steady state and various policies can be applied to meet differing system requirements. In one case the main and interceptor valves may operate simultaneously to give a 'black box' governor behaviour with a linear droop characteristic. Other systems have sequential operation of steam valves producing a stepped droop characteristic sometimes referred to as 'incremental' droop, and a common mode of operation for base load machines is with the interceptor valves fully open, a fine control being afforded by varying only the governor valve openings for normal operation. Hence for accurate governor studies, account should be taken of these differing control methods.

6.6 Summary and conclusions

It has been found that the electrohydraulic governing system is capable of massive improvements in increasing both the transient stability margin (i.e. the first rotor angle forward swing) and the damping of subsequent rotor oscillations. This is achieved by the ability of the governor to directly influence the power balance equation during transient disturbances by superimposing a velocity damping effect on the prime mover torque. However true velocity damping is only obtained by compensating for the control valve and steam transport delays. This can be achieved by phase advancing the speed signal input by an analogue filter or by using correct amounts of acceleration or electrical power feedback signals.

Fast valve closure was another highly effective method for increasing the stability margin due to the reduction of the initial rotor acceleration and during an extended fault, this may prevent the operation of the overspeed trip thus keeping the set in synchronism with the system.

In all the controls discussed the valves were closed at various speeds during the fault. Although this reduces the first forward swing, the power

imbalance immediately after the fault when the electrical load is restored, is greater causing a larger underswing. This is made worse by the slower opening rate of the valves but it does not have a deleterious effect on the stability margins.

Increasing the gain and dynamical response of the governor in general improved every aspect of generator performance. This includes the terminal voltage recovery, a quality which is not widely appreciated. Fig.6.9 shows the terminal voltage response improvements obtained with both standard speed governing (curve (b)) and with acceleration feedback (curve (c)) compared to the uncontrolled response (curve (a)).

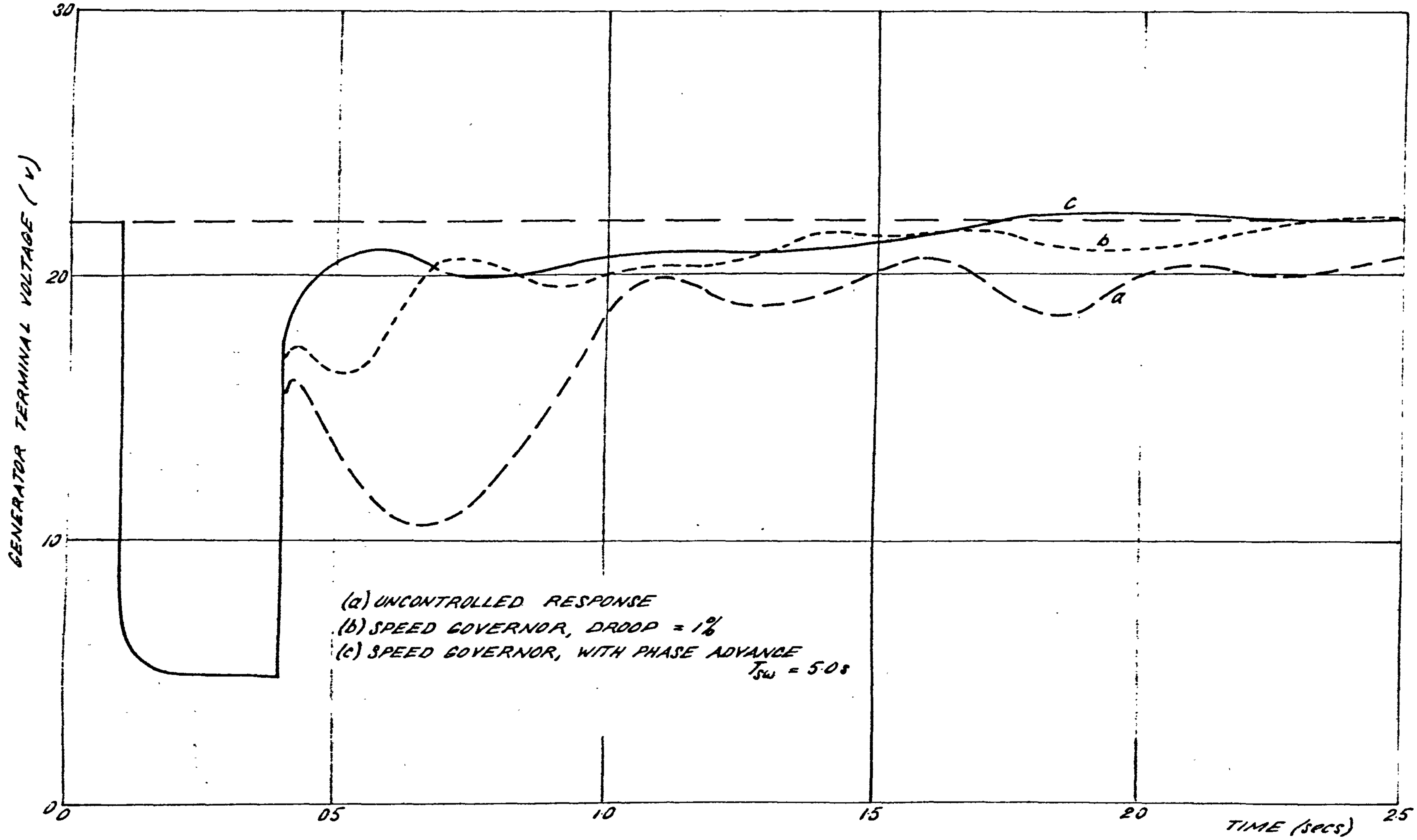

ELECTRO - HYDRAULIC GOVERNOR STUDY - TERMINAL VOLTAGE IMPROVEMENTS

6.9 9/1

7 COMBINATION OF HIGH SPEED EXCITATION AND TURBINE CONTROLS

7.1 Introduction

In the previous chapters the effects of high speed excitation and turbine control systems on turbogenerator transient performance have been studied acting separately. The most effective controls for each case were formulated using well established analogue techniques with emphasis applied to the practical realisation of the systems on turbogenerators in the immediate future. Longer term investigations into true optimal controllers using analogue[66] and digital[26,28] techniques are under way for which investigations, this thesis can be regarded as preliminary work. The present project would not be complete without studying simultaneous action of high speed excitation and turbine controls to ensure compatibility and that no interaction effects exist. Another factor to be clarified is the trade-offs between using either thyristor excitation systems, or electrohydraulic governors, or both in a particular case in preference to the conventional slower acting systems such as diode excitation and mechanical/hydraulic governor, because of the increased capital outlay of the new systems. The best assessment would be obtained by multimachine studies for a specific example and this would determine any interaction effects between machines in close proximity with differing controls. However this short study of the single machine case is only intended as a general performance check for the compatibility of the two systems.

7.2 Effects of simultaneous fast action of standard AVR and governor controls

Fig.7.1 shows the results of combining various AVR and governor response without any form of additional stabilising technique.

Curves (a) and (b) show the effect of 4% and 1% governor droops respectively when the response of both control systems was high. This produced similar performance changes to the action of the governor alone, i.e. the transient stability margin and the damping of oscillations was improved by the lower droop figure. The effect of slowing down the regulator response but with fast governor control is shown by comparing curves (b) and (d). It is seen that the slow regulator gives an improved second swing but after this it is superseded by the performance with the faster regulator. This is at variance with the findings of the studies of excitation acting alone where increasing excitation response gave an overall weakening of the damping capability. The action of the

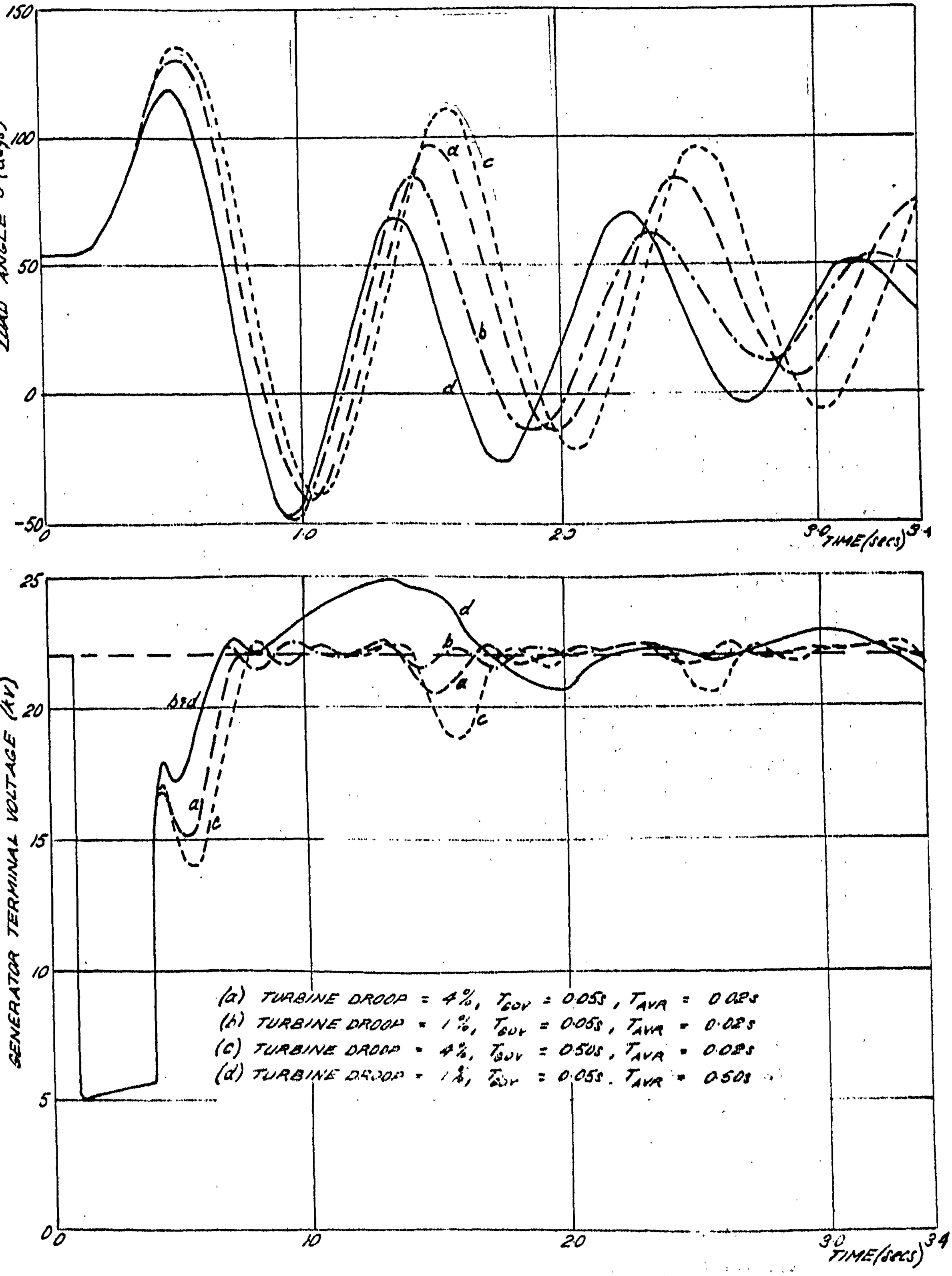

EFFECTS OF SIMULTANEOUS ACTION OF AVR AND GOVERNOR

FIG 7.1

governor seems to reverse this trend in the later stages of the transient. In addition the excitation system had little contribution to the transient stability margin on the first swing when acting simultaneously with a fast governor. A slow governor and fast excitation gave the worst results of the various combinations as shown by curve (c).

The best terminal voltage recovery was obtained when the AVR was working in conjunction with a fast 1% droop governor system. With a slow AVR (T_{FN} = 0.5 sec) although the line voltage returned to its original value in about 300 ms after fault removal, there was subsequently a large overshoot. With fast excitation and high performance governing however, the excitation recovered quickly and remained relatively constant to within 2½% of the pre-fault value for the duration of the transient rotor oscillations.

7.3 Effects of simultaneous high speed controls with stabilising terms

In Chapter 5 it was found that the extremely damped response obtained with acceleration control of excitation was deteriorated under voltage regulator action. Fig.7.2 shows that including the effects of a fast governor on this combination partially restores the damping and gives a much reduced first swing. In addition, the voltage control is more effective with smaller fluctuations in the transient period.

In Fig.7.3, curve (b) shows the effect of including an acceleration term in the governor with a fast AVR controlling the excitation. The inclusion of exciter effects gains a small reduction of the first forward swing but this is followed by a larger increase of the underswing compared to the action of the governor alone (curve (a)). However, almost perfect terminal voltage recovery was achieved in less than 200 ms after fault clearance with a minimal oscillation thereafter.

Introducing stabilising terms into both excitation and governor systems had little extra benefit than using governor stabilisation only (curve (c) of Fig.7.3. In this case the two acceleration terms had a combined effect in increasing the effective moment of inertia which was embodied by a further decrease in the frequency of the long slow oscillation after the initial fast transient had subsided.

7.4 Conclusions

It was found that when both fast excitation and governor controls acted simultaneously each system contributed to the improvement of transient performance and negligible interaction effects were present. The total

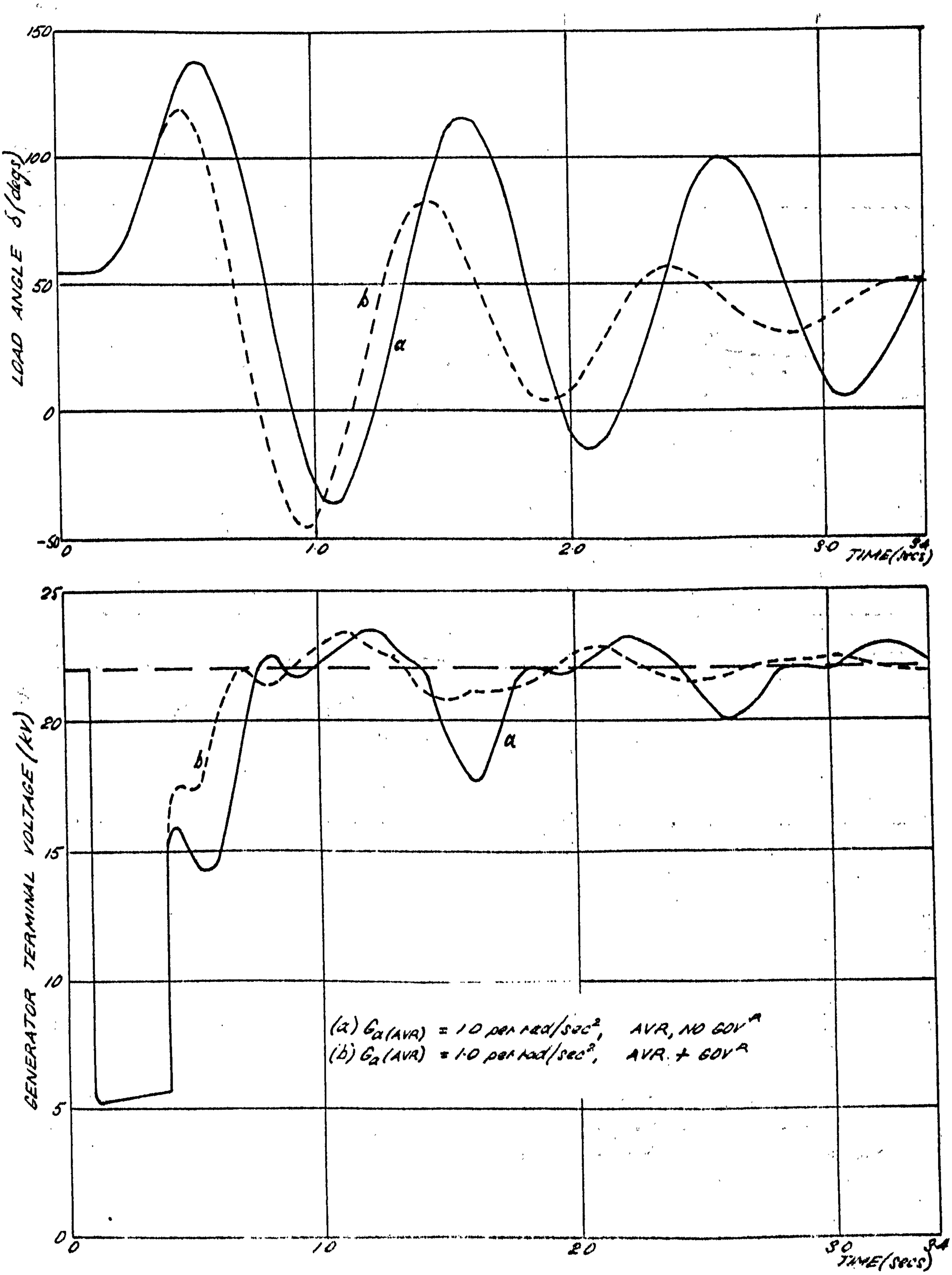

DUAL AVR AND GOVERNOR CONTROL WITH ACCELERATION FEEDBACK IN EXCITER

FIG 7.2

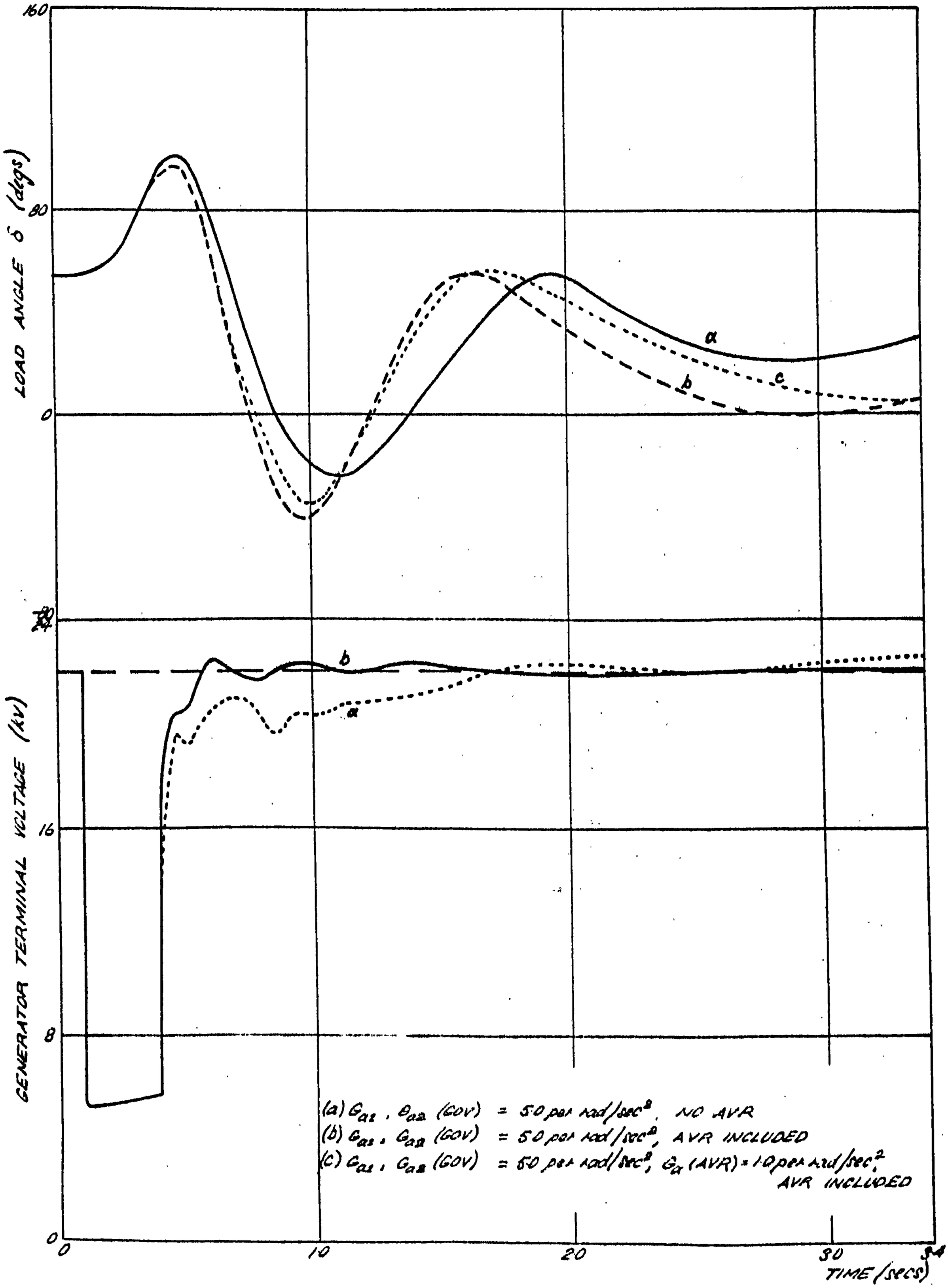

DUAL AVR AND GOVERNOR CONTROL WITH ACCELERATION FEEDBACK IN GOVERNOR

FIG 7.3

reduction of the first rotor angle excursion with combined control was 55^{o} representing a great improvement in the transient stability margin which it is doubtful could be achieved by any other means. The major portion of the improvement of the rotor system dynamics was brought about by the governor, whilst the excitation was more effective in controlling the generator terminal voltage as might be expected. In their respective controls, the two systems assisted each other, so that the best overall performance regarding both the rotor angle swings and the terminal voltage recovery was obtained with voltage feedback in the excitation system, and rotor dynamic signals of velocity and acceleration controlling the prime mover.

It is quite likely that both high speed excitation and governor controls will appear together on turbogenerators in the near future as the systems become more widely accepted. The cost of an electrohydraulic governor system is at present much higher than its mechanical counterpart but the static thyristor system (transformer fed) is relatively inexpensive as there is no rotating exciter. This system is becoming increasingly popular especially in North America, as an added advantage is that there is a saving of about 25 feet in the overall length of the set.

In the past, for combating stability problems, the tendency has been to concentrate on fast excitation systems, but the results of these studies indicate that electronic governing would be a better solution. When serious voltage fluctuations exist, especially those of short duration that do not cause appreciable rotor movement, then fast thyristor excitation would be the effective solution. These conditions would occur with arc furnace loads, electrolytic smelting, or large motor start-up currents, and generators with local loads of these types at Neepsend Power Station near Sheffield have been converted to thyristor excitation by CEGB[67].

8 INSTRUMENTATION FOR MEASURING TURBOGENERATOR ELECTRICAL AND DYNAMICAL QUANTITIES

8.1 General

In order to implement the control policies developed in the previous chapters, novel instrumentation has to be designed to satisfy the requirement of high speed of operation. Other factors to be considered if the instrumentation is to be used for permanent monitoring on a turbo-generator are the intrinsic stability, signal to noise ratio, and equipment reliability.

In general the purpose of the instrumentation is to produce a voltage analogue signal proportional to the mean value of the quantity being measured. It is usually necessary to use an electro-mechanical transducer or transformer to provide the input for the electronic circuitry.

8.2 Descriptions of circuits

8.2.1 Armature voltage measuring circuits

The standard method of voltage measurement is probably not fast enough for high speed control purposes but is outlined here for completeness.

The machine line voltages are transformed down to about 110 volts by three V.T's (see Fig.8.1). This is then rectified by a three phase full wave bridge and passed through a simple passive low-pass filter in order to attenuate the 300 Hz ripple. Due to the high gain of modern AVR's, a filter with a time constant ofmore than 50 milliseconds is usually required which gives an attenuation of 40 dB at 300 Hz for a single stage filter.

A method which gives a time delay of only 10ms on a single phase waveform without any filtering has been developed from previous work[7]. This employs a data sampling device which samples and holds the peak value of the AC waveform every half cycle. The system is shown in diagrammatic form in Fig.8.2. If this were extended to three phase operation an even better response of 3.3 ms could be achieved.

The principle of the analogue data sampler is illustrated by Fig.8.3a. The analogue information on input 1 is buffered by amplifier A1 which has a very low output impedance. This enables capacitor C to charge up rapidly to the instantaneous input voltage when the FET is switched ON by a pulse appearing on input 2. The pulse duration is just sufficient to enable the capacitor to attain full charge at the maximum input voltage and upon removal

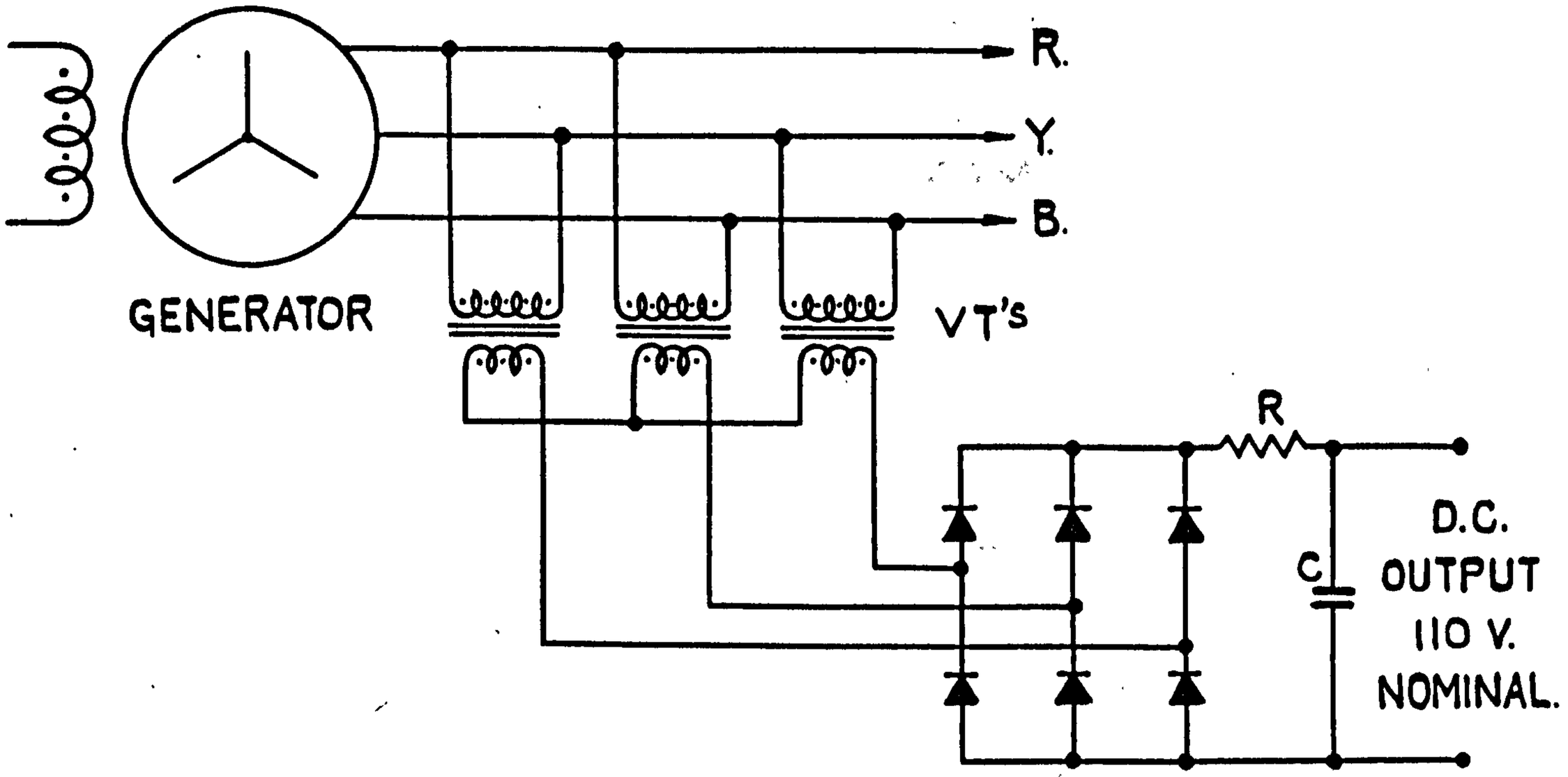

ARMATURE VOLTAGE MEASUREMENT.

FIG.8.1.

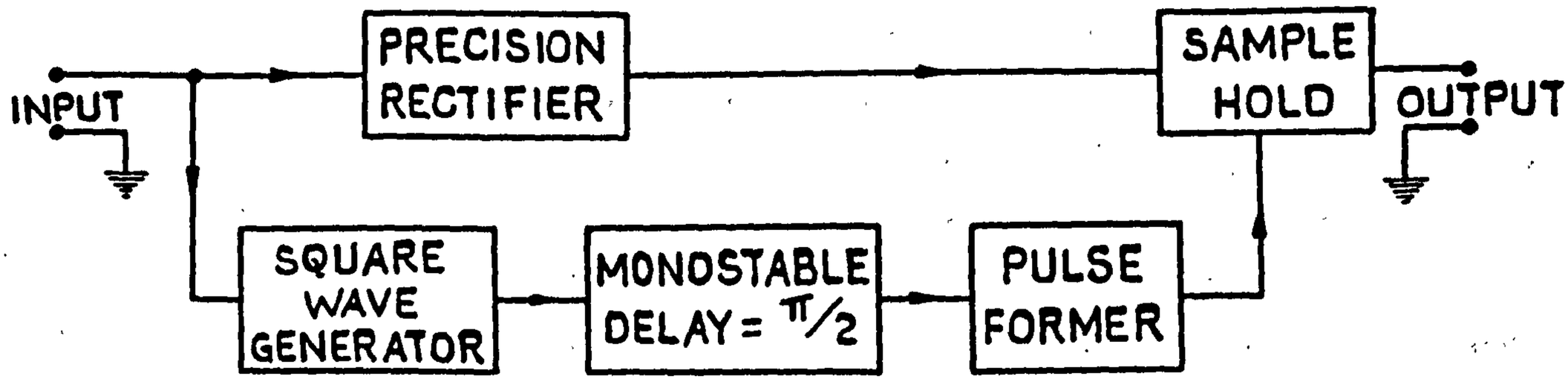

(a) LAYOUT DIAGRAM.

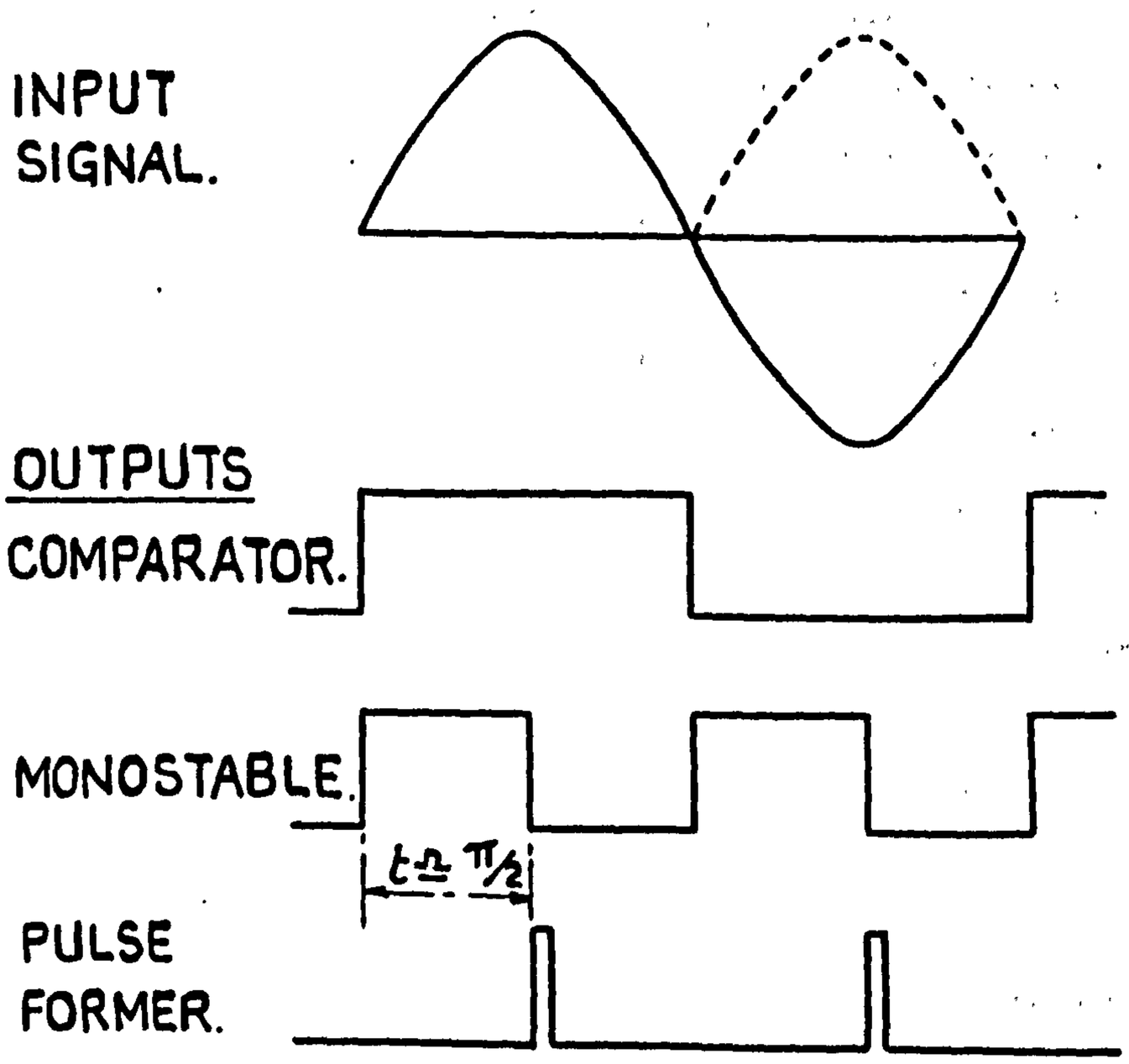

(b) OPERATION.

SAMPLE HOLD VOLTAGE TRANSDUCER.

FIG. 8.2.

of this pulse the FET switches OFF leaving the charge on the capacitor to leak away through the input impedance of amplifier A2 until the next 'sample' occurs. If the input impedance of the amplifier A2 is very large then the output signal will remain almost constant between samples as very little charge is lost by the capacitor. The circuit of Fig.8.3b is a unity gain amplifier which satisfies the requirements for both of the amplifiers A1 and A2 by having an FET input stage giving high input impedance and an emitter follower output stage giving low output impedance. Both input and output stages are supplied from FET constant current sources and diode D1 is included to offset the base-emitter voltage drop of Q3. A capacitor C1 is required in close proximity to the drain of Q1 to eliminate spurious oscillations which may occur due to the combination of high impedance and junction capacitance.

Returning to the layout of the voltage transducer of Fig.8.2, the input AC voltage is divided into two channels, in one of which it is full wave rectified in a precision rectifier circuit so that two positive peaks may be sampled per cycle, whilst in the other channel the sampling pulses are formed. This is done by first converting the sinusoidal waveform into a square wave which then drives a monostable and a pulse former respectively in order to produce sampling pulses with manually adjustable delay with respect to the input waveform. The operation is described by the waveform diagram of Fig.8.2b and the full circuit is given in Fig.8.4. The precision rectifier consists of amplifier systems A2 and A3 and is preferred to a standard rectifier bridge in order to ensure that the two peaks per cycle are exactly the same height, otherwise a fundamental frequency component would appear in the analogue output signal. Amplifier system A3 operates as a unity gain straight forward amplifier to one input channel, to which is added another channel with a gain of 2 which has undergone half wave rectification in amplifier system A2. Due to both amplifiers being inverting, the output during the first half cycle is:

$$E_o = -\{\sin \omega t + 2\ (-\sin \omega t)\}\ \hat{E} = \hat{E} \sin \omega t$$

and during the negative half cycle

$$E_o = -\left\{\sin\left(\omega t + \frac{\pi}{2}\right)\right\}\hat{E} = \hat{E} \sin \omega t \quad \left(0 < \omega t < \frac{\pi}{2}\right)$$

Hence full wave rectification is achieved and because the rectification diodes D3 and D4 are in the feedback loop, non linearity is decreased to a very small value.

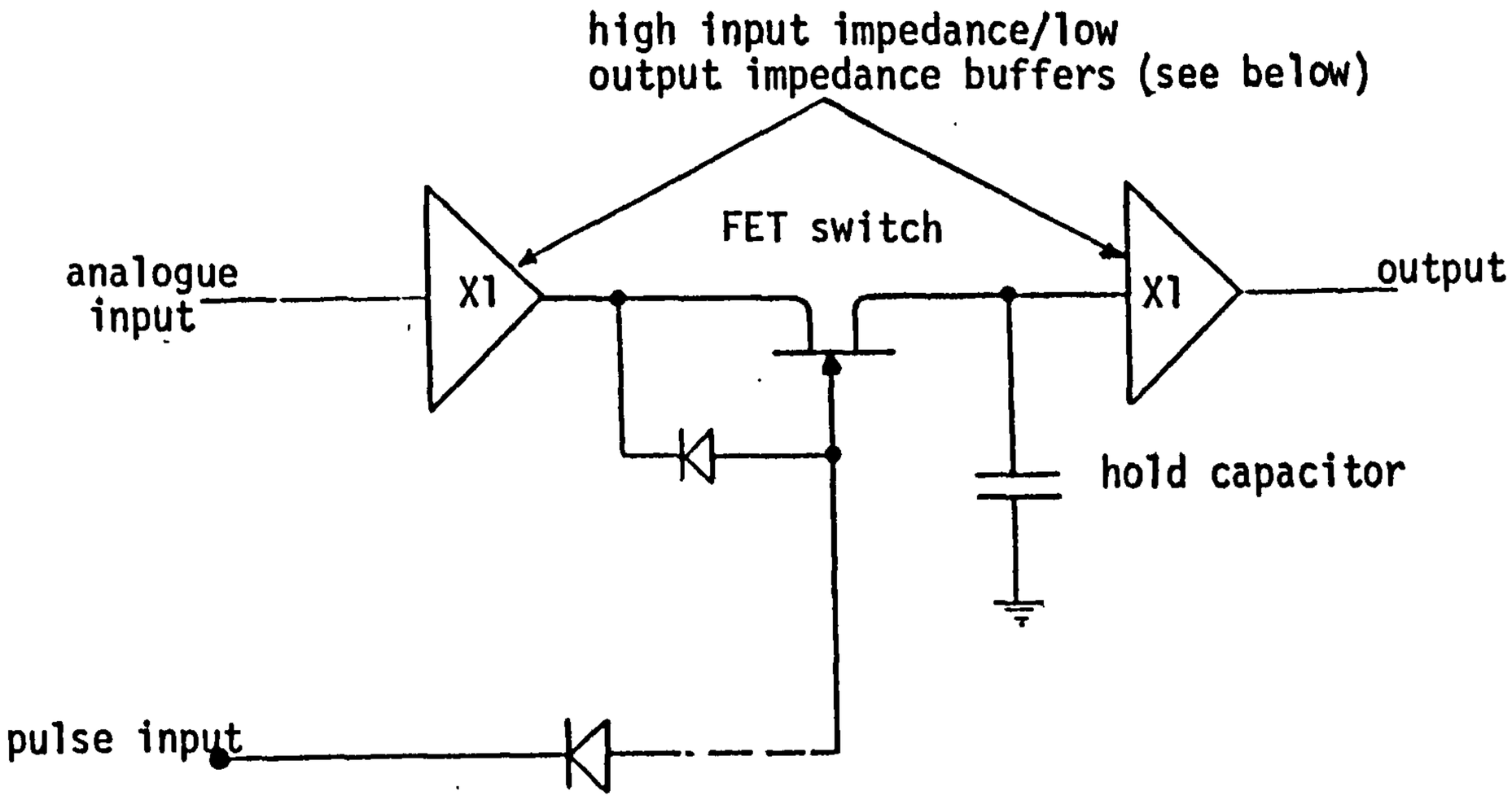

(a) SAMPLE-HOLD CIRCUIT

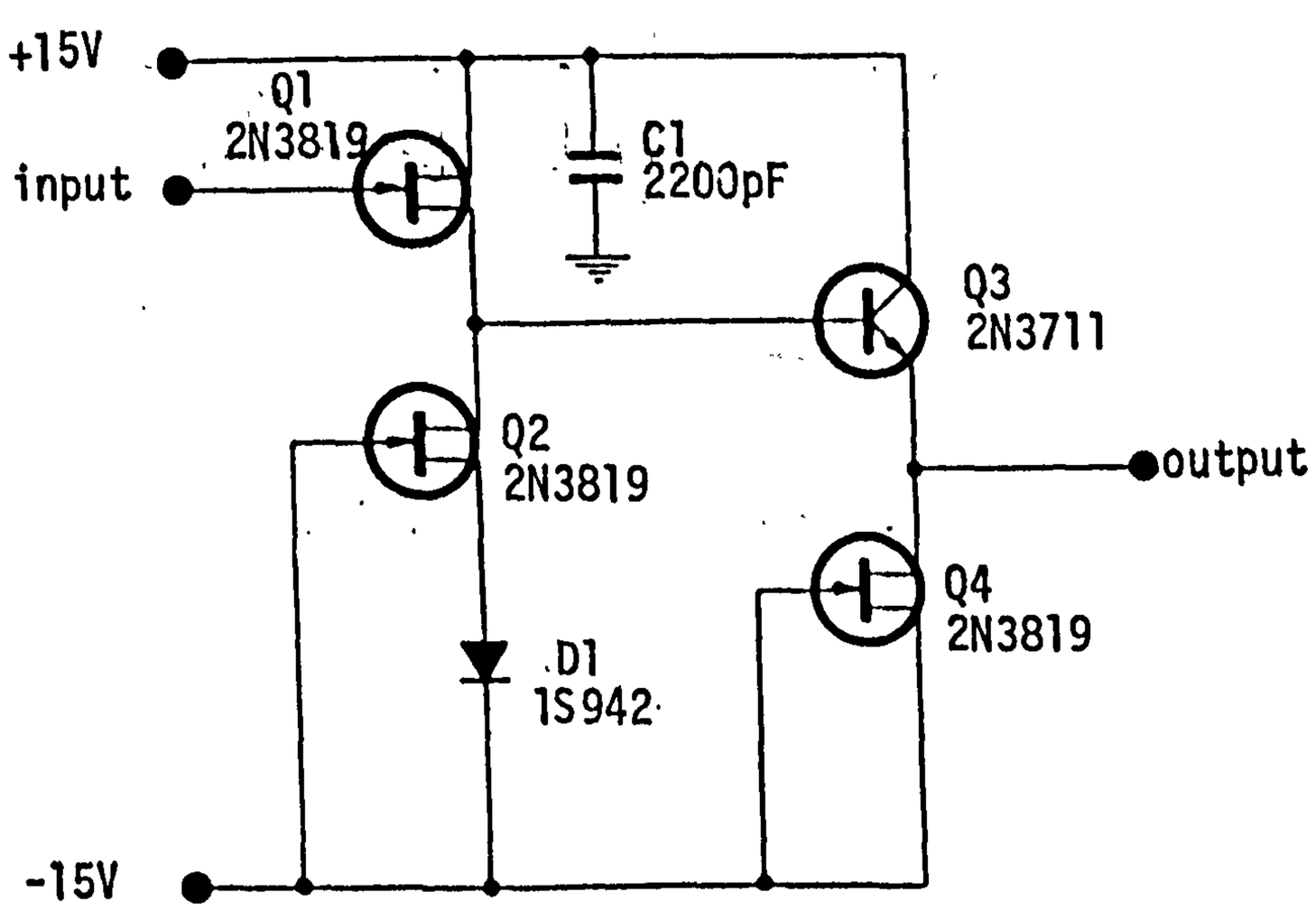

(b) AMPLIFIER (UNITY GAIN BUFFER)

DETAILS OF SAMPLER

FIG. 8·3

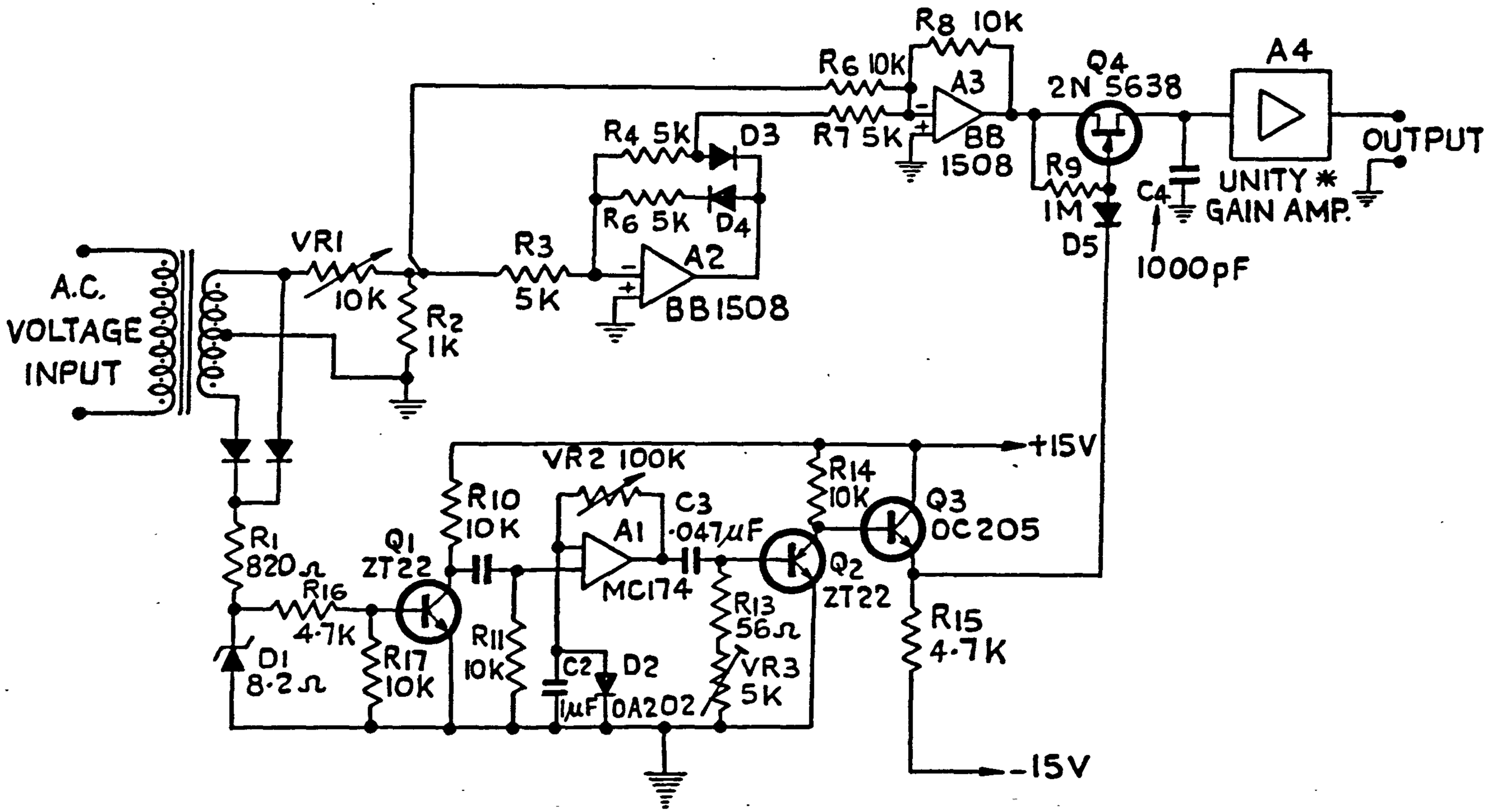

* SEE FIG. 8.3 b.

FIG. 8.4

VOLTAGE TRANSDUCER CIRCUIT.

Amplifier A3 also acts as the input buffer for the sample hold circuit Q4 which has been described earlier.

In the sample pulse forming circuit, Q1 acts as a switch to produce a square wave from the input sine wave voltage, which drives the monostable circuit formed by the integrated circuit operational amplifier A1 and gives smaller variations in delay time due to temperature than a discrete transistorised circuit. The output of the monostable is differentiated to form pulses by C13, R13 and VR2, and the latter is used for adjusting the pulse width. Positive pulses are then amplified by Q2 and Q3 forming the sampling pulses which traverse almost the full negative to positive rail voltages.

8.2.2 AC current measuring circuits

The same circuit as the peak sampling voltage transducer may be used if the signal waveform is reasonably clean. However if the signal is taken from a shunt a certain amount of noise may be present or if a current transformer is used the waveform may be distorted by heavy harmonics.

If this is the case then it is better to measure the average value of the signal rather than the peak and this can be performed using the same sampled data philosophy as before thus keeping the response time of the transducer to a very low value.

The principle is to take a number of samples of the signal in each half cycle which are stored and read into an averager at the end of the half cycle. The system shown in Fig.8.5 contains only six sampling FET switches for simplicity, in practice probably more would be required. The astable multivibrator generates a square wave which is six times the input frequency and synchronised to it (see Fig.8.6). This is used to form 6 sets of equally displaced sampling pulses by the ring counter and pulse forming circuit in order that gates 1-6 are switched sequentially throughout the half cycle. The first five switches sample the input voltage at equal intervals and distribute the information on the capacitors C1-C5. Amplifier A1 is an FET input type operational amplifier so that no leakage of the charges on the capacitors occurs and at the end of the half cycle the output of this amplifier is proportional to the average value of the five sampled voltages on C1-C5. This is read off by gate 6 which transmits the information to C6 at the end of the half cycle. This is buffered as before to give a low impedance output signal.

Although the sampling switch system would seem to be very complex, it is

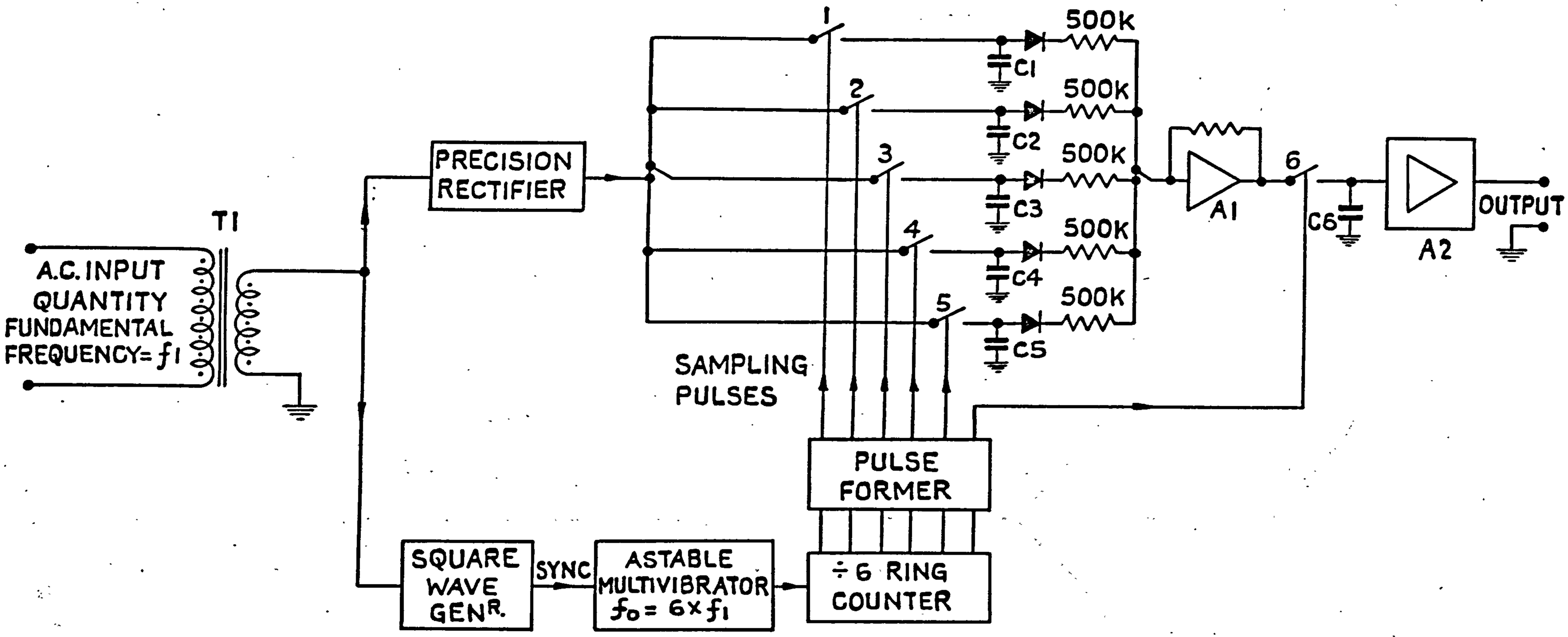

FIG. 8.5.

CIRCUIT FOR MEASURING THE AVERAGE VALUE OF AN A.C. QUANTITY.

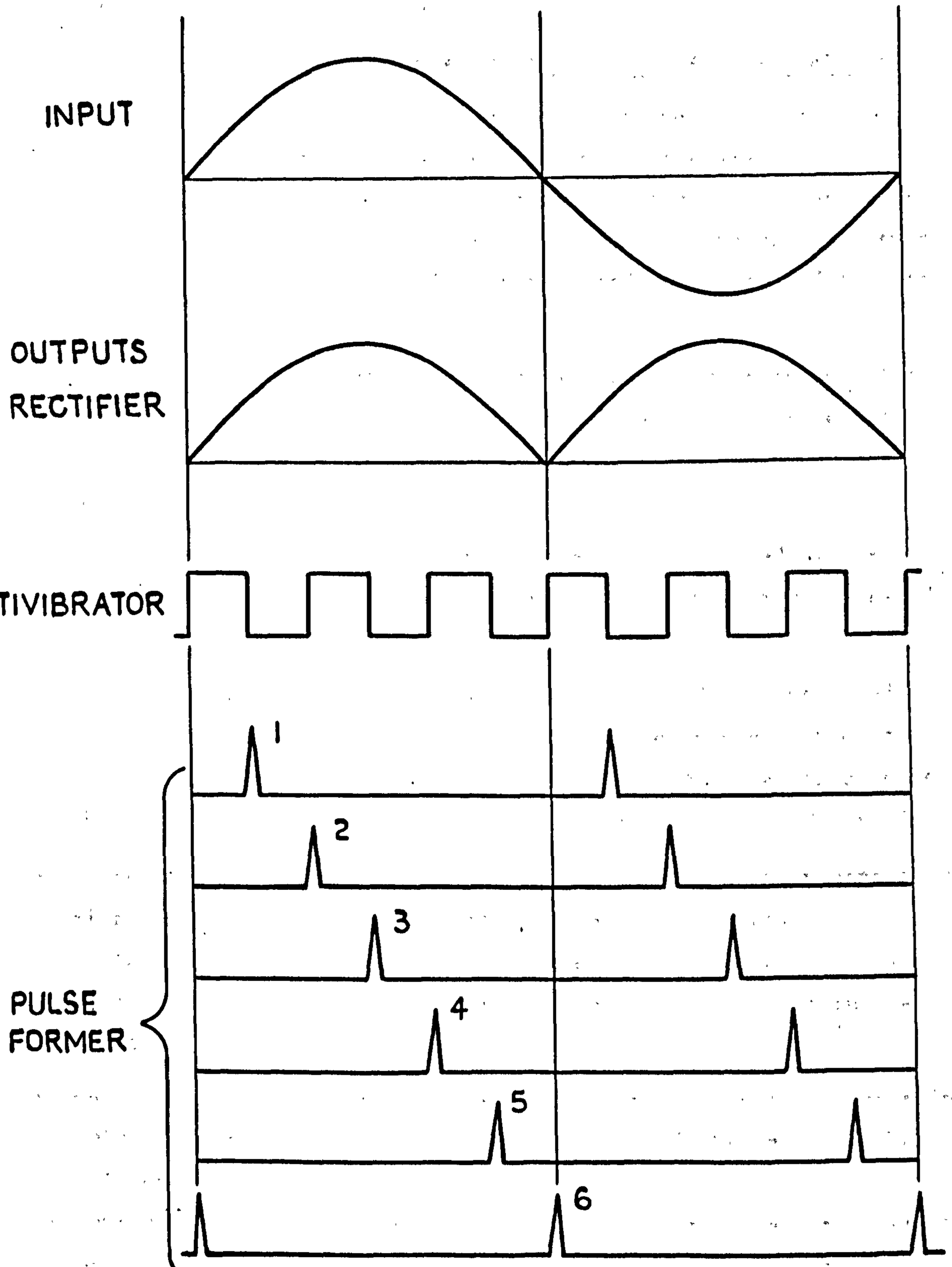

WAVEFORM DIAGRAMS FOR AVERAGE VALUE TRANSDUCER.

FIG. 8.6.

now possible to obtain most of the circuit in integrated form thus reducing the number of physical components. At the present time up to sixteen FET switches together with associated drive logic (i.e. ring counter and pulse former)are available in a single package.

8.2.3 Circuit for measuring turbogenerator shaft rotational velocity

For the purpose of shaft velocity measurement a magnetic (or photo-electric) type pick up is preferred as the mounting of the associated toothed wheel on the shaft is simpler than mounting a tachogenerator, which would require access to the end of the shaft. Also, for accuracy and speed of response, a high frequency ($\geq$ 1000 Hz) is required which is difficult to obtain from a tachogenerator.

In the prototype system a 20-toothed wheel was used giving an output of 1000 pulses per second. The electronic circuitry measures the time between pulses which is converted into a frequency dependent signal (i.e. velocity) by taking the reciprocal.

For control purposes a velocity deviation signal is required, and to obtain this the signal is backed off to zero with the input signal at exactly 1000 Hz.

The circuit of the transducer is shown in Fig.8.7. The input waveform (Fig.8.8a) is applied to the Schmitt Trigger Q3/Q4 which produces two sets of alternate square waves (Figs.8.8b and 8.8c). These are used to produce 30V pulses (Figs.8.8f and 8.8g) by the pulse forming circuits Q2/Q1 and Q5/Q6.

These pulses are used to sample-hold and reset the linear ramp generator Q7/C7 producing an analogue output proportional to the time between pulses (Fig.8.8h). An analogue divider is used to take the reciprocal of this output and finally a comparator stage backs off the steady state signal at synchronous speed

To set up the circuit, the input is supplied from an oscillator operating at exactly 1000 Hz ($\equiv$ synchronous speed). The slope of the ramp is then adjusted by R16 until the sampled voltage equals the zener voltage of D1 giving zero output. It is preferable to use a reference diode for D1 as in the prototype a certain amount of drift was experienced with a standard zener diode, caused by the zener voltage varying with temperature.

8.2.4 Shaft acceleration measurement

The acceleration tranducer is driven from the output of the velocity circuit described above and differentiates this output using a data-sampled

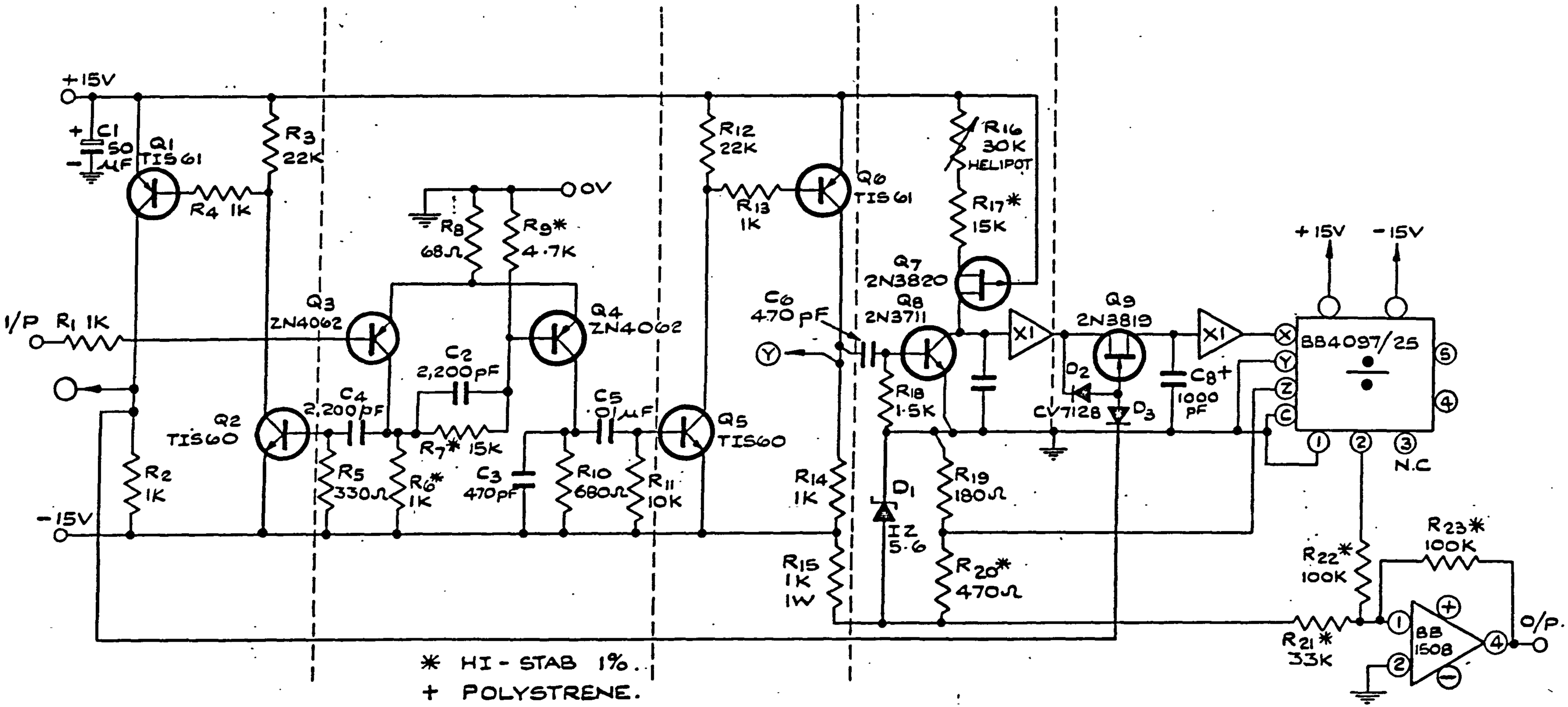

ANALOGUE SHAFT VELOCITY MEASUREMENT CIRCUIT.

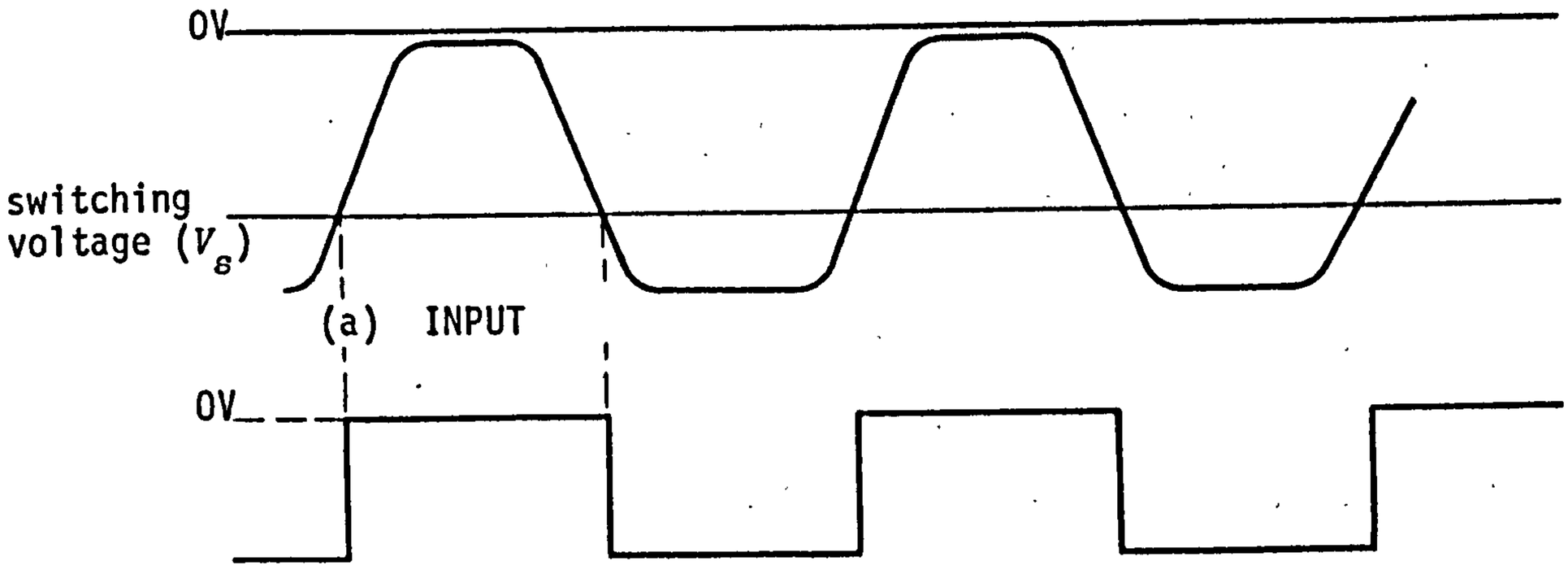

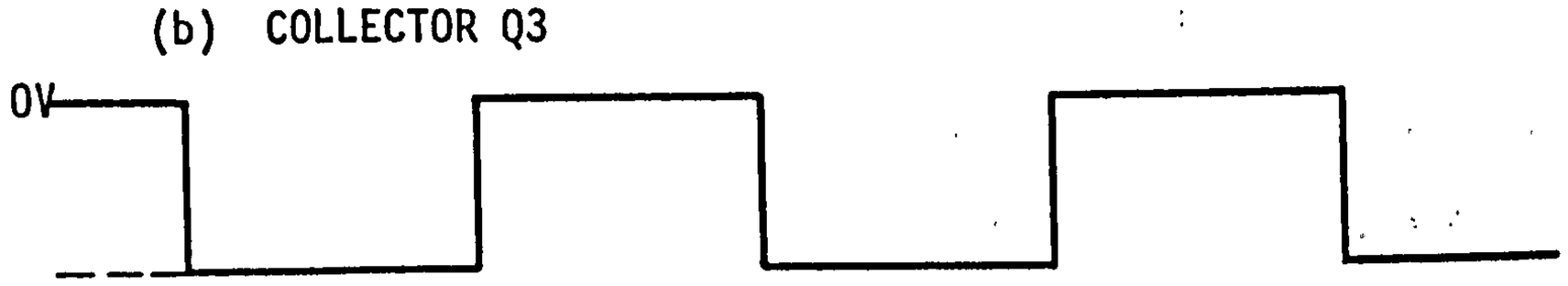

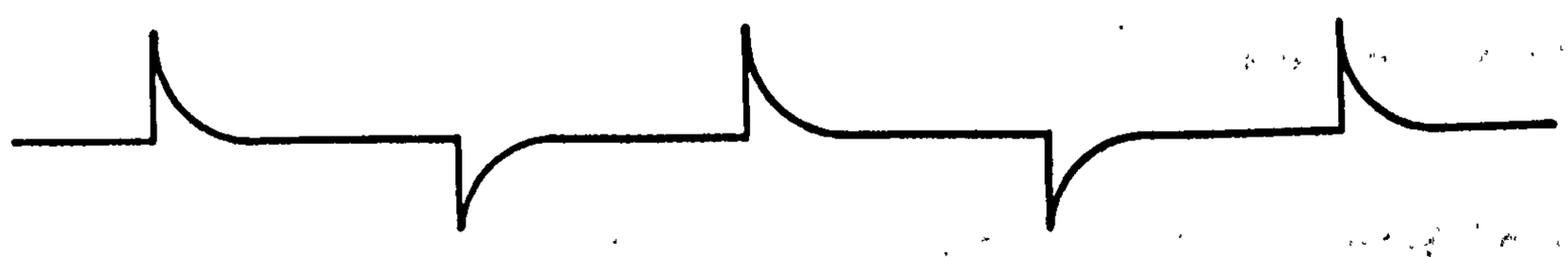

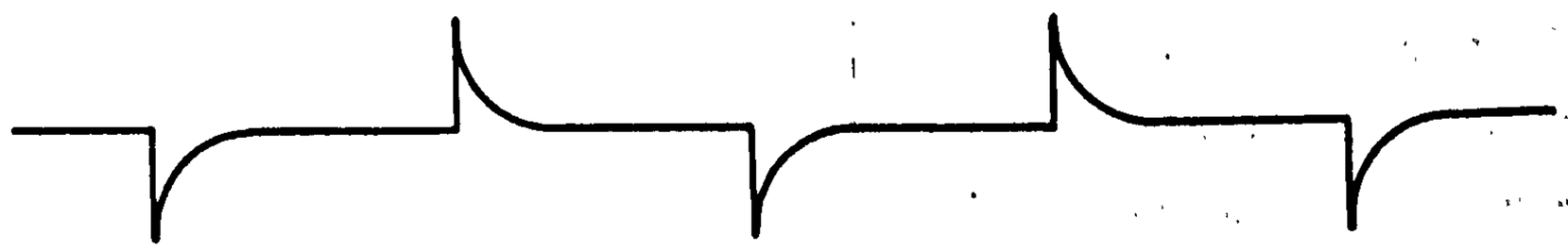

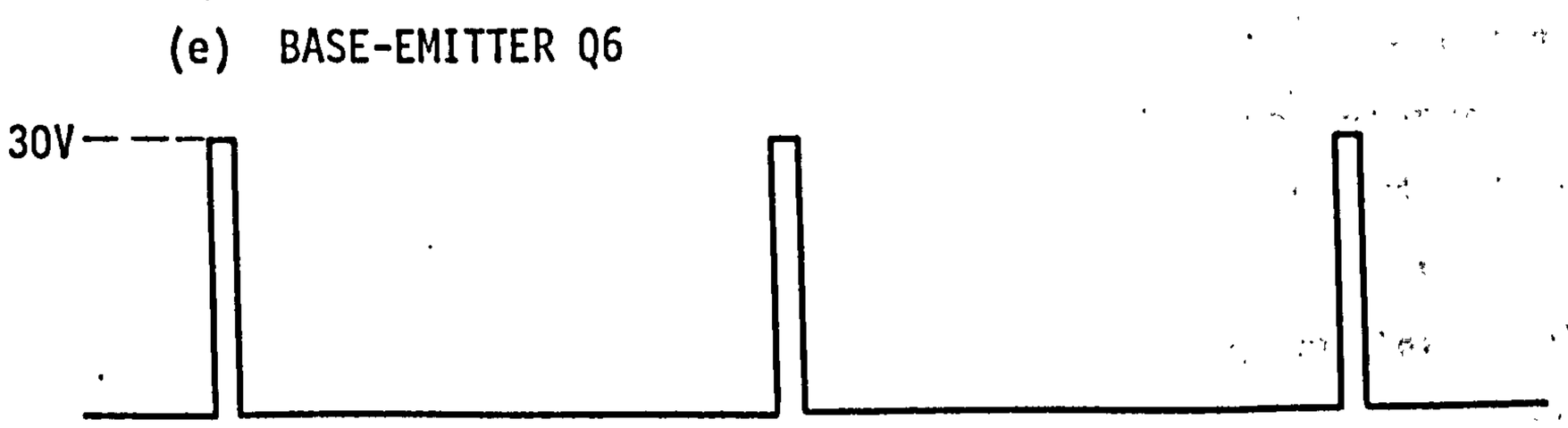

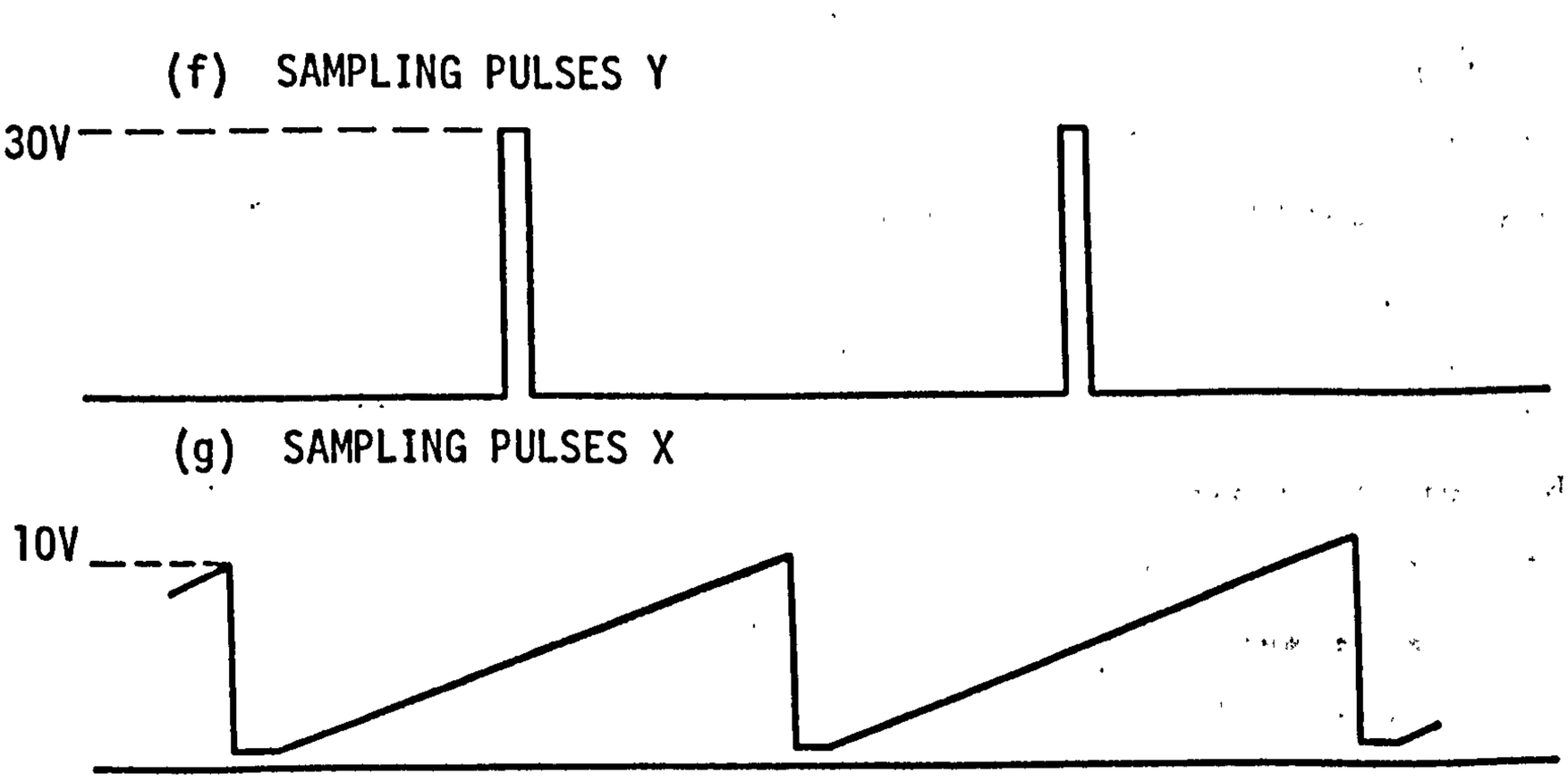

SPEED TRANSDUCER WAVEFORMS

FIG. 8·8

delay principle. This is illustrated by Fig.8.9a which shows an enlarged portion of elemental length, of the curve V = F(t) shown in Fig.8.9b (where V is velocity and t is time). For two points which differ by Δt on the time axis, the differential f'(t) approximates to:

$$f'(t) = \frac{f(t + \Delta t) - f(t)}{\Delta t}$$

Thus the operation of differentiation is reduced to a difference equation which can be easily implemented without the noise problems associated with standard methods of differentiation.

To implement this equation the function f(t) (velocity input) is delayed by the sampling time Δt to produce the function $f(t + \Delta t)$, and then the two functions are subtracted in a comparator. The delay line consists of three data samplers in cascade, the centre one being supplied with alternate pulses to the outer two to give the required delay. The operation is explained by Fig.8.9b and the circuit is given in Fig.8.10.

An input filter of a multiple-feedback design is included to remove any noise and sampling spikes passed on from the velocity transducer. It is designed to give a fast roll-off at high frequencies together with a very small phase shift in the low frequency region. The signal next passes through a line of three data samplers as mentioned earlier. Only four buffer amplifiers are required in this line up as the central two perform the dual roles of high impedance buffer and low impedance current source. The first data sampler operates on the incoming signal to give sampled values of f(t) using the X sampling pulses which are also generated by the velocity transducer. The Y pulses are used to drive the next sampler which delays f(t) by some period which is less than the sampling time. In the last sampler the X sampling pulses are used again delaying the input signal by a full sampling period Δt. The outputs from the first and third samplers are subtracted using a differential input operational amplifier to give an output signal proportional to acceleration.

8.2.5 Rotor angle meter circuit

The study of rotor angle swing curves is the most usual method of assessing turbogenerator transient performance in system stability studies. However standard methods of measurement employing phase sensitive detector circuits, which are normally used for steady state indications, are inadequate for the study of transient oscillations because of the slow response. The instrument described here employs a data sampler and gives

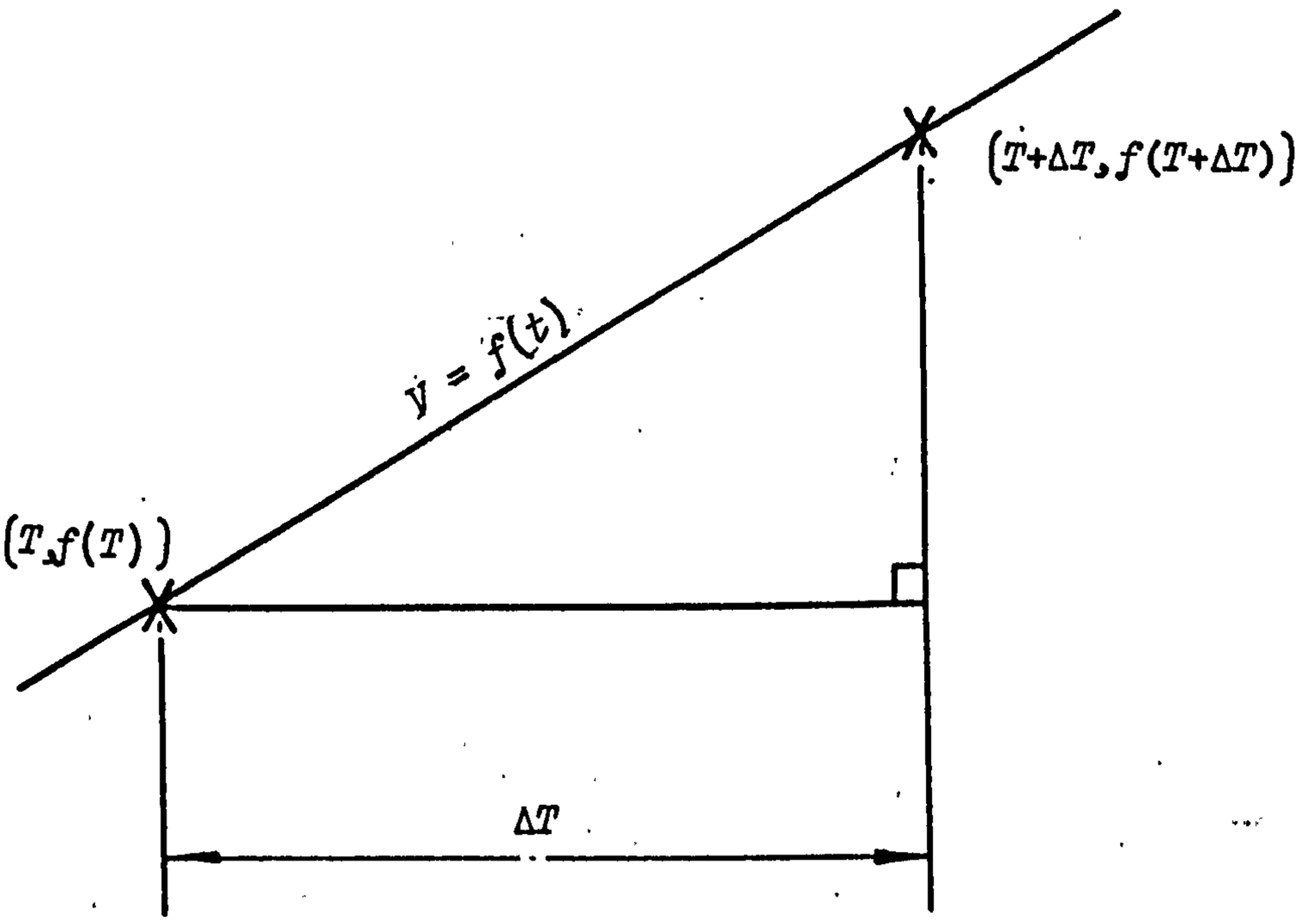

(a) ENLARGED PORTION OF CURVE $y = f(t)$ OF ELEMENTAL LENGTH

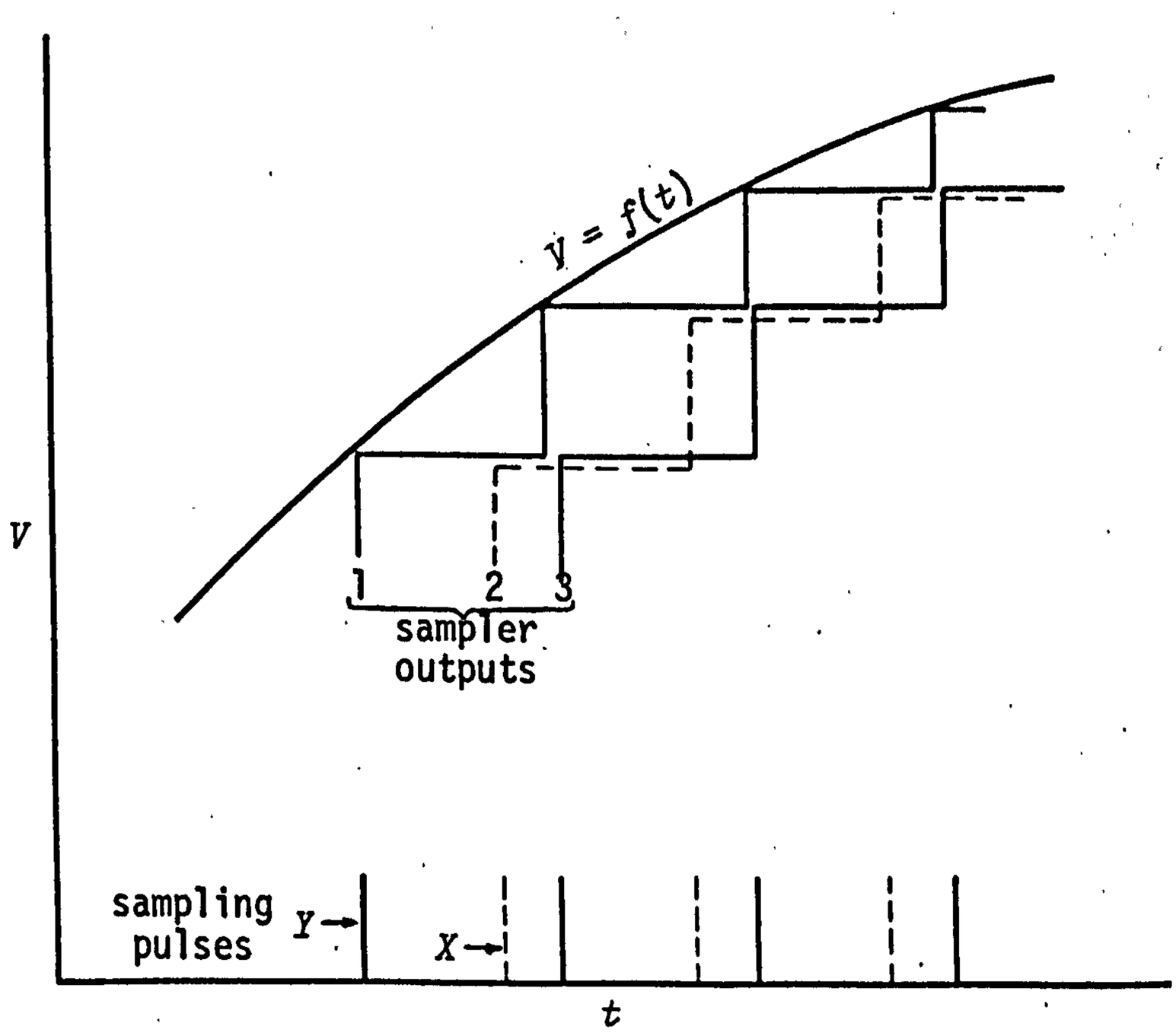

(b) FUNCTION $f(t)$ DELAYED BY SAMPLING TIME ΔT

PRINCIPLE OF OPERATION OF DATA-SAMPLED DIFFERENTIATOR

FIG. 8.9

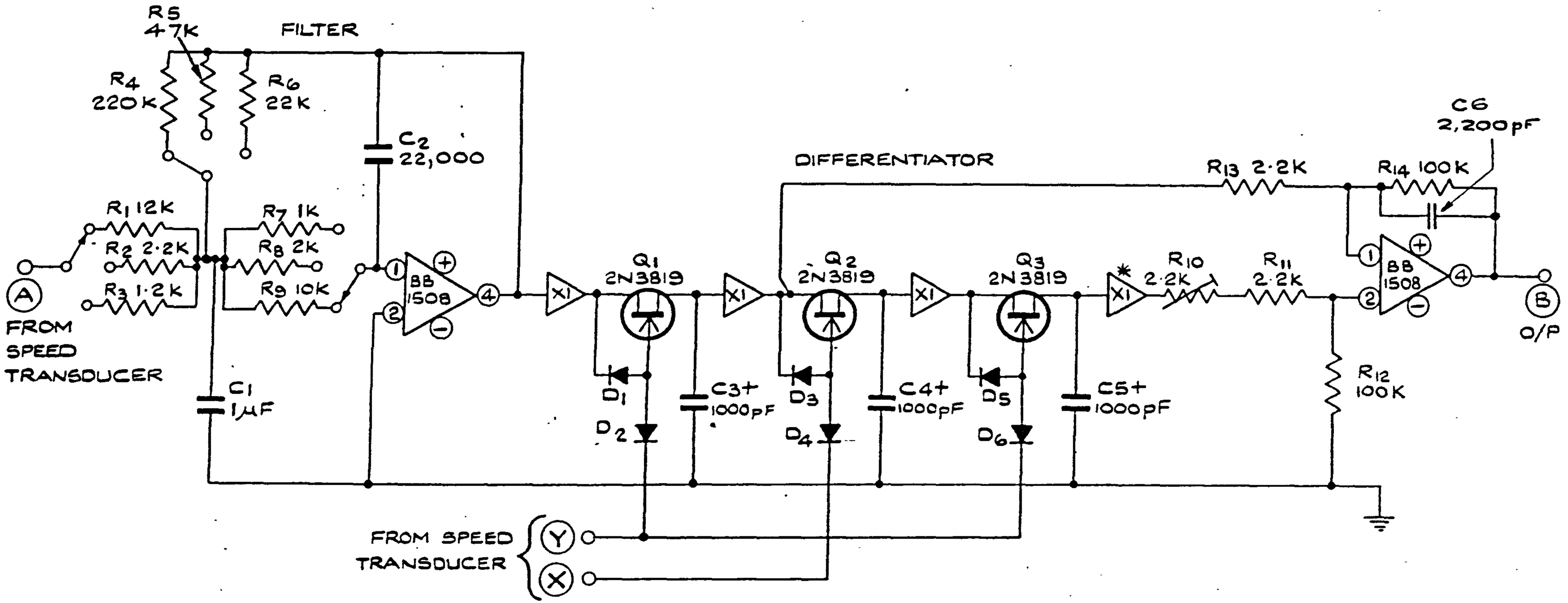

ALL RESISTORS · 1% HI - STAB

\+ POLYSTYRENE

* THIS AMPLIFIER HAS D1 REPLACED BY A 5K POT (R15)

$D_1 - D_6$ GERMANIUM DIODES TYPE CV7128

ANALOGUE SHAFT ACCELERATION MEASURING CIRCUIT.

FIG 8.10

a response which is in effect only limited by the input data rate from the appropriate transducer. In most cases this is a magnetic pick up operated by a projection of magnetic material attached to the turbogenerator shaft. This gives one pulse per revolution and the response time is therefore 20 ms. Inputs are also possible from higher frequency tacho's or toothed wheel/ magnetic probe systems by using bi-stable frequency dividers.

The schematic layout is shown in Fig.8.11 and the waveforms in Fig.8.12. Pulses from the shaft sensor (or from the bi-stable divider if a high frequency transducer is used) are used to reset an integrating type ramp generator after passing through a shaping unit. The output of the ramp generator is then sampled using pulses derived from the AC reference input voltage. For machine rotor angle measurement this is derived from the generator terminal voltage but if system angle is required, then the reference voltage is taken from the reference busbar. The timing of the sampling pulses can be delayed over a 180^{o} range to enable zero setting of the instrument with the machine on no-load.

The following description refers to the circuit diagram of Fig.8.13.

Transistors Q1 and Q2 shape the input pulses from the shaft transducers into square pulses of controlled duration for resetting the ramp generator Q3/A1. An integrated circuit amplifier is preferred here to discrete devices, to obtain the necessary linearity over the relatively long charging period (20 ms). The circuit operates as a pure integrator which is being continuously reset and relaxed by transistor Q3 which acts as switch to discharge C3 at the end of every cycle. The charging rate of C3 after Q3 has switched off depends upon the resistor VR1 which sets the calibration of instrument in volts per degree. Transistor Q7 produces square waves from the AC input voltage which drive the circuit of amplifier A2 acting as a monostable multivibrator. This is used to delay the sampling pulses appearing after the pulse amplifier Q8/Q9, and the amount of this delay can be altered by VR3 which varies the rate of charging of C6 and hence the time before the monostable returns to its stable state. Thus the instrument can be set to read $0-360^{o}$, $-180^{o}-0-+180^{o}$, or any other 360^{o} spread by adjusting the initial position of the sampling pulses with respect to the ramp.

The sample-hold unit consists of an FET chopper Q4 and capacitor C4 which stores the sampled voltage every cycle. The buffer amplifier has an operational amplifier output A3 in order to introduce a back-off

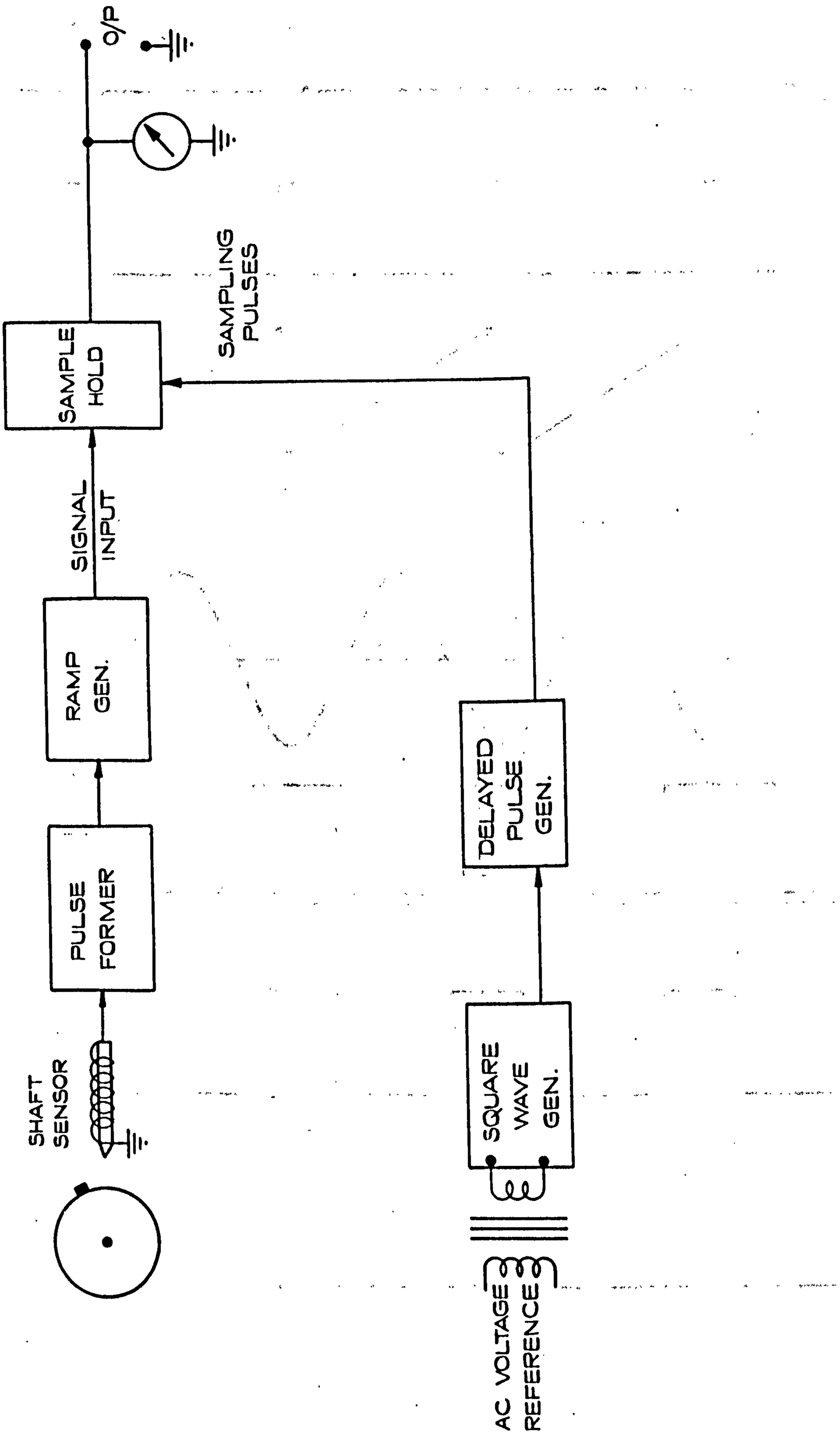

SCHEMATIC LAYOUT OF ROTOR ANGLE INDICATOR

FIG 8.11

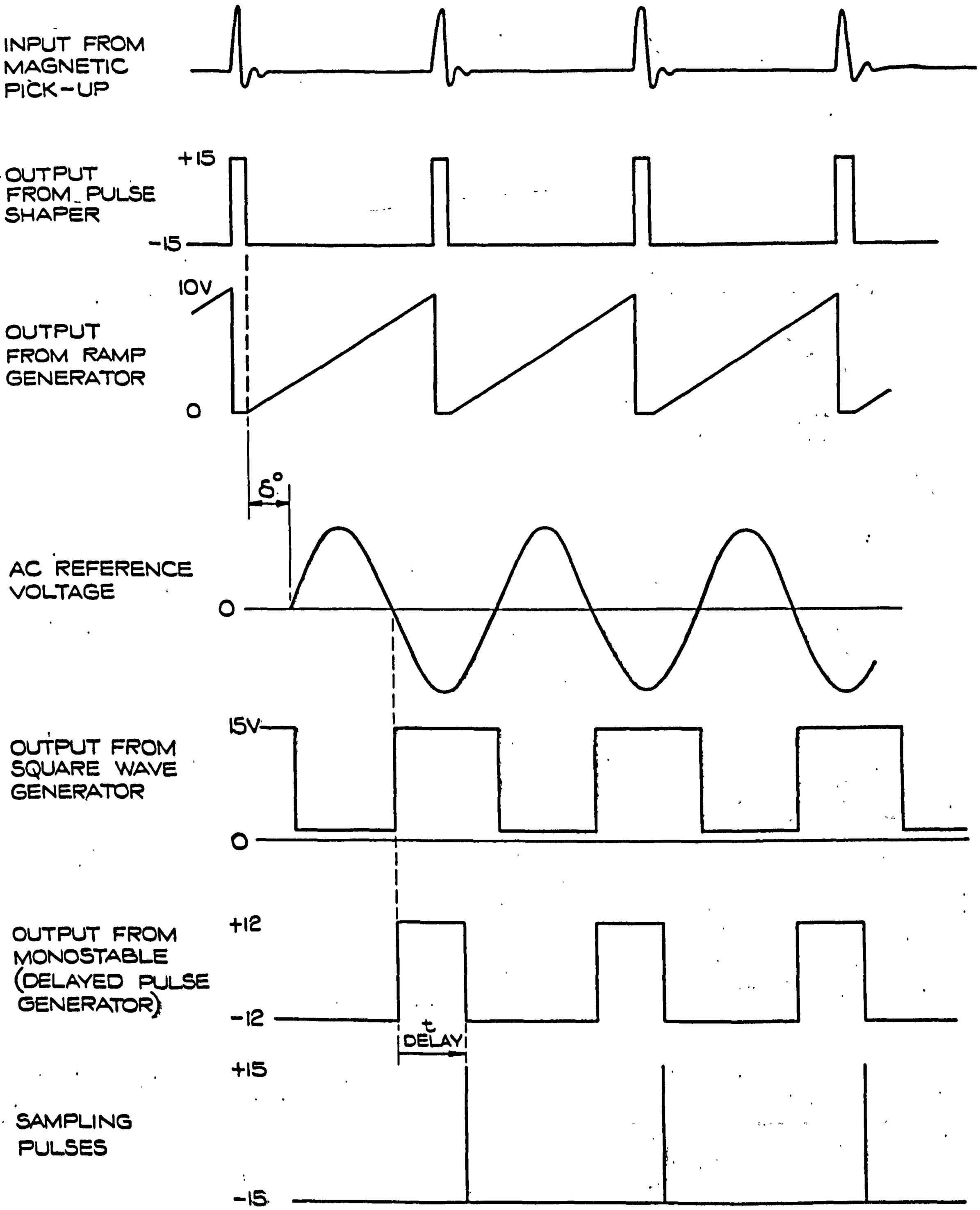

WAVEFORMS FOR ROTOR ANGLE INDICATORS
(FOR THE DELAY SHOWN ABOVE, THE OUTPUT IS ZERO)

FIG 8.12

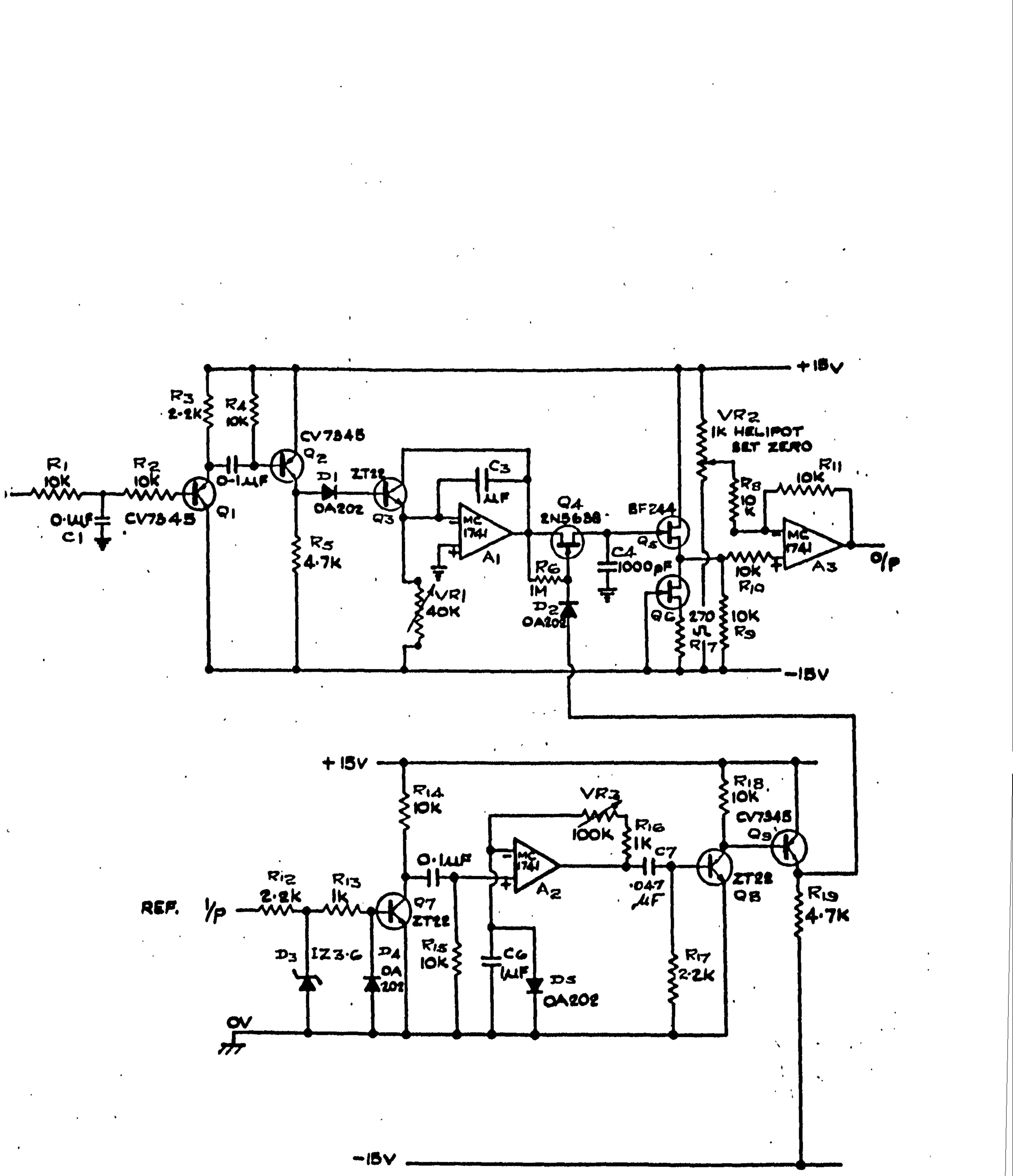

CIRCUIT DIAGRAM OF ROTOR ANGLE METER

FIG.8,13

voltage which is used in conjunction with the delay control VR3 to give a completely flexible range and zero setting facility. For example, if it is desired that the instrument should read $-90^{o}/0/270^{o}$ with a calibration of 5 volts per 180^{o}, the ramp slope is first adjusted to give 10 volts maximum ramp height by VR1. The sampling pulse delay is then altered to give 2.5 volts at the output with potentiometer VR2 at mid travel (i.e. the ramp is being sampled $\frac{1}{4}$ way along). VR2 is then altered to zero the instrument.

8.3 Performance and operation of the data sampled measuring instrumentation

Prototypes of all the previously described fast response instrumentation were assembled and tested on a laboratory alternator with the exception of the average value circuit (Fig.8.5). This was because of cost limitations and the fact that the peak sampling transducer was perfectly adequate for the laboratory machine as the waveforms were noise and distortion-free.

Special circuit cards for velocity and acceleration measurement (Fig.8.14) were manufactured and supplied to CEGB for incorporation in their portable thyristor excitation equipment used during system tests at Doncaster Power Station. The bunching of the semiconductors forming the buffer amplifiers is intentional to eliminate spurious oscillations due to stray capacitance in the high impedance circuits.

The rotor angle meter was constructed as a general instrument for laboratory or site measurements (Fig.8.15) and another unit is to be constructed at C.A.Parsons for use in site tests on electronically governed turbogenerators.

8.3.1 Voltage and current transducers

The same circuits were used for both voltage and current measurement as part of a combined group research project on a laboratory alternator system. the results of which will be published in future theses.

Fig.8.16a shows the sampling pulses and their relative position with respect to the rectified input waveform and Fig.8.16b is an oscillogram of the AC component of the DC output. The effect of the finite sampling time is to cause spikes and the mismatch of the positive and negative samples produces a square type waveform. Some filtering may be beneficial but as the maximum error was less than 0.1% this was not attempted.

Fig.8.17 shows the high linearity obtained by the sampling technique.

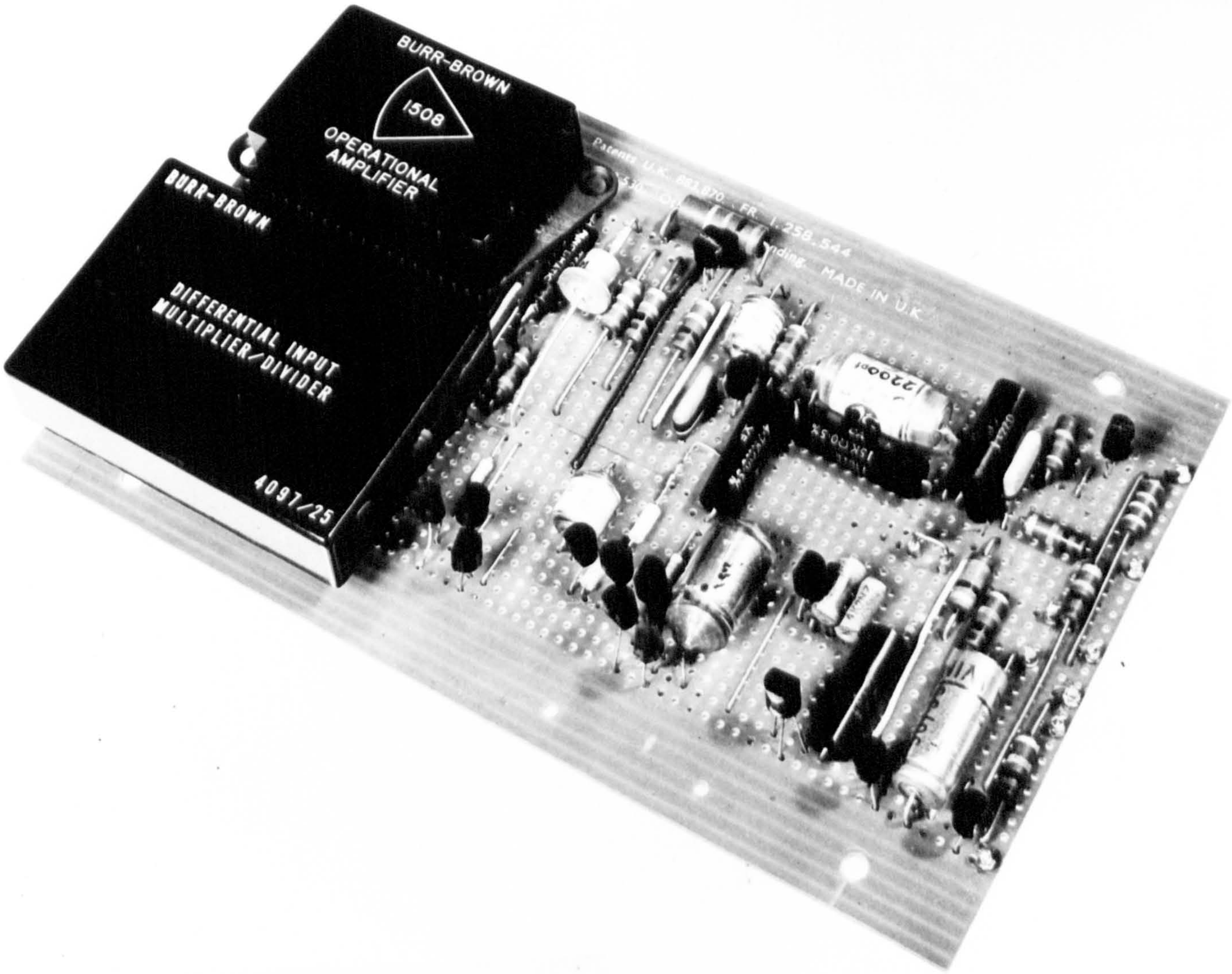

(a) VELOCITY TRANSDUCER CIRCUIT CARD

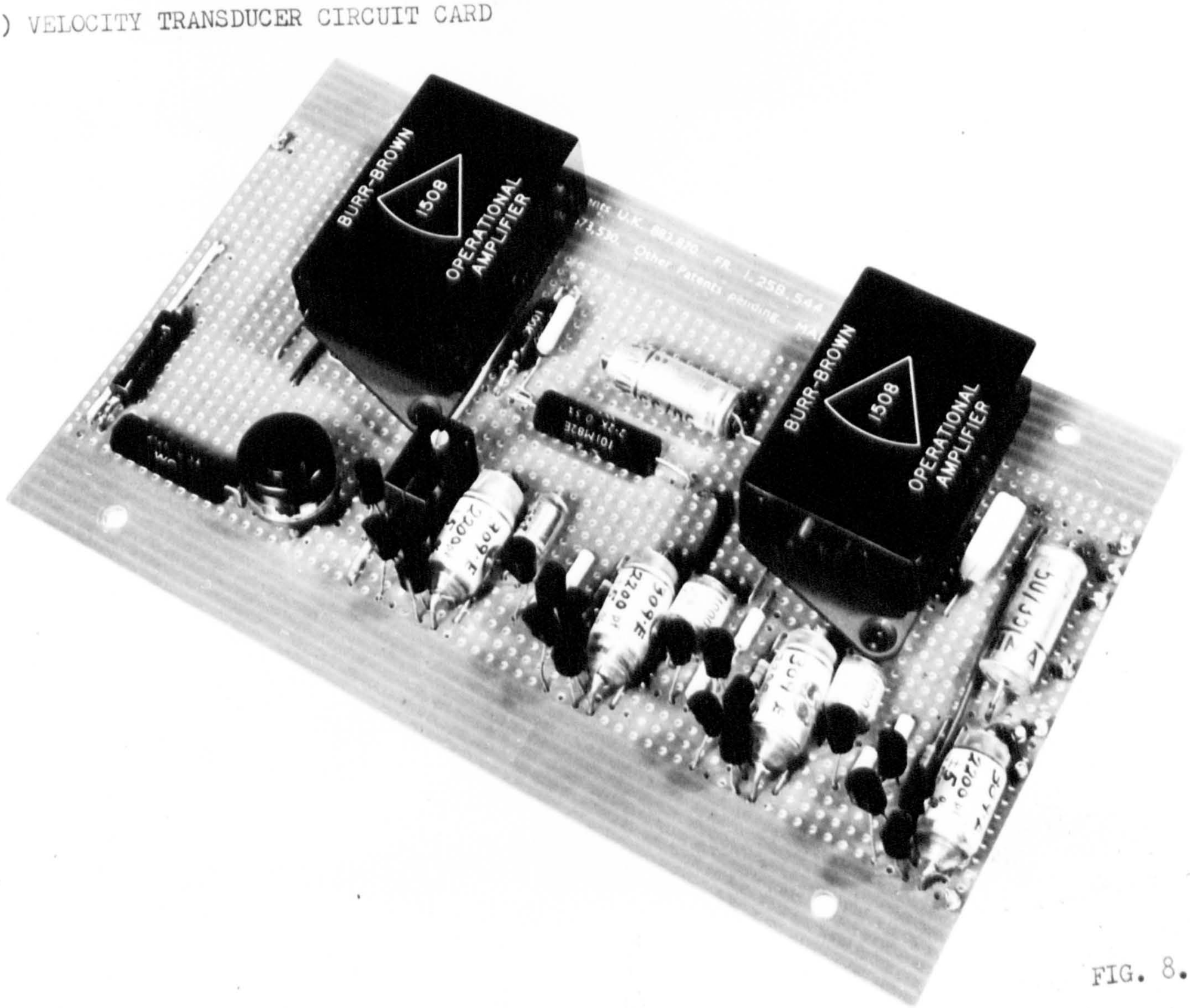

FIG. 8.14

(b) ACCELERATION TRANSDUCER CIRCUIT CARD

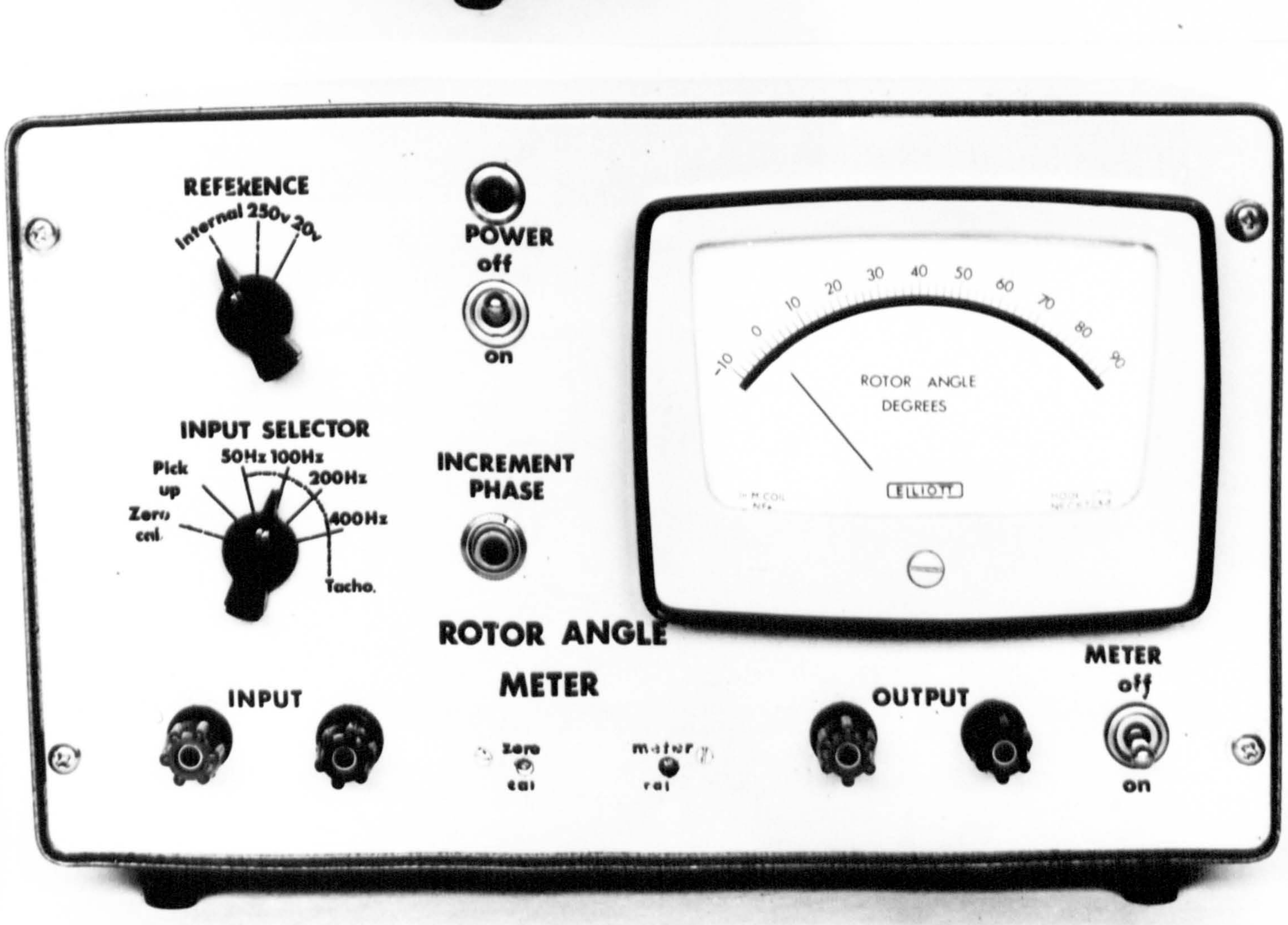

PORTABLE ROTOR ANGLE METER

FIG. 8.15

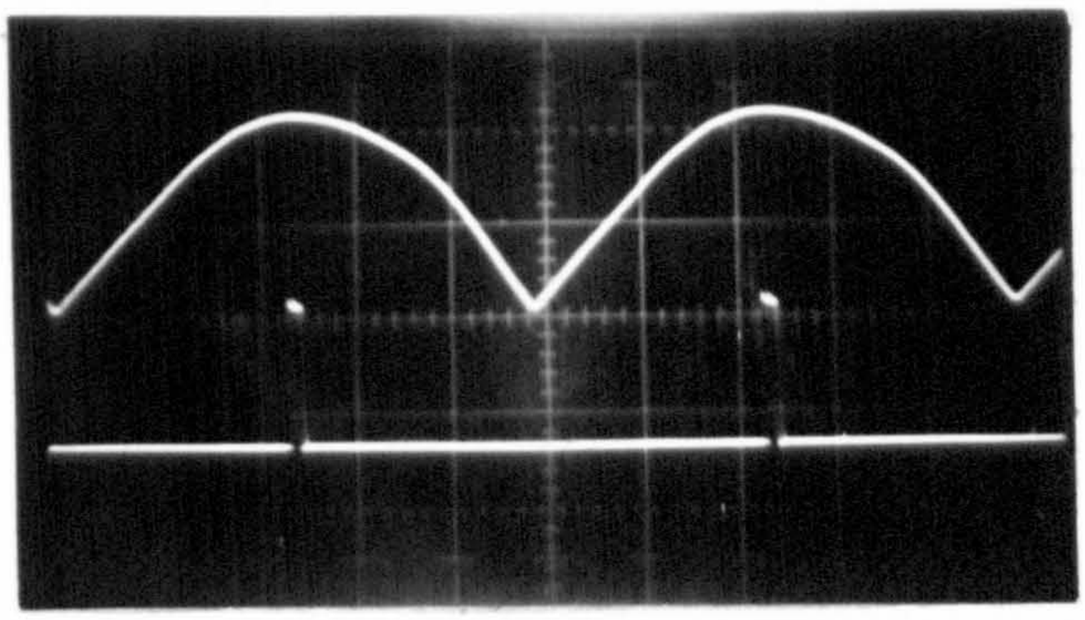

X_1 = 5V/cm

X_2 = 10V/cm

Y = 2mS/cm

(a) RECTIFIED WAVEFORM AND SAMPLING PULSES

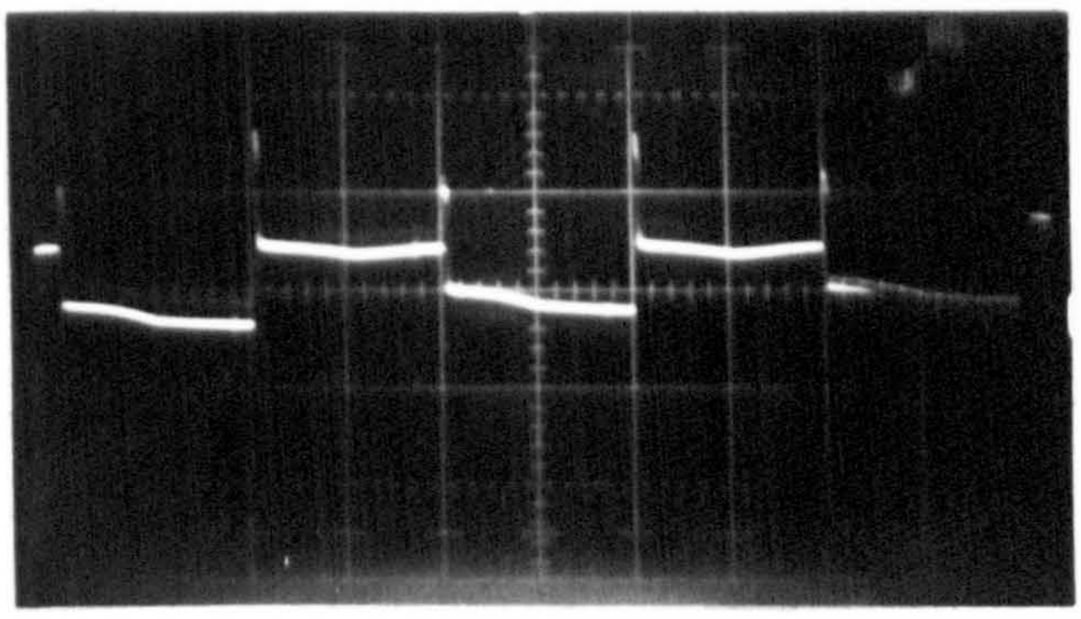

X = 10mV/cm

Y = 5mS/cm

(b) A.C. COMPONENT OF OUTPUT WAVEFORM

OSCILLOGRAMS SHOWING VOLTAGE TRANSDUCER OPERATION

FIG 8.16

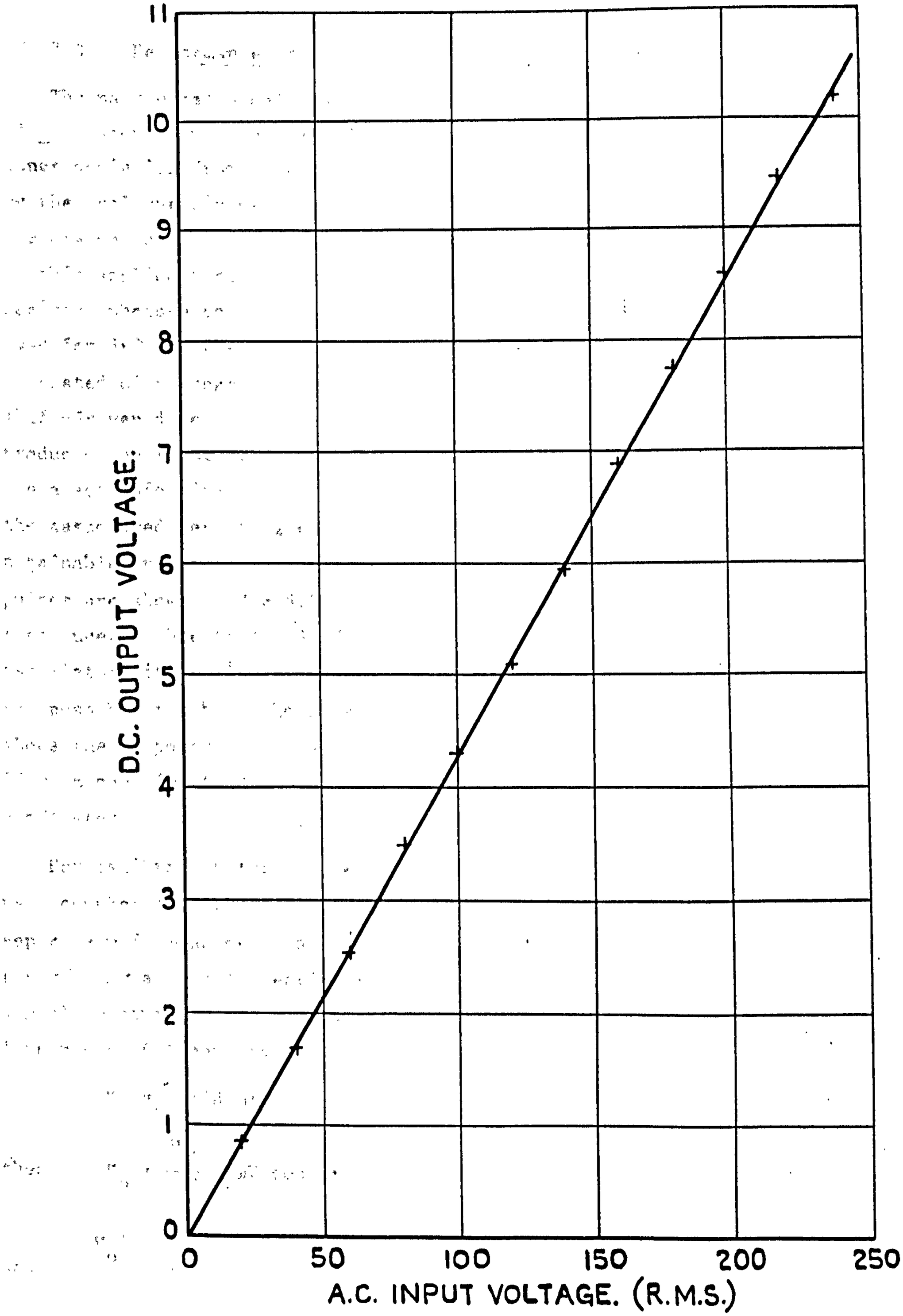

CALIBRATION OF VOLTAGE TRANSDUCER.

FIG.8.17.

8.3.2 Performance of velocity and acceleration transducers

The narrow range calibration of the speed transducer for a deviation of ± 8% around synchronous speed is given in Fig.8.18. Outside this range deviation from linearity was noticeable which was probably caused by the analogue divider module used which had a best accuracy of 2% in the divide mode. However wide range speed measurement is not required in this application. Fig.8.19a shows the output pulses from a specially designed photo-electric sensor on a 30 MW set at Doncaster Power Station used for driving the instrument during system tests in 1970. The pick up consisted of a tungsten-filament lamp, photo-transistor detector and a shaft-driven disc with 20 slots milled out around the perimeter. This produced the input frequency of 1000 Hz at synchronous speed required for the electronic circuitry. Fig.8.19b is the ramp function, together with the associated resetting pulses, and illustrates the extreme linearity attainable by using FET constant current sources. The two sets of 30 volt pulses are shown in Fig.8.19c which are also supplied to the acceleration transducer. Due to the difficulty of obtaining a frequency modulated oscillator with a linear sweep of frequency with respect to time, it was not possible to check the speed of response directly. However Fig.8.19d shows the response to a logarithmic sweep of frequency from 800 Hz to 1500 Hz supplied from a Bruel and Kjoer type 1014 beat frequency oscillator.

For calibrating the acceleration circuit only the sampling pulse inputs were connected to the velocity transducer, the main signal being supplied separately from an oscillator. In this manner it was possible to examine the circuit as a differentiator. The calibration for a sine wave input signal is given in Fig.8.20 and it is seen that the effective gain increases linearly with frequency for if

$$V_i = \hat{V} \sin \omega t,$$

then $$V_o = \frac{dV_i}{dt} = \omega \hat{V} \cos \omega t$$

and $$\left|\frac{V_o}{V_i}\right| \quad \alpha \ \omega$$

Figs.8.21a-8.21c show the effect of different frequencies on the phase lead provided by the differentiator. Due to the finite sampling time this

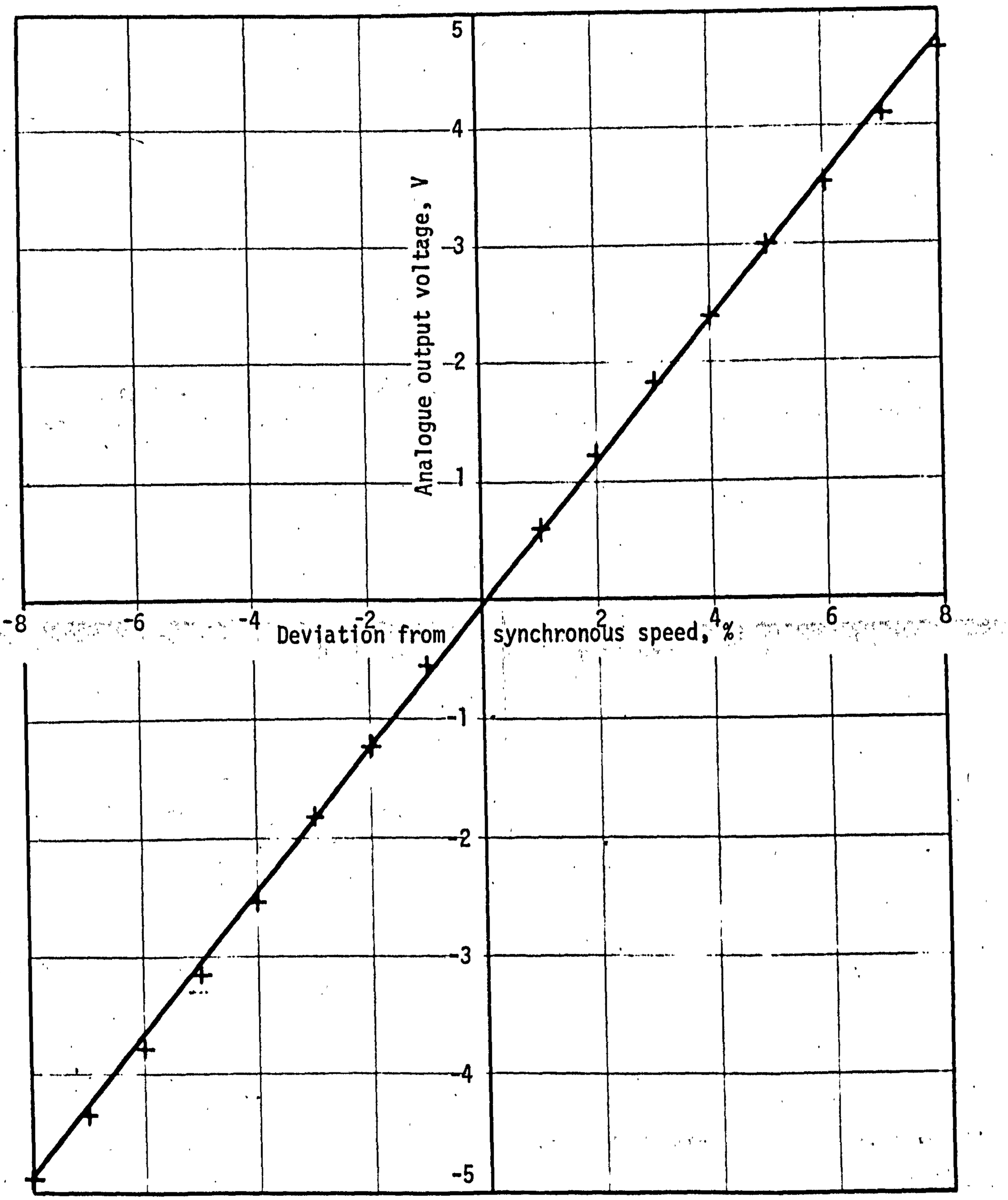

SPEED TRANSDUCER CALIBRATION

FIG. 8·18

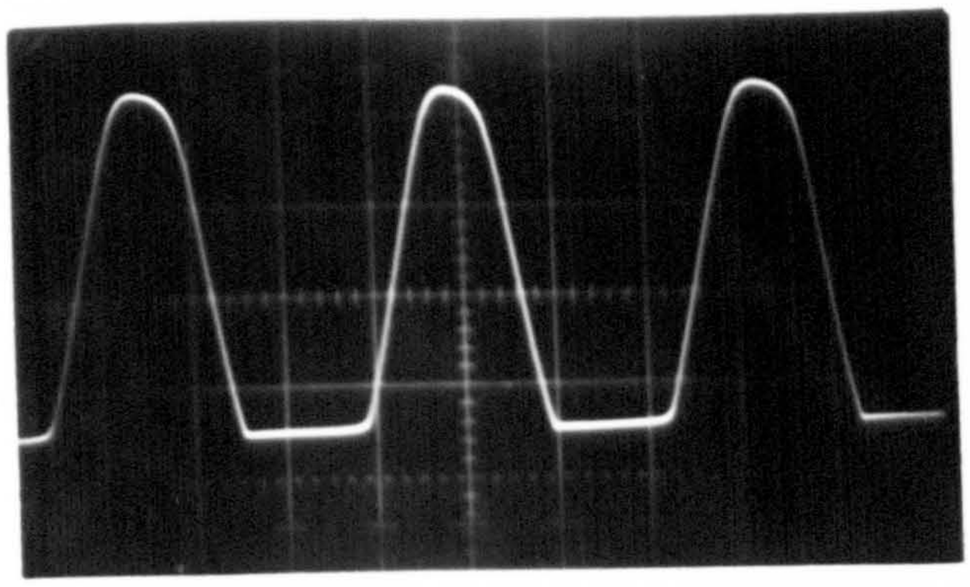

(c) INPUT PULSES FROM PHOTO-ELECTRIC SENSOR (f = 1kHz)

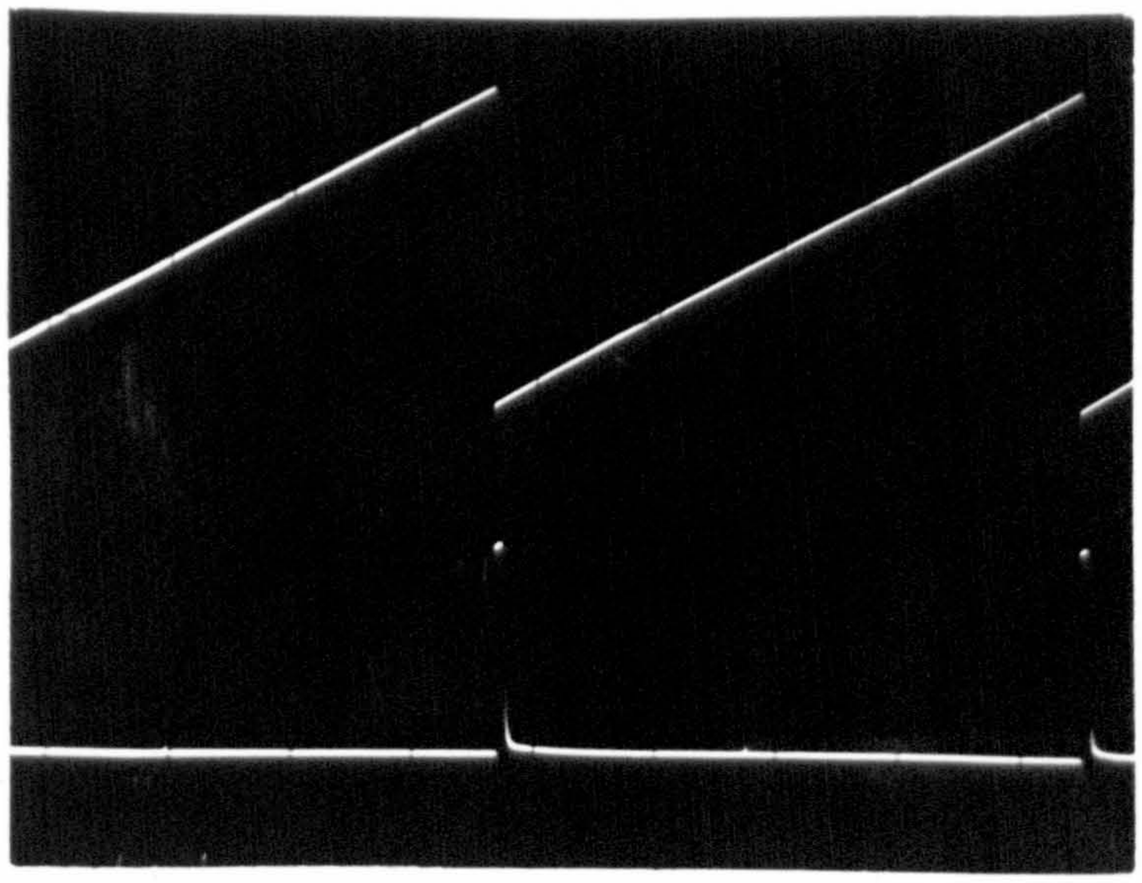

(b) RAMP AND RESETTING PULSES

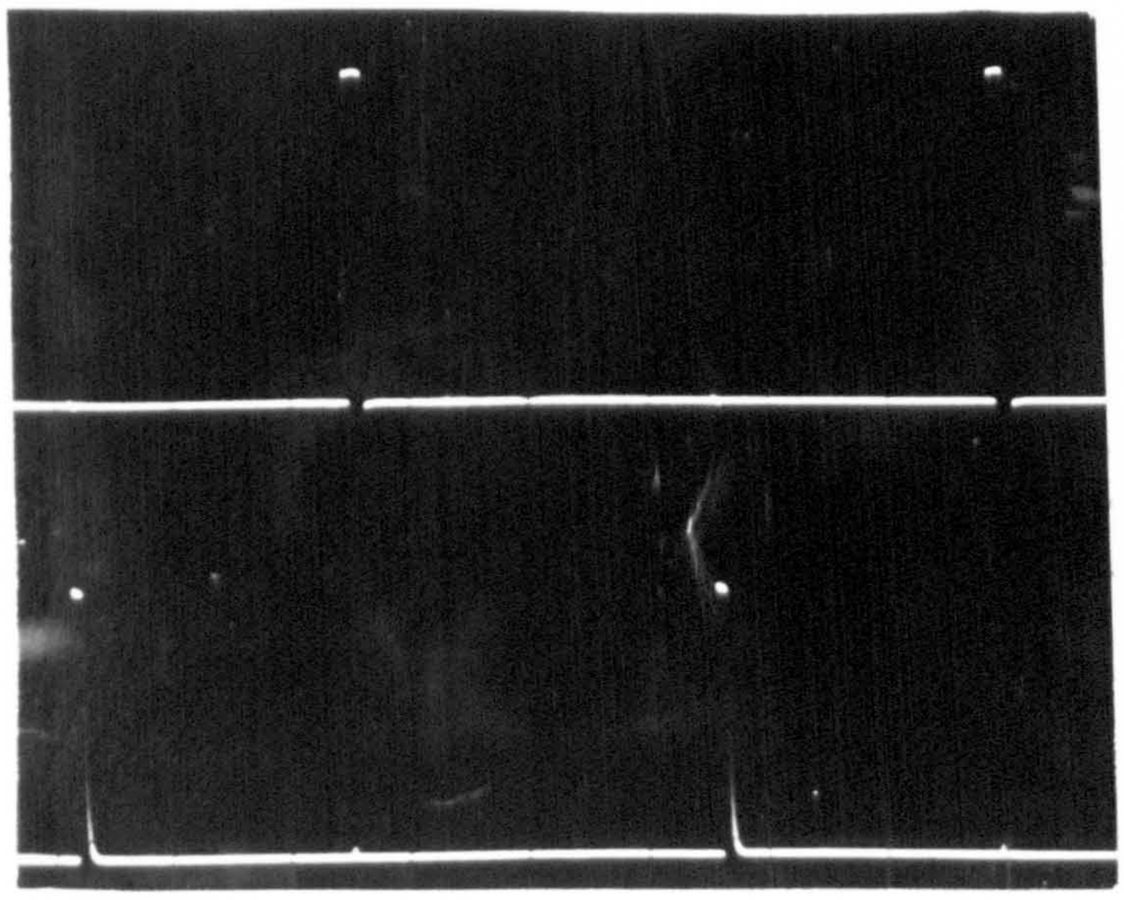

(c) SAMPLING PULSES FOR ACCELERATION TRANSDUCER

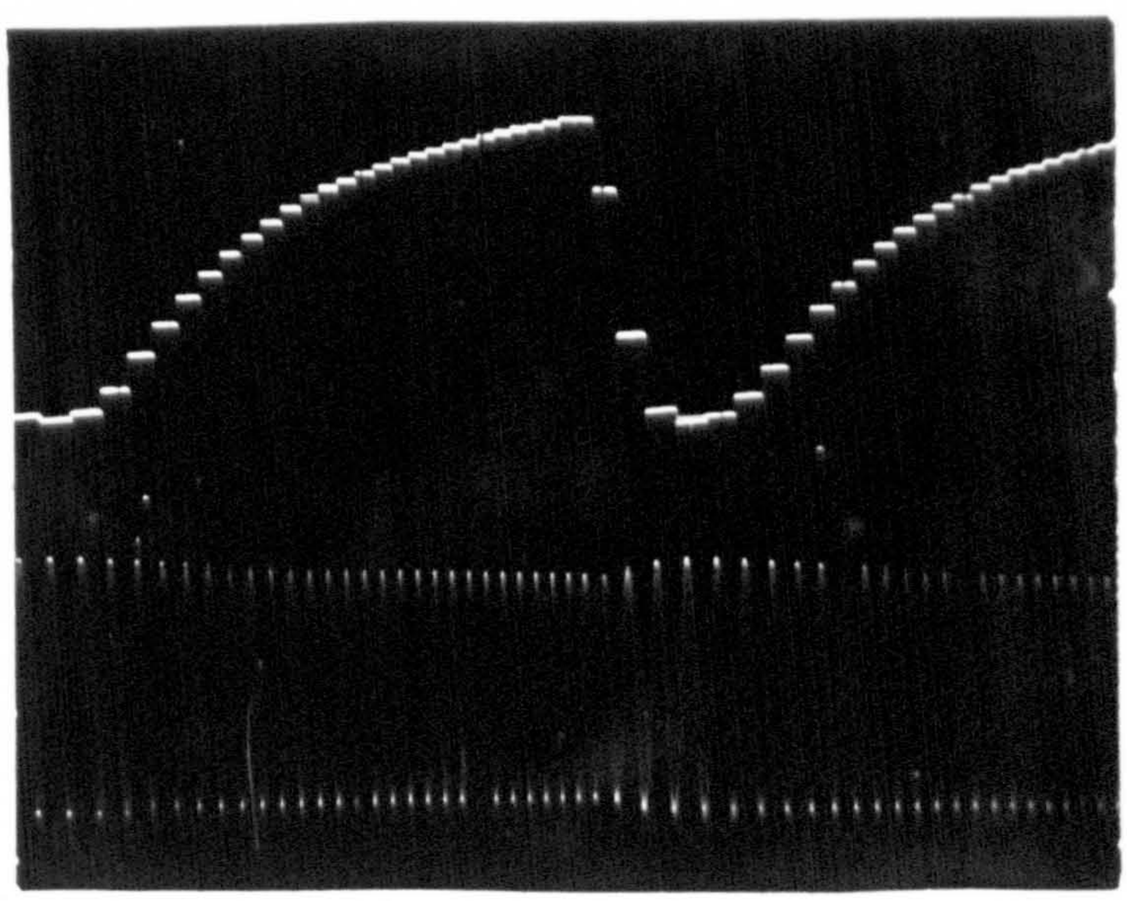

(d) RESPONSE TO LOG SWEEP OF FREQUENCY
UPPER = OUTPUT LOWER = INPUT

VELOCITY TRANSDUCER WAVEFORMS

FIG 8.19

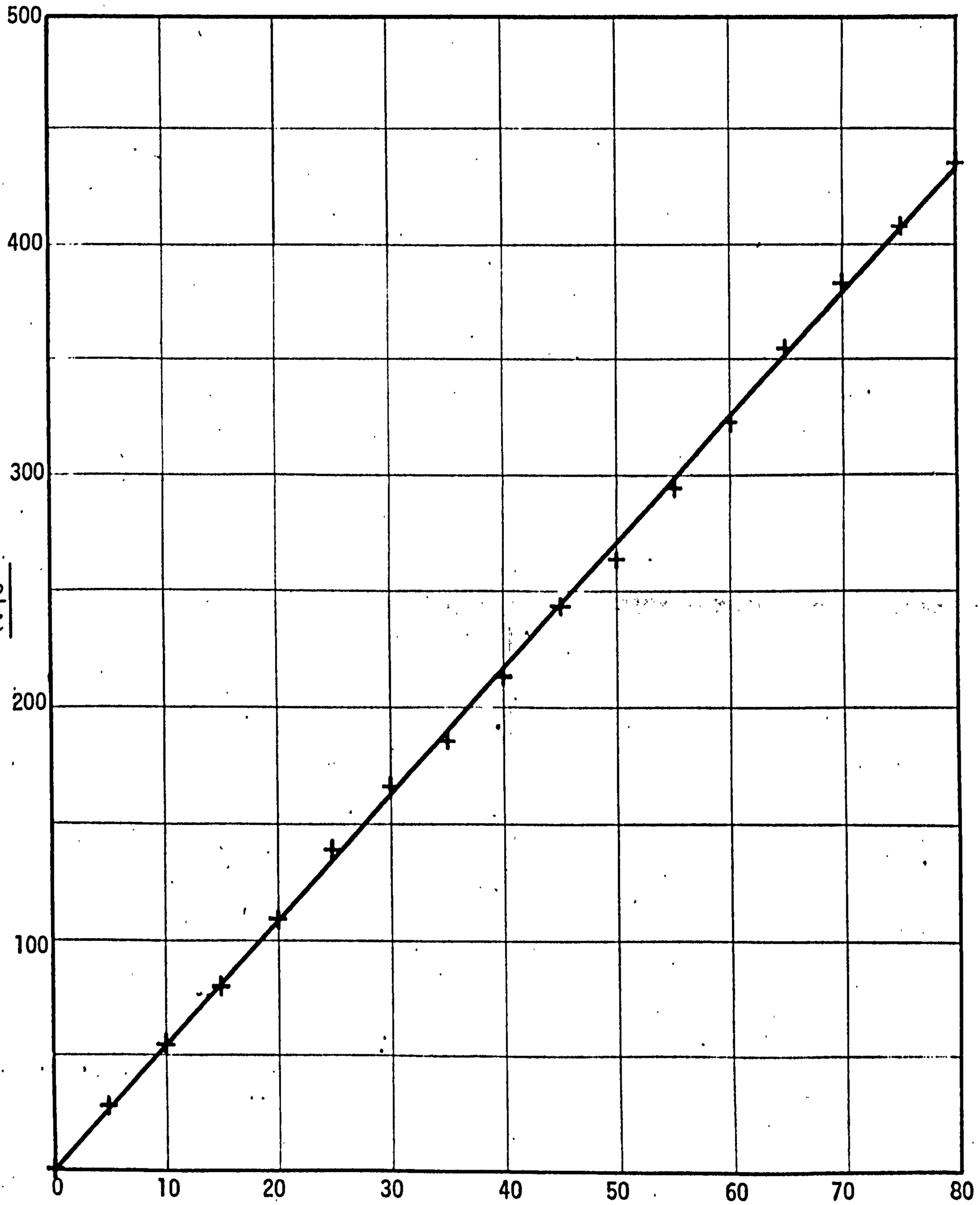

DATA-SAMPLED DIFFERENTIATOR CALIBRATION

FIG. 8·20

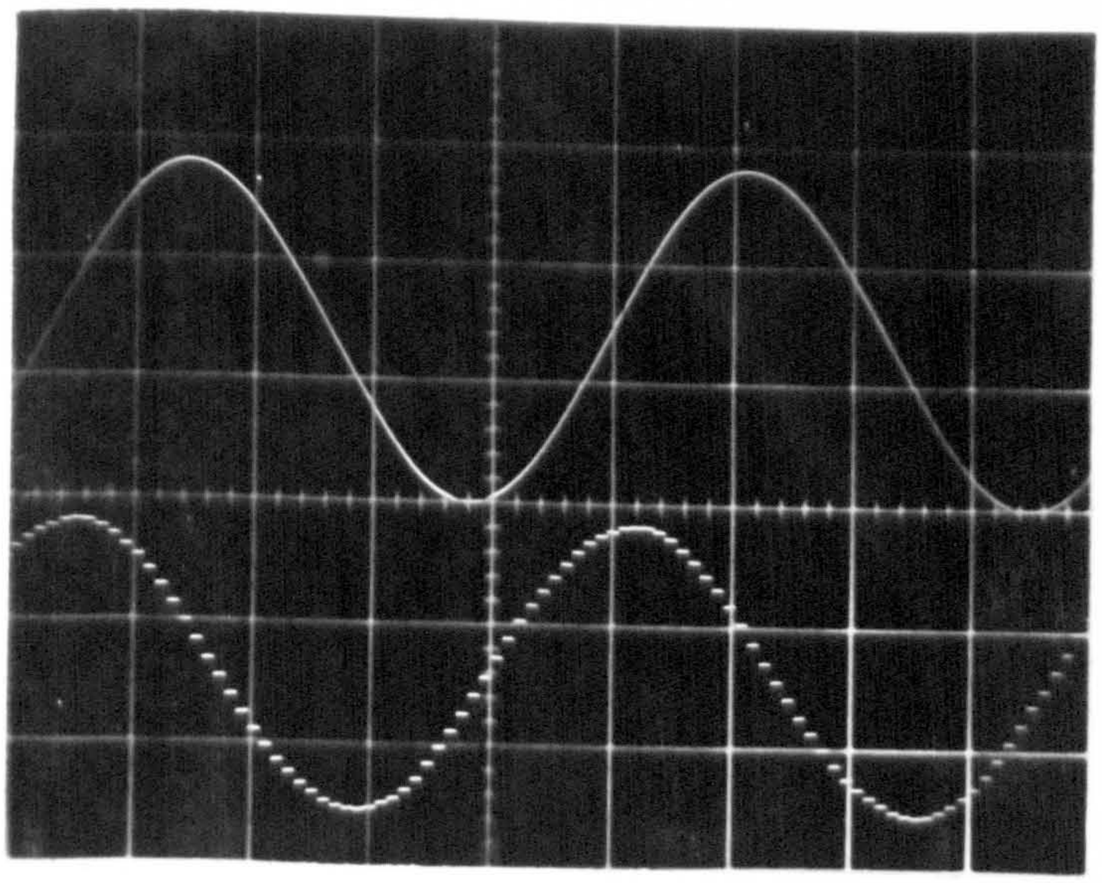

(a) SINE WAVE f = 20Hz

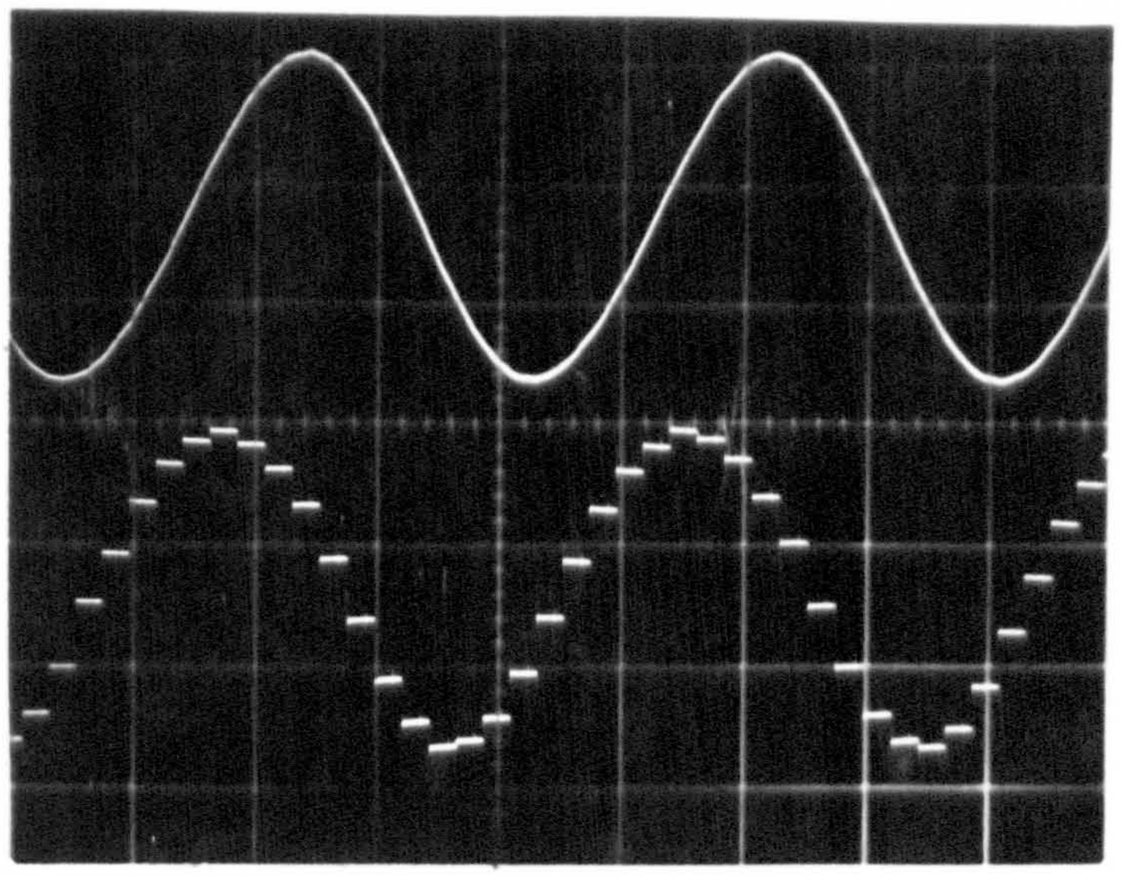

(b) SINE WAVE f = 60 Hz

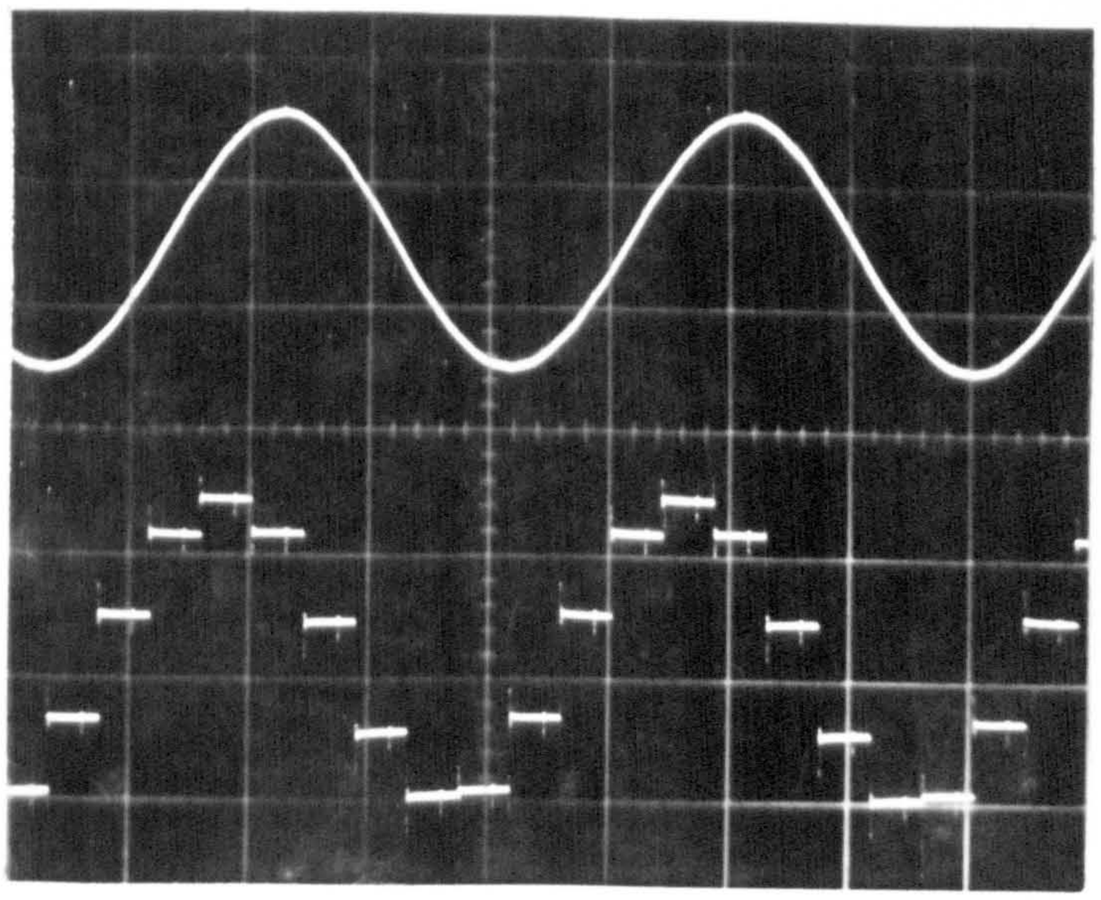

(c) SINE WAVE f = 100 Hz

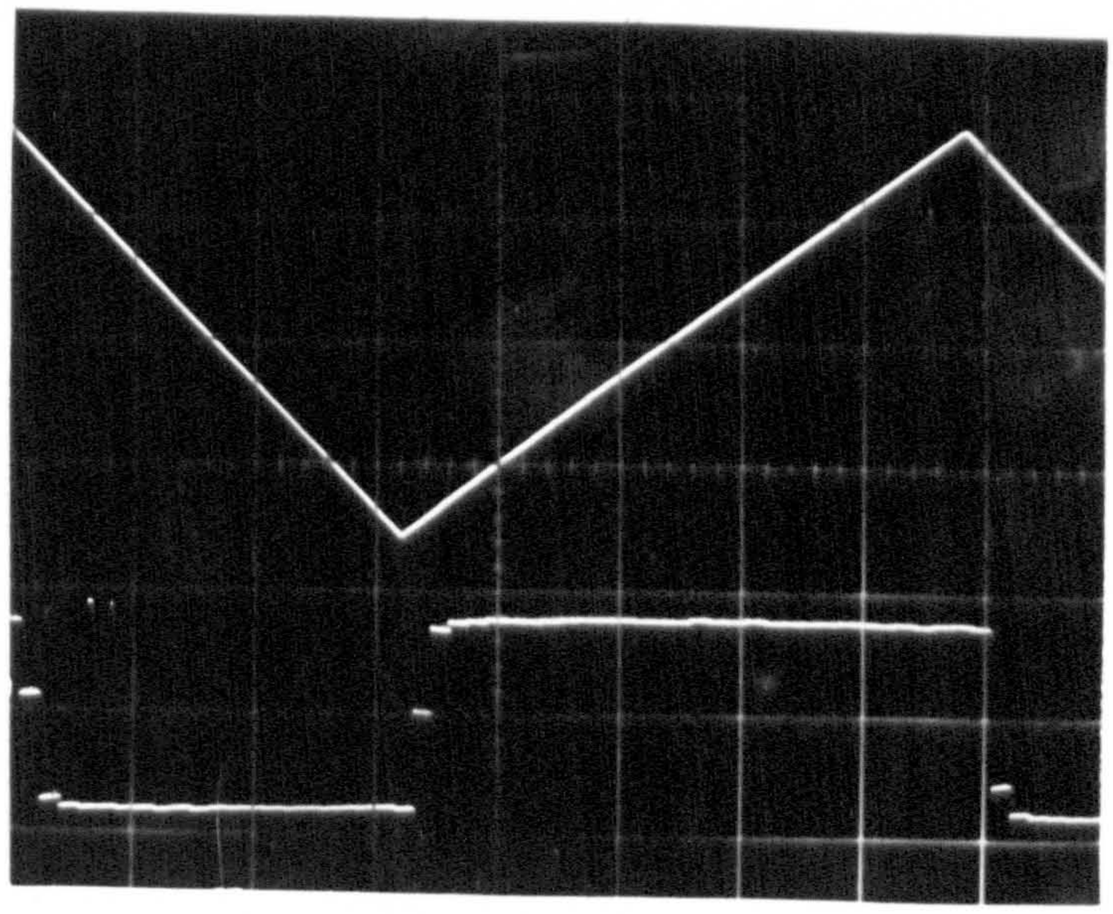

(d) TRIANGULAR WAVE f = 20 Hz

$t_s = 1/m\,S$

DIFFERENTIATION USING ACCELERATION TRANSDUCER

FIG 8.21

deteriorated with increasing frequency and in theory 90° phase lead would only be obtained with an infinitesimally small sampling period. To counteract this the phase lead may be set correctly at any desired frequency by offsetting one channel of the output differencing amplifier by adjusting R10 (Fig.8.10). Fig.8.22 shows the combined phase frequency characteristics of the filter and differentiator for the three switch positions, with the system set for 90° phase lead at approximately 1 Hz. This is the approximate frequency of the transient oscillations of a large turbogenerator after a fault has been applied.

Fig.8.21d shows the effect of using the acceleration transducer to differentiate a triangular waveform. When the slope of the input signal changes sign, the output takes only between 2-3 ms to respond after which it remains reasonably constant giving a measure of the slope of the input waveform.

When the transducers were set up on the Doncaster machine it was observed that large harmonic and spurious fluctuations were present in the acceleration signal and to a lesser extent in the velocity signal. The instrumentation was removed and rechecked only to be found satisfactory, and so the shaft sensor was suspected. On removing the cover of this is was observed that oil from a leak in the main excitor bearing was penetrating inside the sensor housing. Flying droplets of oil were interrupting the light path causing the spurious fluctuations in output. On closer examination of the velocity transducer output waveform it was noticed that the harmonic fluctuations consisted of a 50 Hz component which varied in amplitude and random steps of voltage which were in the same relative position in each cycle and constant in amplitude. The former phenomena was attributed to vibration of the shaft in the bearings and the latter to machining inaccuracies of the toothed wheel.

Unfortunately an outage of the machine was not possible before the power system tests, which was necessary for removing the toothed wheel/probe assembly to rectify the faults. In the circumstances it was decided to include heavy additional filtering to reduce the unwanted oscillations but this severely impaired the response of the instrumentation so that the signals produced were far from analogues of shaft velocity and acceleration. The results of the tests are given in Chapter 9.

8.3.3 Performance of rotor angle meter

The calibration of the rotor angle meter operating from two sine wave 50 Hz inputs is given in Fig.8.23. The varying phase differences were

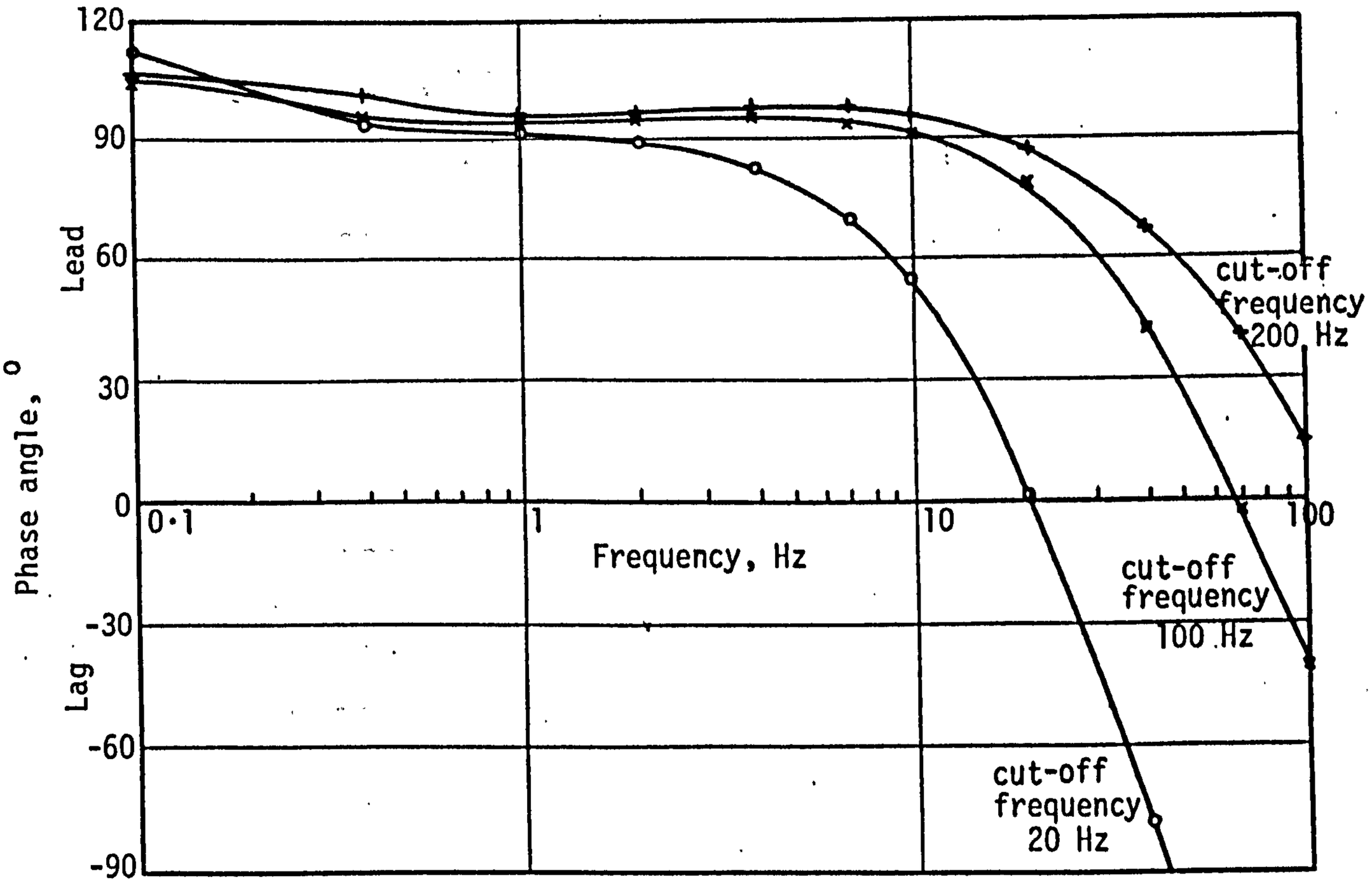

PHASE-FREQUENCY CHARACTERISTICS OF DIFFERENTIATOR

FIG. 8·22

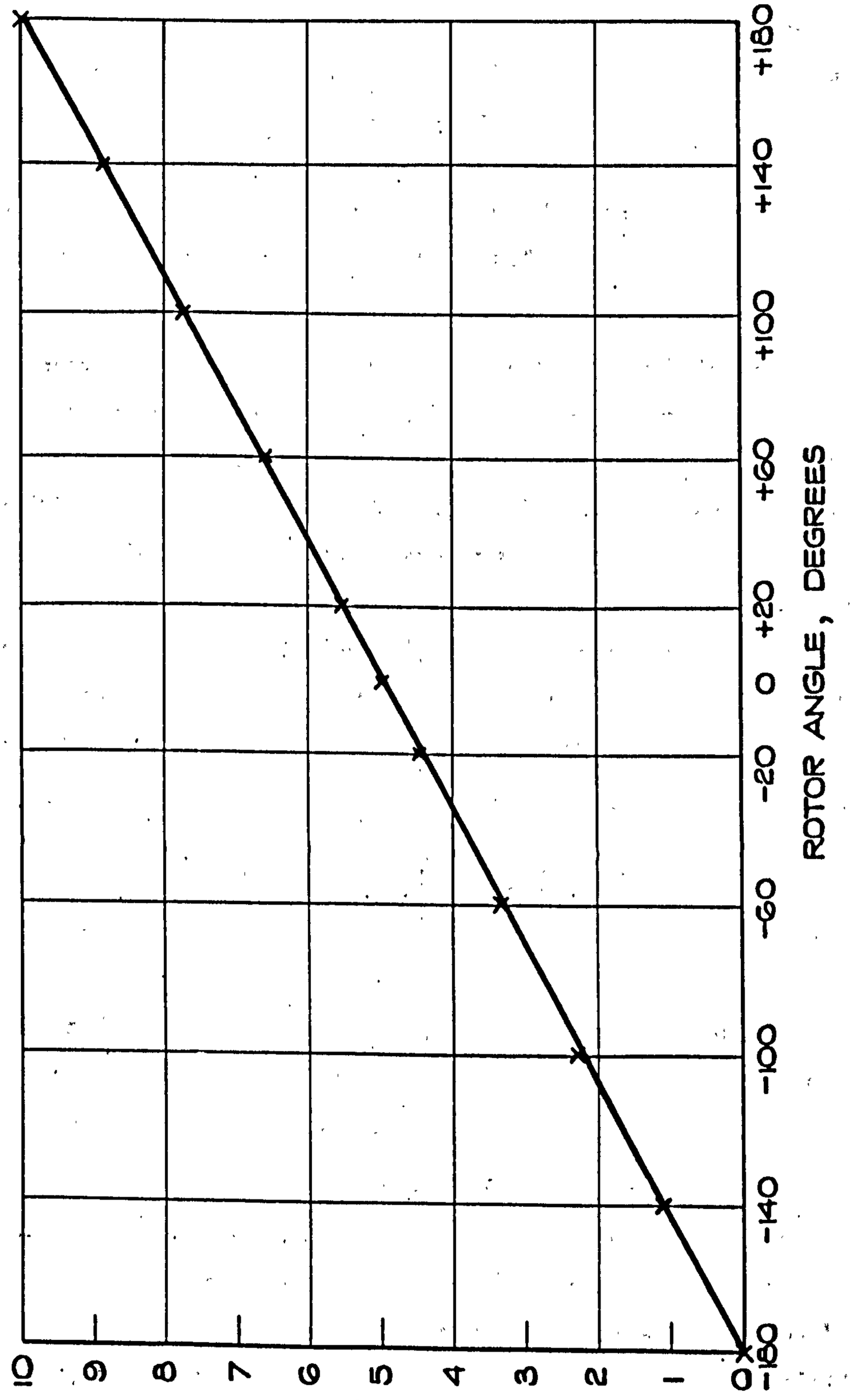

CALIBRATION OF ROTOR ANGLE METER

FIG. 8.23

obtained using a phase shifting transformer with a vernier scale but an additional check was provided by an accurate phase meter.

The unit has operated satisfactorily both from a high frequency 400 c/s tacho[16] and from a single shaft projection giving a 50 Hz input. In order to operate from higher frequencies the 3 stage binary counter of Fig.8.24 was added in the input circuit. This enables inputs of 400, 200 and 100 Hz to be used. The overall wiring diagram of the manufactured portable instrument (Fig.8.15) is shown in Fig.8.25.

Fig,8.26 shows oscillograms of the output of the rotor angle meter during measurements of transient behaviour on a Mawdsley's micro-alternator set. Both figures show the effect of a step change in prime mover torque produced by altering the control signal of the thyristor converter which controlled the DC drive motor. In Fig.8.26a the machine was within the transient stability limit but a larger step was used in Fig.8.26b causing pole slipping. As the disturbance was removed after 250 ms the rotor pulled back into synchronism after one pole slip and the oscillations were damped out. The effect of the sample-hold can just be perceived from Fig.8.26b as a 'stepped' effect when the waveform is changing rapidly.

8.4 Future work on fast response instrumentation

8.4.1 Further development of existing instruments

Most of the circuits exhibited slow drifting of the outputs due to temperature causes and efforts to compensate this should be made in future designs. However due to the wide range of integrated circuits now available almost all of the circuitry could be converted to this form with consequent reduction of temperature drift problems.

Although unsatisfactory results were obtained from the velocity and acceleration transducers at Doncaster, this was not the fault of the electronic equipment as explained earlier. However a development of the system is proposed which will not be effected by errors in the machining of the toothed wheel and will probably give a better rejection of shaft vibration signals. The schematic is shown in Fig.8.27b and the arrangement of the pick up unit which contains two sensors is shown in Fig.8.27a. The angular spacing between the sensors is just less than the span of each tooth and magnetic pick-ups are used to eliminate the problems of dirt and oil which occurred on the Doncaster machine.

As a tooth passes the first sensor it produces a pulse which resets the ramp generator. Subsequently it passes the second sensor and produces another pulse which samples the ramp waveform. Hence the output depends

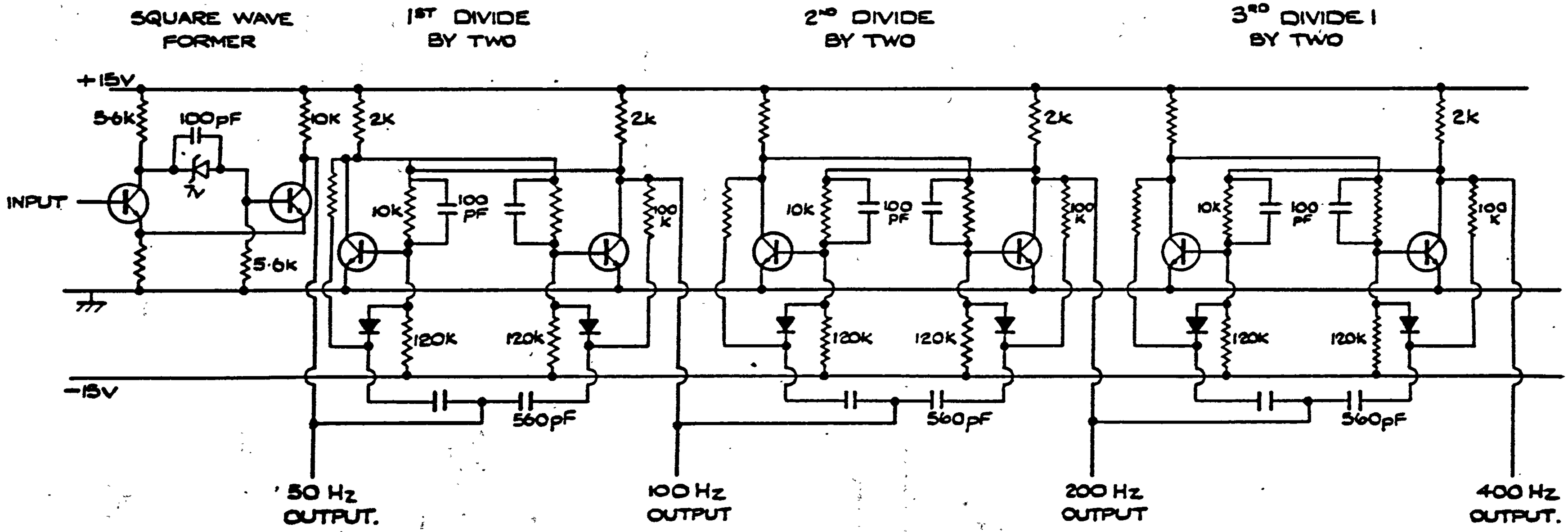

ALL TRANSISTORS TYPE ZT84.

CIRCUIT DIAGRAM OF SIGNAL PREPARATION MODULE

FIG.8.24

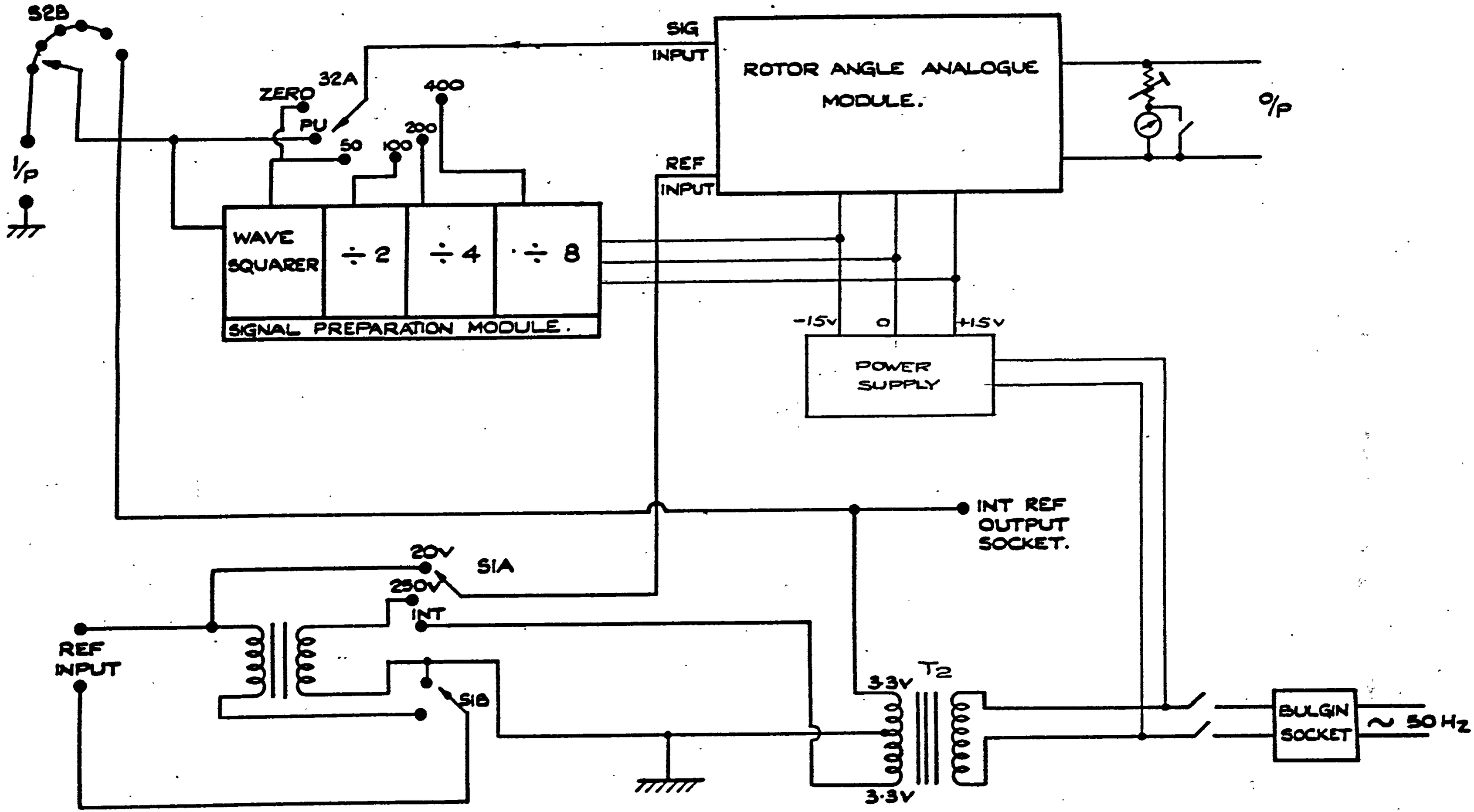

SCHEMATIC LAYOUT OF ROTOR ANGLE METER.

FIG 8.25

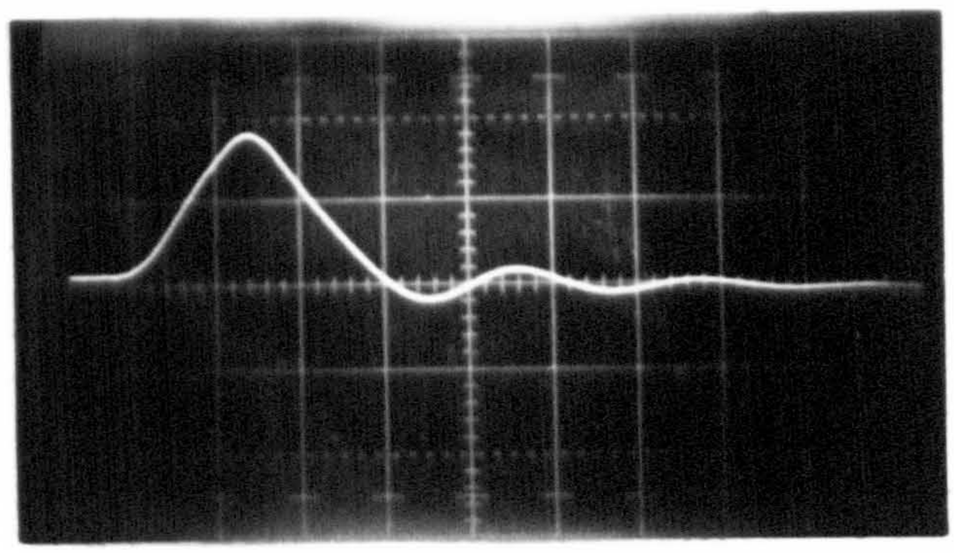

X = 2v/cm

Y = 05 s/cm

(a) TRANSIENT

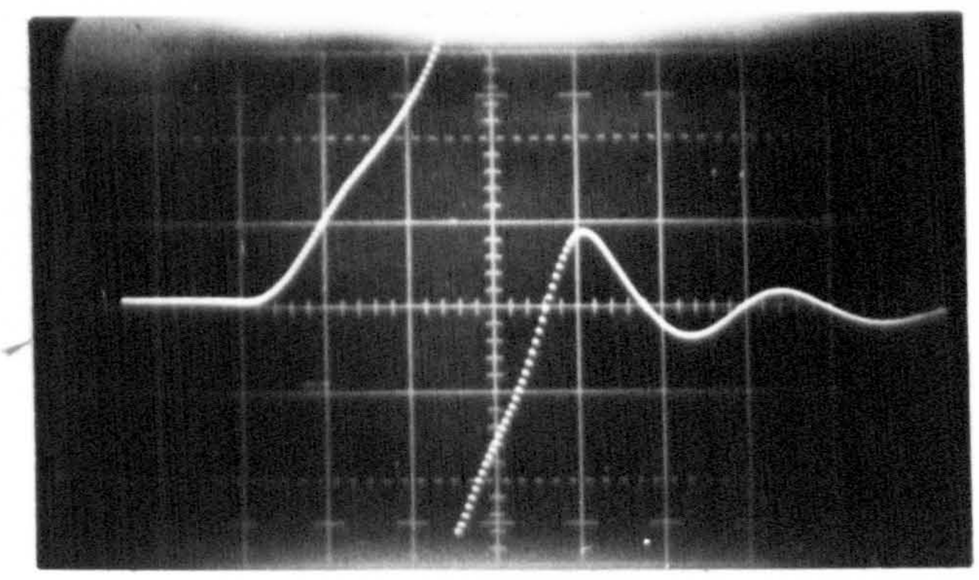

X = 2v/cm

Y = 0.5s/cm

(b) POLE SLIP

OSCILLOGRAMS OF OUTPUT OF ROTOR ANGLE METER MONITORING PERFORMANCE OF MICROMACHINE

FIG 8.26

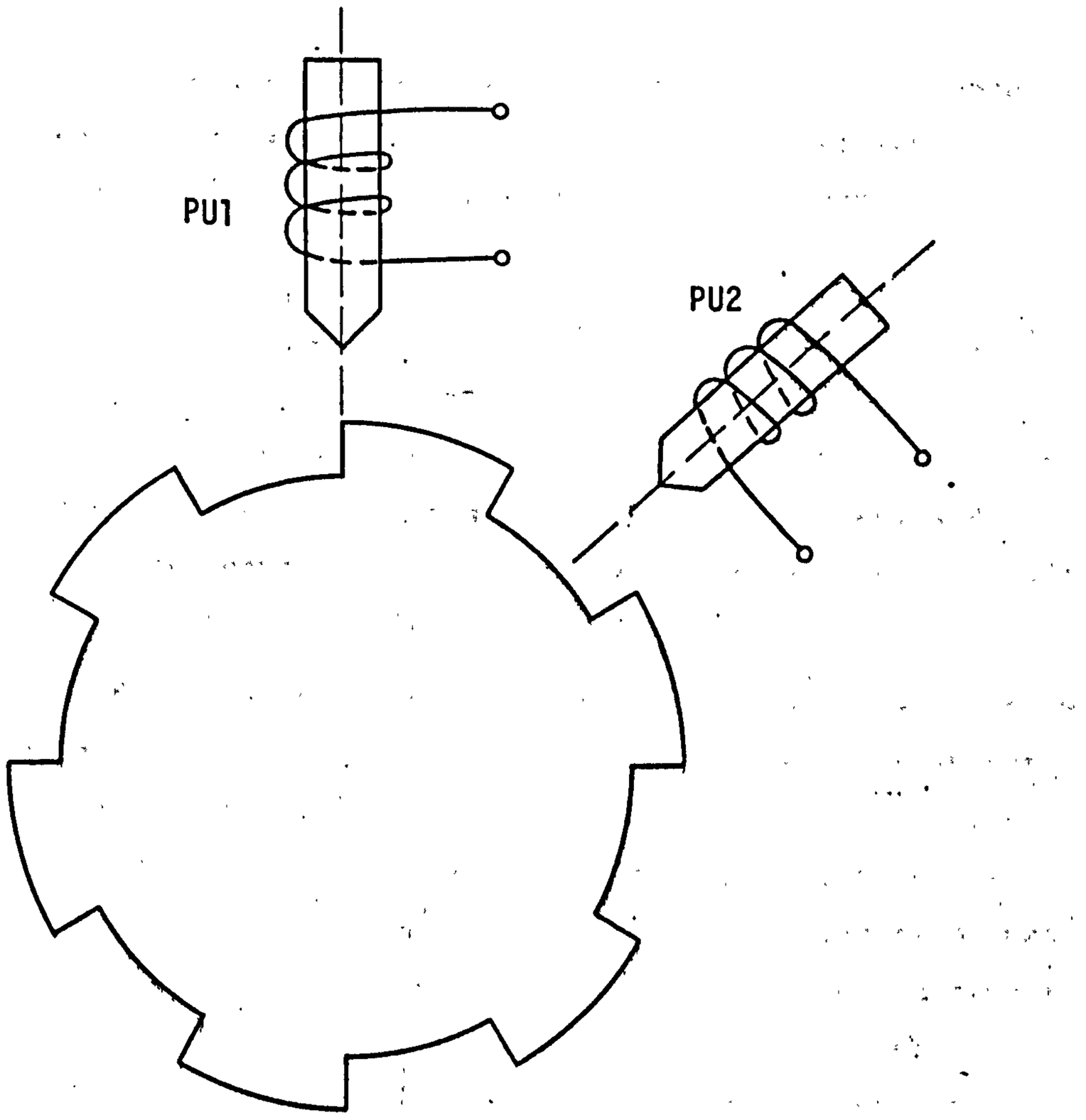

(a) ARRANGEMENT OF PICK-UP UNIT

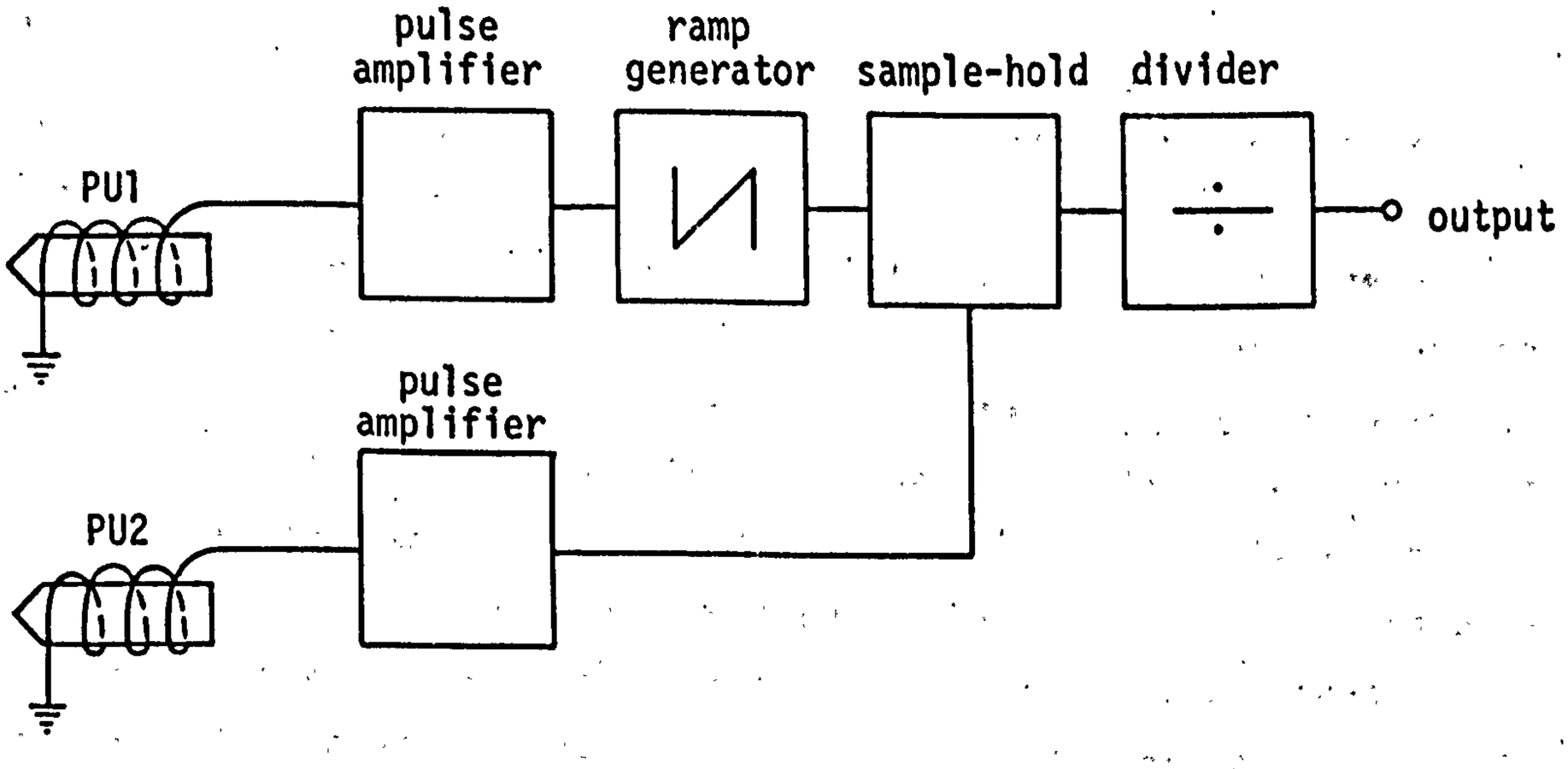

(b) BLOCK DIAGRAM

PROPOSED VELOCITY TRANSDUCER USING TWO PICK-UPS

FIG. 8·27

upon the time taken for each single tooth to travel the angular distance between the two probes (which is constant) and not the time between consecutive teeth passing a single probe which would depend upon the accuracy of the spacing.

8.4.2 Elimination of vibration components using multiple pick-up heads

By employing magnetic instead of photoelectric pick-ups and by using the double pick-up system previously described, it is envisaged that some of the difficulties experienced on the Doncaster set, namely oil droplets and machining errors, can be overcome. However the remaining problem of shaft vibration is the most complex and difficult to eliminate.

As far as the sensor is concerned there are two vibration modes which will affect the signal output. These are torsional oscillations and transverse displacement vibrations. The first is caused by the interaction of the various masses of the turbine and generator rotors through the torsional elasticity of the shaft. Thus the system is analogous to a series of masses and springs which can be excited by electrical and mechanical disturbances in the generator or turbine giving rise to a number of natural frequencies. The effects are almost impossible to remove completely, but extensive work by Ontario Hydro of Canada has shown that there is usually a node somewhere along the shaft where all the torsional oscillation frequencies are minimised. However this may not be a suitable siting for mounting a toothed wheel if say it occurs inside a turbine or the generator casing and two or more wheels may have to be used. These are placed where the oscillations are in opposite phase so that when theoutputs are added together the unwanted frequencies are cancelled.

The second type of vibration is caused by axial excursions of the shaft and gives rise to two effects in the sensor output. The displacement velocity component will be picked up by the probe so that the frequency of the output pulses will be modulated continuously. In addition the air gap between the probe and the wheel will change and thus causes voltages to be generated between pulses as well as variations in the pulse amplitude. To reduce these effects multiple sensors must be employed which are spaced evenly around the wheel. Fig.8.28 shows various probe configurations and the directions of a spurious velocity component s of the shaft with respect to each probe. If a separate velocity measuring circuit is driven from each probe and the outputs summated for each configuration, then the indicated velocity in each case is:

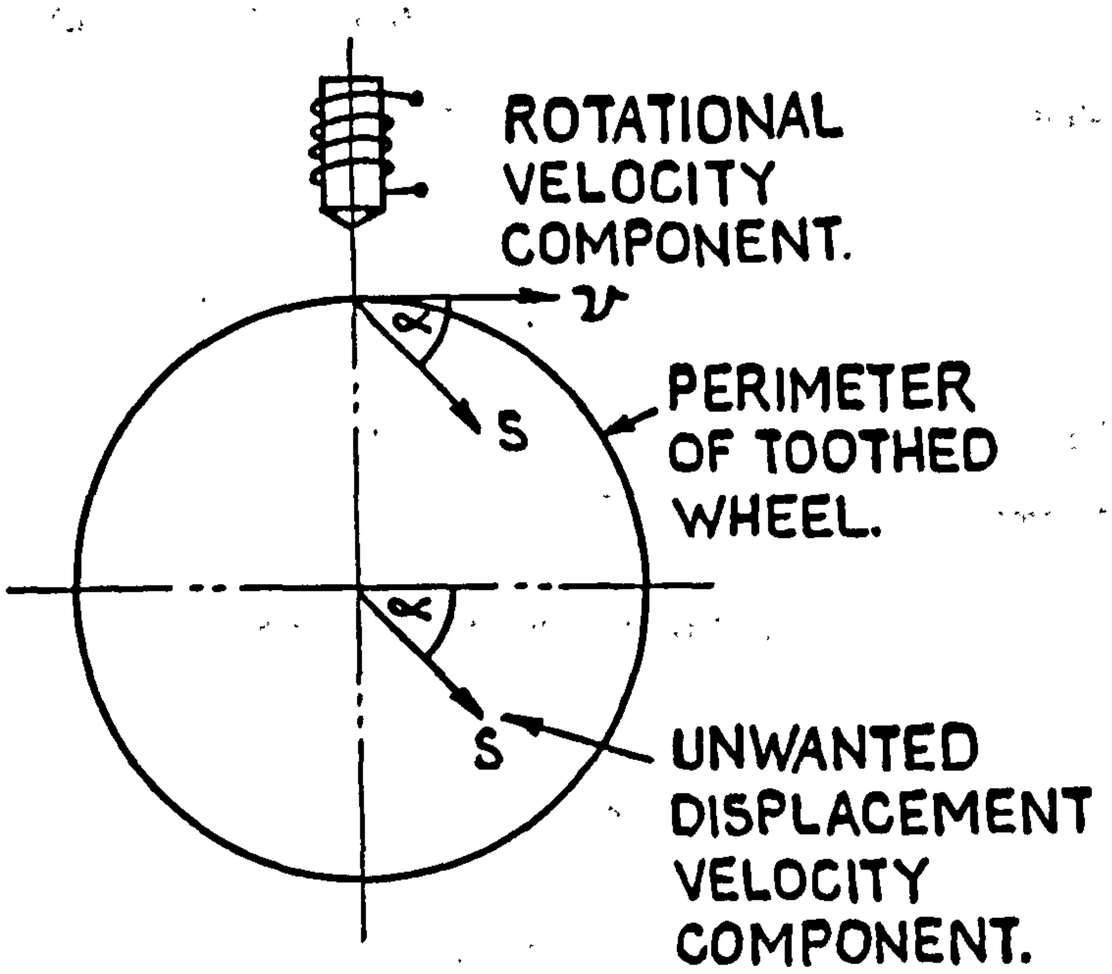

(a) SINGLE PROBE.

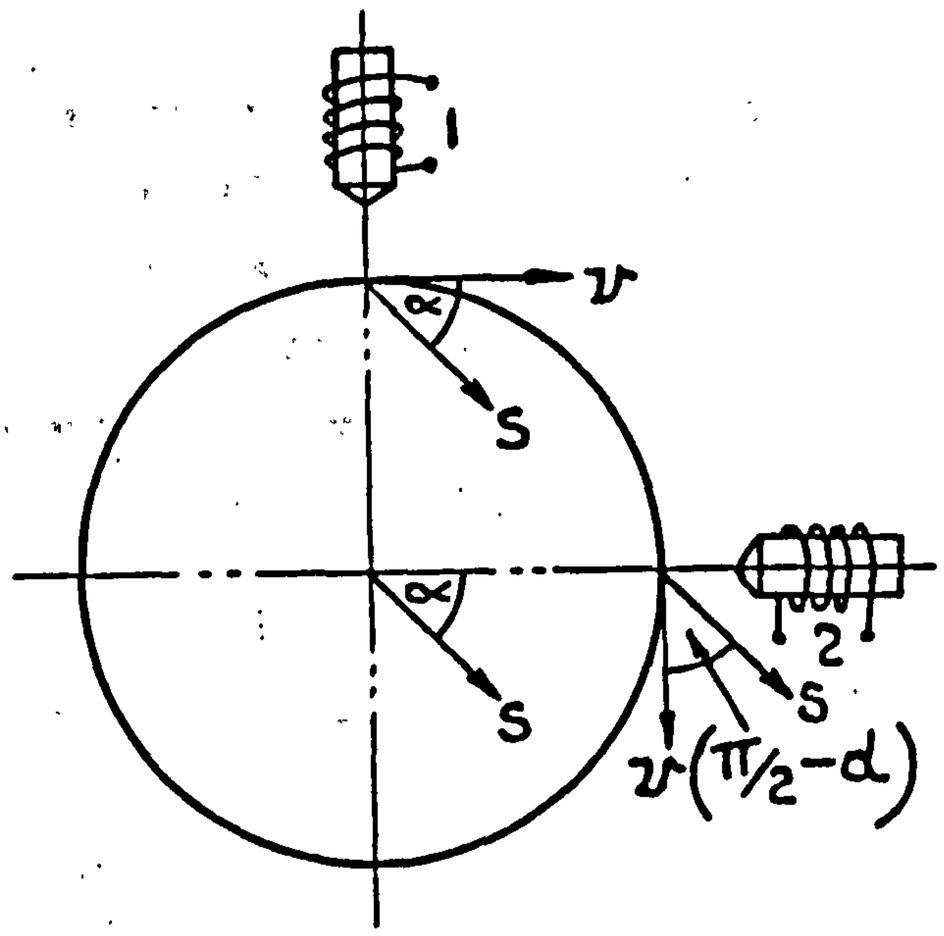

(b) 2 PROBES AT 90°

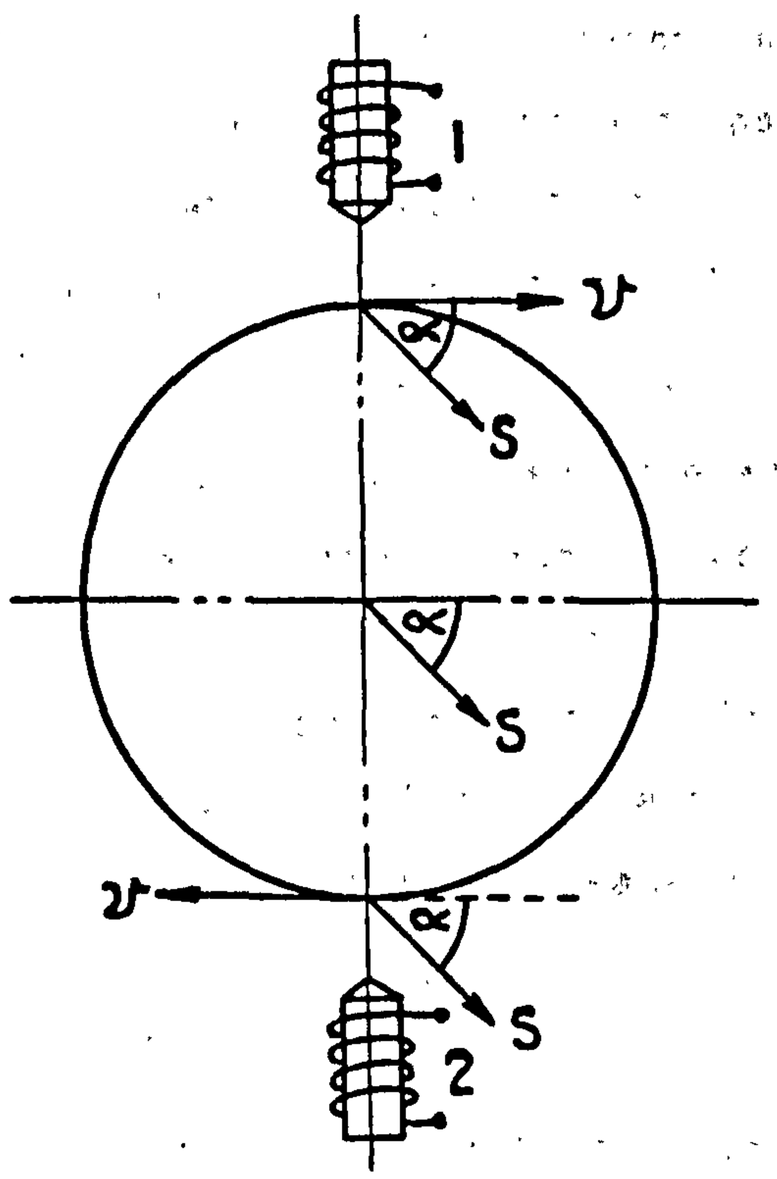

(c) 2 PROBES AT 180°

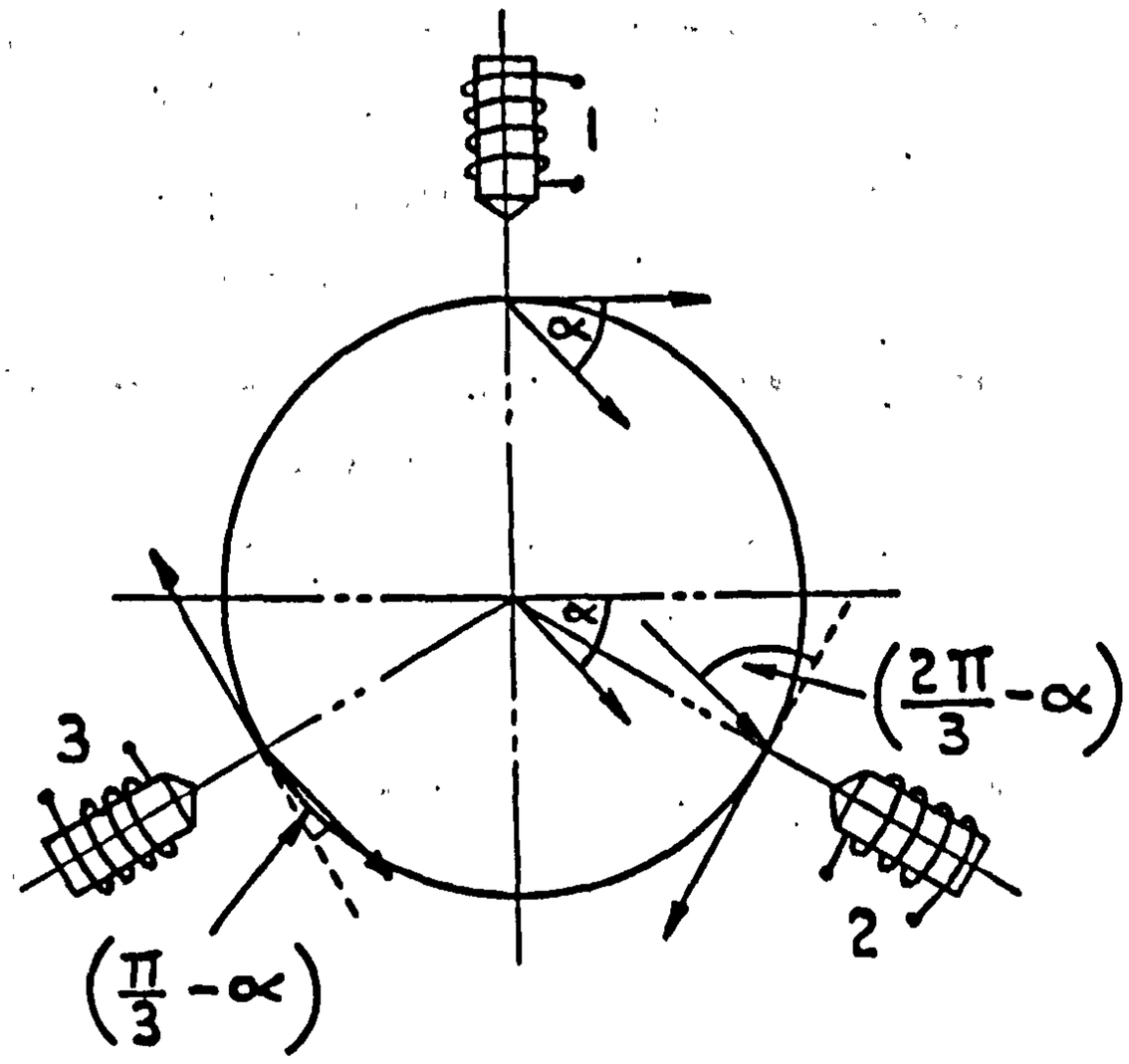

(d) 3 PROBES AT 120°

EFFECT OF ERRONEOUS DISPLACEMENT VELOCITY COMPONENTS ON VARIOUS MULTIPLE PROBE CONFIGURATIONS.

FIG.8.28.

(a) Single probe,

$$V = k\ (\nu + s\ \cos\alpha)$$

(where V is the indicated velocity in volts, k isthe calibration in volts/ cm/sec, ν is the shaft rotational velocity and s is the erroneous displacement velocity at some arbitrary angle α)

(b) Two probes at 90^{o} apart,

$$V = k\ (\nu + s\ \cos\alpha) + k\ (\nu + s\ \sin\alpha) = k\ \{2\ \nu + s\ (\cos\alpha + \sin\alpha)\}$$

(c) Two probes at 180^{o} apart,

$$V = k\ (\nu + s\ \cos\alpha) + k\ (\nu + s\ \cos\alpha) = 2k\nu$$

(d) Three probes at 120^{o} spacing,

$$V = k\ (\nu + s\ \cos\alpha) + k\ (\nu + s\ \cos\ (\tfrac{2\pi}{3} - \alpha)) + k\ (\nu + s\ \cos\ (\tfrac{\pi}{3} - \alpha))$$
$$= 3k\nu$$

It is seen from the above that axial velocity effects can be removed completely from the output signal by using two probes placed diammetrically opposite or three probes spaced equally by 120^{o}. In fact it can be similarly shown that for any higher number of probes symmetrically placed around the wheel the axial velocity effects are nulled.

The effects of variations of the air gap due to eccentric excursions are more difficult to analyse and are still under investigation. Fig.8.29 shows an exaggerated amount of eccentricity of the wheel ℓ at some arbitrary angle α to the fixed reference frame shown. The situation shown is an instantaneous picture as in practice α and ℓ will be modulated in a complex harmonic fashion by the vibrations. The variation of the effective air gap g between a probe, at same angle θ to the reference frame, is desired with respect to ℓ and α in order to investigate ways of minimising their effects on the probe output

The equation of the perimeter of the wheel of radius r, with respect to the fixed centre O, will be

$$(\chi - X)^2 + (y - Y)^2 = r^2 \qquad \ldots(8.1)$$

where X and Y are the coordinates of the wheel centre p.

In order to convert to polar form we may write for any point Q on the circumference,

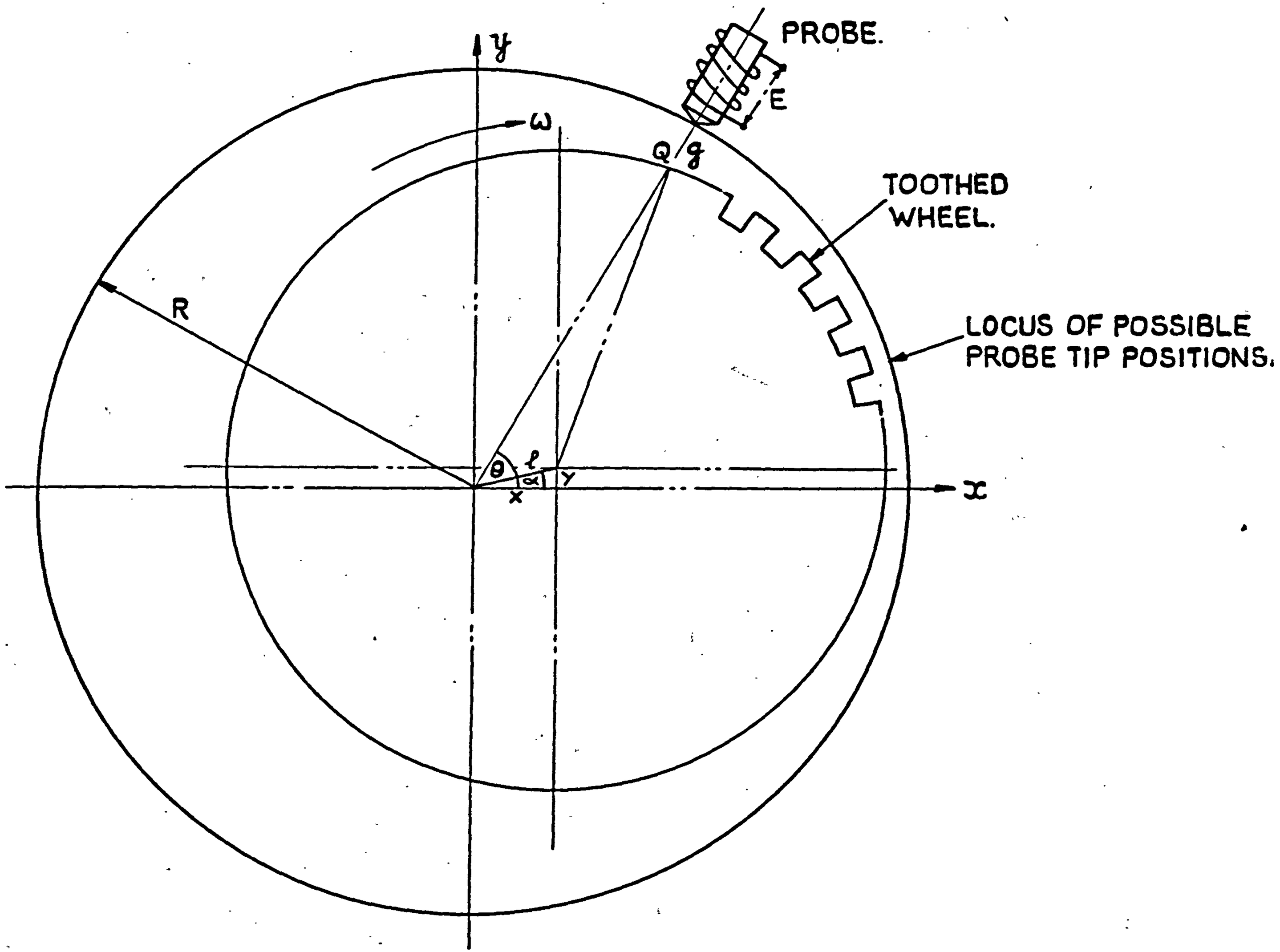

EFFECT OF ECCENTRICITY ON MAGNETIC PROBE.

FIG.8.29.

$$\left.\begin{aligned} x^2 + y^2 &= r'^2 \\ x &= r' \cos\theta \\ y &= r' \sin\theta \end{aligned}\right\} \qquad \ldots(8.2)$$

Also
$$\left.\begin{aligned} X &= \ell \cos\alpha \\ Y &= \ell \sin\alpha \end{aligned}\right\} \qquad \ldots(8.3)$$

Substitution of (8,2) and (8,3) in (8,1) gives

$$r'^2 - 2\ell r' \cos(\theta-\alpha) + \ell^2 = r^2 \qquad \ldots(8.4)$$

The roots of (8.4) are

$$r' = \ell\cos(\theta-\alpha) \pm \sqrt{r^2 - \ell^2 \sin^2(\theta-\alpha)}$$

For the situation considered in Fig.8.28 it can be seen that

$$r' = \ell\cos(\theta-\alpha) + \sqrt{r^2 - \ell^2 \sin^2(\theta-\alpha)}$$

Hence
$$g = R - \ell\cos(\theta-\alpha) - \sqrt{r^2 - \ell^2 \sin^2(\theta-\alpha)} \qquad \ldots(8.5)$$

Here we have the desired relationship of g in terms of α and ℓ for a probe at a certain angle θ. However, the effect of variations of the gap g on the voltage output of the probe must now be determined in order to deduce a method of minimising the effect.

The construction of the probe is merely a solenoid which is wound on a permanently magnetised type core. This is a simple straight core for most industrial applications but owing to the possibility of stray fields being present in the magnetic circuit, a U-shaped core is usually employed on turbogenerators. The core is extended to a tip which lies in close proximity to the toothed wheel and as a tooth passes the probe tip at speed there is a rapid change in reluctance, and hence the flux in the magnetic circuit, causing a voltage to be developed in the coil.

Now the flux $= \dfrac{\text{m.m.f.}}{\text{reluctance}} = \dfrac{\sigma\mu\mu_o A}{g}$

where the m.m.f. σ is provided by the permanent magnetism of the iron core. The permability of the air gap $\mu\mu_o$ is constant and if it is assumed that the area A through which the flux acts is also constant (i.e. the leakage flux does not change) then we may write

$$\phi = \frac{k}{g} \quad \text{(where } k = \sigma\mu\mu_o A \text{ and is assumed constant)} \qquad \ldots(8.6)$$

The open circuit voltage developed by the probe will be proportional to the rate of change of flux $\frac{d\phi}{dt}$ and so differentiating equation (8.6) we obtain:

$$\frac{d\phi}{dt} = \frac{-k}{g^2}.\frac{dg}{dt} \qquad \ldots(8.7)$$

In order to differentiate equation (8.5) to obtain $\frac{dg}{dt}$, partial derivatives must be used:

$$\frac{dg}{dt} = \frac{\partial g}{\partial \ell}.\frac{d\ell}{dt} + \frac{\partial g}{\partial \alpha}.\frac{d\alpha}{dt} \qquad \ldots(8.8)$$

and from (8.5)

$$\frac{\partial g}{\partial \ell} = -\cos(\theta-\alpha) + \frac{\ell \sin^2(\theta-\alpha)}{\sqrt{r^2-\ell^2\sin^2(\theta-\alpha)}} \qquad \ldots(8.9)$$

$$\frac{\partial g}{d\alpha} = -\ell\sin(\theta-\alpha) - \frac{\ell^2 \sin(\theta-\alpha)\cos(\theta-\alpha)}{\sqrt{r^2-\ell^2\sin^2(\theta-\alpha)}}$$

Combining equations (8.7), (8.8) and (8.9) above gives

$$\frac{d\phi}{dt} = \frac{k}{(R-\ell\cos(\theta-\alpha)-\sqrt{r^2-\ell^2\sin^2(\theta-\alpha)}} \left\{ \left[\cos(\theta-\alpha) \frac{\ell^2\sin^2(\theta-\alpha)}{\sqrt{r^2-\ell^2\sin^2(\theta-\alpha)}} \right] \dot{\ell} + \left[\ell\sin(\theta-\alpha) + \frac{\ell^2\sin(\theta-\alpha)\cos(\theta-\alpha)}{\sqrt{r^2-\ell^2\sin^2(\theta-\alpha)}} \right] \dot{\alpha} \right\} \qquad \ldots(9.10)$$

It is difficult to draw any conclusions as to the effect of combining the outputs of multiple probes for reducing spurious generated voltages by inspecting the above equation due to its complexity. However the preceeding analysis forms a basis for proceeding with future work. It would seem that the most practical approach would be to calculate the eccentricity errors for various multiple probe configurations by programming equation (8.10) on the digital computer. As the velocity errors $\dot{\ell}$ and $\dot{\alpha}$ will be eliminated by the previous analysis (Fig.8.28) they can be replaced by constants and the variations in $\frac{d\phi}{dt}$ calculated for a full range of values of ℓ and α using practical values forR and r.

It should be noted that the latter mentioned eccentricity problems only arise with magnetic probe systems which at present turbogenerator manufacturers and generating utilities seem to favour. This is mainly because of their ruggedness and environmental suitably as discussed earlier. However it may be worth while in the long term to develop more suitable photo-electric systems which would overcome the eccentricity problem and with the advent of new components such as the gallium arsenide laser and high response detectors, a faster system could be produced with greatly increased accuracy.

8.4.3 Extension ofthe instrumentation for measuring other parameters

It is conceivable that many other quantities could be measured using the principles developed in the preceding sections. To exemplify, the rotor angle meter could be adapted for measuring the angle between any two signals enabling machine phase angle to be measured. Power factor could then be obtained very easily by passing the signal through an analogue cosine function generator. Multiplying outputs from the power factor, voltage and current transducers in an analogue multiplier would produce a measurement of electrical power. Reactive power would require a sine function generator for taking the sine of the phase angle. Having obtained the rotor and phase angles, other resolved quantities could be obtained such as V_d, V_q, I_d and I_q which may be required for more advanced control systems.

8.5 Conclusions

A complete instrumentation package for measuring generator quantities has been developed which satisfies the requirement of high speed of response for use in thyristor excitation and electronic governor control systems for increasing transient stability limits. The circuits in the main were developed for experimental work on laboratory 'micromachines' although the velocity and acceleration transducers were used for controlling a 30 MW machine during power system tests. For permanent measurements on a large machine the circuitry would have to be modified to achieve better temperature stability and long term reliability. This should not be difficult due to the wide range of integrated circuits which have become available since the commencement of the project.

All the new transducers described employ data sampler output stages. This technique now finds extensive application in the input stages of analogue to digital convertors and it follows therefore that the information from the instrumentation could be easily digitised giving increased accuracy and resolution. This is the most convenient form for logging the information for future study and will also find application in digital control systems which are being contemplated atthe present time.

9 SITE TESTS FOR VERIFICATION OF TURBOGENERATOR MODELS AND CONTROL POLICIES

9.1 Introduction

Pure theoretical studies are of little value unless the results can be complemented by practical tests on actual systems. In the field of power system stability, initial experiments are usually performed on laboratory micromachines or small industrial alternators as the opportunities for large scale site testing are infrequent and costs are extremely high. However the author was fortunate in being invited to participate in tests by CEGB North Eastern Region on a 30 MW set at Doncaster Power Station (No.2 Unit) which took place in July/August 1970. The overall purpose was the assessment of turbogenerator behaviour with thyristor excitation under dynamic, asynchronous and transient conditions. The author's involvement was mainly with the latter and included the planning, simulation and instrumentation for a series of 3 phase fault tests at full load. Unless specific mention is made to the contrary, these are the only tests referred to in following as the results for the remainder are, at the time of writing, confidential CEGB internal material.

The tests were designed to investigate the effect of the following control configurations on the generator transient performances:

(a) Exciter fed thyristor excitation.

(b) Generator/transformer fed thyristor excitation.

(c) Rate of change of voltage stabilisation.

(d) Acceleration feedback stabilisation.

It was intended to perform a number of tests at both leading and lagging power factor but unfortunately it was possible to apply a series of only four faults to the generator, which rather limited the scope of the investigation.

The tests provided an opportunity for checking the accuracy of the computer modelling techniques developed in Chapter 2, and provision was made in the test programme for the measurement of a limited number of machine parameters. A number of performance predictions were also carried out before the test data for both planning and security purposes. These were conservatively estimated so that the worst case performance could be checked, and as the generator swings were much smaller in the tests, the results of the initial predictions are not recorded here.

9.2 Test details

9.2.1 Ancillary equipment

The test machine (GEC No. 99952/2) was a fully air cooled 30 MW unit driven by a two cylinder turbine, and the excitation current was normally supplied from a DC exciter controlled by an electromechanical automatic voltage regulator. For the majority of the tests the designed excitation system was replaced by a thyristor converter and electronic AVR system, which was connected through to the slip rings by a temporary terminal board adjacent to the generator. This equipment was a newly designed portable spare excitation system for installation on generators up to 60 MW output, in the event of an exciter failure, and the operation during the system tests constituted thorough proving trials. Fig.9.1 shows the equipment installed in the basement of Doncaster B Power Station during July 1970, and the component parts of transformer, circuit breaker, thyristor bays, and AVR cubicle can be distinguished. The velocity and acceleration transducer cards described in Chapter 8 were mounted in the AVR cubicle, and input drive pulses were supplied from a shaft mounted photo-electric pick-up arrangement (Fig.9.2). This was mounted as a unit on the exterior of the exciter outboard pedestal bearing, and contained a shaft driven wheel containing 20 holes which modulated a parallel light beam produced by a tungsten filament lamp and lens assembly. The light pulses were picked up by a phototransistor receiver head which provided the necessary input for the velocity transducer. In order to drive the relatively long length of cable to the equipment which was situated in the basement, a machine mounted buffer amplifier was provided. The photo-electric heads were supplied by the author and Fig.9.3 shows the relative displacement of these with respect to the wheel inside the pick-up unit. The original wheel was replaced by one with slots instead of holes after an initial trial period, due to the maloperation referred to in Chapter 8. Although this gave a slight improvement on the pitch errors, the performance was still unsatisfactory, mainly due to environmental problems with the photo-electric system, which were unavoidable with the unsatisfactory condition of the exciter bearing, as mentioned previously. The reason for the substantial pitch errors encountered was that basically the diameter of the wheel was too small. If this had been larger then the effect of standard machining inaccuracies on the spacing of the teeth, would have been reduced, but redesign of the unit was not possible before the tests. The effects of shaft vibration were fairly small however and this was due to the unit having its own double bearings with a semi-flexible coupling to the main turbogenerator shaft.

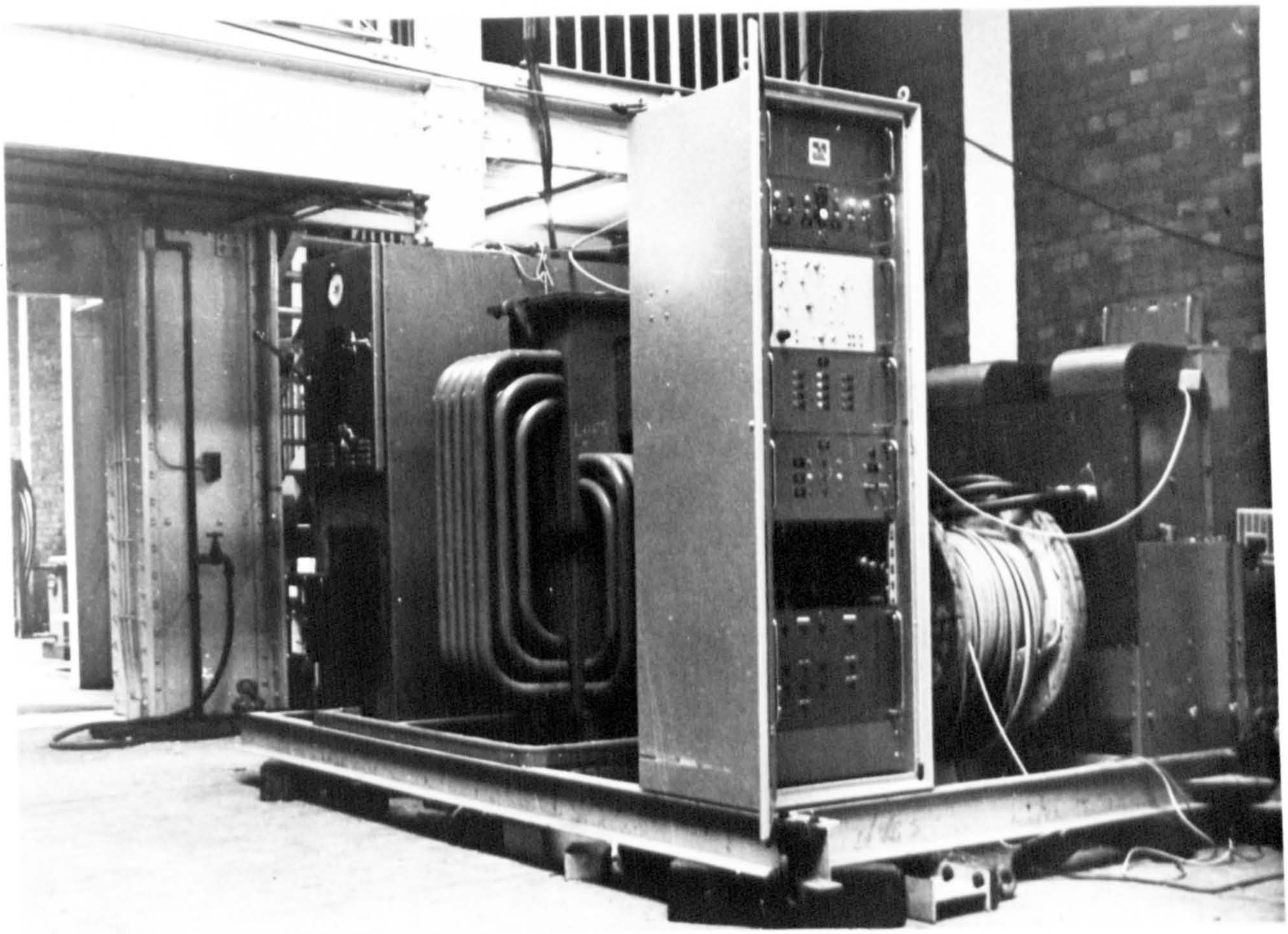

CEGB PORTABLE THYRISTOR EQUIPMENT INSTALLED AT DONCASTER POWER STATION, JULY 1970

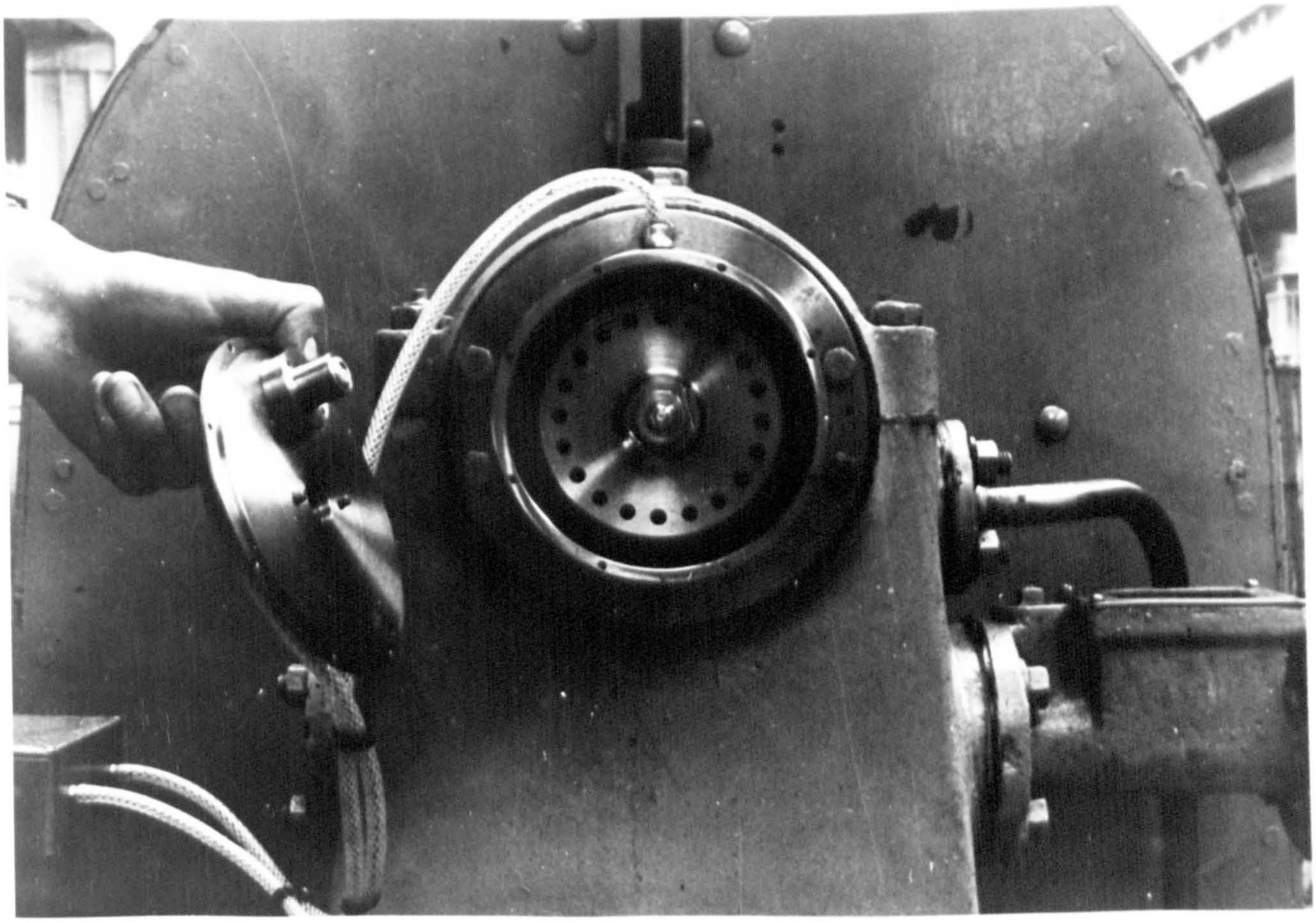

SPEED/ACCELERATION PICK UP UNIT MOUNTED ON OUTBOARD EXCITER BEARING OF DONCASTER MACHINE

FIG. 9.2.

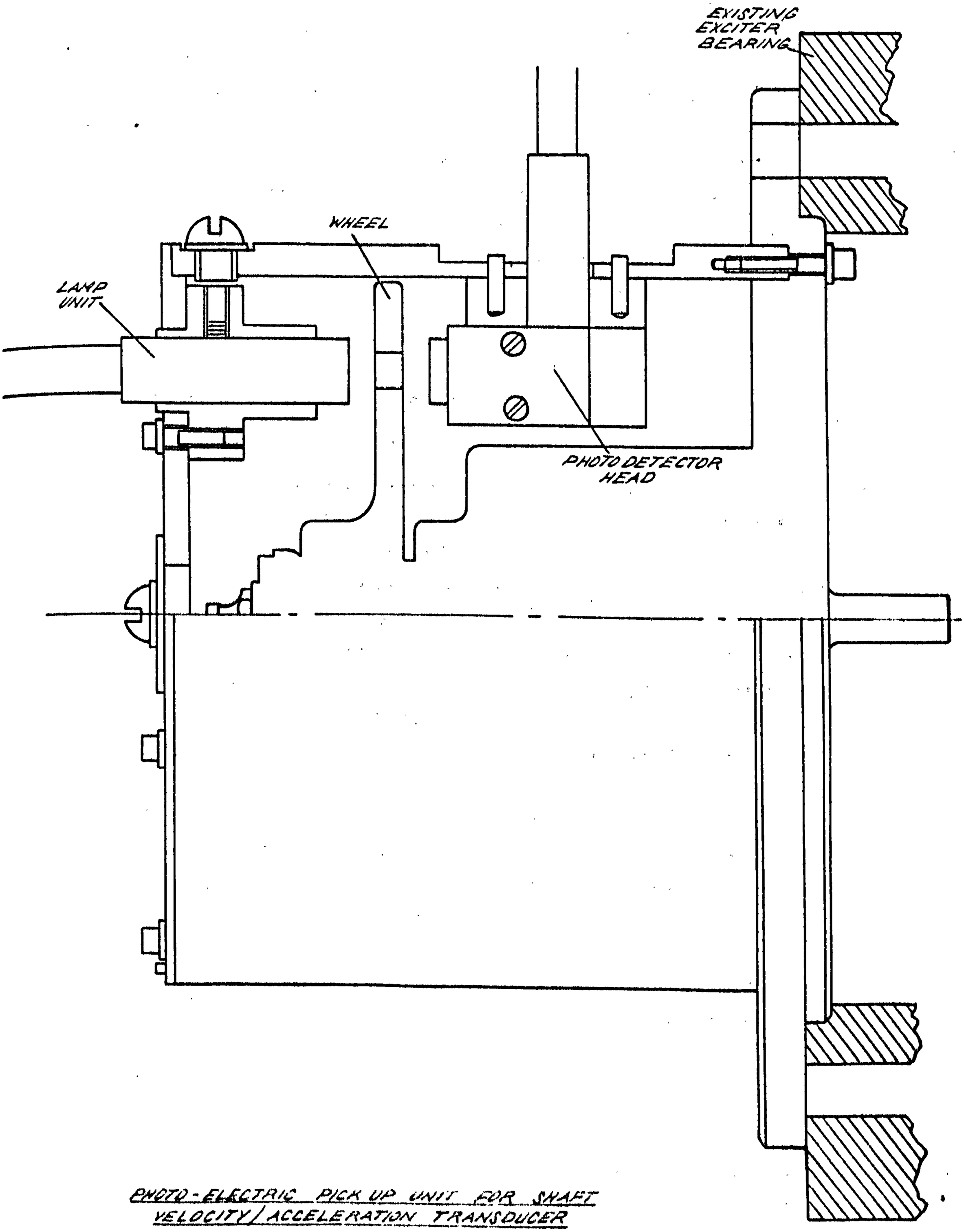

PHOTO-ELECTRIC PICK UP UNIT FOR SHAFT VELOCITY/ACCELERATION TRANSDUCER

FIG 9.3

Recordings of the results were obtained on ultra-violet oscillographs at three points, i.e. underneath the control room, adjacent to the thyristor equipment, and at the grid access point (Doncaster Central). At the first recording station, the electrical quantities stator voltage, stator current, field voltage, field current, power, rotor angle and system angle were recorded by means of shunts, transducers and other instrumentation. Precision metering was also provided for accurate measurements of the initial condition settings. In the basement, recordings were made of the outputs of the thyristor convertor and the acceleration transducer whilst at the remote grid the busbar voltage fluctuations were measured.

A special control panel was installed for the test, which contained the fault initiation switch and emergency field boost push button in addition to the normal manual controls for the thyristor excitation.

9.2.2 - System arrangement for fault tests

Fig.9.4 shows the re-organisation of the power system local to the power station for the fault tests. Only the test machine (No.2 Unit) was synchronised on to the main station busbars, the remaining three being connected to the reserve bars as shown, together with the local load outlets. For the purpose of applying the fault, the two 66 kV circuit breakers on the sending end of a redundant double circuit transmission line (Mexborough) were utilised. A jumper connection was made at the local terminal tower between the two lines as shown on the diagram, and a three phase short circuit clear of ground was connected on the open side of the Mexborough 2 breaker. This breaker was initially open and was closed to apply the fault, the Mexborough 1 breaker being used to clear the fault after a specified time interval determined by a time delay relay. The No.2 machine auxiliaries were supplied from the reserve station busbar, the voltage of which remained relatively constant during the fault, and a direct connection was made from the test machine to the West Melton 132 kV grid switching station. Both these measures were intended to produce a 'single machine to infinite busbar' situation which could be accurately represented by digital computer modelling techniques. The connections to the thyristor excitation transformer are described in the next section.

9.2.3 - Description of tests

Four transient tests were performed in which symmetrical 3-phase faults were applied to the machine as described in the preceeding section. Table 2 gives the relevant initial conditions for the tests and the generator, transmission

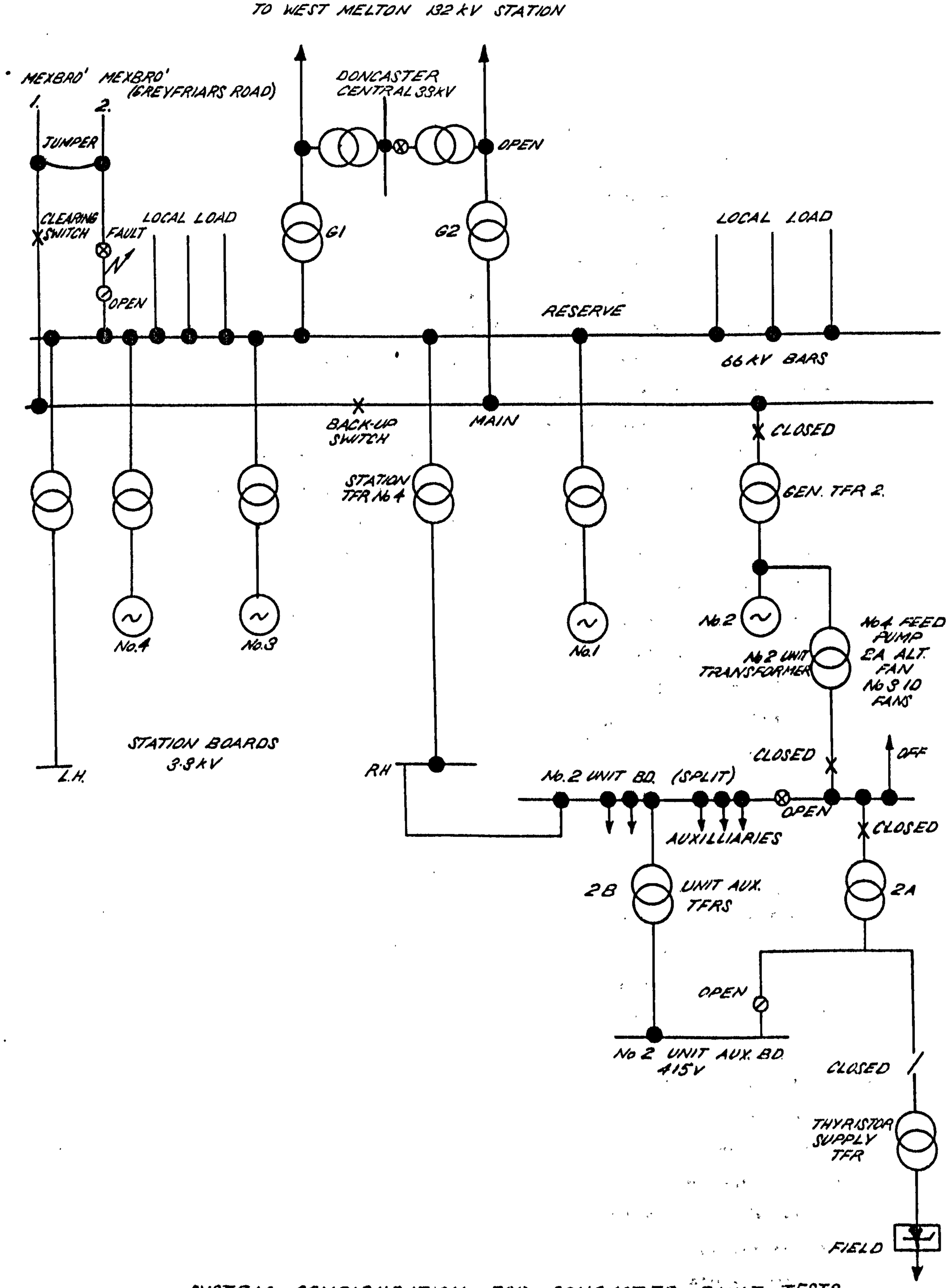

SYSTEM CONFIGURATION FOR DONCASTER FAULT TESTS

FIG 9.4

network and control system parameters are given in Appendix 11.3.

Tests 1-3 were carried out at full load, lagging power factor, with a nominal load angle and fault duration of 60° and 200 ms respectively. The fourth test was again performed at full load but this time at a leading power factor with a load angle of 79°. The fault duration was reduced to 136 ms to prevent instability. In tests 1 and 2 only voltage control feedback was used in the excitation system, and test 1 was performed with the thyristor supply transformer connected to No.2 Unit auxiliary board, which remained at a constant voltage (see Fig.9.4). This represented an exciter fed thyristor excitation system where the excitation supply is not depleted during a fault. In test 2 however, the thyristor transformer was connected across the output terminals of the test generator via No.2 unit transformer in order to represent a transformer fed static thyristor system and to make performance comparisons with the former configuration. In tests 3 and 4 the configuration of test 1 was adopted to reduce complication and an acceleration feedback term was added to the output of the AVR at the input to the thyristor control circuits. It appeared from the results of test 3 that the acceleration gain was much too low to have any appreciable effect, due to the attenuation introduced by the extra filtering, and so for test 4 the gain was increased by a factor of 10. In order to obtain the correct test conditions the tappings on both the generator and grid transformer 2 were altered and these are also given in Table 2.

9.3 Results of fault tests

9.3.1 Performance of instrumentation

In general the results of the tests were marred by the poor performance of certain items of instrumentation. One was the acceleration transducer which has been referred to earlier, but the major drawback was caused by the failure of the main rotor angle measuring device during each fault, which was probably caused by the reduction in voltage of the reference signal. A back up instrument was also used which was a slow acting type of questionable accuracy, but in the event, this had to be relied upon for all the transient measurements. (The author's rotor angle meter unfortunately could not be fitted.) The field current signal was obtained from a shunt but the output was so low compared to the galvanometer drive requirements, that a very small deflection was obtained, and little confidence can be expressed in this result. Due to the chopped waveform produced by the thyristors, heavy filtering was required to obtain an acceptable analogue signal for recording.

However this introduced too large a time delay and the final graphs were produced by measuring the areas of each pulsation in the DC waveform with a planimeter to obtain the average value per cycle. (This trace was obtained at the basement recording station.) The measurement of electrical power was facilitated by a small analogue computer and the multiplication of voltage current and power factor was accomplished by analogue function circuits which performed well. Armature voltage and current were recorded directly as AC quantities.

9.3.2 Assessment of recordings

Results taken from the original recordings are shown as the full line curves of Figs.9.6-9.9.

Figs.9.6 and 9.7 give a comparison between exciter fed and transformer fed thyristor excitation systems respectively. In the case of test 1 (Fig.9.6), full forcing voltage (2 p.u. based on CMR value) was available during the fault due to the large AVR input voltage error. In Fig.9.7, the depletion of the AC supply to the thyristors in test 2 due to the generator terminal voltage depression, caused a lowering of the excitation voltage during the fault, which increased the first forward angle swing by about 3^{o}. Although this is small, it would have been increased if identical fault durations had been accomplished, but in test 2 the fault time was about 3% less than that used in test 1. This was caused by the spread in the timing relay intervals and the breaker operating times. In both field voltage oscillograms, a large negative field forcing effect occurred directly after fault removal which would be produced by the rate of change of voltage stabilising term. This would also slow down the recovery of the terminal voltage as found in Chapter 5 but due to the fast thyristor excitation negligible overshoot occurred.

The results of test 3 (Fig.9.8) show very little difference to those of Fig.9.6 without the acceleration signal as the gain was too small. A slight reduction in the first rotor angle swing is observed but this is probably fortuitous. In Fig.9.9 which shows the results of test 4 however, the larger acceleration gain caused full positive and negative swings of the field voltage. Unfortunately due to the limited test programme, an uncontrolled test could not be performed in order to determine the effectiveness of this control signal. It was apparent however that very little damping had been introduced if any, as the behaviour was more oscillatory than in any of the other tests. The heavy filtering in the acceleration channel is illustrated by the slow build up

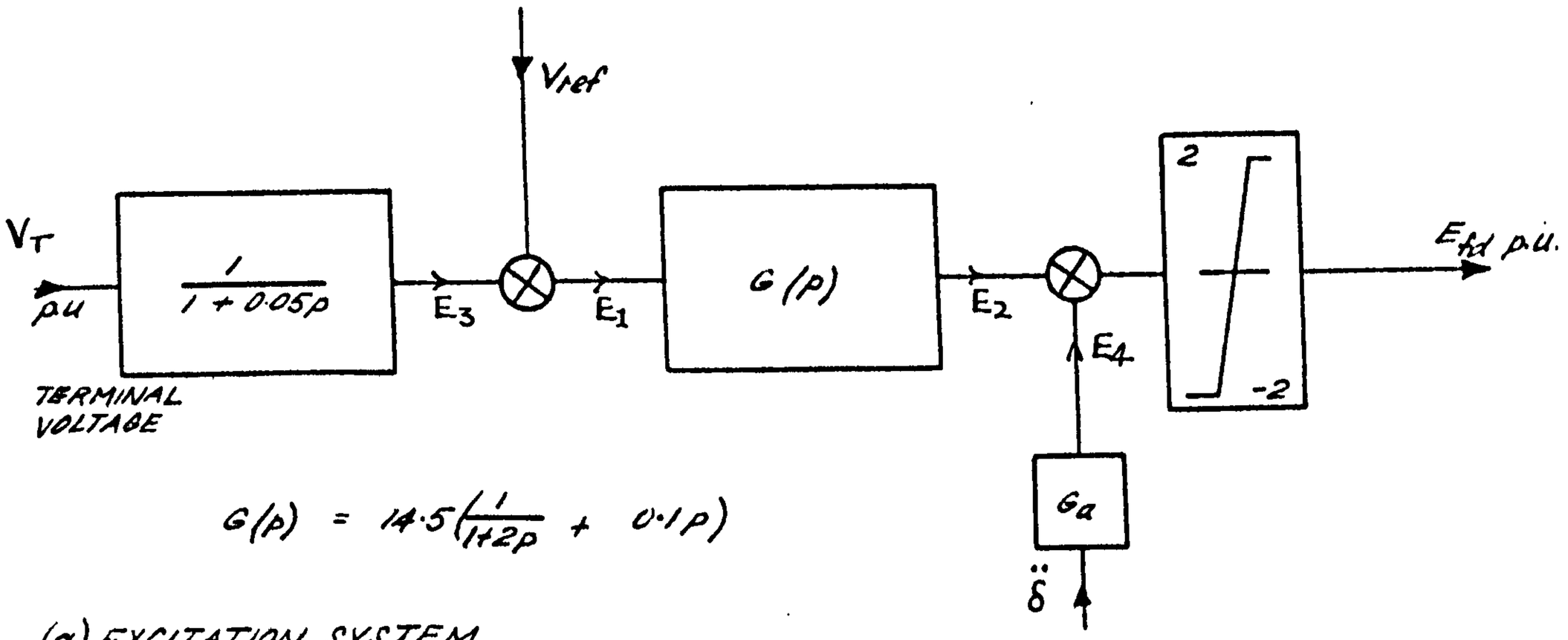

$$G(p) = 14.5\left(\frac{1}{1+2p} + 0.1p\right)$$

(a) EXCITATION SYSTEM

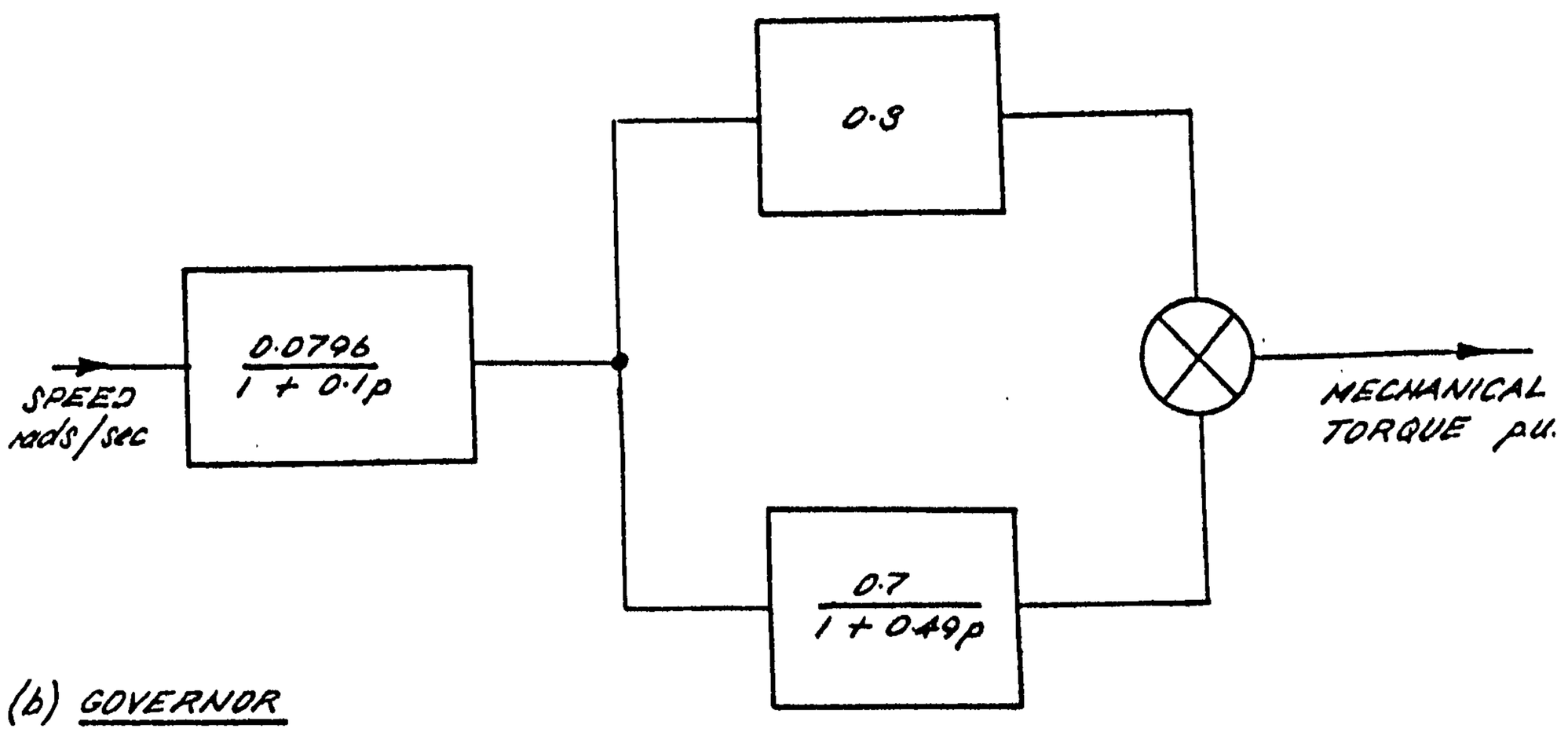

(b) GOVERNOR

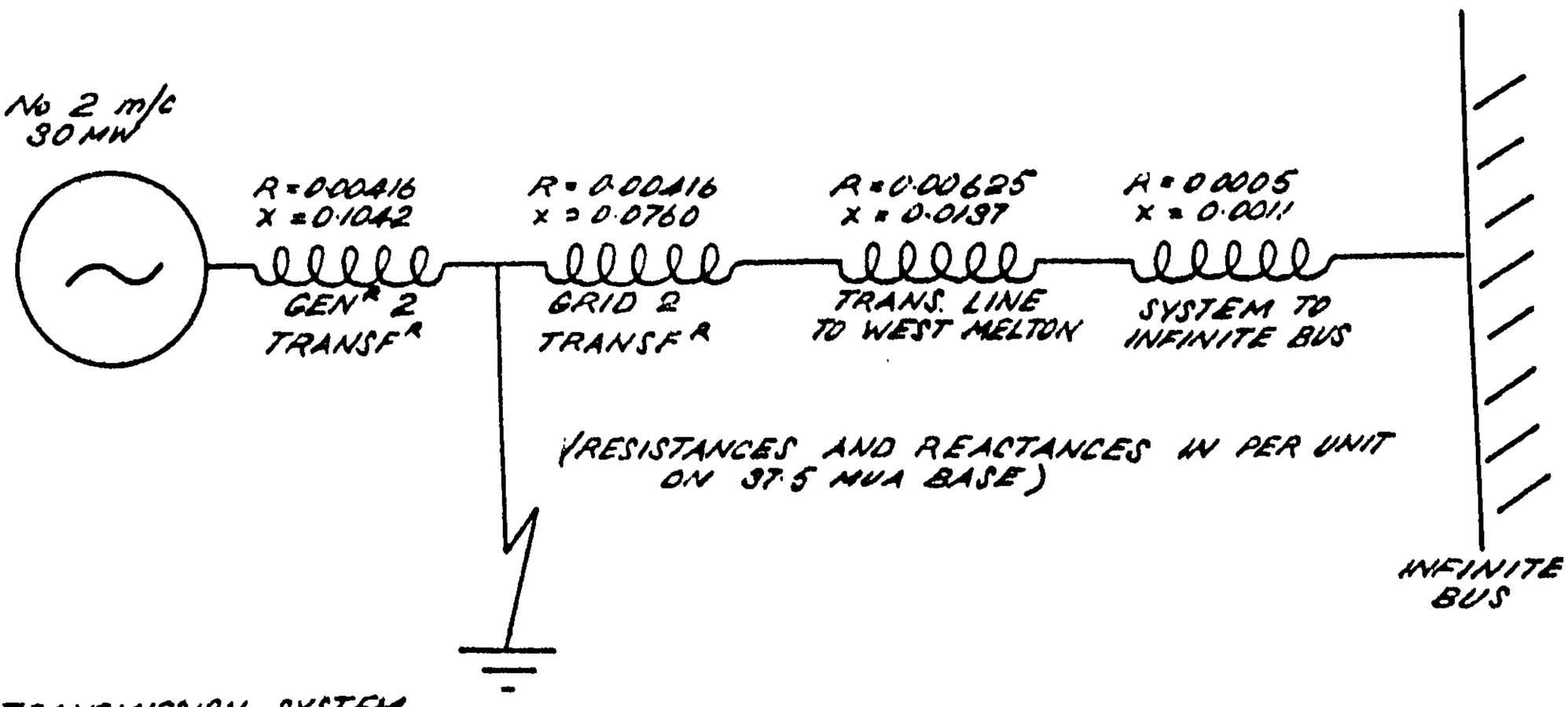

(c) TRANSMISSION SYSTEM

COMPUTER REPRESENTATIONS FOR DONCASTER FAULT TESTS

FIG 9.5

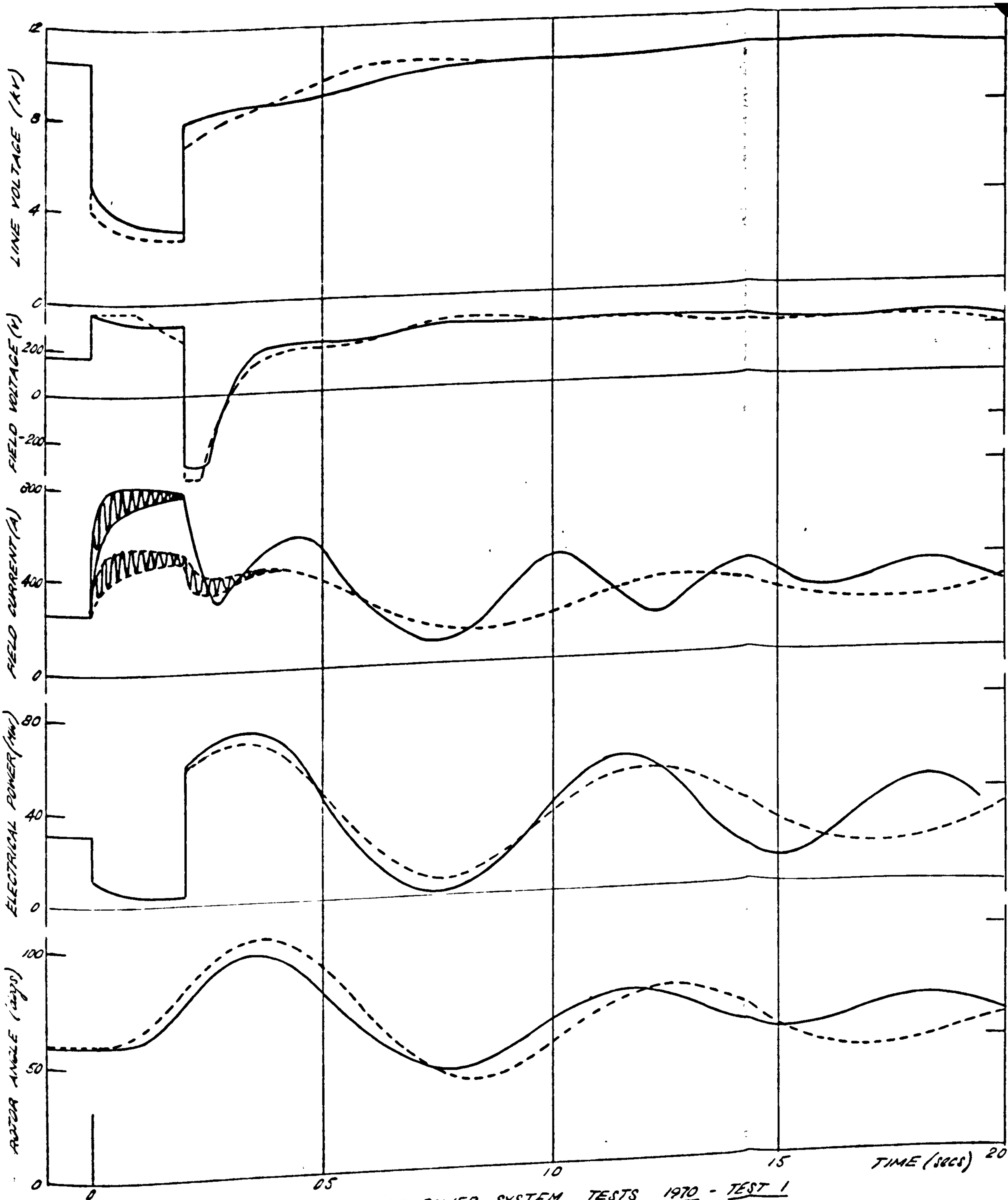

DONCASTER POWER SYSTEM TESTS 1970 - TEST 1

EFFECT OF 3 PHASE FAULT WITH THYRISTOR EXCITATION CONTROL FED FROM CONSTANT VOLTAGE SUPPLY

FIG 9.6

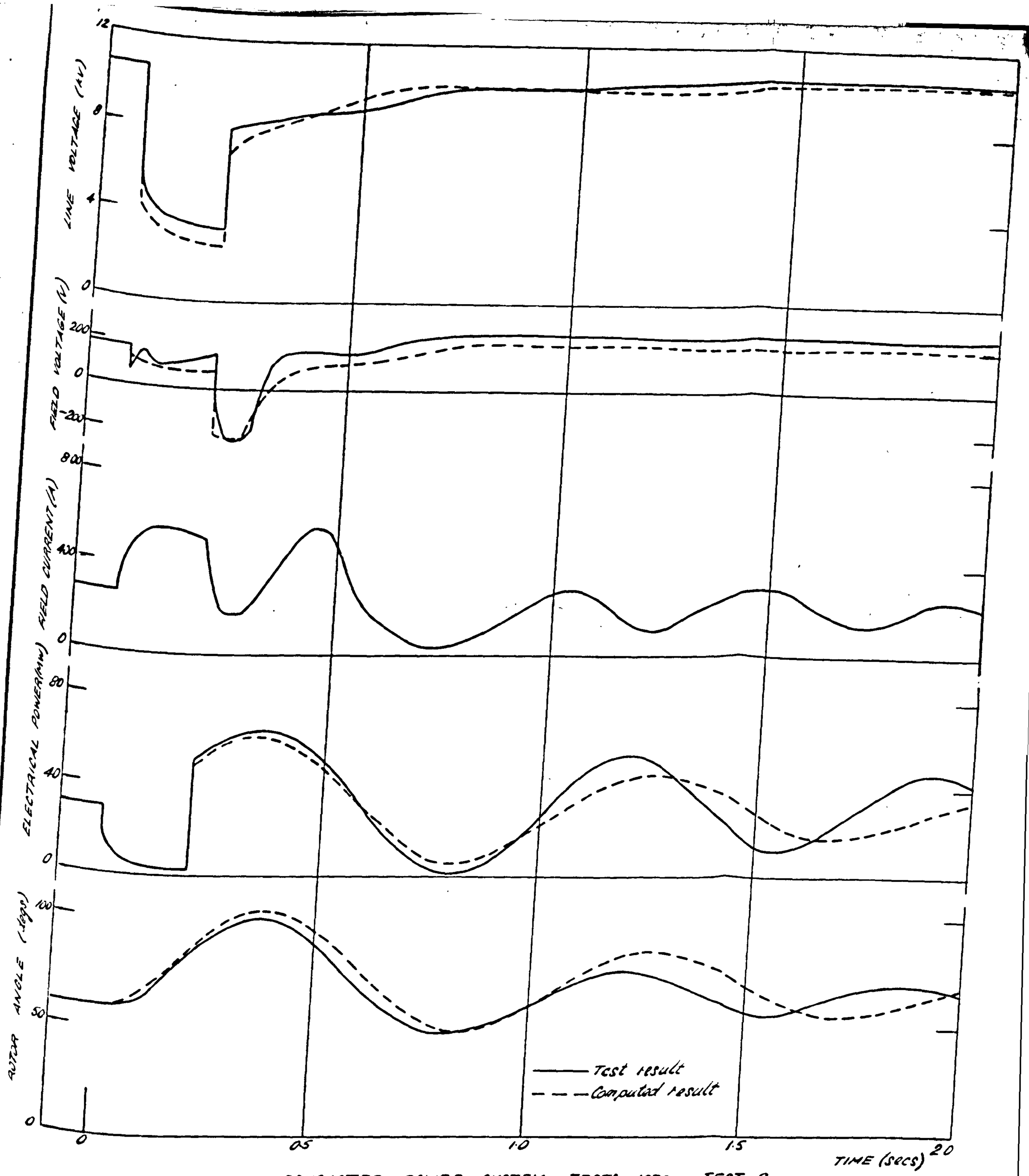

DONCASTER POWER SYSTEM TESTS 1970 - TEST 2

EFFECT OF 3-PHASE FAULT WITH THYRISTOR EXCITATION CONTROL FED FROM MACHINE TERMINALS

FIG 9.7

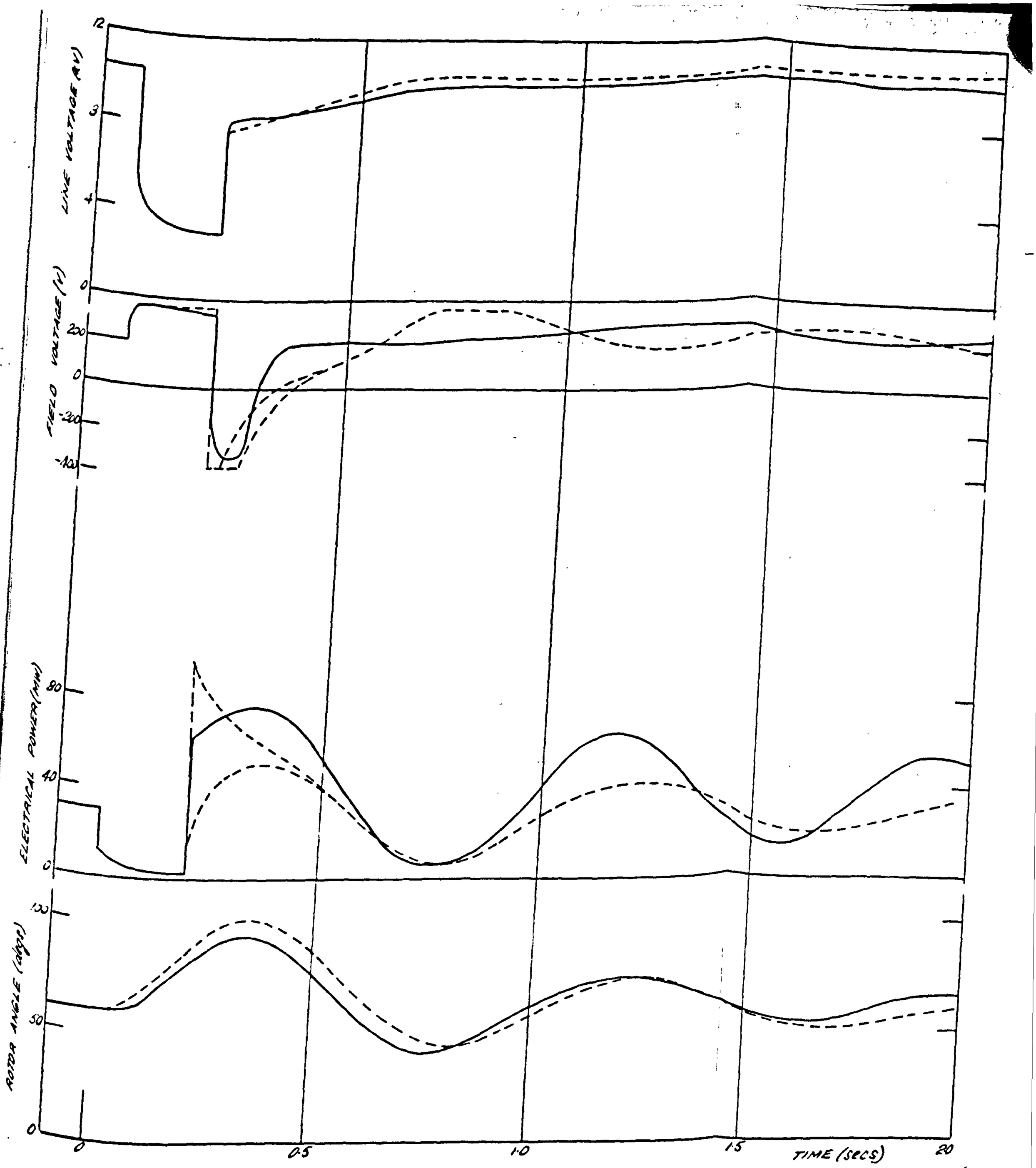

DONCASTER POWER SYSTEM TESTS 1970 - TEST 3

EFFECT OF 3 PHASE FAULT AT LAGGING POWER FACTOR WITH MODERATE ACCELERATION FEEDBACK

FIG 9.8

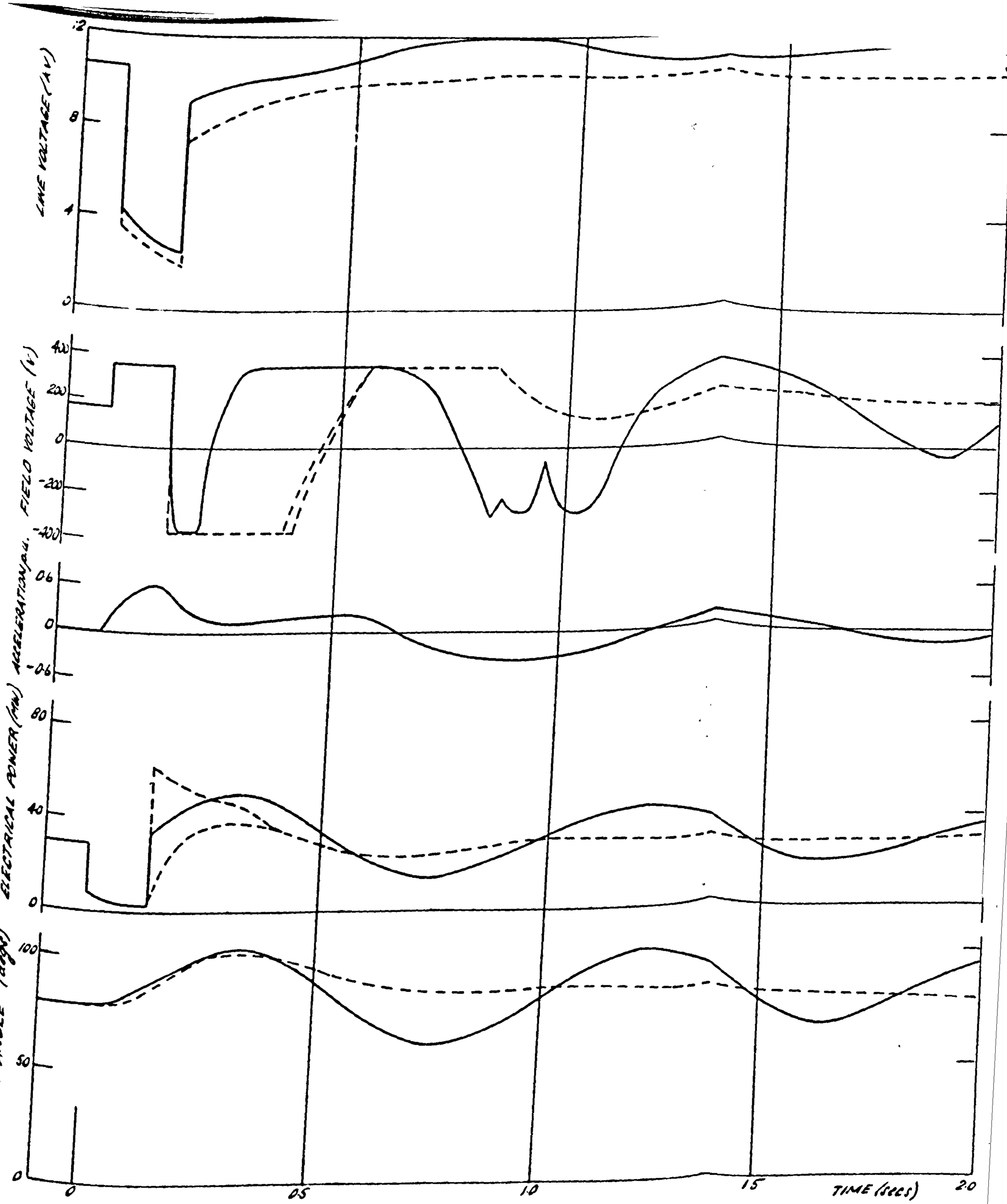

DONCASTER POWER SYSTEM TESTS 1970 TEST 4

EFFECT OF 3 PHASE FAULT AT LEADING POWER FACTOR WITH HIGH ACCELERATION FEEDBACK

EIA 9.9

Substituting equation (9.3) in (9.1) gives

$$E_2 + E_2T_1p = K_1E_1 + \frac{K_2}{T_3}E_3 - \frac{K_2K_3V_T}{T_3} + \left(\frac{K_2T_1E_3}{T_3} - \frac{K_2K_3T_1V_T}{T_3}\right)p$$

$$\therefore \quad \left[E_2 + \frac{K_2K_3}{T_3} - \frac{K_2}{T_3}E_3\right]T_1p = K_1E_1 - E_2 + \frac{K_2}{T_3}E_3 - \frac{K_2K_3V_T}{T_3} \qquad \ldots(9.4)$$

Hence to solve the complete AVR equations, two integrators are required for operation on equations (9.2) and (9.4). The first integrator output I(1) gives values of E_3 and the second integrator output I(2) satisfies the relationship:

$$I(2) = E_2 + \frac{K_2K_3}{T_3} - \frac{K_2}{T_3}E_3$$

$\therefore$ the output of the AVR, E_2, is calculated each step as:

$$E_2 = I(2) + \frac{K_2}{T_3}E_3 - \frac{K_2K_3}{T_3}$$

To this is added the signal from the acceleration stabilising channel E_4 to obtain the final voltage applied to the field, E_{fd}.

Only the output of the thyristor bridge was limited as the AVR amplifiers were operating at very low voltage levels, most of the gain being provided by the thyristor convertor. For test 2 the limits and gain of the thyristor amplifier were modified by the per unit value of terminal voltage to simulate AC supply variations to the convertor when fed from the generator terminals.

For the governor the simple representation of mechanical/hydraulic systems of Chapter 3 was employed. Few details of the actual governor parameters of the Doncaster machine were available and so corresponding values for a similar 30 MW set at Goldington were used (see Fig.9.5).

9.4.2 Results of computer simulations and comparison with tests

The computed results are shown as the dashed curves on Figs.9.6-9.9. Some difficulty was experienced in representing the initial condition settings for the tests (see Table 2). The main causes of the trouble were eventually traced to erroneous values of system reactances, which arose because of unusually low tap numbers on the generator transformer, and in addition, the shunt rating for the measurement of field current was 600 amps instead of the originally assumed value of 500 amps. Problems were also encountered in obtaining the correct conditions using the measured values of MVA and MVAr to

obtain power factor. More compatible results were produced by recycling the power factor to obtain the measured rotor angle setting for each test. From numerous trials at matching the initial conditions, it appeared that the reactive power measurement was in error, which is a probability, since the power factor was near unity and it is common to experience similar difficulties in the measurement of active power at near-zero power factor conditions.

Considering the lack of reliable turbogenerator data and the instrumentation difficulties, the results of the simulation were very encouraging especially for tests 1 and 2 where the performance was not complicated by the acceleration channel. Close simulation of the field and armature voltages for the whole of the transient was obtained in test 1 with good comparisons of the computed and measured power and rotor angle for the first second. The actual field current diverged widely from the computed result in both amplitude and frequency but this was due to errors caused by the small sensitivity of this channel and the results should be disregarded. However the 50 Hz oscillations predicted by the computer programme were distinguishable. In both tests 1 and 2 the predicted rotor angle swings were higher than the test result, whilst the opposite effect was found in the case of the power swings. This is an unlikely situation, and could have been due to the slow response of the rotor angle measuring instrument. The simulation of the field voltage was less accurate in the generator fed thyristor excitation system of test 2, which suggests that the representation may be inadequate. In particular a noticeable transient was produced on the depressed voltage immediately after fault application which was not present on the predictions. This may have originated from the transformer but it is more likely to have been caused by the effect of the depressed voltage on the firing circuitry.

The computed results shown in Figs.9.8 and 9.9 for tests 3 and 4 give the intended performances in the tests assuming correct functioning of the acceleration transducer. In both cases a damping effect should be expected and in test 2 this is almost critical. The effect of the acceleration transducer filtering was to produce a large deterioration of the expected performance causing near undamped oscillations in test 2.

9.5 Summary and conclusions

The foregoing chapter has illustrated various aspects of the planning, performing and computer simulations of large scale tests of turbogenerator transient performance. The suitability of fast thyristor excitation systems

under adverse conditions of system transients has been verified, but the overall purpose of establishing the effectiveness of an acceleration stabilising signal on these systems has not reached a satisfactory conclusion. The fact that this was due to inadequacies in the measuring equipment, leads to the important conclusion that developments in hardware must keep abreast of the theories that require them. It is also essential that all aspects of the instrumentation channels are perfected, as in this case although the electronic equipment functioned perfectly the troubles arose in the transducer that provided the input drive.

Concerning the comparison of the two different thyristor excitation schemes it was found that little deterioration in the transient stability margin was produced by the generator fed system. This leads to a possible explanation that the excitation has a large influence in the period between fault removal and the peak of the first swing where both systems function identically. During longer system depressions however, the exciter fed system should have a marked superiority.

Finally, from the simulations of tests 1 and 2, some confidence can be expressed in the mathematical model developed for the project due to the good comparisons obtained.

10 CONCLUSIONS AND FURTHER WORK

These final conclusions contain a summary of the separate conclusions of the preceeding chapters, together with more general comments on the whole work. Where applicable, any suggestions for future study are discussed with each item rather than left until the end.

The specific conclusion to be drawn from the work is that for the sole purpose of transient performance improvements, the new prime mover control devices, rather than excitation systems, hold the most promise. A large step in the reduction of the practical limitations of previous governor designs has been achieved by the introduction of the electrohydraulically actuated system, opening up the field for new control philosophies. Intense developments in these systems are presently taking place and their incorporation into new plant will increase. Hence future studies of controls for increased transient performance should be directed towards the capabilities of the governor system, which is a reverse of the previous practice in which excitation control has received the most attention. Although with fast thyristor excitation systems it is possible to bring about both substantial electrical and mechanical transient performance improvements, these are not in sympathy and it is best to adhere to a voltage control policy in the excitation. The demands for fast voltage control are probably few but the low cost of the static thyristor system makes it attractive, so that in the future the system may be incorporated in many power networks where neither voltage or stability problems exist. Hence there is a likelihood of dual high speed controls appearing in future systems. From Chapter 7 it was found that this arrangement was perfectly acceptable, the two systems being mutually compatible and the best overall performance was achieved with systems stabilising terms in the governor, and voltage feedbacks in the excitation system.

With the pure analogue control discussed an optimum critically damped response could not be obtained without deteriorating other aspects of the performance. Thus a logical extension of the work would be an investigation of the capabilities of digital control, especially since digital computers are installed in all the new large power stations. Presently these are mainly used for monitoring purposes with only limited control duties, but as speed and reliability aspects are improved then direct digital control of turbogenerators will become a viable proposition.

From Chapter 4 it was found that nearly all the normal parameters of the

generator had some effect on the transient behaviour, and the results of these investigations should be of interest to generator manufacturers. Although in most cases the improvements were small these can often be achieved at little or no extra cost and rather than create entirely new designs, the studies were intended to assist the general trends so that the transient performance capability can be taken into account at the design stage.

Regarding the mathematical modelling of turbogenerators, it was shown in Chapter 2 that the versatility and accuracy of the digital computer makes it an ideal medium for transient response analyses. Computer simulation techniques were developed to a very high accuracy level but unfortunately a serious deficiency exists in compatible parameters for the higher order models. This is seriously limiting the validation of the latest computer models and future research into methods of acquisition of accurate turbogenerator parameters, in particular those of the damping circuits, is of paramount importance. The effects of including stator transients in the computer model were widely illustrated and the author believes that these terms provide a large contribution to the transient behaviour and should not be neglected. This is demonstrated by the rotor angle backswing effect and the production of 50 Hz components in the rotor circuits. However, the energy exchanges that produce backswing and the link between this property and the fundamental frequency components are not fully understood and would benefit from further investigations.

The work reported in Chapters 8 and 9 served to complement the theoretical material of the initial chapters with a practical approach. The effective improvement of transient stability requires a fast dynamical response of both the controlling device and the instrumentation used to obtain the necessary control signals. The development of instrumentation for providing additional stabilising signals has lagged behind the advances in the control areas, and novel instrumentation had to be designed for the Doncaster tests. The development work was commenced in 1967 and was perhaps ambitious, as although excellent performance was obtained from the electronic circuitry, unsatisfactory operation was produced by the machine mounted transducer. This was a direct result of the fast response of the system as the errors would not have been apparent with slow acting instrumentation. The major advances in digital systems now make possible the design of much improved instrumentation, and it is hoped to perform a further set of tests in the near future for which the Doncaster series will be valuable experience.

11 APPENDICES

11.1 Summary of equations of standard computer model for turbogenerator transient behaviour

(a) Differential equations

These are solved by an integration technique.

Electrical:

$$
\begin{array}{|c|}
\hline
p\psi_{fd} \\
p\psi_{kd} \\
p\psi_{kq} \\
pi_d \\
pi_q \\
\hline
\end{array}
=
\begin{array}{|c|}
\hline
\left[-\omega_o \dfrac{R_{fd}}{\chi_{\ell fd}}\left(1-\dfrac{X_1}{\chi_{\ell fd}}\right)\right] \\
\left[\omega_o \dfrac{R_{kd}}{\chi_{\ell kd}} \cdot \dfrac{X_1}{\chi_{\ell kd}}\right] \\
0 \\
-F \\
N\omega \\
\hline
\end{array}
\times
\begin{array}{|c|}
\hline
\left[\omega_o \dfrac{R_{fd}}{\chi_{\ell fd}} \cdot \dfrac{X_1}{\chi_{\ell kd}}\right] \\
\left[-\omega_o \dfrac{R_{kd}}{\chi_{\ell kd}}\left(1-\dfrac{X_1}{\chi_{\ell kd}}\right)\right] \\
0 \\
-E \\
M\omega \\
\hline
\end{array}
$$

$$
\begin{array}{|c|c|c|c|c|c|c|}
\hline
\psi_{fd} & \psi_{kd} & \psi_{kq} & i_d & i_q & V_{fd} & V_b \\
\hline
\end{array}
$$

$$
\times
$$

$$
\begin{array}{|ccccccc|}
\hline
0 & 0 & \left[-\dfrac{R_{kq}}{\chi_{\ell kq}} \cdot \dfrac{X_2}{\chi_{mq}}\right] & G\omega & -L & 0 & 0 \\
0 & 0 & 0 & C & -K\omega & 0 & 0 \\
\left[-\dfrac{R_{fd}}{\chi_{\ell fd}} \cdot X_1\right] & \left[-\dfrac{R_{kd}}{\chi_{\ell kd}} X_1\right] & 0 & -D\omega & -J & 0 & 0 \\
0 & 0 & \left[-\dfrac{R_{kq}}{\chi_{\ell kq}} \cdot X_2\right] & 0 & -B & A\sin\delta & 0 \\
0 & 0 & 0 & 0 & 0 & -I\cos\delta & 0 \\
\hline
\end{array}
$$

$$
+
\begin{array}{|c|}
\hline
\left[\omega_o \dfrac{R_{fd}}{\chi_{\ell fd}} \cdot \dfrac{X_1}{\chi_{\ell kd}}\right] \\
\left[-\omega_o \dfrac{R_{kd}}{\chi_{\ell kd}}\left(1-\dfrac{X_1}{\chi_{\ell kd}}\right)\right] \\
0 \\
-F \\
N\omega \\
\hline
\end{array}
$$

Mechanical:

$$
p\omega = \frac{\omega_o}{2H}\left[T_L - T_i - \omega_o\left(\frac{X_1}{\chi_{\ell fd}}\psi_{fd} + \frac{X_1}{\chi_{\ell kd}} - (X_1+\chi_{\ell d})\frac{i_d}{\omega_o}\right) i_q - \omega_o\left(\frac{X_2}{\chi_{\ell kq}}\psi_{kq} - (X_2+\chi_{\ell q})\frac{i_q}{\omega_o}\right) i_d - k_d\omega\right]
$$

$$
p\delta = \omega
$$

The constants X_1, X_2, A-G, and I-N are defined as follows:

$$X_1 = \frac{X_{md} X_{\ell kd} X_{\ell fd}}{X_{md}X_{\ell kd}+X_{md}X_{\ell fd}+X_{\ell kd}X_{\ell fd}} = X_d'' - X_{\ell d}$$

$$X_2 = \frac{X_{mq} X_{\ell kq}}{X_{mq}+X_{\ell kq}} = X_q'' - X_{\ell q}$$

$$A = \frac{\omega_o}{X_1+X_{\ell d}-X_t}$$

$$B = \frac{\omega_o X_1}{X_{\ell fd}(X_1+X_{\ell d}-X_t)}$$

$$C = \frac{\omega_o}{(X_1+X_{\ell d}-X_t)} \left[R_a+R_t+X_1^2\left(\frac{R_{fd}}{X_{\ell fd}^2}+\frac{R_{kd}}{X_{\ell kd}^2}\right)\right]$$

$$D = \frac{(X_2+X_{\ell q}+X_t)}{(X_1+X_{\ell d}-X_t)}$$

$$E = \frac{X_1^2 \omega_o^2}{X_{\ell fd}X_{\ell kd}(X_1+X_{\ell d}-X_t)} \left[\frac{R_{kd}}{X_{\ell kd}} - \frac{R_{fd}}{X_{\ell fd}} \frac{(X_{md}+X_{\ell kd})}{X_{md}}\right]$$

$$F = \frac{X_1^2 \omega_o^2}{X_{\ell fd}X_{\ell kd}(X_1+X_{\ell d}-X_t)} \left[\frac{R_{fd}}{X_{\ell fd}} - \frac{R_{kd}}{X_{\ell kd}} \frac{(X_{md}+X_{\ell fd})}{X_{md}}\right]$$

$$G = \frac{\omega_o X_2}{X_{\ell kq}(X_1+X_{\ell d}-X_t)}$$

$$I = \frac{\omega_o}{(X_2+X_{\ell q}+X_t)}$$

$$J = \frac{\omega_o}{(X_2+X_{\ell q}+X_t)} \left[R_a+R_t+\frac{X_2^2 R_{kq}}{X_{\ell kq}^2}\right]$$

$$K = \frac{(X_1+X_{\ell d}+X_t)}{(X_2+X_{\ell q}+X_t)}$$

$$L = \frac{X_2^2 \omega_o^2 R_{kq}}{X_{mq} \cdot X_{\ell kq}(X_2+X_{\ell q}+X_t)}$$

$$M = \frac{\omega_o \cdot X_1}{X_{\ell fd} \cdot (X_2+X_{\ell d}+X_t)}$$

$$N = \frac{\omega_o X_1}{X_{\ell kd}(X_2+X_{\ell d}+X_t)}$$

(b) Auxiliary equations (executed after each integration step)

$$\psi_d = \frac{X_1}{X_{\ell fd}}\psi_{fd} + \frac{X_1}{X_{\ell kd}}\cdot\psi_{kd} - (X_1 + X_{\ell d})\frac{i_d}{\omega_o}$$

$$\psi_q = \frac{X_2}{X_{\ell kq}}\psi_{kq} - (X_2 + X_{\ell q})\frac{i_q}{\omega_o}$$

$$p\psi_q = \frac{X_1}{X_{\ell fd}}p\psi_{fd} + \frac{X_1}{X_{\ell kd}}\cdot p\psi_{kd} - (X_1+X_{\ell d})\frac{pi_d}{\omega_o}$$

$$p\psi_q = \frac{X_2}{X_{\ell kq}}\cdot p\psi_{kq} - (X_2 + X_{\ell q})\frac{pi_q}{\omega_o}$$

$$V_d = p\psi_d - R_a\, i_d - \omega\psi_q$$

$$V_q = p\psi_q - R_a\, i_q + \omega\psi_d$$

$$E_{tm} = \sqrt{V_d^2+V_q^2}$$

$$i_{fd} = \frac{\omega_o}{X_{\ell fd}}\left[\left(1 - \frac{X_1}{X_{\ell fd}}\right)\psi_{fd} - \frac{X_1}{X_{\ell kd}}\psi_{kd} + \frac{X_1}{\omega_o}\, i_d\right]$$

$$T_e = \omega_o\,(\psi_d\, i_q - \psi_q\, i_d)$$

$$P = V_d\, i_d + V_q\, i_q$$

$$Q = V_q\, i_d - V_d\, i_q$$

11.2 Digital computer programme for turbogenerator transient performance

The digital computer programme is written in IBM360 Fortran IV language and is built around the equations of Appendix 11.1 and the initial condition equations of Section 2.3.3. The programme statements are stored on magnetic disk, and access and data input is gained via card input. Both tabulated results and a line printer graph plot are available, the latter being for rough assessment only as the accuracy is limited by the printer typset spacing. The Fortran statements are reproduced in the following pages and the flow chart is given in Fig.11.1.

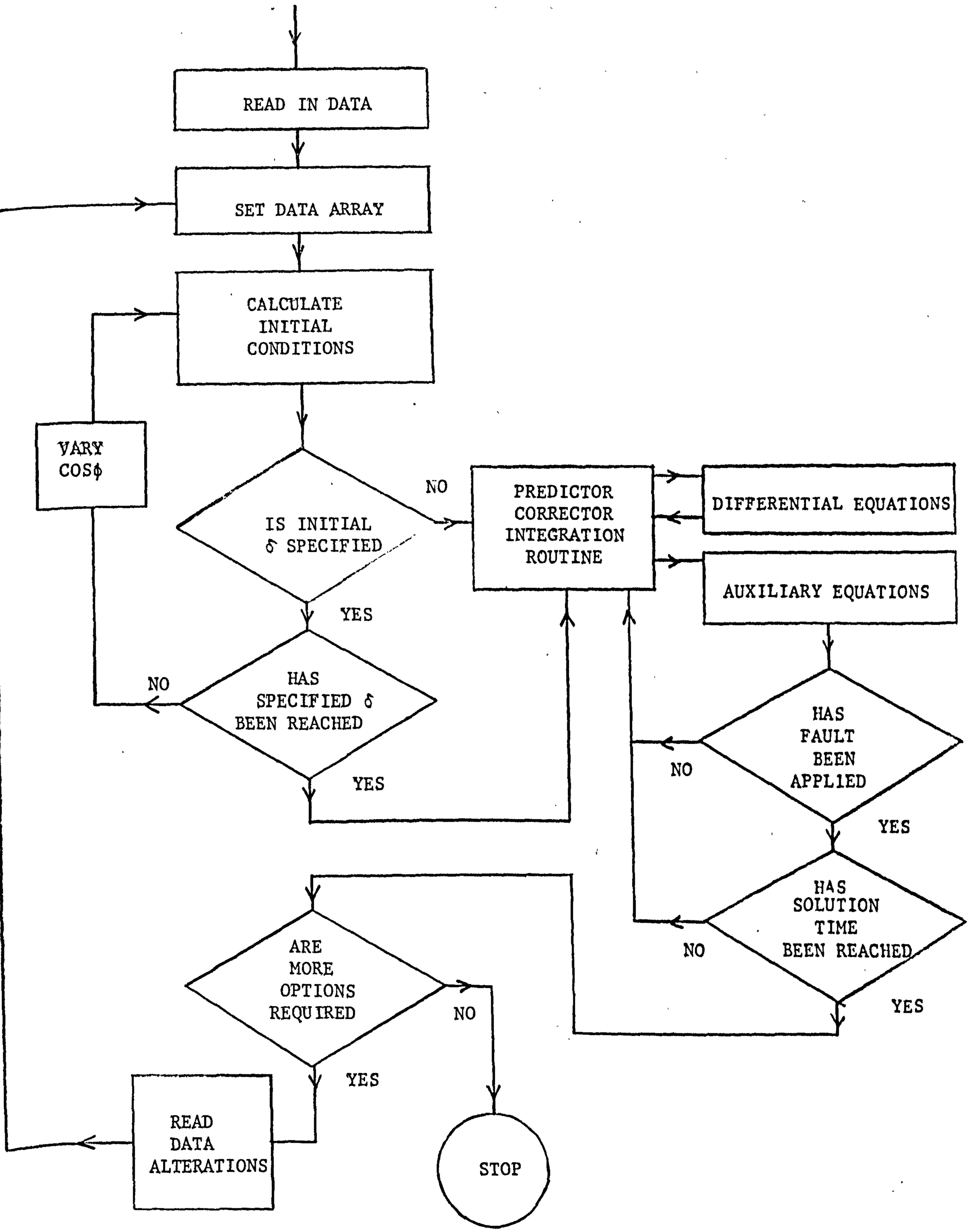

DIGITAL COMPUTER PROGRAMME FLOW CHART

FIG. 11.1

```
      TRANSIENT STABILITY STUDY OF A SINGLE TURBO-GENERATOR
      REPRESENTATION INCLUDES ONE DAMPER COIL IN EACH AXIS
      REAL K1,K2
      REAL ID,IQ,IA,IFD,IQ,LAD,LAFD,LFDD,LAD,IF,IAP,I,L,LP
      EXTERNAL FNA
      EXTERNAL OUTP
      DIMENSION Y(17),DY(17),AUX(16,17),PRM(20),DATA(6,12)
      DIMENSION AA(500),BB(500),CC(500),DD(500),EE(500)
      COMMON A1,A2,A3,A4,A5,A6,WO,W,VFD,PFD,XLD,XLFD,RKD,XKD,RKQ,XKQ,XMQ
     1,A7,A8,RA,PT,X1,VB,TL,TG,H
      COMMON VREF,V1,K1,K2,T1,T2,GV1,GEN,TV1,TEN,TD,TV,TA,E1,DW1,DW2
      COMMON AREF,VR1,VQ,VRLIM,VRLOW,VFDO,VA,GD,GV,GA,GTH,TH1,IQ,IFDO,K,
     1TF,TFC,TREC,TSOL,XTF,XTFC,XTR,RTF,RTFC,RTR,AA,BB,CC,DD,EE,THETA,EF
     2D,IF,VL,AP,WREF1,WREF2,TL1,TL2,TLO,LOGIC,PR,GA1,GA2,TIC,TIO,T2C,T2
     3O,DW1M,DW2M,VG,VI,WT,TSW,TSV,FTT
      CALL ERRDMP
      I=0.
      READ(5,1)(DATA(1,I1),I1=1,12)
      READ(5,2)(DATA(2,I2),I2=1,12)
      READ(5,3)(DATA(3,I3),I3=1,11)
      READ(5,4)(DATA(4,I4),I4=1,12)
      READ(5,5)(DATA(5,I5),I5=1,11)
      READ(5,6)(DATA(6,I6),I6=1,5)
    1 FORMAT(12F6.4)
    2 FORMAT(12F6.4)
    3 FORMAT(11F6.4)
    4 FORMAT(12F6.5)
    5 FORMAT(11F6.5)
    6 FORMAT(5F6.4)
    7 FORMAT(I2)
    8 FORMAT(2I2,F6.4)
  420 FORMAT(1H1,'          TRANSIENT PERFORMANCE OF TURBOGENERATOR
     1WITH HIGH SPEED CONTROLS ')
  421 FORMAT('-------------------------------------------------
     1-------------------------------------------------'//)
   15 FORMAT(6X,'ARMATURE RESISTANCE                    RA = ',F8.5/
     1'          FIELD RESISTANCE                     RFD = ',F8.5/
     2'          DIRECT AXIS MUTUAL REACTANCE         XMD = ',F8.5/
     3'          QUADRATURE AXIS MUTUAL REACTANCE     XMQ = ',F8.5/
     4'          DIRECT AXIS LEAKAGE REACTANCE        XLD = ',F8.5/
     5'          QUADRATURE AXIS LEAKAGE REACTANCE    XLQ = ',F8.5/
     7'          FIELD LEAKAGE REACTANCE             XLFD = ',F8.5/
     8'          DIRECT AXIS DAMPER LEAKAGE REACTANCE XKD = ',F8.5/
     9'          QUAD. AXIS DAMPER LEAKAGE REACTANCE  XKQ = ',F8.5/
     1'          DIRECT AXIS DAMPER RESISTANCE        RKD = ',F8.5/
     2'          QUADRATURE AXIS DAMPER RESISTANCE    RKQ = ',F8.5/
     3'          INERTIA CONSTANT                       H = ',F8.5//)
   16 FORMAT(6X,'TRANSMISSION REACTANCE BEFORE FAULT     X1 = ',F8.5/
     1'          TRANSMISSION REACTANCE DURING FAULT   XTF = ',F8.5/
     2'          TRANSMISSION REACTANCE AFTER FAULT    XTFC = ',F8.5/
     3'          TRANSMISSION REACTANCE AFTER RECLOSE  XTR = ',F8.5/
     4'          TRANSMISSION RESISTANCE BEFORE FAULT   RT = ',F8.5/
     5'          TRANSMISSION RESISTANCE DURING FAULT  RTF = ',F8.5/
     6'          TRANSMISSION RESISTANCE AFTER FAULT   RTFC = ',F8.5/
     7'          TRANSMISSION RESISTANCE AFTER RECLOSE  RTR = ',F8.5//)
   57 FORMAT('          POWER FACTOR                    COS(PHI) = ',F8.5,
     1'   LEADING')
   58 FORMAT('          POWER FACTOR                    COS(PHI) = ',F8.5,
     1'   LAGGING')
   43 FORMAT('          BUS VOLTAGE                          VB = ',F8.5/
     1)
   44 FORMAT('          FAULT ON AT          T = ',F8.5,' SECS'/
     1'          FAULT CLEARED AT T = ',F8.5,' SECS'/
     2'          RECLOSED AT          T = ',F8.5,' SECS'/)
   45 FORMAT('          EXCITATION PARAMETERS                PRIME MOVER
```

```
46 FORMAT(
   1'        GVT = ',F10.5,'
   2'        TVT = ',F10.5,'
   X' ,F10.5/
   3'        GFN = ',F10.5,'
   4'        TFN = ',F10.5,'
   Y' ,F10.5/
   5'         GP = ',F10.5,'
   6'         TP = ',F10.5,'
   7'         GV = ',F10.5,'
   8'         TV = ',F10.5,'
   9'         GA = ',F10.5,'
   1'         TA = ',F10.5/
   2'        GTH = ',F10.5,'
   3'      VLIM = ',F10.5,'
   4'      VLOW = ',F10.5/)
```

```
                  K1 = ',F10.5/
                  T1 = ',F10.5,',

                  K2 = ',F10.5/
                  T2 = ',F10.5,',

HP DROOP = ',F10.5/
LP DROOP = ',F10.5/
    AREF = ',F10.5/
     GA1 = ',F10.5/
     GA2 = ',F10.5/

     TSW = ',F10.5/
     TSV = ',F10.5/
```

```
406 FORMAT(1H1,'  TIME      ROTOR     FIELD    FIELD    LINE      PHASE
   1  MW        MVAR        SPEED     ACCN     GOV.      INT.    MECH. ')
407 FORMAT('  SECS      ANGLE     VOLTS     AMPS  K.VOLTS   K.AMPS
   1                  RAD/S   RAD/S/S    VALVE    VALVE   TORQUE ')
502 I=I+1.
    RA    =DATA(1,1)
    RFD   =DATA(1,2)
    XMD   =DATA(1,3)
    XMQ   =DATA(1,4)
    XLD   =DATA(1,5)
    XLQ   =DATA(1,6)
    XLFD  =DATA(1,7)
    XKD   =DATA(1,8)
    XKQ   =DATA(1,9)
    RKD   =DATA(1,10)
    RKQ   =DATA(1,11)
    H     =DATA(1,12)
    XT    =DATA(2,1)
    RT    =DATA(2,2)
    XTF   =DATA(2,3)
    RTF   =DATA(2,4)
    XTR   =DATA(2,5)
    RTR   =DATA(2,6)
    TF    =DATA(2,7)
    TREC  =DATA(2,8)
    TSOL  =DATA(2,9)
    TFC   =DATA(2,10)
    RTFC  =DATA(2,11)
    XTFC  =DATA(2,12)
    VA    =DATA(3,1)
    VL    =DATA(3,2)
    OPS   =DATA(3,3)
    AFS   =DATA(3,4)
    WA    =DATA(3,5)
    AREF  =DATA(3,6)
    FIM   =DATA(3,7)
    PE    =DATA(3,8)
    PF    =DATA(3,9)
    DTHETA=DATA(3,10)
    HS    =DATA(3,11)
    PC1   =DATA(4,1)
    PC2   =DATA(4,2)
    GV1   =DATA(4,3)
    GFN   =DATA(4,4)
    GTH   =DATA(4,5)
    GD    =DATA(4,6)
    GV    =DATA(4,7)
    GA    =DATA(4,8)
    VRLIM =DATA(4,9)
```

```
      GA1    =DATA(4,11)
      GA2    =DATA(4,12)
      T1C    =DATA(5,1)
      T2C    =DATA(5,2)
      TVT    =DATA(5,3)
      TFN    =DATA(5,4)
      TD     =DATA(5,5)
      TV     =DATA(5,6)
      TA     =DATA(5,7)
      T1D    =DATA(5,8)
      T2D    =DATA(5,9)
      TSW    =DATA(5,10)
      TSV    =DATA(5,11)
      L      =DATA(6,1)
      LP     =DATA(6,2)
      WRST   =DATA(6,3)
      PRST   =DATA(6,4)
      DEG    =DATA(6,5)
      BASE VOLT-AMPERES
      VAO=VA*1000000.
      BASE STATOR VOLTAGE VO =PEAK PHASE VOLTS
      VO=VL*SQRT(0.666)
      BASE STATOR CURRENT IO =PEAK PHASE CURRENT AMPS
      IO=VAO/VO*2./3.
      WO=2.*3.142*CPS
      BASE INDUCTANCE LAO HENRIES
      LAO=VO/(WO*IO)
      AFS=FIELD CURRENT TO GIVE RATED D/C VOLTS ON AIR GAP LINE
      LAFO=VO/(WO*AFS)
      LAO=XMD*LAO
      BASE FIELD CURRENT IFDO AMPS
      IFDO=LAO*IO/LAFO
      BASE FIELD VOLTAGE VFDO VOLTS
      VFDO=VO*IO/IFDO*1.5
      INITIAL CONDITION SETTING
      XD=XMD+XL0
      XQ=XMQ+XL0
      RTHET=3.14159*DTHET/180.
   34 PY=ATAN(SQRT((1-PF*PF)/(PF*PF)))
      GO TO 38
   39 PY=-ATAN(SQRT((1-PF*PF)/(PF*PF)))
   38 IA=PF/(PF*FTM)
      A=FTM+IA*RA*COS(PY)+IA*XQ*SIN(PY)
      B=IA*XQ*COS(PY)-IA*RA*SIN(PY)
      C=FTM-IA*R1*COS(PY)-IA*X1*SIN(PY)
      D=IA*X1*COS(PY)-IA*R1*SIN(PY)
      FDASH=SQRT(A*A+B*B)
      DEL=ATAN(B/A)
      IF(DEL)200,201,201
  200 DEL=3.141592+DEL
  201 CONTINUE
      FF=FDASH+IA*(XD-XQ)*COS(3.142/2.-PY-DEL)
      VR=SQRT(C*C+D*D)
      SIG=ATAN(D/C)
      DELTA=DEL+SIG
      IF(IP)32,32,130
  130 CONTINUE
      BJ=100.*RTHET/DELTA
      J=IFIX(BJ)
      IF(100-J)71,32,72
   71 IF(PY)33,33,31
   31 PF=1.01*PF
      IF(PF-1.)34,80,80
   80 PF=1.
      GO TO 39
```

```
      IF(PF-1.)39,81,81
81    PF=1.
      GO TO 34
72    IF(FY)73.73,74
74    PF=0.99*PF
      IF(PF-1.)34,80,80
73    PF=1.01*PF
      IF(PF-1.)39,81,81
42    THETA=180.*DELTA/3.14159
      WRITE(6,420)
      WRITE(6,421)
      WRITE(6,15)RA,RFD,XMD,XMQ,XLD,XLQ,XLFD,XKD,XKQ,RKD,RKQ,H
      WRITE(6,16)X1,XTF,XTFC,XTK,R1,RTF,RTFC,PTP
      IF(FY)55,55,56
55    WRITE(6,57)PF
      GO TO 90
56    WRITE(6,58)PF
90    CONTINUE
      IFD=EF/XMD
      K1=1./(PC1*WO)
      K2=1./(PC2*WO)
      WRITE(6,43)VB
      WRITE(6,44)TF,TFC,TREC
      WRITE(6,45)
      WRITE(6,46)GV1,K1,TVT,TLC,TLO,GEN,K2,TEN,T2C,T2O,GD,PC1,TD,PC1.GV,
     1ARMF,TV,GA1,GA,GA2,TA,GTH,TSW,VRLTM,TSV,VRLOW
      WRITE(6,406)
      WRITE(6,407)
      A1=(XMD*XKD)/(XMD*(XLFD+XKD)+XLFD*XKD)
      A2=(XMD*XLFD)/(XMD*(XLFD+XKD)+XLFD*XKD)
      A3=(XMD*XLFD*XKD)/(XMD*(XLFD+XKD)+XLFD*XKD)+XLD
      A4=XMQ/(XMQ+XKQ)
      A5=(XMQ*XMQ/(XMQ+XKQ)-(XMQ+XLQ))
      A6=(A1*A2*RKD/XKD-A1*RFD*(1-A1)/XLFD)
      A7=(A1*A2*RFD/XLFD-A2*RKD*(1-A2)/XKD)
      A8=(A1*RFD*(A3-XLD)/XLFD+A2*RKD*(A3-XLD)/XKD)
      TD=TA*SIN(DEL+FY)
      TQ=TA*COS(DEL+FY)
      VFD=EFD*PFD
      W=WO
      Y(7)=DELTA
      Y(5)=TQ
      Y(4)=TD
      VB1=VB
      Y(1)=((XMD+XLFD)*IFD-XMD*Y(4))/WO
      Y(2)=(XMD*IFD-XMD*Y(4))/WO
      Y(3)=(-XMQ*Y(5))/WO
      Y(6)=0.
      Y(12)=0.0
      Y(14)=0.0
      Y(15)=0.0
      WT=0.0
      PHID=A1*Y(1)+A2*Y(2)-A3*Y(4)/WO
      PHIQ=A4*Y(3)+A5*Y(5)/WO
      TG=(PHID*Y(5)-PHIQ*Y(4))*WO
      TL=TG
      TFL=WA/VA
      TLO=TL
      TL1=.3*TL
      TL2=.7*TL
      T1=T1C
      T2=T2C
      PH=TH
      Y(13)=TH
      Y(8)=TH0/TH
```

```
      Y(16)=PB*Y(8)
      Y(17)=Y(13)*Y(9)
      DW1=Y(8)/K1
      DW2=Y(9)/K2
      DW1M=DW1
      DW2M=DW2
      VG=Y(8)
      VJ=Y(9)
      WREF1=DW1+Y(14)
      WREF2=DW2+Y(14)
      LOGIC=1
      VT=EIM*VQ
      EFD=VFD*VFDO
      ACCN=0.
      E2=EFD/GTH
      E1=E2/GEN
      Y(11)=TEN*E2-TSV*GEN*E1
      EI1=E2
      Y(10)=GVI*VT
      VREF=E1+Y(10)
      VD=EIM*SIN(DEL)
      VQ=EIM*COS(DEL)
      PRMT(1)=0.
      PRMT(2)=TSOL
      PRMT(3)=.001
      PRMT(4)=.05
      PRMT(5)=0.
      PRMT(6)=WRST
      PRMT(7)=0.
       PRMT(8)=PRST
      PRMT(9)=0.
      N=DEQ
      DO 26 II=1,N
      DY(II)=0.
   26 CONTINUE
      DY(7)=1.
      T=0.
      K=0
      CALL  RPCG(PRMT,Y,DY,N,IHLF,FNA,OUTP,AUX)
      CALL  PLOTLX(AA,BB,K,1)
      IF(N-7)340,340,341
  341 CALL  PLOTLX(AA,CC,K,2)
  340 CALL  PLOTLX(AA,DD,K,3)
      CALL  PLOTLX(AA,EE,K,4)
      IF(I-L)500,28,28
  500 READ(5,7)JD
      DO 501 II=1,JD
      READ(5,8)NY,NX,VALUE
  501 DATA(NY,NX)=VALUE
      GO TO 502
   28 STOP
      END
```

```
SUBROUTINE FNA(T,Y,DY)
REAL K1,K2
DIMENSION Y(17),DY(17)
DIMENSION AA(500),BB(500),CC(500),DD(
COMMON A1,A2,A3,A4,A5,A6,WD,W,VFD,RHO
1,A7,A8,KA,R1,XT,VK,FL,TG,H
COMMON VREF,VT,K1,K2,T1,T2,GV1,GFN,TV
COMMON AREF,VR1,VD,VRLIM,VKLIM,VFDD,V
1TF,IFC,IDFC,TSOL,XTF,XTFC,XTK,KTF,KTF
2D,IF,VL,AP,WREFJ,WRFF2,TL1,TL2,TL3,TD
3D,DW1M,DW2M,VG,VI,WT,TSW,TSV,FTT
DY(1)=VFD-RFD*(WD*(1-A1)*Y(1)-WD*A2*Y
DY(2)=-KKD*(WD*(1-A2)*Y(2)-W1*A1*Y(1)
DY(3)=-KKO*(WD*Y(3)+XMO*Y(5))/(XMO+XK
DY(4)=W1*(A1*VFD-VK*SIN(Y(7))+WD*A6*Y
1-W*A4*Y(3)-W*(A5-XT)*Y(5)/W1)/(XTF+A3
DY(5)=W1*(W*A1*Y(1)+W*A2*Y(2)-WD*A4*Y
1XMO*KKO)/(XMO+XKO))*Y(5)-VK*COS(Y(7)
DY(6)=(TI-TG)*WD/(2.*H)
DY(7)=Y(6)
DY(8)=(K1*DW1-Y(8))/T1
DY(9)=(K2*DW2-Y(9))/T2
DY(10)=((VT*VT-Y(10))/TV1
DY(11)=GFN*F1-FTT
DY(12)=(TL-TG-Y(12))/TD
DY(13)=(Y(16)*FFL/TLO-Y(13))/7.
DY(14)=Y(6)-WT
DY(15)=(DY(6)-Y(15))/TA
DY(16)=(VG*PR-Y(16))/.13
DY(17)=(VI*Y(13)-Y(17))/.4
RETURN
END
```

```
      SUBROUTINE OUTP(T,Y,DY,IHLF,N,PRMT)
      REAL K1,K2
      REAL IFD,IA,IAP,ID,IF,IFDD
      DIMENSION Y(1),DY(1),PRMT(1)
      DIMENSION AA(500),BB(500),CC(500),DD(500),EE(500)
      COMMON A1,A2,A3,A4,A5,A6,WD,W,VFD,RFD,XLD,XLFD,RKD,XKD,RKQ,XKQ,XMQ
     1,A7,A8,RA,RT,XT,VR,TL,TG,H
      COMMON VREF,VT,K1,K2,T1,T2,GV1,GFN,TV1,TFN,TD,TV,TA,F1,DW1,DW2
      COMMON AREF,VR1,VQ,VRLIM,VRLOW,VFDD,VA,GD,GV,GA,GTH,TFL,TQ,IFDD,K,
     1TF,TFC,TREC,TSOL,XTF,XTFC,XTR,RTF,RTFC,RTR,AA,BB,CC,DD,EE,THETA,FF
     2D,IF,VL,AP,WREF1,WREF2,TL1,TL2,TLQ,LOGIC,PB,GA1,GA2,T1C,T1Q,T2C,T2
     3Q,DW1M,DW2M,VG,VI,WT,TSW,TSV,F11
408   FORMAT(1X,F6.3,3X,F6.2,3X,F6.1,3X,F7.1,2X,F5.2,4X,F5.2,4X,F6.1,3X
     1,F6.1,4X,F5.1,4X,F5.1,3X,F5.2,3X,F5.2,3X,F5.3,3X,F5.3)
      PHID=A1*Y(1)+A2*Y(2)-A3*Y(4)/WD
      PHIQ=A4*Y(3)+A5*Y(5)/WD
      IFD=(WD*(Y(1)-PHID)-XLD*Y(4))/XLFD
      TG=(PHID*Y(5)-PHIQ*Y(4))*WD
      W=WQ+Y(6)
      ACCN=DY(6)
      PPHIQ=A4*DY(3)+A5*DY(5)/WD
      PPHID=A1*DY(1)+A2*DY(2)-A3*DY(4)/WD
      VQ=PPHIQ+W*PHID-RA*Y(5)
      VD=PPHID-W*PHIQ-RA*Y(4)
      EFM=SQRT(VQ*VQ+VD*VD)
      VT=EFM*VQ
      IF(LOGIC-0)1,1,2
    1 IF(W-WQ)3,3,4
    2 IF(Y(15)-AREF)4,4,5
    5 LOGIC=0
      GOTO 4
    3 LOGIC=1
    4 CONTINUE
      WT=(Y(14)+TSW*Y(6))/TV
      DW1=WREF1-W1-GA1*Y(15)
      DW2=WREF2-WT-GA2*Y(15)
      IF(DW1-DW1M)10,10,11
   10 T1=T1C
      GO TO 14
   11 T1=T1Q
   14 IF(DW2-DW2M)12,12,13
   12 T2=T2C
      GO TO 15
   13 T2=T2Q
   15 DW1M=DW1
      DW2M=DW2
      IF(DW1-1.582/K1)36,36,37
   37 DW1=1.582/K1
   36 IF(DW1+1.582/K1)38,38,39
   38 DW1=-1.582/K1
   39 IF(DW2-1.582/K2)16,16,17
   17 DW2=1.582/K2
   16 IF(DW2+1.582/K2)18,18,19
   18 DW2=-1.582/K2
   19 CONTINUE
      IF(Y(8))6,6,7
    7 IF(Y(8)-1.)8,9,9
    8 VG=Y(8)
      GO TO 100
    9 VG=1.
      GO TO 100
    6 VG=0.
  100 IF(Y(9))46,46,47
   47 IF(Y(9)-1.)48,49,49
   48 VI=Y(9)
```

```
 47 VI=1.
    GO TO 101
 46 VI=0.
101 CONTINUE
    TL1=.3*Y(16)
    TL2=.7*Y(17)
    IF(TL1-.3*TFL)114,114,115
115 TL1=.3*TFL
114 IF(TL1-0.)116,117,117
116 TL1=0.
117 IF(TL2-.7*TFL)118,118,119
119 TL2=.7*TFL
118 IF(TL2-0.)120,121,121
120 TL2=0.
121 TL=TL1+TL2
    FI=VFFI-Y(10)
    FR=GD*Y(12)+GV*Y(14)+GA*Y(15)
    FTT=(Y(11)+1.5V*GFN*FI)/TFN
    F2=FTT+FR
    FFD=GTH*F2
    IF(LOGIC)111,111,122
122 CONTINUE
    IF(FFD-VRLIM)110,110,111
111 FFD=VRLIM
110 IF(FFD-VRLOW)112,113,113
112 FFD=VRLOW
113 CONTINUE
    VFD=FFD/VFDO
    IA=SQRT(Y(4)**2+Y(5)**2)
    DELTA=Y(7)
    THETA=DELTA*180./3.14592
    PF=VD*Y(4)+VQ*Y(5)
    QI=VQ*Y(4)-VD*Y(5)
    RP=QI*VA
    AP=PF*VA
    IAP=IA*10/(SQRT(2.)*1000.)
    VL=VT*SQRT(1.5)/1000.
    IF=IFD*IFDO
    IF(T-PRMT(9))50,40,40
 40 K=K+1
    AA(K)=T
    BB(K)=THETA
    CC(K)=FFD
    DD(K)=IF
    EE(K)=VL
    PRMT(9)=PRMT(9)+PRMT(8)
 50 IF(T-PRMT(7))45,30,30
 30 WRITE(6,408)T,THETA,FFD,IF,VL,IAP,AP,RP,Y(6),ACCN,VG,VI,TL
    PRMT(7)=PRMT(7)+PRMT(6)
 45 IF(T-TF)20,21,21
 20 CONTINUE
    GO TO 29
 21 IF(T-TFC)22,23,23
 22 XT=XTF
    RT=RTF
    VB=0.
    GO TO 29
 23 IF(T-TRFC)24,25,25
 24 XT=XTFC
    VB=VB1
    RT=RTFC
    GO TO 29
 25 IF(T-TSOL)26,27,27
 26 XT=XTR
    RT=RTR
```

```
77 PRINT(5)=1 •
79 RETURN
   END
```

```
      SUBROUTINE HPCG(PRMT,Y,DERY,NDIM,IHLF,FCT,OUTP,AUX)
      DIMENSION PRMT(1),Y(1),DERY(1),AUX(16,1)
      N=1
      IHLF=0
      X=PRMT(1)
      H=PRMT(3)
      PRMT(5)=0.
      DO 1 I=1,NDIM
      AUX(16,I)=0.
      AUX(15,I)=DERY(I)
    1 AUX(1,I)=Y(I)
      IF(H*(PRMT(2)-X))3,2,4
    2 IHLF=12
      GOTO 4
    3 IHLF=13
    4 CALL FCT(X,Y,DERY)
      CALL OUTP(X,Y,DERY,IHLF,NDIM,PRMT)
      IF(PRMT(5))6,5,6
    5 IF(IHLF)7,7,6
    6 RETURN
    7 DO 8 I=1,NDIM
    8 AUX(8,I)=DERY(I)
      ISW=1
      GOTO 100
    9 X=X+H
      DO 10 I=1,NDIM
   10 AUX(2,I)=Y(I)
   11 IHLF=IHLF+1
      X=X-H
      DO 12 I=1,NDIM
   12 AUX(4,I)=AUX(2,I)
      H=.5*H
      N=1
      ISW=2
      GOTO 100
   13 X=X+H
      CALL FCT(X,Y,DERY)
      N=2
      DO 14 I=1,NDIM
      AUX(2,I)=Y(I)
   14 AUX(9,I)=DERY(I)
      ISW=3
      GOTO 100
   15 DELT=0.
      DO 16 I=1,NDIM
   16 DELT=DELT+AUX(15,I)*ABS(Y(I)-AUX(4,I))
      DELT=.0666667*DELT
      IF(DELT-PRMT(4))19,19,17
   17 IF(IHLF-10)11,18,18
   18 IHLF=11
      X=X+H
      GOTO 4
   19 X=X+H
      CALL FCT(X,Y,DERY)
      DO 20 I=1,NDIM
      AUX(3,I)=Y(I)
   20 AUX(10,I)=DERY(I)
      N=3
      ISW=4
      GOTO 100
   21 N=1
      X=X+H
      CALL FCT(X,Y,DERY)
      X=PRMT(1)
```

```
      AUX(11,I)=DERY(I)
220   Y(I)=AUX(1,I)+H*(.375*AUX(8,I)+.7916667*AUX(9,I)
     1-.2083333*AUX(10,I)+.0416667*DERY(I))
23    X=X+H
      N=N+1
      CALL FCT(X,Y,DERY)
      CALL OUTP(X,Y,DERY,IHLF,NDIM,PRMT)
      IF(PRMT(5))6,24,6
24    IF(N-4)25,200,200
25    DO 26 I=1,NDIM
      AUX(N,I)=Y(I)
26    AUX(N+7,I)=DERY(I)
      IF(N-3)27,29,200
27    DO 28 I=1,NDIM
      DELT=AUX(9,I)+AUX(9,I)
      DELT=DELT+DELT
28    Y(I)=AUX(1,I)+.3333333*H*(AUX(8,I)+DELT+AUX(10,I))
      GOTO 23
29    DO 30 I=1,NDIM
      DELT=AUX(9,I)+AUX(10,I)
      DELT=DELT+DELT+DELT
30    Y(I)=AUX(1,I)+.375*H*(AUX(8,I)+DELT+AUX(11,I))
      GOTO 23
100   DO 101 I=1,NDIM
      Z=H*AUX(N+7,I)
      AUX(5,I)=Z
101   Y(I)=AUX(N,I)+.4*Z
      Z=X+.4*H
      CALL FCT(Z,Y,DERY)
      DO 102 I=1,NDIM
      Z=H*DERY(I)
      AUX(6,I)=Z
102   Y(I)=AUX(N,I)+.2969776*AUX(5,I)+.1587596*Z
      Z=X+.4557372*H
      CALL FCT(Z,Y,DERY)
      DO 103 I=1,NDIM
      Z=H*DERY(I)
      AUX(7,I)=Z
103   Y(I)=AUX(N,I)+.2181004*AUX(5,I)-3.050965*AUX(6,I)+3.832865*Z
      Z=X+H
      CALL FCT(Z,Y,DERY)
      DO 104 I=1,NDIM
1040  Y(I)=AUX(N,I)+.1747603*AUX(5,I)-.5514807*AUX(6,I)
     1+1.205536*AUX(7,I)+.1711848*H*DERY(I)
      GOTO(9,13,15,21),ISW
200   ISTEP=3
201   IF(N-8)204,202,204
202   DO 203 N=2,7
      DO 203 I=1,NDIM
      AUX(N-1,I)=AUX(N,I)
203   AUX(N+6,I)=AUX(N+7,I)
      N=7
204   N=N+1
      DO 205 I=1,NDIM
      AUX(N-1,I)=Y(I)
205   AUX(N+6,I)=DERY(I)
      X=X+H
206   ISTEP=ISTEP+1
      DO 207 I=1,NDIM
      DELT=AUX(N-4,I)+1.333333*H*(AUX(N+6,I)+AUX(N+6,I)-AUX(N+5,I)+
     1AUX(N+4,I)+AUX(N+4,I))
      Y(I)=DELT-.9256198*AUX(16,I)
207   AUX(16,I)=DELT
      CALL FCT(X,Y,DERY)
      DO 208 I=1,NDIM
```

```
     1AUX(N+6,I)-AUX(N+5,I)))
      AUX(16,I)=AUX(16,I)-DELT
208   Y(I)=DELT+.0743801?*AUX(16,I)
      DELT=0.
      DO 209  I=1,NDIM
209   DELT=DELT+AUX(15,I)*ABS(AUX(16,I))
      IF(DELT-PRMT(4))210,222,222
210   CALL FCT(X,Y,DERY)
      CALL OUTP(X,Y,DERY,IHLF,NDIM,PRMT)
      IF(PRMT(5))212,211,212
211   IF(IHLF-11)213,212,212
212   RETURN
213   IF(H*(X-PRMT(2)))214,212,212
214   IF(ABS(X-PRMT(2))-.1*ABS(H))212,215,215
215   IF(DELT-.02*PRMT(4))216,216,201
216   IF(IHLF)201,201,217
217   IF(N-7)201,218,218
218   IF(ISTEP-4)201,219,219
219   IMOD=ISTEP/2
      IF(ISTEP-IMOD-IMOD)201,220,201
220   H=H+H
      IHLF=IHLF-1
      ISTEP=0
      DO 221  I=1,NDIM
      AUX(N-1,I)=AUX(N-2,I)
      AUX(N-2,I)=AUX(N-4,I)
      AUX(N-3,I)=AUX(N-6,I)
      AUX(N+6,I)=AUX(N+5,I)
      AUX(N+5,I)=AUX(N+3,I)
      AUX(N+4,I)=AUX(N+1,I)
      DELT=AUX(N+6,I)+AUX(N+5,I)
      DELT=DELT+DELT+DELT
2210  AUX(16,I)=8.962963*(Y(I)-AUX(N-3,I))-3.361111*H*(DERY(I)+DELT
     1+AUX(N+4,I))
      GOTO 201
222   IHLF=IHLF+1
      IF(IHLF-10)223,223,210
223   H=.5*H
      ISTEP=0
      DO 224  I=1,NDIM
     0Y(I)=.00390625*(80.*AUX(N-1,I)+135.*AUX(N-2,I)+40.*AUX(N-3,I)+
     1AUX(N-4,I))-.1171875*(AUX(N+6,I)-6.*AUX(N+5,I)-AUX(N+4,I))*H
     0AUX(N-4,I)=.00390625*(12.*AUX(N-1,I)+135.*AUX(N-2,I)+
     1108.*AUX(N-3,I)+AUX(N-4,I))-.0234375*(AUX(N+6,I)+18.*AUX(N+5,I)-
     29.*AUX(N+4,I))*H
      AUX(N-3,I)=AUX(N-2,I)
224   AUX(N+4,I)=AUX(N+5,I)
      X=X-H
      DELT=X-(H+H)
      CALL FCT(DELT,Y,DERY)
      DO 225  I=1,NDIM
      AUX(N-2,I)=Y(I)
      AUX(N+5,I)=DERY(I)
225   Y(I)=AUX(N-4,I)
      DELT=DELT-(H+H)
      CALL FCT(DELT,Y,DERY)
      DO 226  I=1,NDIM
      DELT=AUX(N+5,I)+AUX(N+4,I)
      DELT=DELT+DELT+DELT
     0AUX(16,I)=8.962963*(AUX(N-1,I)-Y(I))-3.361111*H*(AUX(N+6,I)+DELT
     1+DERY(I))
226   AUX(N+3,I)=DERY(I)
      GOTO 206
      END
```

```
      SUBROUTINE PLOTLX(X,Y,N,NO)
      DIMENSION IOUT(101),YPR(11),X(1),Y(1)
    8 FORMAT(1H1,60X,' GRAPH NO ',I3,//)
   11 FORMAT(1H ,16X,10(1H.          I          I          I          I
     1    I          I          I          I          I          I))
   10 FORMAT(1H ,9X,11F10.4)
   14 FORMAT(1H ,F11.4,5X,101A1)
      YMIN=Y(1)
      YMAX=YMIN
      DO 4 J=1,N
      IF(Y(J)-YMIN)2,3,3
    3 IF(Y(J)-YMAX)4,4,5
    2 YMIN=Y(J)
      GO TO 4
    5 YMAX=Y(J)
    4 CONTINUE
      YSCALE=(YMAX-YMIN)/100.
      WRITE(6,8)NO
      YPR(1)=YMIN
      DO 9 K=1,9
    9 YPR(K+1)=YPR(K)+YSCALE*10.0
      YPR(11)=YMAX
      WRITE(6,10)(YPR(IP),IP=1,11)
      WRITE(6,11)
      IF(NO-1)16,16,17
   16 CONTINUE
      IBLANK=32
      CALL MINC(IBLANK)
      ISYM=88
      CALL MINC(ISYM)
   17 CONTINUE
      DO 15 I=1,N
      DO 13 IX=1,101
   13 IOUT(IX)=IBLANK
      JP=((Y(I)-YMIN)/YSCALE)+1.0
      IOUT(JP)=ISYM
      WRITE(6,14)X(I),(IOUT(IX),IX=1,101)
   15 CONTINUE
      RETURN
      END
```

11.3 Turbogenerator and transmission system parameters used in the studies

11.3.1 Typical 500 MW turbogenerator parameters

(a) Generator

The following turbogenerator parameters are based upon an early 500 MW design, where the damping is provided by the solid iron circuits alone as no copper damper winding is included. The symbols are defined in the Nomenclature Section.

Generator rating	588 MVA, 500 MW 22 kV, 3000 rpm
Armature resistance, R_a	.0031 p.u.
Field resistance, R_{fd}	.0012 p.u.
Direct axis mutual reactance, χ_{md}	2.59 p.u. (unsat.)
Quad. axis mutual reactance, χ_{mq}	2.52 p.u. (unsat.)
Direct axis leakage reactance, $\chi_{\ell d}$	0.21 p.u.
Quad. axis leakage reactance, $\chi_{\ell q}$	0.20 p.u.
Field leakage reactance, $\chi_{\ell fd}$	0.162 p.u.
Direct axis damper leakage reactance, $\chi_{\ell kd}$	0.0204 p.u.
Quad. axis damper leakage reactance, $\chi_{\ell kq}$	0.0204 p.u.
Direct axis damper resistance, R_{kd}	0.0174 p.u.
Quad. axis damper resistance R_{kq}	0.07 p.u.
Inertia constant H	4.44 secs.

(b) Transmission system

Total transmission reactance before disturbance	0.2 p.u.
Total transmission reactance during disturbance	0.1 p.u.
Total transmission reactance after disturbance	0.2 p.u.

(c) Excitation system

The following are the parameters for the standard fast thyristor excitation system and the nomenclature refers to the symbols shown on Fig.5.1.

Voltage transformer/rectifier gain, G_{vt}, 0.0005 per volt

Voltage transformer/rectifier time constant, T_{vt}, 0.01 s

AVR gain G_{fn}	66 per volt
AVR time constant T_{fn}	0.01 s
Thyristor convertor gain G_{th}	50 per volt
Exciter positive forcing limit V_{lim}	800 volts (2.5 p.u.)
Exciter negative forcing limit V_{low}	-600 volts

(d) Governing system

The following are the parameters for the standard electrohydraulic governing system and the nomenclature refers to Fig.3.14.

Governor gain, K_1, K_2	0.318 (1% droop) 0.0796 (4% droop)
Valve time constants T_1, T_2	0.05 s
Transducer time constant T_v	0.01 s
Reheater lag T_{rh}	7.0 s
HP steam transport lag T_{HP}	0.13 s
IP/LP steam transport lag T_{LP}	0.4 s
HP torque complement K_{HP}	0.3
LP torque complement K_{LP}	0.7

11.3.2 Parameters of Doncaster No.2 30 MW machine used for simulation of fault tests

(a) Generator

The parameters were in general obtained from three sources. From the manufacturers' design information (GEC) a calculation was performed based on Kilgore[40] using an in-house computer programme of C.A. Parsons & Co. Ltd. These parameters are denoted by a letter K. Other parameters supplied by the manufacturers are denoted by a letter M and data supplied by CEGB both from test and calculations, by the letter C.

Generator rating	37.5 MVA, 30 MW 11.8 kV, 3000 rpm
Armature resistance, R_q	0.0015 p.u. (C)
Field resistance, R_{fd}	0.00068 p.u. (C)
Direct axis mutual reactance, χ_{md}	1.516 p.u. (K)
Quad. axis mutual resistance, χ_{mq}	1.482 p.u. (K)

Direct axis leakage reactance, $X_{\ell d}$	0.158 p.u. (K)
Quad. axis leakage reactance, $X_{\ell q}$	0.158 p.u. (K)
Field leakage reactance, $X_{\ell fd}$	0.105 p.u. (K)
Direct axis damper leakage reactance, $X_{\ell kd}$	0.0209 p.u. (K)
Quad. axis damper leakage reactance, $X_{\ell kq}$	0.0114 p.u. (K)
Direct axis damper resistance, R_{kd}	0.00882 p.u. (C)
Quad. axis damper resistance, R_{kq}	0.00882 p.u. (C)
Inertia constant, H	5.0 (M)

(b) Transmission system

(See Fig.9.5c)

Total transmission reactance before fault	0.195 p.u.
Total transmission reactance during fault	0.1042 p.u.
Total transmission reactance after fault	0.195 p.u.
Total transmission resistance before fault	0.01507 p.u.
Total transmission resistance during fault	0.00416 p.u.
Total transmission resistance after fault	0.01507 p.u.

(c) Excitation system

(See Fig.9.5a)

Transfer function is given by:

$$G(p) = \frac{E_{fd\ p.u.}}{E_{tm\ p.u.}} = 14.5\left(\frac{1}{1+2p} + 0.1p\right)$$

Also, acceleration gain, Ga = 6 per rad/sec^2 (Test 3)

Ga = 60 per rad/sec^2 (Test 4)

Excitation limits $\pm$ 2 p.u. (360 volts)

Voltage transformer lag 0.05 s

(d) Governor

This was assumed to be identical to a similar unit at Goldington Power Station[6].

Governor gain	0.0796 (4% droop)
Governor → HP lag	0.1 s
LP/IP lag	0.49 s
HP torque complement	0.3
LP torque complement	0.7

TABLE 1

DEGREES OF COMPLEXITY OF TURBOGENERATOR MODELS

Model No.	Number of d-axis dampers	Number of q-axis dampers	Damper constant	Stator transients	Field transients	Number of differential equations	Description
1	-	-	-	-	-	2	Classical representation
2	-	-	X	-	X	3	Field transients or 'flux decay' included
3	-	1	-	-	X	4	Quadrature axis damping only
4	1	1	-	-	X	5	Full damping stator transients neglected
5	1	1	-	X	X	7	'Standard' model stator transients included
6	1	2	-	X	X	8	High and low frequency quadrature axis damping circuits
7	∞	∞	-	X	X	7*	Non linear damping representation

*Non-linear differential equations

TABLE 2

INITIAL CONDITION SETTINGS FOR DONCASTER FAULT TESTS

Quantity	Test No. 1	2	3	4
Terminal power (MW)	29,7	29,8	30,0	29,5
*Terminal reactive power (MVAr)	2.02	2.72	1,15	-12,1
System angle (degrees)	59,5	58	60	79
Stator volts (kV)	10.54	10,60	10,56	10,60
Stator amps (A)	1576	1588	1590	1663
Field volts (v)	182	180	186	166
Field amps (A)	264	267.5	264	228
Genr. transformer tap position	2	2	2	8
Grid transformer tap position	5	6	6	6
Fault duration (mS)	203	197	196	136
Connections to thyristor transformer	unit aux.	No.2 unit	unit aux.	unit aux.
Gain of acceleration channel (field volts per rad/sec^2)	0	0	6	60

* Not relied upon for simultations

NOMENCLATURE

The parameters given below are those not defined specifically in the text or diagrams.

Suffix notation

d	direct axis
q	quadrature axis
a	armature
f	field
k	damper
t	transmission system
m	mutual
ℓ	leakage
o	per unit base

Superfix notation

'	transient
''	subtransient

Per unit quantities

A,B,C,D,E,F,G, I,J,K,L,M,N, X_1,X_2	multiple impedance constants as defined by Appendix 11.1
E_f	field voltage referred to stator
E_{tm}	generator terminal voltage
E'	voltage behind transient reactance
i_d,i_q	direct and quadrature axis armature currents
i_{fd}	field current
i_{kd},i_{kq}	direct and quadrature axis damper winding currents
i_{kq1},i_{kq2}	high and low reactance quadrature axis damper winding currents for complex model
I_a	armature current
I_d,I_q	direct and quadrature axis armature currents
I_{fd}	Field current

} Steady state values

k_d	mechanical damping constant
K_{dm}	electrical damping constant

NOMENCLATURE (Cont'd)

K_e	exciter gain
K_g	governor (droop) gain
K_H	high pressure turbine torque complement
K_L	low/intermediate pressure turbine torque complement
L_{md}	direct axis mutual inductance
M_{fd}	mutual inductance between field and direct axis armature coils
M_{df}	mutual inductance between direct axis armature coil and field coil
M_{kd}	mutual inductance between direct axis damper and armature coils
M_{dk}	mutual inductance between direct axis armature and damper coils
P	electrical power (active)
P_B	boiler pressure
P_R	reheater pressure
Q	electrical power (reactive)
R_a	armature resistance
R_{fd}	field resistance
R_{kd}, R_{kq}	direct and quadrature axis damper winding resistance
R_{kq1}, R_{kq2}	resistance of high and low quadrature axis dampers for complex model
R_t	transmission system resistance
T_e	electrical torque
T_{FL}	full load prime mover torque
T_i	mechanical losses torque
T_L	prime mover torque
T_{LO}	initial condition setting of prime mover torque
V_b	busbar voltage

NOMENCLATURE (Cont'd)

V_d, V_q	direct and quadrature axis armature voltages
V_d', V_q'	voltages behind direct and quadrature axis transient reactances
V_{fd}	field voltage
V_T	armature voltage
χ_d	direct axis synchronous reactance
χ_d'	direct axis transient reactance
χ_{fd}	total field reactance
χ_{kd}, χ_{kq}	direct and quadrature axis total damper reactances
χ_{kq1}, χ_{kq2}	high and low quadrature axis damper winding total reactances for complex model
$\chi_{\ell d}$ $\chi_{\ell q}$	direct and quadrature axis armature leakage reactances
$\chi_{\ell fd}$	field leakage reactance
$\chi_{\ell kd}, \chi_{\ell kq}$	direct and quadrature axis damper leakage reactances
χ_{md}, χ_{mq}	direct and quadrature axis mutual reactances
χ_q	quadrature axis synchronous reactance
χ_t	transmission reactance

Other quantities

E_{ao}	base armature voltage, volts
E_{fd}	field voltage, volts
E_{fdo}	base field voltage, volts
H	inertia constant, kW-secs/kVA
I_{ao}	base armature current, amps
i_{eq}	field current to produce 1 p.u. armature voltage on open circuit, amps
L_{ao}	base armature inductance, Henrys
L_{afd}	mutual inductance between armature and field, Henrys
Se	exciter saturation function

NOMENCLATURE (Cont'd)

T_d'	direct axis transient short circuit time constant, seconds
T_d''	direct axis subtransient short circuit time constant, seconds
t	time, seconds
VA_o	base volt amperes
δ	system load angle, radians
δ'	generator rotor angle, radians
$\dot{\delta}$	shaft speed deviation, rads/sec,
$\ddot{\delta}$	shaft acceleration, rads/sec,
ϕ	phase angle, radians
ψ_d, ψ_q	direct and quadrature axis armature fluxes
ψ_{fd}	field flux
ψ_{kd}, ψ_{kq}	direct and quadrature axis damper winding fluxes
ψ_{kq1}, ψ_{kq2}	high and low reactance damper winding fluxes for complex model
ψ_T	total air gap flux
ω	shaft speed rads/sec,
ω_o	synchronous speed, rads/sec,
p	differential operator, d/dt

REFERENCES

1 LYON, G. Some experience with a British network analyser. Proc.IEE, Vol.97(II), 1950, pp697-725

2 ADAMSON, C., and El-SERAFI, A.M.S. Representation of saliency on AC network analysers. ibid, Vol.104c, 1956, p108

3 DINELEY, J.L. Study of power system transient stability by a combined computer. ibid, Vol.III(1), 1964, pp107-114

4 ALDRED, A.S. Electronic analogue computer simulation of multi-machine power system networks. ibid, Vol.109a, No.45, 1962

5 MILES, J.G. Analysis of overall stability of multi-machine power systems. ibid, Vol.109a, No.45, 1962

6 SHACKSHAFT, G. A general purpose turbo-alternator model. ibid, Vol.110(4), 1963, pp703-713

7 SHUM, L.Y.S. The optimal control aspects of power systems in the transient state. Ph.D. thesis, L955, University of Newcastle, 1967

8 BALDWIN, C.J. and BYERLY, R.T. Recent advances in the digital simulation of power system distrubances. Proc. PICA Conf., Paper No. D and C4

9 HUMPAGE, D. and STOTT, B. Predictor corrector methods of numerical integration in digital computer analyses of power system transient stability Proc. IEE, Vol.112(8), 1965

10 RUPERT, R. Micromachines and micronetwork study of the problems of transient stability by the use of models similar electromechanically to existing machines and systems. CIGRE, Paris, 1950, Paper No. 338

11 HAMMONS, T.J. and PARSONS, A.J. Design of microalternator for power system stability investigations. Proc. IEE, Vol.118(10), Oct. 1971, pp1421-1441

12 PARK, R.H. Two reaction theory of synchronous machines. Trans. AIEE, Vol.49, 1930

13 PARK, R.H. Two reaction theory of synchronous machines II. ibid, Vol.52, 1950

14 ADKINS, B. The general theory of electrical machines. Chapman and Hall, 1964

15 JONES, C.V. The unified theory of electrical machines. Butterworths, 1967

16 RANKIN, A.W. Per unit impedances of synchronous machines, Part I. Trans. AIEE, Vol.64, 1945, p569

17 RANKIN, A.W. Per unit impedances of synchronous machines, Part II. ibid, Vol.64, 1945, p839

18 HARRIS, LAWRENSON and STEPHENSON. Per unit systems. Cambridge University Press, 1970

19 KAMINOSONO, H. and UYEDA, K. New measurements of synchronous machine quantities. IEEE Trans., Vol.PAS-87, No.11, 1968, pp1908-1918

20 HUMPAGE, W.D. and SAHA, T.N. Digital computer methods in dynamic response analyses of turbogenerator units. Proc.IEE, Vol.114(8), 1967

21 HARLEY and ADKINS, B. Calculation of the angular backswing following a short circuit of a loaded alternator. ibid, Vol.117(2), 1970

22 DINELEY, J.L. and MORRISS, A.J. The dynamic interaction of closely coupled synchronous generators. IEEE Paper No.71 TP71-PWR

23 JACKSON, W.B. and WINCHESTER, R.L. Direct and quadrature-axis equivalent circuits for solid rotor turbogenerators. IEEE Trans., Vol.PAS-88, No.7, 1969, pp1121

24 MEHTA, D.B. and ADKINS, B. Transient torque and load angle of a synchronous generator following several types of system disturbance. Proc.IEE, Vol.107A, 1960, pp61-74

25 SHACKSHAFT, G. Effect of oscillatory torques on the movement of generator rotors. ibid, Vol.117(10), 1970, pp1969-1974

26 PODOLSBY, L.B. OSBORNE, R.L. and HEISER, R.S. Digital electro-hydraulic control for large steam turbines. Proc. 14th Int. ISA Power Instrument. Symposium, May 1971, pp40-41

27 EGGERS, C.W. Direct digital control comes of age. Westinghouse Engineer, July 1969, pp98-103

28 EVANS, F.J., NGO, Y.H. and OUTHRED, H.R. The on-line digital and optimal control of generator excitation systems. CIGRE Paper No.32-05, 1972

29 CUNEEN, W.J. and KOPPEL, H.H. D.D.C. picks up steam. Proc. 14th Int. ISA Power Inst. Symposium, May 1971, pp29-34

30 WRIGHT, W.F., HAWLEY, R. and DINELEY, J.L. Brushless thyristor excitation systems. IEE Paper No.T72 226-4

31 IEEE Committee Report. Computer representation of excitation systems. IEEE Trans, Vol.PAS-87, No.6, June 1968, pp1460-1464

32 FENWICK, D.R. Fast excitation systems. Electrical Times 29 Dec. 1960

33 McCLYMONT, K.R., MANCHUR, G., ROSS, R.J. and WILSON, R.J. Experience with high speed rectifier excitation systems. IEEE Winter Power Meeting New York, N.Y., Jan 29-Feb 3, 1967

34 CRENSHAW, M.L., MILLER, W.J., SCHULZ, R.P. and TEMOSHOCK, M. Althyrex excitation system with power system stabiliser. IEEE Paper No.70Cp563-PWR, July 1970

35 SCHINDLER, P.B., NEASHAM, D.L., JENKINS, K and NAIK, K.R. A brushless thyristor exciter. Proc. of 8th Universities Power Engineering Conf., Bath University, Jan. 1973

36 DANDENO, P.L., KARAS, A.N., McCLYMONT, K.R. and WATSON, W. Effect of high speed rectifier excitation systems on generator stability limits. IEEE Trans., Vol.PAS-87, Jan. 1968, pp190-200

37 WATSON, W. and COULTES, M.E. Static exciter stabilising signals on large generators - mechanical problems. IEEE Transactions, Paper No. T72-2280

38 ADAMSON, C. and HINGORANI, N.G. High voltage direct current power transmission. Garraway, 1960

39 BARNEY, G.C. Method of rapidly reversing current in highly inductive loads. Proc.IEE, Vol.113(12), Dec.1966, pp2031-2034

40 KILGORE, L.A. Calculation of synchronous machine constants. Trans. AIEE, Dec.1931, pp1201-1214

41 SAY, M.G. The performance and design of alternating current machines. Pitman, London, 3rd Ed. 1958

42 DUBE, C and LEMAY, J. Improvement in system stability with effective static excitation control. Paper D and C3, PSCC Conf. Proc., Rome 1969

43 MORRISS, A.J. Some aspects of the transient performance and control of synchronous generators. Ph.D. thesis, University of Newcastle, 1970

44 RICHARDSON, P., HAWLEY, R. and WOOD, J.W. Insulation levels for turbo-generator rotors. IEEE Winter Power meeting, 1971

45 BYERLY, R.T., KEAY, F.W. and SKOOKLUND, J.W. Damping of power oscillations in salient pole machines with static exciters. IEEE Transaction Paper No.69.TP735-PWR

46 DEMELLO, F.P. and CONCORDIA, C. Concepts of synchronous machine stability as affected by excitation control. IEEE Transactions Paper No.68.TP129-PWR

47 GLAVITSCH, H. Möglichkeiten der Verbesserung der Stabilität und der Spannungregelung von synchronmaschinen mit Hilfe der Gleichrichtererregung Electrotechnik u. Maschinenbau (Austria), Vol.85, No.2, 1968

48 SCHLIEF, F.R., HUNKINS, H., MARTIN, G.E. and HATTON, E.E. Excitation control to improve powerline stability. IEEE transactions, Paper No. 31TP 67-51

49 SHIER, R.M and BLYTHE, A.L. Field tests of dynamic stability using a stabilising signal and computer program verification. IEEE Transactions Vol.PAS-87, pp315-322, Feb. 1968

50 DINELEY, J.L., MORRISS, A.J. and PREECE, C. Optimised transient stability from excitation control of synchronous generators. IEEE Transaction. Vol.PAS-87, No.8, August 1968, pp1696-1705

51 SHACKSHAFT, G. Results of stability tests on an underexcited 120 MW generator. Proc. IEE, Vol. 119, No.2, Feb. 1972, pp175-188

52 CHORLTON, A. and SHACKSHAFT, G. Comparison of accuracy of methods for studying stability Northfleet exercise. Electra No.23, 1972 pp9-49 (CIGRE publication)

53 MASON, T.H., AYLETT, P.D. and BIRCH, F.H. Turbogenerator performance under exceptional operating conditions. Proc. IEE, Vol.106A, 1959, p357

54 DINELEY, J.L. and KENNEDY, M.W. Influence of governors on power-system transient stability. ibid, Vol.111, pp98-106, January 1964

55 DINELEY, J.L. and POWNER, E.T. Power system governor simulation. ibid, pp115-124

56 BROWN, P.G., de MELLO, F.P, LENFEST, E.H. and MILLS, R.J. Effects of turbine energy control, and transmission on transient stability. IEEE Trans. Vol.PAS-89, No.6, July/August 1970

57 de MELLO, F.P., EWART, D.N., TEMOSHOK, M. and EGGENBERGER, M.A. Turbine energy controls aid in power system performance. Proc. Amer. Power Conf. Vol.28, pp438-445, 1966

58 BYERLY, R.T. Power system stability - effect of control system performance. (See Ref.65)

59 EGGENBERGER, M.A. An electrohydraulic control system for reheat turbines. Proc. Amer. Power Conf. pp351-361, Vol.27, April -965

60 HAM, P.A.L. Control requirements for large turbines, Inst. M.C. Symposium. Turbine and Compressor Control, City University London, April 1972

61 BIRNBAUM, M. and NOYES, E.G. Electrohydraulic control for improved availability and operation of large steam turbines. ASME-IEEE, Nat. Power Conf., Albany, N.Y. 1965

62 EGGENBERGER, H.A. Introduction to the basic elements of control systems for large steam turbine generators. G.E. Tech. Manual GET-3096A

63 FENWICK, P.J. DINELEY, J.L. and HAM, P.A.L. A study of the effect on transient stability of a digital electro-hydraulic governor. Proc. of PSCC Conf. Grenoble, 1972

64 HUGHES, F.M. Electrical governor control of turbine generators. Ph.D. thesis, UMIST, 1969

65 IEEE Tutorial Course Text. The role of prime movers in system stability. Course text 70M29-PWR

66 IYER, S.N. Optimum control of a turbogenerator including an exciter and governor. IEEE paper No.71, TP70-PWR

67 FAIRNEY, W. LODGE, I. and TOMS, J.E. Thyristor excitation alternators. Conf. on power thyristors and their applications, 6-8 May 1969, IEE Conf. Publication No.53.